INVESTIGATION INTO THERMAL-FLUID PROPERTIES OF HYBRID FERROFLUIDS AS HEAT TRANSFER FLUIDS

by

Solomon Olanrewaju Giwa

Submitted in partial fulfilment of the requirements for the degree

Philosophiae Doctor in Mechanics

Department of Mechanical and Aeronautical Engineering

University of Pretoria

October 2019

Supervisors: Prof. Mohsen Sharifpur and Prof. Josua P. Meyer

Abstract

Title: Investigation into thermal-fluid properties of hybrid ferrofluids as heat transfer fluids.

Supervisors: Prof M. Sharifpur and Prof J.P. Meyer

Department: Mechanical and Aeronautical Engineering

Degree: PhD (Mechanics)

Over two decades of extensive research on nanofluids have established them as a better cooling media than traditional fluids such as ethylene glycol (EG) and water. Recently, hybrid nanofluids have emerged as advanced thermal transport media with improved thermal and fluid properties relative to nanofluids. Experimentally, limited studies have been carried out on the thermo- and thermomagnetic convection heat transfer of nanofluids in cavities. However, there is a dearth of documentation on the thermo- and thermomagnetic convection of hybrid nanofluids in cavities in the public domain.

In this study, the thermo-convection heat transfer (Q_{av}) performance of three magnetic hybrid nanofluids (MHNFs) contained in a rectangular cavity was experimentally investigated with and without magnetic stimuli. Aqueous MWCNT-ferrofluid (AMF) [MWCNT-Fe_2O_3/deionised water (DIW)], aqueous Al_2O_3-ferrofluid (AAF) [Al_2O_3-Fe_2O_3/DIW] and bi-aqueous Al_2O_3-ferrofluid (BAAF) [Al_2O_3-Fe_2O_3/EG-DIW] were formulated for volume concentrations (φ) of 0.05 to 0.40 vol.%. Key nanofluid formulation parameters of dispersion fraction, sonication time and amplitude were optimised to improve stability of the MHNFs. Stability, characterisation and thermal properties (μ and κ at 20-40 °C) of the MHNFs were carried out using standard instruments. AMF, BAAF, AAF, DIW and EG-DIW were charged into a rectangular cavity subjected to differential heating of the opposite vertical walls under varying ΔT of 20 to 35 °C. Samples of AMF, BAAF and AAF with the highest heat transfer

were thereafter charged into the cavity where the walls (bottom, top and side) were exposed to magnetic stimuli (4.89 – 21.95 mT).

Stable MHNFs were formulated according to the optimised parameters as verified using an ultraviolet visible spectrophotometer and visible inspection techniques. The images of the transmission electron microscope for the MHNFs showed an even suspension of the nanoparticles into DIW and EG-DIW. An increase in temperature and φ was observed to enhance κ_{eff} of AMF, BAAF and AAF by 3.83% to 14.17%, 2.14% to 12.56% and 2.21% to 10.51% respectively. Temperature rise detracted μ_{eff} and φ enhanced it for AMF, BAAF and AAF with augmentation of 11.83% to 28.79%, 1.66% to 13.33% and 4.55% to 20.43% respectively. With the MHNFs, higher κ_{eff} and lower μ_{eff} were recorded in comparison with the monoparticle nanofluids of Fe_2O_3, which made the MHNFs beneficial for convective heat transfer studies. Additionally, models were developed for predicting the κ_{eff} and μ_{eff} of AMF, BAAF and AAF from the obtained experimental data.

Without magnetic stimuli, the Q_{av} of AMF, BAAF and AAF was enhanced at $\varphi \leq 0.20$ vol.% and attenuation was the case beyond $\varphi = 0.20$ vol.%. Optimum Q_{av} enhancements of 11.2%, 10.09% and 10.79% were achieved for AMF (at 0.05 vol.%), BAAF (at 0.05 vol.%) and AAF (at 0.10 vol.%) respectively. Models were proposed for estimating the Nu_{av} of AMF, BAAF and AAF. The vertical imposition of the magnetic stimuli on the sidewall of the cavity led to maximum enhancements of Q_{av} by 4.48%, 4.02% and 4.31% for the AMF, BAAF and AAF samples respectively. These values were recorded for magnetic stimuli of 21.95 mT for AMF and AAF, and 11.84 mT for AAF. The MHNFs were observed to yield higher Q_{av} than monoparticle nanofluids of Fe_2O_3 with and without magnetic stimuli.

Conclusively, the κ_{eff}, μ_{eff} and Q_{av} of AMF, BAAF and AAF were found to be better than those of the monoparticle nanofluids of Fe_2O_3, which revealed the benefit of NP hybridisation for engineering application, especially in thermo- and thermomagnetic convection studies.

Publications

The following publications have been prepared as this study progressed:

Journals papers

1. S.O. Giwa, M. Sharifpur and J.P. Meyer, Experimental study of thermo-convection performance of hybrid nanofluids of Al_2O_3-MWCNT/water in a differentially heated square cavity, International Journal of Heat and Mass Transfer, Vol. 149, 119072, 2020.

2. S.O. Giwa, M. Sharifpur and J.P. Meyer, Effects of uniform magnetic induction on heat transfer performance of aqueous hybrid ferrofluid in a rectangular cavity, Applied Thermal Engineering, Vol. 170, 115004, 2020.

3. S.O. Giwa, M. Sharifpur, Marjan Goodarzi and J.P. Meyer, Influence of base fluid, temperature, and concentration on the thermo-physical properties of hybrid nanofluids of alumina-ferrofluid, **In Press** in Journal of Thermal Analysis and Calorimetry (JTAC), https://doi.org/10.1007/s10973-020-09372-w

4. M. Sharifpur, S.O. Giwa, H. Ghodsinezhad, K. Lee and J.P. Meyer, Experimental investigation into cavity flow natural convection of zinc oxide-water nanofluids, Accepted in the special issue of Heat Transfer Engineering.

5. S.O. Giwa, M. Sharifpur and J.P. Meyer, Thermal transport performance of bi-aqueous hybrid ferrofluid in an enclosure under magnetic stimulus, submitted to International Journal of Thermal Sciences, manuscript number: THESCI_2019_1554.

6. S.O. Giwa, M. Sharifpur and J.P. Meyer, Experimental investigation into heat transfer performance of water-based magnetic hybrid nanofluids in a rectangular cavity exposed to magnetic excitation, International Communications in Heat and Mass Transfer, manuscript number: ICHMT-D-19-01065.

7. S.O. Giwa, M. Sharifpur, O. Mahian, J.P. Meyer and S. Wongwises, Experimental measurement of viscosity and electrical conductivity of water-based γ-Al_2O_3/MWCNT

hybrid nanofluids, submitted to Journal of Molecular Liquids, manuscript number: is going to be submitted to the special issue of Journal of Thermal Analysis and Calorimetry (JTAC).

8. S.O. Giwa, M. Sharifpur, O. Mahian, J.P. Meyer and S. Wongwises, Experimental determination of viscosity and electrical conductivity of water-based hybrid ferrofluids, is going to be submitted to the special issue of Journal of Thermal Analysis and Calorimetry (JTAC).

9. A comprehensive review of magnetohydrodynamic convection behaviours of nanofluids in non-square enclosures (submitted to the supervisor for final corrections).

10. A review of magnetic field influence on natural convection heat transfer performance of nanofluids in square cavities (submitted to the supervisor for final corrections).

11. M. Behi, S.O. Giwa, M. Sharifpur, J.P. Meyer, M. Behnia, Review of recent developments on colloidal nano-engineering fluids (under final revision to be submitted).

Conference papers

12. S.O. Giwa, M. Sharifpur and J.P. Meyer, Heat transfer enhancement of dilute Al_2O_3-MWCNT water based hybrid nanofluids in a square cavity, International Heat Transfer Conference (IHTC-16), Beijing, China, August 10-15, 2018.

13. S.M.S. Murshed, M. Sharifpur, S.O. Giwa and J.P. Meyer, Trend of experimental natural convection of nanofluids, 14th International Conference on Heat Transfer, Fluid Mechanics and Thermodynamics (HEFAT 2019), 22 -24 July 2019, Wicklow, Ireland.

Chapter in a book

14. S.M.S. Murshed, M. Sharifpur, S.O. Giwa and J.P. Meyer, Stability evaluation, measurements and presentations of convective heat transfer characteristics of nanofluids. Accepted book chapter for “The art of measuring in thermal science”, by CRC Press (Taylor and Francis, Series: Heat Transfer, Series Editor: Prof Afshin Ghajar), manuscript number: 1570481883.

Dedication

This work is dedicated to the LORD Almighty, the Father of our Lord Jesus Christ; the Source of life.

Acknowledgements

I am forever grateful for the huge role played by my father, the late Alhaji D.A. Giwa, who laid the solid foundation for my education, upon which God helped me to build my life. The immeasurable efforts and rare sacrifices of my beloved wife (Mrs. Omolara L. Giwa) and +lovely children (Ms. Opeyemi B. Giwa, Master Kingdom O. Giwa and Master Ayanfe O. Giwa) during this study are acknowledged and forever appreciated. I love you all.

The fatherly figure and the financial and moral support provided by Prof. J.P. Meyer (Head of Department, Mechanical and Aeronautical Engineering, University of Pretoria, South Africa) are highly appreciated. Prof. M. Sharifpur, a rare gem and a worthy supervisor, is specially acknowledged for his undiluted support and guidance in all ramifications through this study. I thank you all for your tutelage. The moral and technical support afforded by Mr. Chris Govender and Mr. Donald Keetse, which kept me going, is duly appreciated.

Finally, I want to acknowledge Olabisi Onabanjo University for the opportunity to undertake my doctoral degree at the University of Pretoria, South Africa. The financial support provided by the National Research Foundation of South Africa under the Renewable and Sustainable Energy Doctoral Scholarships is also highly appreciated.

Table of Contents

List of Figures

List of Tables

Nomenclature

A	Area of cavity	m^2
AAE	Average absolute error	%
Ag	Silver	
AIN	Aluminium nitride	
Al	Aluminium	
Al_2O_3	Aluminium oxide	
AR	Aspect ratio	
Au	Gold	
B	Dimensionless heat source length	
CC	Carboxymethyl cellulose	
CNT	Carbon nanotube	
Co_3O_4	Cobalt oxide	
C_p	Specific heat capacity at constant pressure	J/kg K
CTAB	Cetyl trimethyl ammonium bromide	
Cu	Copper	
CuO	Copper oxide	
Da	Dimensionless heat source location	
DIW	Deionised water	
DW	Distilled water	
DWCNT	Double-walled carbon nanotube	
EDL	Electrical double layer	
EG	Ethylene glycol	
EG-DIW	Ethylene deionised water	
EO	Engine oil	
Fe	Iron	
Fe_2O_3	Iron (III) oxide	
Fe_3O_4	Iron (II) oxide	
G	Graphene	
G	Gravitational acceleration	9.81 m/s^2
GA	Gum arabic	
GL	Glycerol	
GNF	Green nanofluid	
GO	Graphene oxide	
GON	Graphene oxide nanosheet	
Gr	Grashof number	
h	Coefficient of convective heat transfer	W/m^2K
H	Height	m
Ha	Hartmann number	
HEG	Hydrogen exfoliated graphene	
HNF	Hybrid nanofluid	
HNP	Hybrid nanoparticle	
L	Length of cavity	m

m	Gradient	
$\dot{m}$	Mass flow rate	kg/s
MAE	Mean absolute error	
MgO	Magnesium oxide	
MHNF	Magnetic hybrid nanofluid	
MNF	Magnetic nanofluid	
MO	Mineral oil	
MOD	Margin of deviation	
MSE	Mean standard error	
MWCNT	Multi-walled carbon nanotube	
ND	Nanodiamond	
Ni	Nickel	
NF	Nanofluid	
NP	Nanoparticle	
Nu	Nusselt number	
P	Heating power	W
PG	Propylene glycol	
Pr	Prandtl number	
PVP	Polyvinyl pyrolidone	
PW	Paraffin wax	
Q	Heat transfer rate	W
Ra	Rayleigh number	
Re	Reynolds number	
RMSE	Root mean standard error	
SD	Standard deviation	
SDBS	Sodium dodecyl benzene sulfonate	
SDS	Sodium dodecyl sulphate	
SiC	Silicon carbide	
SiO_2	Silicon oxide	
SiO_x	Silicon oxides	
SWCNT	Single-walled carbon nanotube	
t	Student's *t* test	
T	Temperature	°C
TiO_2	Titanium oxide	
TO	Transformer oil	
V	Volume	m^3
W	Water	
W	Width	m
X	Ratio of hybrid nanoparticles	wt.%
Zn	Zinc	
ZnO	Zinc oxide	
ΔT	Temperature difference	°C

Greek letters

Δ	Difference	
ρ	Density	m^3/kg
β	Thermal coefficient of expansion	1/k
μ	Dynamic viscosity	mPa.s
σ	Electrical conductivity	µS/cm
κ	Thermal conductivity	W/m K
φ	Volume concentration of nanoparticles	vol.%
δ	Uncertainty	
∂	Partial differential	

Subscripts

M	Weight of nanoparticles	g
W	Wall	
e	Enhancement	
eff	Effective	
av	Average	
s	Sample	
w	Water	
S	Side	
in	Input	
i	Inlet	
o	Outlet	
1	First	
2	Second	
h	Hot	
c	Cold	
Exp	Experiment	
Pred	Predicted	
b	Bias	
B	Bulk	
p	Precision	
cal	Calibration	

Chapter 1

INTRODUCTION

1.1 BACKGROUND

The trio of population, economic and technological growth is the primary drivers for the ever-increasing global energy demand. These drivers have collectively impacted negatively on the environment leading to climate change, which is currently of global concern. The growing trend of global warming and the adverse effect on our environment are worrisome to the global communities and gave rise to the slogan “Sustainability” in terms of energy and environment as promoted by the United Nations (UN). The UN has championed different global agendas towards resolving several environmental and energy issues confronting our world. The latest agenda is the 17-point Sustainable Development Goals (SDGs) initiated in 2016, which will run until 2030. To deal with the issue of energy sustainability, the UN aimed to engage SDG 7 (ensure access to cheap, dependable, sustainable and modern-day energy for all) by recommending that energy efficiency be doubled globally by 2030 as one of the five targets under SDG 7 [1].

The current global technological advancement in communication, electronics, power plants, computing and power systems has called for improvement in the energy efficiency of devices, components and machinery. With the state-of-the-art technologies, the critical need to remove the high degree of heat flux generated at a faster rate without causing material damage and system failure demands an efficient thermal management method. Traditional working fluids such as engine oil (EO), water, propylene glycol (PG) and ethylene glycol (EG) as cooling media in heat transfer devices (electronic components, heat exchangers, transformers, solar panels, microprocessors, micro heat sinks, etc.) have been employed for some decades now. The heat transfer capacity of the conventional fluids has reached its threshold due to the generally low thermal conductivity values of these fuilds [2]. Surface

extension (fins), miniaturisation, surface modification and surface area/volume ratio reduction of thermal equipment are methods used to improve the heat transfer of thermal systems. However, they are presently reaching their practicable limits [3, 4].

The limitations have ignited extensive research, and in 1873, Maxwell [5] first proposed the concept of engineering an energy-efficient fluid through the improvement of the thermophysical properties of conventional fluids. With solid materials known to possess a higher κ than that of conventional working fluids, Maxwell suspended micro-sized metal into base fluids and observed an improvement in κ_{eff} of the microparticle fluids. However, drawbacks such as clogging, erosion, sedimentation and considerable pressure drop were reported [3, 5]. Ahuja conducted an identical study to that of Maxwell by suspending micro-sized particles of polystyrene in a base fluid of sodium chloride and glycerine [3, 6]. A significant improvement in κ_{eff} was reported relative to that of base fluid. Similar problems as noticed by Maxwell were also reported by Ahuja, which made this idea unfeasible for decades.

To solve the problems associated with the use of microparticles to improve the κ of conventional fluids, Masuda and co-workers [7] were the first to engage nano-sized particles to enhance the κ of traditional fluids. They suspended nano-scaled particles of SiO_2, TiO_2, and Al_2O_3 in water and noticed an enhanced κ_{eff} without the flaws associated with the use of micro-scaled particles reported by Maxwell and Ahuja. This innovation and subsequent studies [8–10] produced newly engineered fluids as advanced cooling media. In 1995, Choi named this novel fluid “nanofluid” [10]. For over two decades now, extensive studies have been carried out on the thermal properties (μ, κ, ρ, etc.) of different types of nanofluids formulated using various nanoparticles (metals, non-metals and carbon-based) suspended in different base fluids (water, EG, EO, PG, TO, etc.) [11–15]. The improvements in the thermal properties established for nanofluids (over the base fluids) have spurred researches on their

heat transfer capacities as thermal transport media for forced and natural convection applications [16–20].

1.2 PROBLEM STATEMENT

Owing to the advantage and wide application of natural convection, different nanofluids have been studied for their heat transfer performances in various cavity configurations (under varying thermal and boundary conditions) [21–25]. Most of these works were carried out using numerical techniques with limited numbers experimentally researched [26]. Generally, discrepancies in findings were observed. The progression in research has brought about studies on the influence of an external magnetic field on the thermo-convection heat transfer of nanofluids in cavities [27–32]. The imposition of a magnetic field on the cavity is an active means of manipulating the heat transfer characteristics of nanofluids. As a recurring trend, most studies in this regard have been conducted mainly using numerical techniques, while experimental works have remained very scarce in the public domain. It is worth noting that these studies were conducted using monoparticle nanofluids; very few were carried out using ferrofluid (nanofluids with magnetic characteristics).

As a passive way of enhancing the thermal properties of nanofluids, a new class of nanofluid coined “hybrid nanofluid” has emerged on the horizon [33, 34]. The experimental determination of the thermal properties of hybrid nanofluids is presently receiving increasing attention with a limited number of publications [33–38]. However, very few studies have reported the heat transfer performance of hybrid nanofluids in cavities [39, 40]. Also, none of the research in the available literature was conducted experimentally and in the presence of an external magnetic stimulus. In this context, it was evident that the thermo-convection of hybrid nanofluids in cavities under the influence of a magnetic stimulus had to be experimentally examined.

1.3 AIM

The aim of the study was to experimentally investigate the thermo-convection performance of magnetic hybrid nanofluids (MWCNT-Fe_2O_3/deionised water, Al_2O_3-Fe_2O_3/deionised water and Al_2O_3-Fe_2O_3/ethylene glycol-deionised water) in a cavity with and without magnetic stimuli.

1.4 OBJECTIVES

The specific objectives of the study were as follows:

1. to formulate stable MWCNT-Fe_2O_3/deionised water, Al_2O_3-Fe_2O_3/deionised water and Al_2O_3-Fe_2O_3/ethylene glycol-deionised water, magnetic hybrid nanofluids (MHNFs), by way of the optimisation of the sonication time and amplitude, and dispersion fraction of surfactants;
2. to characterise the formulated MHNFs in terms of their morphology and stability using a transmission electron microscope and ultraviolet visible spectrophotometer respectively;
3. to measure the thermal properties of MHNFs at various volume concentrations and temperatures;
4. to investigate the thermo-convection performance of MHNFs with and without magnetic stimuli;
5. to develop correlations for the prediction of the thermal properties and Nusselt number of MHNFs.

1.5 SCOPE

In the study, three types of nanoparticles (NPs) and two types of base fluids were used in the formulation of MHNFs, which were at low volume concentrations (0.05 - 0.4 vol.%). The measurement of the thermal properties (thermal conductivity and viscosity) was carried out under atmospheric and static conditions. Furthermore, the thermal properties were measured

at low temperatures (20 - 40 °C). The thermo-convection experiments were conducted using a rectangular cavity as the test cell under atmospheric conditions. The thermal baths were kept between 15 to 50 °C to maintain the heated sidewalls of the cavity at varying temperature gradients of 20 to 35 °C. Both flow rates and temperature measurements were automatically acquired by way of a data logger into a personal computer.

1.6 ORGANISATION OF THESIS

An overview of the arrangement of the chapters of the thesis is provided in this section. The thesis consists of eight chapters in total. Chapter 1 presents a general introduction of the study carried out. It starts with the background of the problems that led to the advent of nanofluid and thereafter, the problem, purpose, objectives and scope of the study are provided. Chapter 2 provides a detailed literature review covering the morphology, stability, thermal conductivity and thermo-convection of both monoparticle nanofluids and hybrid nanofluids. Chapter 3 provides details of the experimental set-up, especially that of the measurement of the thermal properties of MHNFs and thermo-convection characteristics of MHNFs in a cavity with and without magnetic stimuli. This chapter also contains the validation of the cavity, data reduction, uncertainty estimation and model development.

Chapter 4 presents the results for the formulation of stable MHNFs and their morphology. In Chapter 5, the measurements are provided, and the correlations proposed for viscosity and thermal properties of MHNFs are presented and discussed. Chapter 6 covers the presentation and discussion of the results for the thermo-convection behaviour of the MHNFs in the cavity without magnetic stimuli. Chapter 7 covers the thermo-magnetic convection behaviour of MHNFs in the cavity. Chapter 8 presents a general conclusion of the thesis and suggests recommendations for future study.

Chapter 2

LITERATURE REVIEW

2.1 INTRODUCTION

The advent of nanotechnology a few decades ago led to its application in various fields of study. Nano-scaled materials have been employed in the field of heat and fluid transfer as advanced fluids with improved thermal and flow properties relative to conventional fluids. An overview of how NPs and HNPs were conceptualised and used in the formulation of nanofluids and hybrid nanofluids respectively is presented. In addition, details of the stability tests, characterisation techniques and thermophysical properties relating to nanofluids and hybrid nanofluids are provided. Furthermore, the performances of different nanofluids and hybrid nanofluids in various cavities for thermo-convection applications under varying thermal conditions are highlighted. The focus was on the influence of magnetic stimulus on the thermophysical properties and thermo-convection of nanofluids in different configurations of the enclosure. It is worth mentioning that the literature review was primarily carried out using experimental studies, most especially for the thermo-convection heat transfer performance of nanofluids and hybrid nanofluids in cavities except for the thermomagnetic convection performance of hybrid nanofluids where numerical techniques were reported.

2.2 CONCEPT OF MONOPARTICLE NANOFLUID AND HYBRID NANOFLUID

Nanofluids are engineered colloids containing NPs with less than 100 nm. Nano-engineered materials have been studied as advanced materials in the field of heat and fluid transfer since the pioneering work of Masuda et al. [7]. They investigated the κ_{eff} of nano-scaled materials (SiO_2, TiO_2 and Al_2O_3) suspended in water and found that the κ_{eff} was better than that of water. Also, this work solved the problems initially encountered with the use of micro-scaled particles suspended in conventional fluids [5, 6]. The breakthrough recorded by Masuda and

co-workers in enhancing the κ of water led to several studies in this regard by suspending various types of NPs in traditional fluids. NPs of metals, metal oxides, metal carbides, metal nitrides, carbon (nanotubes/graphene sheets) and biomass were suspended at various volume fractions/concentrations or weights in base fluids (water and organic liquids (EG, PG and TO) or a mix of both) [16, 41–49]. It should be noted that researchers started with the measurements of κ_{eff}, then μ_{eff}, and thereafter ρ_{eff}, σ_{eff}, $C_{p\text{-}eff}$, etc. of nanofluids.

Based on the idea that the κ of solid materials, especially metals, is higher than the κ of conventional fluids, nanofluid was created through the reduction of the size of the materials to nano-scale and their suspension into traditional fluids. Similarly, hybrid nanofluid was conceptualised on the premise that NPs had different thermophysical properties and combining two or more dissimilar NPs at different ratios or weights could help improve these properties through synergy [33]. Both Chopkar et al. [38] and Jana et al. [33] appeared to pioneer studies on the measurements of the thermal properties (κ in this case) of hybrid nanofluids because their works were published in the same year (2007), with the former a few months before the latter. Chopkar et al. [38] reported κ enhancement of 50 to 150% for Al_2Cu and Ag_2Al HNPs suspended in water and EG when φ = 0.2 to 1.5 vol.% relative to the respective base fluids. However, Jana et al. [33] demonstrated that DIW-based Cu, CNT and Au nanofluids had higher κ than DIW-based CNT-Cu and CNT-Au nanofluids. Jha et al. [34] reported that the κ of Cu-MWCNT suspended in DIW and EG was higher than that of EG- and DIW-based MWCNT nanofluids, which corroborated the results of Chopkar et al. [38] and was consistent with the work of Wei et al. [50].

2.3 NANOFLUID FORMULATION AND CHARACTERISATION TECHNIQUES

2.3.1 Nanofluid Formulation Methods

Monoparticle nanofluids and hybrid nanofluids were formulated through the suspension of NPs and HNPs respectively into conventional fluids, namely base fluids, of which their

stability is very important to the measurement of thermophysical properties and convective studies. Fundamentally, nanofluids and hybrid nanofluids are formulated using a one- and a two-step process. By this, the latter entails two processes, namely (i) synthesis of NPs or HNPs in the powdery form and (ii) suspension of NPs or HNPs into the base fluids. The most-reported process in the literature is the two-step process of nanofluids and hybrid nanofluids formulation, especially for metallic oxide and carbon nanotube NPs and HNPs. This is connected to the likelihood of large-scale production of nanofluids and hybrid nanofluids for industrial application and cost-effectiveness. The shortcoming of the two-step process relates to the sedimentation and agglomeration of NPs and HNPs due to the Van der Waals forces of attraction among the particles [51]. The one-step process consists of the simultaneous production of nanofluids and hybrid nanofluids by way of synthesis and suspension of NPs and NHPs in the base fluids. This technique offers the advantage of improved stability and homogeneity of nanofluids and hybrid nanofluids, and the elimination of laborious processes such as storing and drying compared with the single-step process by reducing NPs and HNPs agglomeration [6, 51]. Conversely, the industrial use of this method is not practicable except for fluids with low vapour pressure and it is also capital intensive [52]. Various techniques were reported in the literature for the one-step process [6, 53, 54].

2.3.2 Nanofluid Characterisation Techniques

Numerous techniques have been reported in the literature for the characterisation of nanofluids and hybrid nanofluids for their NP and HNP shapes, sizes, distribution, functional groups, crystalline structure, surface morphology, dispersion, elemental composition, saturation, magnetisation, etc. These techniques include Raman spectroscopy, Fourier transform infrared spectroscopy, high-resolution transmission electron microscopy, X-ray diffractometer, scanning electron microscopy, dynamic vibrating sample magnetometer, transmission electron microscopy, light scattering and energy-dispersive X-ray spectroscopy

[35, 36, 55–59]. The most-used technique for characterising nanofluids and hybrid nanofluids is transmission electron microscopy (TEM), followed by scanning electron microscopy (SEM) and X-ray diffractometer (XRD). The characterisation techniques mostly used are often engaged as a stand-alone technique or with other techniques for nanofluid and hybrid nanofluid characterisation. TEM is used to determine the size, shape and dispersion of NPs and HNPs in nanofluids and hybrid nanofluids, respectively, while SEM detects the surface morphology and elemental mapping. XRD is used to show the crystalline structure and grain size of NPs and HNPs contained in nanofluids and hybrid nanofluids, respectively.

2.4 NANOFLUID STABILITY IMPROVEMENT AND TESTS

2.4.1 Stability of Nanofluids

The suspension of NPs and HNPs in various base fluids introduces charges into the base fluids, which leads to the formation of an electrical double layer (EDL) around the particle surface [60]. Therefore, nanofluids and hybrid nanofluids are referred to as electrically conducting fluids. By applying a potential across, oppositely charged electrodes tend to attract the NPs or HNPs and EDL. EDL formation is strongly connected to volume fraction, size and surface charge of the particles and concentration of ions in the base fluids. Stability and even distribution of NPs or HNPs in the base fluids are vital in the application of nanofluids and hybrid nanofluids because nanofluid and hybrid nanofluid thermophysical (mostly thermal conductivity and viscosity) and optical properties, and efficiency are significantly related to the concentration of NPs or HNPs in the suspension [61, 62]. The enhancement of the stability of nanofluids and hybrid nanofluids to avoid agglomeration and sedimentation using the two-step process has led to the utilisation of four techniques, namely the mechanical (sonication), surfactant addition, surface modification and pH control techniques.

2.4.2 Techniques for Improving Nanofluid Stability

2.4.2.1 Sonication

Sonication is one of the techniques deployed for obtaining a homogeneous mixture of NPs or HNPs as they are suspended in selected base fluids to achieve stable nanofluids and hybrid nanofluids. Several studies demonstrated that sonication had an effect on κ_{eff}, absorbance wavelength, μ_{eff}, cluster size, surfactants, diameter of CNTs and particle size [55, 63–68]. The sonication time was investigated for durations of a few minutes to several hours. It can be concluded that an optimum sonication time (mainly due to the Brownian motion of NPs or HNPs) occurs where the parameter investigated either reduces (for μ_{eff} and κ_{eff}) or increases (for CNT diameter, particle and cluster size). An optimum sonication time ranging from 12 min [69] to 60 h [65] has been reported in the literature for different nanofluids and hybrid nanofluids studied. This reflects the necessity to optimise sonication time in relation to other parameters to achieve improved stability. However, this is mostly not the case for most of the studies on the formulation of nanofluids and hybrid nanofluids, except very limited studies which have optimised the sonication parameters [63, 64, 70].

2.4.2.2 Addition of Surfactants

Surfactants are complex chemical compounds that create an electrostatic repulsion to overcome magnetic attraction (for magnetic NPs) and the Van der Waals interaction between NPs or HNPs and avoid the sedimentation of NPs or HNPs in the base fluid [71]. The primary reason for using surfactants in monoparticle nanofluid or hybrid nanofluid formulation is to aid the stability of NPs or HNPs suspended in the base fluids [71]. Surfactants lower the interfacial tension between NPs or HNPs and base fluid to enhance the stability of nanofluids and hybrid nanofluids. The use of surfactants promotes the stability of nanofluids and hybrid nanofluids by increasing EDL between NPs or HNPs. Surfactants such as sodium dodecyl sulphate (SDS), sodium dodecyl benzene sulfonate (SDBS), gum Arabic, oleic acid, cetyl trimethyl ammonium bromide (CTAB), polyvinyl pyrolidone (PVP),

nanosperse AQ, dodecyl trimethyl ammonium bromide and hexa decetyl trimethyl ammonium bromide were utilised for the stability of nanofluids and hybrid nanofluids [53, 62, 72–76]. An increase in κ_{eff}, zeta potential, surface tension and μ_{eff} of nanofluids and hybrid nanofluids due to the use of surfactants has been reported in the literature [53, 61, 66, 70]. However, the effectiveness of surfactants at >60 °C was reported to reduce due to a weak bond between it and NPs or HNPs, which finally broke and led to sedimentation and thus instability of nanofluids and hybrid nanofluids [72]. Different surfactants have been used by various researchers to stabilise nanofluids and hybrid nanofluids formulated from diverse NPs and HNPs suspended in different base fluids [22, 55, 70, 76–79]. Therefore, it can be concluded that the stability of nanofluids and hybrid nanofluids based on the use of surfactants is dependent on the type and nature (magnetic or not) of NPs or HNPs, and the base fluid type (ionic or non-ionic).

2.4.2.3 Control of pH

The stability of nanofluids and hybrid nanofluids can be manipulated using pH. The suspension of NPs or HNPs into base fluid produces surface electric charges on the resultant nanofluid and hybrid nanofluid with the modification of the base fluid pH value. The surface electric charges affect the stability of nanofluid and hybrid nanofluid. Altering the pH value farther from the isoelectric point (IEP) enhances the nanofluid and hybrid nanofluid stability. The pH of nanofluid and hybrid nanofluid determines the IEP of the suspension, and this can be altered to sustain the stability through avoiding sedimentation and agglomeration. Additionally, the surface electric charge can be determined using zeta potential. Zeta potential measures the repulsion between NPs or HNPs and increases with a rise in the particles suspended into the base fluid [76, 80]. A high zeta potential (absolute value) indicates the stability of nanofluids and hybrid nanofluids due to a strong electrostatic repulsion between NPs or HNPs, while low zeta potential shows instability due to the weak

electrostatic repulsion of particles. With a zeta potential value of >60 mV, a very stable nanofluid is formulated, a value of >30 mV implies a stable nanofluid, whereas <20 mV indicates weakness in nanofluid stability [54, 61, 76]. Zawrah et al. [76] reported the modification of pH of Al_2O_3/water nanofluid (with a surfactant of SDBS) from 5 to 10 using NaOH because the IEP of the nanofluid was around 6.3. Similar pH alterations to attain stable nanofluids and hybrid nanofluids were carried out in other studies [15, 63, 66, 81, 82].

2.4.2.4 Functionalisation of Nanoparticles

The surface modification or functionalisation of NPs or HNPs is another technique employed to improve the stability of nanofluids and hybrid nanofluids. This method of enhancing the stability of nanofluids and hybrid nanofluids is surfactant-free. Although this technique has been discussed in a few studies, compared with others with and without the use of surfactants, it is a promising method for the formulation of more stable nanofluids and hydrid nanofluids [62, 65, 83]. Owing to the importance of the stability of nanofluids and hybrid nanofluids, the measurement of this parameter is key to the further use of nanofluids and hybrid nanofluids in terms of the thermophysical property measurements and convective heat transfer studies.

2.4.3 Stability Test Methods

2.4.3.1 Visual Inspection

The simplest method to check the stability of nanofluids and hybrid nanofluids is by visual inspection. In other words, it is a visual observation of the nanofluid and hybrid nanofluid samples on daily or weekly or monthly intervals to see how the NPs or HNPs sediment with time. This is not a scientific method of checking the stability of nanofluids and hybrid nanofluids, as reported in the literature [62, 64, 84, 85]. However, this method is always used in addition to other stability monitoring techniques that are scientific in nature [62, 64, 70, 84, 85].

2.4.3.2 Zeta Potential

Zeta potential is a method used to determine the stability of nanofluids and hybrid nanofluids. As earlier stated, the zeta potential of nanofluids and hybrid nanofluids is strongly connected to the repulsive force between the NPs or HNPs. This technique is one of the techniques most used to measure the stability of nanofluids and hybrid nanofluids, as reported in the literature by several authors [37, 56, 57, 76, 82]. The degree of stability of nanofluids and hybrid nanofluids can be determined using this method based on the obtained zeta potential values. It is worth mentioning that this stability-checking technique is often used along with others.

2.4.3.3 Ultraviolet Visible Spectrophotometer

This method appears to be the most used of all the techniques employed in the monitoring of the stability of nanofluids and hybrid nanofluids. Either the transmittance or absorbance of the nanofluids and hybrid nanofluids at the determined peak wavelength can be used as an indicator to monitor the stability of nanofluids and hybrid nanofluids [63, 68, 70, 86–88]. One notable advantage of this technique is the ability to monitor stability constantly at regular time intervals over a period of time spanning weeks and months [89], which other methods cannot offer. Thus it provides an instantaneous measurement of the stability of nanofluids and hybrid nanofluids. Similar to other techniques, it is always used along with other methods such as visual inspection and zeta potential.

2.4.3.4 Viscosity and Thermal Conductivity Check

The stability of nanofluids and hybrid nanofluids is also monitored by measuring their thermophysical properties over a period of time. Garbadeen et al. [22] and Joubert et al. [88] monitored the stability of MWCNT/DIW and Fe_2O_3/DIW nanofluids for 250 min and 20 h respectively by measuring μ_{eff}. Likewise in other studies, Yu et al. [90] and Ijam et al. [86] monitored the stability of Fe_3O_4/keresene and GO/DIW-EG (60:40) nanofluids by measuring their κ_{eff} for 360 min and 7 days respectively. The use of κ_{eff} to monitor the stability of nanofluids was corroborated by the work of Wang et al. [66], which reported a strong

relationship between κ_{eff} and the stability of nanofluids (Al_2O_3/W and Cu/W). The literature on monitoring nanofluid stability showed that two or more of these reported techniques were used for stability check of nanofluids and hybrid nanofluids.

2.5 THERMOPHYSICAL PROPERTIES OF NANOFLUID

2.5.1 Thermal Conductivity

The public domain is inundated with publications on κ_{eff} of different nanofluids. Since hybrid nanofluids are emerging advanced fluids, a few works have been published on the thermal property, κ_{eff}. The various mechanisms (static and dynamics) proposed to be responsible for the uncharacteristic enhancement of κ_{eff} due to the suspension of NPs in various base fluids were extensively reviewed by Aybar et al. [12]. The static mechanisms assumed NPs to be stationary in nanofluids and these include interface thermal resistance, nanolayering, fractal geometry, aggregation and percolation, while the dynamic mechanisms presumed random motion of NPs in nanofluids such as Brownian motion and nano-scale convection.

Masuda and co-workers [7] were the first to measure the κ_{eff} of nanofluids and reported 30% enhancement of κ of water by suspending alumina NPs (13 nm) in water at φ = 4.3 vol.%. Choi and Eastman [10] showed a 3.5-fold enhancement of κ_{eff} for water-based Cu nanofluid at φ = 20 vol.%. The results stating that κ_{eff} was enhanced through the suspension of NPs into base fluids were also supported by some other studies conducted thereafter [8, 9, 16, 91]. Recently, the κ_{eff} of nanofluids and hybrid nanofluids as a function of temperature and φ has been widely reported. Several studies revealed that the κ_{eff} of nanofluids and hybrid nanofluids was enhanced with an increase in temperature and φ [44, 66, 96, 73, 82, 89, 90, 92–95]. Wang et al. [66] reported that the κ_{eff} of Al_2O_3/DIW and Cu/DIW nanofluids was enhanced by 15% and 18% for weight fraction of 0.8% at room temperature. Furthermore, Agarwal et al. [94] showed 30% and 31% enhancements of κ_{eff} for DW- and EG-based Al_2O_3 nanofluids when φ = 2.0 vol.% and temperature of 70 °C. Using Fe_2O_3/EG and Fe_3O_4/EG

nanofluids, Pastoriza-Gallego et al. [69] published κ_{eff} enhancements of 2% to 15% and 1% to 11% respectively at φ = 0.011 to 0.069 vol.% and 10 to 50 °C.

Hybrid nanofluids was proposed as a passive method for improving the thermal propeties of nanofluids. Some studies were carried out on the κ_{eff} of hybrid nanofluids using two different NPs suspended in various base fluids [35, 50, 59, 73, 79, 97–100]. Chen et al. [73] and Askari et al. [59] reported κ_{eff} enhancements of 27.75% (0.05 vol.% MWCNT and 0.02 vol.% Fe_2O_3 at room temperature) and 14% to 32% (0.1 – 1.0 wt.% at 20 – 40 °C) for MWCNT-Fe_2O_3/W and Fe_3O_4-G (20:80)/DIW nanofluids respectively. Also, Kakavandi et al. [58] and Asadi et al. [99] showed maximum κ_{eff} enhancements of 33.0% (0.05 – 0.75 vol.% and 25 – 50 °C) and 45.0% (0.125 – 1.5 vol.% and 25 – 50 °C) for MWCNT-SiC (50:50)/W-EG and Al_2O_3-MWCNT/TO nanofluids respectively. Additionally, Sundar et al. [35] published 17.8%, 13.4%, 13.6% and 14.6% enhancements for the κ_{eff} of DW, 20 DIW:80 EG, 40 DW:60 EG and 60 DW:40 EG-based ND-Fe_3O_4 (72:28) nanofluids respectively.

Furthermore, the κ_{eff} of green nanofluids (GNFs), palm kernel fibre and mango bark, was observed to enhance as temperature and φ increased with the palm kernel fibre nanofluid having an enhancement of 16.1% (60 °C and 0.5 vol.%) in comparison with EG-DIW (50:50) [41, 101]. Yarmand et al. [102] reported the κ_{eff} of hybrid nanofluid (0.02 – 0.6 wt.% and 20 – 40 °C) formulated using synthesised NPs of fruit bunch and GO NPs suspended in EG. They recorded a maximum enhancement of 6.47% at 0.06 wt.% and 40 °C. Khdher et al. [48] also determined the κ_{eff} of Al_2O_3 NPs suspended in green base fluid (bioglycol), EG and PG and found enhancements of 17%, 9% and 3.6% (1.0 vol.% and 30 °C) respectively. These studies signal the potential of green nanofluids and hybrid nanofluids in the near future. As an active technique for enhancing the thermophysical properties of magnetic nanofluids (magnetic types), an analysis of the influence of a magnetic stimulus on the κ_{eff} of magnetic nanofluids has been conducted by a few authors, such as pioneers Xuan and co-workers [42,

103–106]. Similarly, Shahsavar et al. [107] showed that exposing Fe_3O_4-CNT (1:2,1:1,2:1)/W nanofluid to a magnetic stimulus enhanced the κ_{eff} of Fe_3O_4-CNT (1:2)/W nanofluid by 152.95% (at 35 °C and 480 mT) as against 45.41% enhancement without exposure to a magnetic stimulus. Azizian et al. [103] showed that the exposure of TiO_2/DIW and Fe_3O_4/DIW nanofluids to a magnetic field strength of 32 mT only enhanced Fe_3O_4/DIW nanofluid (by 169%) because TiO_2/DIW nanofluid was not magnetic. For both magnetic nanofluid and hybrid nanofluid, it was reported that the presence of a magnetic stimulus enhanced κ_{eff} and an increase in the magnetic field strength was noticed to increase κ_{eff} further. An optimum could be reached in κ_{eff} enhancement depending on the strength of the magnetic stimulus, φ, type and nature of NPs, base fluid and temperature studied.

It is worth noting that the correlations developed for the κ_{eff} of nanofluids could not be used to predict the κ_{eff} of hybrid nanofluids due to the former underestimating the latter [55, 68, 84, 108–110] and because hybrid nanofluids yielded higher κ_{eff} than nanofluids (formulated using the base NPs) [37, 38, 50, 58, 71]. The thermal properties of different hybrid nanofluids are presented in Table 2.1.

2.5.2 Viscosity

Studies showed that the κ_{eff} of nanofluids were found to be relatively lower than that of μ_{eff}. This property measured the flow of nanofluid due to internal resistance. The suspension of NPs and HNPs into base fluids led to an increase in μ_{eff}. The increment in μ_{eff} accompanied a corresponding increase in κ_{eff} (as φ increased) through enhanced heat transfer of nanofluid for engineering applications but at a penalty of high pumping power. Therefore, the phenomenon described is seen as a possible flaw in using nanofluids as thermal transport media. It is important to note that at high φ, high μ_{eff} overrides the benefit of high κ_{eff} and hence leads to deterioration instead of augmentation of heat transfer when nanofluid is used

Table 2.1: Thermophysical properties of hybrid nanofluids.

Author	HNPs (ratio)	Base fluid	Properties	Temp.	φ (vol. %)	Enhancement (%)	Surfactant
Chopkar et al. [38]	Al_2Cu, Ag_2Al (Al=70%; Cu & Ag=30%)	EG & DIW	κ	Room temp.	0.2 – 1.5	50 – 150%	Oleic acid
Jha et al. [34]	Cu/MWCNT & MWCNT	EG & DIW	κ	26.5 – 48.9	0.6 – 4.0	14.8 – 210 (DIW) 3.6 – 20.2 (EG)	Functionalised
Jana et al. [33]	Au, CNT, Cu, CNT-Cu & CNT-Au (1.5-2.5)	DIW	κ	Room temp	0.3 & 0.5 (CNT) 1.4 (Au) & 0.05-0.3 (Cu)	74 (Cu)	Laurate salt
Sundar et al. [35]	ND-Fe_3O_4 (72%:28%)	DW & DW-EG mixtures	κ, μ, & σ	20 – 60	0.05 – 0.2	13.4 – 17.8 (κ) 1.5X – 2.19X (μ)	-
Sundar et al. [95]	ND-Co_3O_4 (67%:33%)	DW & DW-EG mixtures	κ & μ	20 – 60	0.05 – 0.5 wt.%	9.0 – 16.0 (κ) 1.15X – 1.11X (μ)	-
Baby and Ramaprabhu [83]	f-MWCNT-f-HEG (50:50 wt.%)	DIW & EG	κ	25 – 50	0.5 – 5.0	20 (DIW); 3 (EG)	-
Baby and Sundara [111]	CuO-f-HEG (20:80 wt.%)	DIW & EG	κ & σ	25 – 50	0.5 – 5.0	90 (DIW); 23 (EG)	-
Kannaiyan et al. [112]	Al_2O_3-CuO	DIW-EG (80:20)	ρ, μ, & ρ	20 – 60	0.05 – 0.2	45	-
Harandi et al. [109]	f-MWCNT- Fe_3O_4 (50:50)	EG	κ	25 – 50	0.1 – 2.3	30	-
Esfe et al. [75]	Ag-MgO (50:50)	DW	κ & μ	Room temp	0 – 2	-	CTAB
Mousavi et al. [55]	CuO-MgO-TiO_2 (5 diff. ratios)	DW	κ, μ, ρ, C_p & surface tension	15 – 60	0.1 – 0.5	-	SDS
Abbasi et al. [114]	MWCNT-Al_2O_3 (1:1)	DIW	κ	Room temp	0.1	20.68	GA
Sundar et al. [96]	CNT-Fe_3O_4 (26:74)	DW	κ & μ	20 – 60	0.1 & 0.3	28.46 (κ); 1.5X (μ)	Nanosperse AQ
Zadkhast et al. [115]	MWCNT-CuO (50:50)	DIW	κ	25 – 50	0.05 – 0.6	30.38	-
Wei et al. [50]	SiC-TiO_2 (50:50 wt.%)	Diathermic oil	κ & μ	17 – 43	0.1 – 1.0	8.39 (κ)	Oleic acid
Esfe et al. [116]	MWCNT-TiO_2 (10:90 & 55:45)	EO	μ	15 – 55	0.25 – 1.0	-	-
Akilu et al. [37]	SiO_2-CuO/C (80:20 wt.%)	GL-EG (60:40 wt.%)	C_p, κ, & μ	30 – 80	0.5 – 2.0	1.15X (μ); 21.1 (C_p); 26.9 (κ)	-
Hamid et al. [117]	TiO_2-SiO_2 (40:60 vol.%)	EG	κ	30 – 70	0.5 – 3.0	21	-
Hussien et al. [122]	MWCNT-G	DW	μ	27 – 57	0.075 – 0.25 wt.%	2.8 – 10.3	PVP (1:1)

Author	HNPs (ratio)	Base fluid	Properties	Temp.	φ (vol. %)	Enhancement (%)	Surfactant
Kakavandi and Akbari [58]	MWCNT-SiC (50:50 wt.%)	W-EG (50:50 vol.%)	κ	25 – 50	0.05 – 0.75	33	-
Sundar et al. [118]	GO-Co_3O_4 (67:33 wt.%)	EG & DW	κ & μ	20 – 60	0.05 – 0.2	EG (μ=1.42X & κ=11.85) & DW (μ=1.70X & κ=19.14)	-
Qing et al. [97]	SiO_2-G	Naphthenic mineral oil	κ, μ, & σ	20 – 100	0.01 – 0.08 wt.%	κ (80 (HNF) & 29 (NF)); μ (29.7 (HNF) & 12.87 (NF); σ (557-97)	-
Bahrami et al. [119]	Fe-CuO (50:50 wt.%)	W-EG (20:80 vol.%)	μ	25 – 50	0.05 – 1.5	57 – 70	-
Suresh et al. [82]	Al_2O_3-Cu (90:10 wt.%)	DIW	κ & μ	Room temp	0.1 – 2.0	1.47 – 12.11 (κ); 8 – 115 (μ)	SLS
Eshgarf et al. [120]	MWCNT-SiO_2 (50:50 vol.%)	EG-W (50:50 vol.%)	μ	27.5 – 50	0.0625 – 2.0	20,000	Functionalised
Esfe et al. [110]	DWCNT-ZnO (10:90)	EG	κ	30 – 50	0.045 – 1.90	24.9	-
Esfe et al. [121]	SWCNT-MgO (20:80)	EG	κ	30 – 50	0.05 – 2.0	32	-
Parsian and Akbari [98]	Al_2O_3-Cu (50:50)	EG	κ	25 – 50	0.125 – 2.0	24 – 28	-
Afrand et al. [123]	SiO_2-MWCNT (50:50 vol.%)	EO	μ	25 – 60	0.0625 – 1.0	27.6 – 37.4	-
Nadooshan et al. [100]	Fe_3O_4-MWCNT (50:50)	EG	μ	25 – 45	0.1 – 1.8	-	-
Esfahani et al. [124]	ZnO-Ag (50:50)	W	κ	25 – 50	0.125 – 2.0	-	Surfactant
Asadi et al. [99]	Al_2O_3-MWNCT	Thermal oil	κ & μ	25 – 50	0.125 – 1.5	45 (κ) & 81 (μ)	-
Rostamian et al. [125]	CuO-SWCNT (50:50 vol.%)	EG-W (40:60)	κ	20 – 50	0.02 – 0.75	36.2	-
Afrand et al. [126]	Fe_3O_4-Ag (50:50 vol.%)	EG	μ	25 – 50	0.0375 – 1.2	-	-
Sundar et al. [79]	ND-Ni (85:15 wt.%)	DW	κ & μ	30 & 60	0.1 & 0.3	16.65 & 23.24 (μ); 10.23 & 29.39 (κ)	Nanosperse AQ
Sundar et al. [127]	MWCNT-Fe3O4 (26:74 wt.%)	DW	κ & μ	20 – 60	0.1 & 0.3	1.27X & 1.5X (μ); 13.88 & 28.46 (κ)	Nanosperse AQ
Esfe et al. [128]	CNT-Al_2O_3	W	κ	30 – 60	0.02 – 1.0	-	-
Kumar et al. [129]	Cu-Zn (50:50)	EO, VO, paraffin	μ, κ & FP	30	0.1 – 0.5	Cu-Zn/VO (best)	SDS

Author	HNPs (ratio)	Base fluid	Properties	Temp.	φ (vol. %)	Enhancement (%)	Surfactant
Alirezaie et al. [62]	MWCNT-MgO (10:90)	EO	μ	25 – 50	0.0625 – 1.0	-	GA
Esfe and Sarlak [130]	CuO-MWCNT (85:15)	EO	μ	5 – 55	0.05 – 1.0	43.52	-
Menbari et al. [63]	CuO-Al_2O_3	DW	μ	20 – 21 (room temp)	0.001 – 0.06	-	SHMP
Esfe and Arani [131]	MWCNT-SiO_2 (40:60)	EO	μ	5 – 55	0.05 – 1.0	25	-
Ebrahimi and Saghravani [71]	Fe_3O_4-CuO	DIW	κ	25 – 50	3 – 7	-	TMAH
Sundar et al. [36]	ND-Ni (84:16 wt.%)	DW & EG	σ	24 – 65	0.02 – 0.1	199.52 – 200.23 (EG); 1339.81 – 853.13 (κ)	-
Zawawi et al. [84]	Al_2O_3-SiO_2; Al_2O_3-TiO_2; TiO_2-SiO_2	PAG	μ	30 – 80	0.02 – 1.0	μ=20.50 (Al_2O_3-TiO_2/PAG); κ=2.41 (Al_2O_3-SiO_2) at 30 °C.	-
Hamid et al. [132]	TiO_2-SiO_2 (20:80 vol.%)	W-EG (60:40 vol.%)	κ & μ	30	0.5 – 3.0	4.4 – 19.9 (κ); 10.7 – 26.1 (μ)	-
Askari et al. [59]	Fe_3O_4-G	DIW	μ, κ, & ρ	20 – 40	0.1 – 1.0	14 – 32	-
Naddaf et al. [74]	G-MWCNT (1:1)	Diesel oil	σ & κ	5 – 100	0.05 – 0.5 wt.%	-	Oleic acid and HA
Chen et al. [73]	MWCNT-Fe_2O_3 (0.05:0.02 wt.%)	W	κ	Room temp	MW-0.05 wt.%; Fe_2O_3-0.01 – 0.16 wt.%	27.75	NaDDBS
Nabil et al. [52]	TiO_2-SiO_2 (50:50 vol.%)	DW-EG (60:40 vol.%)	κ & μ	30 – 80	0.5 – 3.0	22.8 (κ); 62.6 (μ)	-
Shahsavar et al. [107]	Fe_3O_4-CNT (1:2; 1:1; 2:1)	W	κ & μ	25 – 35	-	45.41 (no magnet); 152.95 (magnet)	TMAH (Fe_3O_4) & GA (CNT)
Aparna et al. [68]	Al_2O_3-Ag (50:50; 30:70; 70:30)	DW	κ	25 – 52	0.005 – 0.1	23.82	PVP

as a coolant in thermal equipment. However, at low φ, which indicates low μ_{eff}, nanofluid is highly beneficial as a heat transfer fluid.

Several studies determined the μ_{eff} of nanofluids using various NPs and base fluids [15, 18, 49, 56, 57, 60, 93, 133–135]. This property of nanofluids is reportedly dependent on several parameters such as φ, temperature, pH, NP size and shape, sonication time and intensity [11]. The emergence of hybrid nanofluids has also led to the measurement of their μ_{eff} [37, 50, 55, 59, 75, 79, 96, 100]. For both nanofluids and hybrid nanofluids it was generally observed that temperature rise caused μ_{eff} to reduce, while an increment in φ resulted in the augmentation of μ_{eff}. Additionally, studies showed that hybrid nanofluids had lower or higher μ_{eff} than nanofluids formulated from the base NPs (depending on the density of the doped NPs), because of the synergetic benefit of NP hybridisation [37, 50, 82, 97]. For example, Akilu et al. [37] reported that the μ_{eff} of SiO_2-CuO/C (80:20)/G-EG (60:40) nanofluid was lower than that of SiO_2/G-EG (60:40) nanofluid, which was formulated from SiO_2 as the base NPs. In contrast, Qing et al. [97] published μ_{eff} enhancements of 29.7% and 12.87% for SiO_2-G/TO and G/TO nanofluids respectively, showing that hybrid nanofluid had a higher μ_{eff} than that of monoparticle nanofluid. This finding supported the work of Suresh et al. [82] by revealing that hybrid nanofluid (Al_2O_3-Cu (90:10)/DIW) had a higher μ_{eff} than nanofluid (Al_2O_3/DIW). The differences in the densities of the base and doped NPs could be strongly related to this observation.

Sharifpur et al. [101], Adewumi et al. [136] and Kallamu et al. [137] reported the μ_{eff} of GNFs formulated by suspending synthesised NPs of mango bark, coconut fibre carbon and banana fibre into DIW, EG-DIW (60:40) and DIW respectively. They showed that the μ_{eff} of GNFs followed the same pattern as those of nanofluids under increasing temperature and φ. Adewumi et al. [136] and Kallamu et al. [137] reported μ_{eff} augmentation of 50% (1 wt.% and 60 °C) and 22% (60 °C and 1.5 vol.%) for the coconut fibre carbon and banana fibre

nanofluids in comparison with EG-DIW and DIW respectively. Furthermore, Yarmand et al. [102] were the first to formulate and measure the μ_{eff} of hybrid green-metallic nanofluid, which was prepared by suspending synthesised NPs of fruit bunch and GO NPs into EG. They reported maximum μ_{eff} enhancement of 4.16% (0.06 wt.% and 40 °C) relative to EG.

The impact of magnetic stimulus as an active method of manipulating the μ_{eff} of magnetic nanofluids and MHNFs has been studied [107, 138–142]. Amani et al. [138] studied the effect of a magnetic stimulus (100 – 400 G) on the μ_{eff} of $MnFe_2O_4$/DIW nanofluid (0.25 – 3.0 vol.%) at 20 to 60 °C. They observed that μ_{eff} was augmented with an increasing magnetic field strength with a maximum enhancement of 1.38-fold for 3.0 vol.% at 60 °C, relative to no magnetic presence condition. Malekzadeh et al. [142] measured the μ_{eff} of Fe_3O_4/DIW nanofluid (φ = 0.1 – 1.0 vol.%) under a magnetic stimulus range of 130 to 550 G and at 20 to 45 °C. They found that the μ_{eff} was enhanced by 20% to 175% at 550 G for the φ and temperature studied. Using hybrid nanofluid, Shahsavar et al. [107] investigated the influence of magnetic stimuli (120 – 480 mT) and temperature 25 to 35 °C on the μ_{eff} of Fe_3O_4-CNT (1:2,1:1,2:1)/W nanofluids. The results showed that the μ_{eff} enhanced with an increase in magnetic field strength and detracted with a rise in temperature with Fe_3O_4-CNT (1:2)/W nanofluid, yielding the maximum μ_{eff} values.

2.5.3 Density

The ρ_{eff} of nanofluids is a key property that directly relates to *Nu*, *Re*, *Ra*, friction factor and pressure drop in convective heat transfer. As one of the thermal properties of nanofluids, this property has seldom been studied. However, a few studies reported the ρ_{eff} of nanofluids, rarely as a stand-alone property [13] but mainly together with other thermal properties [18, 43, 69, 86, 143]. Some studies reported enhancement of ρ_{eff} with an increase in φ [13, 18, 60, 86, 143] and others reported a reduction with a rise in temperature [13, 43, 86, 143]. The observed augmentation of ρ_{eff} was due to nanofluids having a higher ρ_{eff} than base fluids as φ

increased. Shoghl et al. [60] reported that ρ_{eff} was enhanced for W-based MWCNT, Al_2O_3, MgO, ZnO, TiO_2 and CuO nanofluids as φ increased from 0.01 to 2.0 wt.% and reduced as temperature increased 30 to 40 °C. A similar observation was published by Sharifpur et al. [13], who studied the influence of φ = 1.0 to 6.0 vol.% and 10 to 40 °C on the ρ_{eff} of SiO_2-W, MgO-GL, SiO_x-EG/W (60%:40%) and CuO-GL nanofluids. In addition, Ijam et al. [86] studied the ρ_{eff} of GONs-DIW/EG (60:40) nanofluid for φ = 0.01 to 0.10 wt.% at a temperature range of 25 to 45 °C and recorded 1.134 to 1.000% reduction in ρ_{eff} (at 0.10 wt.% and temperatures of 25 – 45 °C) relative to the base fluid.

Furthermore, Yarmand et al. [102] for the first time measured the ρ_{eff} of EG-based hybrid green-metallic nanofluid and reported a maximum enhancement of 0.09% at 20 °C when φ = 0.06 wt.%. Studies on the ρ_{eff} of hybrid nanofluids are very limited in the public domain as only Askari et al. (Fe_3O_4-G/DIW nanofluid) [59] and Mousavi et al. (CuO-MgO-TiO_2/DW nanofluid) [55] have published in this regard. Yarmand et al. [102], Askari et al. [59] and Mousavi et al. [55] reported identical trends as generally observed for the influence of φ and temperature on the ρ_{eff} of nanofluids. Again, they showed that the measured ρ_{eff} values for EG-based hybrid green-metallic nanofluid and hybrid nanofluids agreed well with those estimated using an empirical (density mixture) model. Mousavi and co-workers [55] recorded ρ_{eff} reduction of 1.32% to 2.08% at φ = 0.5 vol.% and 55 ° C, in relation to DW, for the five different hybrid nanofluids studied. Additionally, there is a dearth of information on the effect of magnetic stimulus on the ρ_{eff} as a function of temperature and φ in the open literature.

2.5.4 Specific Heat Capacity

Another significant thermophysical property of nanofluid is $C_{p\text{-}eff}$. It is critical for enthalpy, energy and exergy analysis. Limited studies have been published on the $C_{p\text{-}eff}$ determination of nanofluids relating to φ and temperature increment in comparison with that of μ_{eff} and κ_{eff}.

The $C_{p\text{-}eff}$ of nanofluids is primarily reported along with other thermophysical properties such as μ_{eff} and κ_{eff}. Basically, $C_{p\text{-}eff}$ is measured under two categories, namely low temperature and high temperature, which depend mainly on the base fluid used in the formulation of nanofluids [144]. For the low-temperature category, conventional base fluids such as DW, EG-DIW, W, EG, DIW, thermal oil, TO, PG, EO and ionic liquids are utilised for suspending NPs, while molten nanosalts are used as base fluids for the high-temperature category. Obviously, the measured $C_{p\text{-}eff}$ values are different from the values of these two types of base fluids, which are also a function of temperature, φ and NP size.

In the open literature, authors have reported disparity in their findings concerning the influence of temperature and φ on the $C_{p\text{-}eff}$ property of nanofluids. Vajjha and Das [145] studied the $C_{p\text{-}eff}$ of three nanofluids (EG-DW (60:40) based Al_2O_3, ZnO and SiO_2) under increasing temperature (42 – 90 °C) and φ (2 – 10 vol.%). A rise in temperature enhanced $C_{p\text{-}eff}$ but an increase in φ caused it to reduce. Also, the $C_{p\text{-}eff}$ of nanofluids was observed to be lower than that of the base fluid. Wang et al. [146] determined the $C_{p\text{-}eff}$ of ionic fluid-based G and MWCNT nanofluids at φ = 0.03 to 0.06 wt.% and 20 to 85 °C. A rise in the temperature enhanced $C_{p\text{-}eff}$, while an increase in φ reduced it with $C_{p\text{-}eff}$ lower than C_p of the ionic base fluid. A similar trend to the one observed by Vajjha and Das [145] and Wang et al. [146] was also reported by Said [61] and Ijam et al. [86]. However, Ijam et al. [86] showed that $C_{p\text{-}eff}$ enhanced for φ < 0.05 wt.% by 3.59% to 5.28% with temperature rise when GO/DW-EG nanofluid was studied at temperatures of 25 to 60 °C and φ of 0.01 to 0.1 wt.%. In constrast to the above studies, Chandran et al. [147] reported that the $C_{p\text{-}eff}$ of ZnO/PG (1.0 – 2.0 vol.%)-PW/W (4.0 – 16.0 wt.%) nanofluid (30 – 60 °C) deteriorated with an increase in temperature but augmented (5.1%) with φ increase.

A complete difference in results was published by Oster et al. [43] on $C_{p\text{-}eff}$ measurements of ionic nanofluids (with four different NPs) as a function of temperature (25 – 90 °C) and φ

(0.5 – 3.0 wt%). They noticed the augmentation of $C_{p\text{-}eff}$ with an increase in both temperature and φ. Nieto De Castro et al. [148] determined the $C_{p\text{-}eff}$ of ionic nanofluid (MWCNT) at φ = 1.0 to 1.5 wt% and 60 to 110 °C. The results showed that temperature increase significantly enhanced $C_{p\text{-}eff}$, whereas a slight augmentation was observed for $C_{p\text{-}eff}$ as φ was increased. Also, the $C_{p\text{-}eff}$ of ionic nanofluid was noticed to be higher than that of the ionic base fluid. With the use of hybrid green-metallic nanofluid, Yarmand et al. [102] reported enhancement of $C_{p\text{-}eff}$ as both temperature and φ increased. At 50 °C, $C_{p\text{-}eff}$ was augmented by 2.25% for φ = 0.06 wt%. However, the work of Mousavi et al. [55] in which the $C_{p\text{-}eff}$ of hybrid nanofluids (CuO-MgO-TiO_2/DW) was measured for the first time differs from the results of Oster et al. [43], Nieto De Castro et al. [148] and Yarmand et al. [102] but agrees with the results of Vajjha and Das [145] and Wang et al. [146] They reported reduction by 1.68% to 2.13% for the hybrid nanofluids studied at temperatures of 15 to 60 °C and φ = 0.1 to 0.5 vol.%.

2.5.5 Electrical Conductivity

The suspension of NPs and HNPs into base fluids creates electric charges, thus making the formulated nanofluids and hybrid nanofluids electrically conducting fluids. The measure of the capability of nanofluids and hybrid nanofluids to conduct electric charges is σ_{eff}. This property is directly and strongly related to electrostatic characteristics (IEP, EDL and zeta potential), φ, NP size, nanosheets φ, and nanosheets charge and stability of nanofluids and hybrid nanofluids [15, 76, 93]. The σ_{eff} of nanofluids and hybrid nanofluids is primarily found in the literature [15, 35, 76, 81, 97] studied along with other thermophysical properties such as κ_{eff} and μ_{eff}, except for a few studies [36, 93].

Numerous studies have been conducted on the effect of temperature and φ on the σ_{eff} of nanofluids and hybrid nanofluids [15, 36, 143, 44, 48, 60, 74, 81, 89, 93, 97]. Adio et al. [81] measured the σ_{eff} of MgO/EG nanofluid as a function of temperature (20 – 70 °C), NP size (20 nm and 100 nm) and φ (0.5 – 3.0 vol.%). They showed that an increase in temperature,

NP size and φ enhanced σ_{eff} with a maximum enhancement of 6 000%. Shoghl et al. [60] examined the σ_{eff} of water-based nanofluids of MgO, ZnO, CNT, Al_2O_3 and CuO at 27 °C and observed that the enhancement of this property depended on an increase in φ and types of NPs. ZnO/W nanofluid yielded maximum σ_{eff} at low φ and CNT/W nanofluid gave the highest σ_{eff} at high φ. Guo et al. [44] reported that the σ_{eff} of SiO_2/EG-W (0 – 100 vol.%) nanofluids for 0.3 wt.% and at 25 to 45 °C was augmented with an increase in temperature and reduction in EG content of base fluid. Using Fe_3O_4/EG nanofluid (at φ = 0.05 – 2.0 wt.% and 25 – 45 °C), Jamilpanah et al. [93] found that σ_{eff} was augmented as temperature and φ increased with 6 202% enhancement at 25 °C for 2.0 wt.%. The observation that increasing temperature and φ enhanced σ_{eff} is corroborated by the works of Naddaf et al. [74] and Adio et al. [15], which engaged hybrid nanofluid and monoparticle nanofluid respectively. Yarmand et al. [102] measured the σ_{eff} hybrid green-metallic nanofluid and noticed enhancement with an increase in both temperature and φ with the highest augmentation of 787.5% achieved for 0.06 wt.% at 45 °C. The results agree with the works of Jamilpanah et al. [93], Naddaf et al. [74] and Adio et al. [15].

However, in studying the σ_{eff} of GO/DW nanofluid in relation to temperature (25 – 60 °C) and φ (0.01 – 0.6 vol.%) temperature, Hadadian et al. [89] noticed that σ_{eff} was enhanced with increasing φ but it declined with increasing temperature. Enhancements of 25,678% and 8,789% were reported for 0.06 vol.% at 25 °C and 60 °C respectively. Khdher et al. [48] determined the σ_{eff} of bioglycol-based Al_2O_3 nanofluid (for φ = 0.1 – 1.0 vol.% and 30 – 80 °C) and reported an enhancement with a rise in temperature and a reduction with an increase in φ. Maximum augmentation of 5 112% was achieved for 0.1 vol.% at 80 °C. Similar results were published by Sundar et al. [36] when the σ_{eff} of hybrid nanofluid (ND-Ni/DW) was investigated for φ = 0.02 to 0.1 vol.% at 24 to 65 °C with maximum enhancements of 1 339.81% (24 °C) and 853.15% (65 °C) respectively for 0.1 vol.%. At room temperature,

Qing et al. [97] reported σ_{eff} enhancements of 557% and 97% for nanofluid and hybrid nanofluid of SiO_2-G/TO and G/TO respectively for φ = 0.01 – 0.80 wt.%. The introduction of the doped NPs of G to the based NPs of SiO_2 to formulate SiO_2-G/TO nanofluid was observed to reduce σ_{eff} of G/TO nanofluid. Additionally, the effects of percolation [60, 143] and counterion condensation on the σ_{eff} of nanofluids were reported [15].

2.5.6 Other Properties

Apart from the thermophysical properties of nanofluids discussed above, there are reports on the measurements of other properties such as flash point [143], contact angle [149], volumetric heat capacity [43], breakdown voltage [143], surface tension [150], extinction coefficient and transmittance [61] and shear stress [150]. So far with hybrid nanofluids, flash point [129] and surface tension [55] are the other measured thermophysical properties found in the open literature.

2.6 THERMO- AND THERMOMAGNETIC CONVECTION OF NANOFLUIDS IN CAVITIES

Natural convection or thermo-convection is a method of heat transfer that is extensively deployed in various areas of application where thermal transport primarily depends on the difference in density of the thermal fluid used. Thermo-convection has been applied to the industry, power generation, nuclear energy, telecommunication, solar energy collectors, aviation, agriculture, geophysics, electronics cooling, etc. For over two decades, nanofluids have been extensively researched and established to possess improved thermal properties compared with those of conventional fluids. Therefore, nanofluids have been studied for their thermo- and thermomagnetic convection in cavities with different shapes [19, 151–154].

Regarding thermo- and thermomagnetic convection of nanofluids, there are considerably more studies on numerical techniques than on experimental methods [26]. In addition, square cavity has been researched more than any other type of cavity and the most investigated thermal boundary condition is the differential heating of the vertical walls with thermal

insulation of the horizontal walls [155, 156]. Furthermore, Al_2O_3 and MWCNT nanofluids were observed to be mostly researched in thermo- and thermomagnetic convection studies [157]. Putra et al. [19] were the first to experimentally investigate the thermo-convection of nanofluids in a cavity. Apart from the use of nanofluids to enhance thermo- and thermomagnetic convection heat transfer, some passive and active methods were deployed experimentally and these include base fluid, cavity inclination, AR, hybrid nanofluid, porous cavity, magnetic stimulus and green nanofluid. Tables 2.2 to 2.4 present the thermo-convection studies carried out for monoparticle nanofluids, green nanofluid and hybrid nanofluid in various types of cavities (square, rectangle, cylinder and triangle). The correlations developed from experimental data of *Nu* are given in Table 2.5. The thermomagnetic convection of nanofluids in square and rectangular cavities is provided in Table 2.6.

2.6.1 Thermo-convection of Nanofluids

2.6.1.1 Square Cavities

Using a square cavity containing ZnO/DIW-EG (75:25, 85:15 and 95:5 vol.%) nanofluid at φ = 5.25 wt.%, the thermo-convection heat transfer performance was investigated experimentally by Li et al. [158]. They observed that the heat transfer of the nanofluid was attenuated relative to DIW-EG. This trend was noticed to increase with a rise in the EG amount contained in the basae fluid. In another study, Kouloulias et al. [159] examined the thermo-convection heat transfer of Al_2O_3/W (0.01 – 0.12 vol.%) nanofluid contained in a square cavity. The results showed that heat transfer of nanofluid was deteriorated compared with the base fluid. In addition, Hu et al. [160] filled a square (vertical) cavity with TiO_2-DIW (3.85 – 10.71 wt.%) nanofluid to study the thermo-convection performance. The heat transfer was deteriorated using nanofluid compared with DIW, which was in agreement with the works of Li et al. [158] and Kouloulias et al. [159]. The reason for the attenuation of the

heat transfer of nanofluids relative to the base fluids was the influence of μ_{eff} and κ_{eff}, poor stability and thermo-convection of base fluids.

The thermo-convection heat transfer of DW-based Al_2O_3 (0.1 – 4.0 vol.%) nanofluid filled into three different square cavities was investigated by Ho et al. [161]. They reported that heat transfer was enhanced at lower φ (0.1 vol.%) for all the cavities and increased with cavity size. In comparison with DW, maximum heat transfer enhancement of 18% was achieved with the largest cavity. A correlation was developed from the experimental data for *Nu* estimation (see Table 2.5). Joshi and Pattamatta [151] examined the thermo-convection performance in a square cavity containing DW-based MWCNT, graphene and Al_2O_3 (0.1 – 0.5 vol.%) nanofluids. *Nu* was observed to be enhanced for MWCNT/DW and Al_2O_3/DW nanofluids at φ = 0.1 vol.% considering the *Ra* range studied. Maximum enhancements of 35%, 20% and 5% were reported for MWCNT/DW, graphene/DW and Al_2O_3/DW nanofluids respectively relative to DW. Joshi and Pattamatta [162] studied the thermo-convection behaviour of DIW-based MWCNT and Al_2O_3 nanofluids in a square cavity. They observed that *Nu* of MWCNT/DIW nanofluid was higher than that of Al_2O_3/DIW nanofluid. Enhancements of 35% and 11% at 0.1 vol.% and 0.3 vol.% respectively were observed for MWCNT/DIW nanofluid when compared with DIW. Garbadeen et al. [22] examined the thermo-convection heat transfer of DIW-based MWCNT/DIW (0 – 1 vol.%) nanofluid in a square cavity. The results showed that the peak heat transfer occurred at φ = 0.1 vol.% and thereafter depreciated as φ increased. The highest enhancement achieved was 45% . Using Al_2O_3-DW (0.25 – 0.77 vol.%) nanofluid in a square cavity, Hu et al. [163] also reported enhancement of heat transfer at low φ (0.25 vol.%) and deterioration at high φ.

Mahian et al. [164] studied the influence of two empirical models and an experiment-derived model on the *Nu* and *h* ratio of SiO_2/W (0.5 – 2 vol.%) nanofluid in a square cavity and a 45°

Table 2.2: Thermo-convection of nanofluids in square cavities.

Author	Nanofluid (φ)	Cavity dimension	*Ra*	Measured properties	Parameters considered	Remark
Kouloulias et al. [159]	γ-Al_2O_3/DIW (0.01 – 0.12 vol.%)	Cubic with 1 x 10^{-3} m^3.	2.5 x 10^9 – 5.2 x 10^9	-	*Nu, h & Ra*	*Nu* and *h* deteriorated with φ increase at different ΔT conditions.
Hu et al. [163]	Al_2O_3/DW (0.25 (1), 0.5 (2) & 0.77 (3) vol.% (wt.%))	Square (180 x 80 x 80 mm^3)	3.09 x 10^7 – 7.05 x 10^7	μ & κ	*Nu, h, Q & Ra*	Heat transfer was augmented at low φ but deteriorated at high φ.
Hu et al. [160]	TiO_2/DIW (3.85, 7.41 & 10.71 wt.%)	Vertical square (180 x 80 x 80 mm^3)	4.04 x 10^7 – 21.07 x 10^7	μ & κ	Nu, h, Q & Ra (Visual)	Heat transfer of NF was less that of DIW.
Joshi and Pattamatta [151]	Al_2O_3/DW, MWCNT/DW & Graphene/DW (0.1, 0.3 & 0.5 vol.%)	Square (40 x 40 x 200 mm^3)	7 x 10^5 – 1 x 10^7	μ & κ	*Nu* & *Ra*	At *Ra*=10^6, DW-based MWCNT & graphene NFs enhanced heat transfer for 0.1 and 0.3 vol.%, whereas at *Ra*=10^7, only MWCNT/DW & Al_2O_3/DW NFs revealed the same at same φ.
Li et al. [158]	ZnO/EG-DW (75:25, 85:15 & 95:5 vol.) (5.25 wt.%)	Square (180 x 80 x 80 mm^3)	5.25 x 10^7 – 1.08 x 10^8	μ & κ	*Q, Nu, h & Ra*	Heat transfer was deteriorated with an increase in EG content.
Giwa et al. [165]	MWCNT-Al_2O_3 (95:5 & 90:10)/DIW (0.1 vol.%)	Square (96 x 96 x 105 mm^3)	2.27 x 10^8 – 4.7 x 10^8	μ & κ	*Q, h, Nu & Ra*	HNFs enhanced heat transfer better than both monoparticle NF of Al_2O_3/DIW and DIW.
Mahian et al. [164]	SiO_2/W (0.5, 1.0, & 2.0 vol.%)	Square and inclined square (45°)	1.0 x 10^5 – 1.0 x 10^6	*ρ, μ, & κ*	*Gr, Nu, h & Ra*	For all the cavities, maximum heat transfer coefficient ratio was observed at *Ra*=10^6 and φ = 0.5 vol.%.
Heris et al. [167]	Al_2O_3, TiO_2, & CuO/turbine oil (0.2 – 0.8 wt.%)	Cube (10 cm) with three inclinations (0°, 45°, & 90°)	3.00 x10^7 – 3.00 x10^8	-	*Nu, h & Ra*	Deterioration of heat transfer for NFs compared with turbine oil.
Kouloulias et al. [168]	Al_2O_3/DIW (0.00026 vol.%)	Cubic (40 mm x 40 mm)	4.1 x 10^9	-	*Pr, Nu, h, q' & V_{avg}*	Mass transfer and velocity characteristics of NFs were enhanced relative to DIW.
Joshi and Pattamatta [162]	MWCNT/DIW (0.1 – 0.5 vol.%) and Al_2O_3/DIW (0.1 – 2 vol.%)	Cuboid (40 x 40 x 200 mm^3)	7 x 10^5 – 1 x 10^7	μ & κ	*Nu* & *Ra*	*Nu* of MWCNT/DIW NF was higher than that of Al_2O_3/DIW, with enhancement at 0.1 and 0.3 vol.%, and 0.1 vol.% respectively.
Garbadeen et al. [22]	MWCNT/DIW (0-1 vol.%)	Cuboid (96 x 96 x 105 mm^3)	1 x 10^8	μ & κ	*Nu, Ra, q & h*	Optimum heat transfer occurred at 0.1 vol.% with 45% enhancement of *h* compared with DIW.
Ho et al. [161]	Al_2O_3/DIW (0.1 – 4 vol.%)	Cuboid (25 x 25 x 60, 40 x 40 x 90, and 80 x 80 x 180)	6.21 x 10^5 – 2.56 x 10^8	μ, ρ, & κ	*Nu, Ra & h*	Enhancement of heat transfer at lower φ (0.1 & 0.3 vol.%) was observed, which increased with cavity size.
Choudhary and Subudhi [166]	Al_2O_3/DW (0.01 & 0.1 vol.%)	Rectangular (120 x 120 x 365 (h) mm^3) with AR (0.3 – 2.5)	10^7 – 10^{12}	-	*Nu, h, δ, Pr & Ra*	At low φ, heat transfer was enhanced but deteriorated at high φ. Heat transfer was noticed to be a function of AR, *Ra* & φ.

inclined square cavity. Results indicated that an increase in φ attenuated *Nu* for both cavities. At $Ra = 10^6$, the inclined square cavity was noticed to enhance *Nu* and *h* ratio at any value of φ; however, this was achieved at φ = 0.5 vol.% and 1.0 vol.% using the square cavity. For both cavities, the optimum *h* ratio was observed at φ and $Ra = 10^6$. Finally, the measurement of thermal properties was emphasised against the use of empirical and previously proposed models. Giwa et al. [165] engaged Al_2O_3-MWCNT (95:5 and 90:10)/DIW) nanofluids at φ = 0.1 vol.% in a square cavity to investigate the thermo-convection performance. They demonstrated that heat transfer was enhanced (with an increase in MWCNT NPs) using hybrid nanofluids in comparison with DIW and Al_2O_3/DIW nanofluid [152]. The highest enhancement of *Nu* = 19.4% and *h* = 9.8% was reported for DIW-based Al_2O_3-MWCNT (90:10 ratio) nanofluid.

Choudhary and Subudhi [166] studied the thermo-convection of Al_2O_3/DW (0.01 and 0.1 vol.%) nanofluid in a rectangular cavity with varying AR of 0.3 to 2.5. They revealed that *Nu* enhancement was dependent on φ, thermal boundary layer, AR and *Ra*. For both samples of nanofluid, *Nu* was observed to be enhanced in comparison with DW. The highest enhancements of 29.5% (at AR = 0.5 and $Ra = 7.89 \times 10^8$) and 14.2% (at AR = 0.3 and $Ra = 1.86 \times 10^8$) were recorded for φ = 0.01 vol.% and φ = 0.1 vol.% respectively. Two correlations were developed from the experimental data for the prediction of *Nu* and the thermal boundary layer of each nanofluid (Table 2.5).

Clearly, a two-way result can be observed in the use of nanofluids in square cavities: (1) outright deterioration of heat transfer irrespective of φ and (2) enhancement of heat transfer to an optimal point related to φ. However, a discrepancy in the result is obviously the case. The formulation and stability of nanofluids may be primarily responsible for the deterioration because most authors did not report on the stability of nanofluids [159], except a few that engaged visual inspection of nanofluid stability [158, 160].

Table 2.3: Thermo-convection of nanofluids in rectangular cavities.

Author	Nanofluids (φ)	Cavity dimension	*Ra*	Measured properties	Parameters considered	Remark
Ilyas et al. [172]	MWCNT/Thermal oil (0 – 1 mass%)	Vertical rectangular (12x4x3 cm^3) with AR=4.	2.5 x 10^5 – 2.7 x10^6	μ, C_p, β and κ	*Nu, h & Ra*	Deterioration of h_{av} (21.3%) and Nu_{av} (35.74%) as φ increased despite high κ_{eff}.
Ho et al. [170]	Al_2O_3/W (1 – 4 vol.%)	Vertical rectangular (l=60mm, b=25mm, h=25mm)	5.78 x 10^5 – 3.11 x 10^6	-	*Nu, h & Ra*	Enhancement of Nu_{av} with φ. Sedimentation has more impact than Brownian motion and Ludwig-Soret effect.
Qi et al. [173]	TiO_2-W (0.1, 0.3 & 0.5 wt.%)	Three rectangles with AR=0.25, 0.5 & 1 and inclined at -45°, 0°, 45° and 90°).	ND	-	*Nu, h Q & Ra*	*Nu* was augmented with increasing φ and *Q*. Highest heat transfer was achieved using a cavity with AR=1 and at 0°.
Nnanna [169]	Al_2O_3/DIW (0.2 – 7.9 vol.%)	Cuboid (35 mm x 40.32 mm x 215 mm)	0.3 x 10^7 – 3.2 x 10^7	-	*Q, Nu, h & Ra*	Heat transfer was augmented at low φ of NF but detracted at higher concentration.
Sharifpur et al. [153]	TiO_2/DIW (0.05 – 0.8 vol.%)	Rectangular (96x103x120 mm^3)	4.9 x 10^8 – 1.47 x 10^9	-	*Q, Ra, Nu*	Heat transfer was enhanced for φ=0.05 – 0.2 vol. and thereafter decreased, with maximum of 8.2% achieved for 0.05 vol.% at ΔT = 50 °C.
Solomon et al. [156]	Al_2O_3/DIW (0.1-0.6 vol.%)	Rectangular with AR=1,2 & 4.	6.9 x 10^6 – 4.0 x 10^8	-	*Q, Ra, h & Nu*	Enhancement of heat transfer was observed to be a function of AR, *Ra* and φ. Highest heat transfer occurred at 0.1, 0.2 and 0.3 vol.% for AR=1, 2 and 4 respectively.
Ghodsinezhad et al. [152]	Al_2O_3/DIW (0.05-0.6 vol.%)	Rectangular (96 x 120 x 102 mm^3)	3.49 x 10^8 – 1.05 x 10^9	μ	*Ra, h & Nu*	Enhancement of *h* up till 0.1 vol.% was observed. At 0.1 vol.%, h was 15% augmented compared with DIW.
Ilyas et al. [176]	f-MWCNT/THO (0.5 – 3 wt.%)	Cuboid (12 x 4 x 3 cm^3)	4.43 x 10^5 – 2.59 x 10^6	μ, ρ, C_p, & κ	*Nu, Pr, Ra & h*	The *h* was enhanced with an increase in φ whereas *Nu* was attenuated.
Solomon et al. [171]	DIW-based mango bark nanofluid (0.01 – 0.5%)	Cuboid (120 x 96 x 103 mm^3)	0.2 x 10^8 – 6 x 10^8	μ & κ	*Nu, Ra & Q*	Deterioration of NF was observed with increase in φ.
Solomon et al. [177]	Al_2O_3/EG (60%)-DIW (40%) (0.05 – 0.4%)	Cuboid (120 x 96 x 103 mm^3)	3 x 10^3 – 1.3 x 10^4 and 1.2 x 10^8 – 4 x 10^8	μ & κ	*Ra, Nu, h & Q*	Heat transfer was enhanced by 10% for the porous cavity at 0.1 vol% and ΔT=50 °C, compared with EG-DIW.
Amiri et al. [143]	MWCNT-hexylamine/TO ((0.001 & 0.005 wt.%)	Rectangle (203 x 100 x 221 mm^3)	ND	μ, ρ, PP, σ, C_p, voltage breakdown, FP, and κ	*Nu & h*	Both *Nu* and *h* were enhanced with φ.

2.6.1.2 Rectangular Cavities

The thermo-convection behaviour of DIW-based Al_2O_3 (0.05 – 0.6 vol.%) nanofluid inside a rectangular cavity was examined by Ghodsinezhad et al. [152]. They showed that *h* was enhanced for φ = 0.05 – 0.1 vol.% and a further increase in φ resulted in attenuation. A maximum augmentation of 15% was recorded for *h* at φ = 0.1 vol.%. They proposed a correlation for predicting *Nu* from *Ra* and φ. Nnanna et al. [169] studied the thermo-convection heat transfer performance in a rectangular cavity containing Al_2O_3/DIW (0.2 – 8 vol.%) nanofluid. They observed that *Nu* was enhanced when $\varphi \leq 2$ vol.% and attenuated for $\varphi > 2$%. The highest *Nu* was reported for φ = 0.2 vol.%. A correlation was proposed to estimate *Nu* as a dependent of *Ra* and φ. A rectangular enclosure containing MWCNT-hexylamine/TO (0.001 – 0.005 wt.%) nanofluids was investigated for the thermo-convection heat transfer performance by Amiri et al. [143]. Their results indicated that *Nu* and *h* of nanofluids were enhanced compared with the base fluid and this increased with φ. Ho et al. [170] studied the thermo-convection of water-based Al_2O_3 (1 – 4 vol.%) nanofluid in a rectangular cavity using both experimental and numerical methods to understand the influence of Brownian motion, Ludwig-Soret effect and sedimentation. The results showed that for both methods, Nu_{av} of nanofluids was better than that of water and increased with a rise in φ. An increase in *Ra* was noticed to enhance $Nu_{av.}$ The influence of sedimentation was more significant than the influence of Ludwig–Soret effect and Brownian motion.

Sharifpur et al. [153] used a rectangular cavity containing TiO_2-DIW (0.05 – 0.8 vol.%) nanofluid to study thermo-convection heat transfer performance. They observed that *Nu* was augmented with an increase in *Ra* and ΔT. Both *Nu* and *Q* were enhanced with $\varphi \leq 0.2$ vol.% and they deteriorated when $\varphi > 0.2$ vol.%, in comparison with DIW. At φ = 0.05 vol.% and ΔT = 50 °C, the highest enhancement of 8.2% was attained. For the first time, thermo-convection of DIW-based green (mango bark) nanofluid with φ = 0.01 – 0.5 vol.% was

conducted by Solomon et al. [171] using a rectangular cavity. The results showed attenuation of *Nu* for all nanofluid samples relative to DIW, though nanofluid with φ = 0.20 vol.% yielded the highest enhancement. In recent work, Ilyas et al. [172] studied the thermo-convection of MWCNT/thermal oil (0 – 1.0 wt.%) nanofluid in a vertical rectangular cavity (AR = 4). They reported that h_{av} and Nu_{av} were attenuated with an increase in φ. Deterioration of 21.3% and 35.7% was observed for h_{av} and Nu_{av} respectively relative to thermal oil at φ = 1.0 wt.%. It was stressed that the observed deterioration was due to high enhancement of μ_{eff} by 62% for φ = 1.0 wt.% despite the high κ_{eff} afforded by MWCNT.

With a rectangular cavity having AR of 1, 2 and 4, Solomon et al. [156] investigated the thermo-convection of Al_2O_3/DIW (0.1 – 0.6 vol.%) nanofluid. The results showed that *h* and *Nu* depended on φ, ΔT and AR. For φ = 0.1, 0.2 and 0.3 vol.%, the highest heat transfer occurred in cavities having AR = 1, 2 and 3 respectively at ΔT = 50 °C. The AR (0.25, 0.5 and 1), Q_{in} (1 – 20 W) and cavity angle (-45° – 90°) of a rectangular cavity containing TiO_2-water (0.10 – 0.50 wt.%) nanofluid were varied to study the thermo-convection [173]. The results showed that *Nu* was augmented as φ and Q_{in} increased. At AR = 1, inclination angle = 0°, and Q_{in} = 20 W, the highest *Nu* was observed.

2.6.1.3 Cylindrical Cavities

Putra et al. [19] examined the thermo-convection of Al_2O_3/DW and CuO/DW (φ = 1 – 4 vol.%) nanofluids in a horizontal cylinder with variation in AR (0.5 – 1.5). They reported that *Nu* was augmented with *Ra* for nanofluids and DW. However, *Nu* of nanofluids was attenuated relative to DW. They attributed the attenuation of nanofluids to ρ_{eff}, AR and φ and suggested an investigation into the effect of particle-slip mechanism and sedimentation. Mahrood et al. [174] studied thermo-convection in a vertical cylinder with varying AR (0.5 – 1.5) containing carboxymethyl cellulose-based TiO_2 and Al_2O_3 nanofluids. They noticed that *Nu* was augmented at $\varphi \leq$ 0.50 vol.% for TiO_2 nanofluid and $\varphi \leq$ 1.0 vol.% for Al_2O_3

nanofluid, and it deteriorated on a further increase of φ. Maximum augmentation of 23.5% and 19.5% was achieved at φ = 0.1 vol.% and 0.2 vol.% for the TiO_2 and Al_2O_3 nanofluids respectively. Increasing AR was noticed to augment *Nu* for both nanofluids.

Suganthi and Rajan [175] experimented with the thermo-convection of ZnO/PG (0.25 – 2.0 vol.%) nanofluid in a cylindrical subjected to both constant heat flux and constant temperature conditions. For both conditions, heat transfer was enhanced with an increase in φ when compared with PG. A maximum augmentation of 4.24% for heat transfer was reported for the constant heat flux condition, while at the cavity cold wall (under constant temperature condition), *h* was improved by 25.6%, both at φ = 2.0 vol.%. The reduction in μ_{eff} and the increase in κ_{eff} of ZnO/PG nanofluid were attributed for the augmentation observed. A correlation was developed from the experimental data for *Nu* prediction. Cadena-de la Peña et al. [154] examined the thermo-convection of MO-based AIN and TiO_2 (0.01 – 0.50 wt.%) nanofluids inside a closed vertical annular cylinder. They showed that for both nanofluids, *Nu* was enhanced when φ = 0.10 wt.% and it deteriorated at higher φ. The h_{av} and Nu_{av} of TiO_2/MO nanofluid were noticed to be higher than those of AIN/MO nanofluid with OA treated AIN/MO nanofluid offering the highest h_{av}. Both h_{av} and Nu_{av} were found to enhance with an increase in *Ra* and a reduction in AR. The highest enhancement of h_{av} and Nu_{av} for TiO_2/MO nanofluid was noticed with φ = 0.10 vol.%, while that of AIN/MO nanofluid occurred at φ = 0.10 vol.%, all at AR = 3.98. They formulated two correlations for the prediction of *Nu*.

With a vertical cylinder having AR of 0.0635 and 0.127 and heated from the bottom wall, the thermo-convection of Al_2O_3/DW (0.21 – 0.75 vol.%) nanofluid was investigated by Ali et al. [178]. Their results showed that *Nu* was augmented with an increase in *Ra* and AR. For both cavities, the augmentation of *Nu* was noticed at $\varphi \leq$ 0.51 vol.% and deterioration occurred

Table 2.4: Thermo-convection of nanofluids in cylindrical and triangular cavities.

Author	Nanofluids (φ)	Cavity dimension	*Ra*	Measured properties	Parameters considered	Remark
			Cylindrical cavity			
Putra et al. [19]	Al_2O_3/DW and CuO/DW (1 & 4 vol.%)	Horizontal cylinder (inner diameter = 40 mm) at AR = 0.5 & 1.	$1.6 \times 10^7 - 9.2 \times 10^7$	ρ, μ, κ, and γ	*Ra*, *Nu* & *h*.	For both NF, heat transfer deteriorated with an increase in AR and φ, and a decrease in *Nu*.
Ali et al. [179]	Al_2O_3/W (0.21, 0.51 & 0.75 vol.%)	Two vertical cylinders (D = 0.2 m) with AR = 0.0635 & 0.127. Heated on the top wall.	$3.0 \times 10^5 - 1.3 \times 10^8$	ρ, μ, and κ	*Ra*, *Q*, *Nu* & *h*.	The *Nu* and *h* of NFs were more deteriorated than W, which is a function of φ and AR.
Cadena-de la Peña et al. [154]	AIN and TiO_2/mineral oil (0.01, 0.1 & 0.5 wt.%)	Annular and vertical (opened) with *AR* of 3.98 & 4.78.	$1.4 \times 10^9 - 3.2 \times 10^{13}$	μ, and κ (at 24 & 40 °C)	*Ra*, *Nu* & *h*	Nu_{av} and h_{av} were improved relative to mineral oil low AR and φ, and high *Ra*. TiO_2/mineral oil NFs performing better than the AIN/mineral oil NFs.
Ali et al. [178]	Al_2O_3/W (0.21, 0.51 & 0.75 vol.%)	Two vertical cylinders (D = 0.2 m) with AR = 0.0635 & 0.127. Heated at the bottom.	$3.0 \times 10^5 - 1.3 \times 10^8$	ρ, μ, & κ	*Ra*, *Q*, *Nu* & *h*	Compared with W, *h* was augmented for 0.21 vol.% and attenuated with φ increase. Heat transfer coefficient was *AR* dependent with higher *h* for lower *AR*.
Mahrood et al. [174]	Al_2O_3 & TiO_2/CC ($0.1 \leq \varphi \leq 1.5$ vol.%)	Vertical cylinder with AR = 0.5, 1.0 & 1.5.	$4.0 \times 10^6 - 3.0 \times 10^7$	n.d.	*q'*, *Nu*, *h* & *Ra*	Heat transfer was enhanced below 0.5 and 1 vol.% with optimum values at 0.1 and 0.2 vol.%, for CC-based TiO_2 and Al_2O_3 NFs respectively. TiO_2 NF was a better heat transfer medium than Al_2O_3 NF. Increasing *AR* was found to enhance heat transfer for both NFs.
Moradi et al. [191]	Al_2O_3/DIW and TiO_2/DIW ($0.1 \leq \varphi \leq 1.5$ vol.%)	Inclined (30°, 60° & 90°) vertical cylindrical (diameter = 80 mm & length = 250 mm) with AR (0.5, 1.0 & 1.5)	$1.2 \times 10^8 - 3.7 \times 10^8$	*P*	*q'*, *Nu*, *h* & *Ra*	Maximum enhancements of *Nu* (6.76% & 2.33% relative to DIW) occurred at 0.2 vol.% and 0.1 vol.% for Al_2O_3/DIW and TiO_2/DIW respectively. *Nu* was noticed to augment with increase in *AR*.
Suganthi and Rajan [175]	ZnO/PG (0.25-2 vol.%)	Cylinder (h=5.2 cm, ID=1.9 cm, OD=2.1 cm)	$10^4 - 10^9$	μ & κ	*Q*, *Nu*, *h* & *Ra*	Enhancement (4.24%) in heat transfer rate with φ for ZnO/PG NF with peak at φ = 2.0 vol.%.
			Triangular cavity			
Mahian et al. [164]	SiO_2/W (0.5, 1.0, & 2.0 vol.%)	Triangular	$1.0 \times 10^5 - 1.0 \times 10^6$	ρ, μ, and κ.	*Gr*, *Nu*, *h* & *Ra*	For all the cavities, the maximum heat transfer coefficient ratio was observed at $Ra=10^6$ and 0.5% concentration.

when φ was further increased. With AR = 0.0635, h was augmented by 40% for φ = 0.21 vol.% and when AR = 0.127, 8% enhancement of h was noticed for φ = 0.51 vol.%. Ali et al. [179] engaged the same nanofluid and cavities but heated them at the top wall. However, they showed that *Nu* was attenuated for nanofluids in comparison with DW. The attenuation was found to depend on AR and φ. Both Ali et al. [179] and Ali et al. [178] proposed correlations for predicting *Nu* as related to φ and *Ra* for AR = 0.0635 and 0.127.

Moradi et al. [180] investigated the influence of cavity inclination (30° – 90°), heat fluxes (500 – 1500 W/m^2) and AR (0.5 – 1.5) on the thermo-convection of DIW-based Al_2O_3 and TiO_2 nanofluids (φ = 0.1 – 1.5 vol.%) in a vertical cylinder heated at the bottom wall. The results showed that *Nu* was enhanced for Al_2O_3/DIW nanofluid, while it deteriorated for TiO_2/DIW nanofluid, compared with DIW. For Al_2O_3/DIW nanofluid, *Nu* was maximally enhanced by 6.76% when φ = 0.20 vol.%, AR = 1.5 and cavity inclination = 30°. They reported that at low *Ra*, *Nu* was significantly influenced by AR, cavity inclination, and φ.

2.6.1.4 Triangular Cavities

The effect of two empirical models and an experiment-based model on the *Nu* and h ratio of SiO_2/W (0.5 – 2.0 vol.%) nanofluid in a triangular cavity was studied by Mahian et al. [164]. They showed that *Nu* deteriorated as φ increased, which was independent of *Ra*. At any *Ra*, h of nanofluids was observed to be higher than that of W. Also, the highest heat transfer for nanofluid was attained at φ = 0.5 vol.%. Additionally, the utilisation of measured thermophysical properties instead of empirical models in thermo-convection studies was stressed.

2.6.1.5 Porous Cavities

The engineering advantage of using porous media as a way of enhancing thermo-convection heat transfer for nanofluids was experimented by Solomon et al. [177]. The work was conducted by using EG (60%)-DIW (40%) based Al_2O_3 (φ = 0.05 – 0.4 vol.%) nanofluid

contained in a rectangular cavity with porous media under ΔT = 20 to 50 °C. They showed that *Nu* was higher for a clear cavity than for a porous cavity. *Ra* increase was observed to enhance *Nu*. At φ = 0.05 vol.%, *Nu* of nanofluid was higher than that of EG (60%)-DIW (40%) and it deteriorated with an increase in φ. Peak enhancement of 10% (*Nu*) was recorded at φ = 0.05 vol.% and ΔT = 50 °C.

2.6.2 Thermomagnetic Convection of Nanofluids

The exceptional heat transfer characteristics of electrically conducting fluids on exposure to magnetic stimulus known as thermomagnetic convection have been studied widely. Thermomagnetic convection has found application in various devices such as astrophysics (orbital stations), magnetic sensors, crystal manufacturing, plasma confinement and microelectronics [181, 182]. Because nanofluids and hybrid nanofluids are known as electrically conducting fluids, several studies have been carried out on their thermomagnetic convection heat transfer performance in various cavities under diverse thermal conditions [27, 29, 183–190]. The public domain has been overwhelmed with various methods for enhancing the thermomagnetic convection of nanofluids and hybrid nanofluids in different shapes of cavities. These methods include cavity inclination, use of porous media, AR, partitioning, baffles, magnetic field inclination, presence of obstacles, heaters and their positioning, use of different types of nanofluids and hybrid nanofluids, and various types and strengths of magnetic fields.

Ghasemi et al. [183] pioneered the study of thermomagnetic convection of nanofluids. They numerically examined the thermomagnetic heat transfer of Al_2O_3/W nanofluid in a square cavity using a uniform magnetic field. With controlling parameters of φ, *Ra* and *Ha*, they revealed that heat transfer was augmented as *Ra* increased and it attenuated as *Ha* increased. Depending on *Ra* and *Ha* values, heat transfer was observed to be either augmented or attenuated as φ increased. However, there is a great scarcity of experimental studies on the

thermomagnetic characteristics of nanofluids in the open literature, while there are no studies on the characteristics of hybrid nanofluids. Based on the focus of this study, the very few experimental works found in the literature were reviewed.

2.6.2.1 Square Cavities

Yamaguchi et al. [192] experimented with the thermo-convection of kerosene-based Mg-Zn ferrite nanofluid contained in a square cavity and exposed to an external magnetic field. The results showed that the exposure of magnetic nanofluid to the magnetic field augmented heat transfer in the cavity in comparison with kerosene. Also, an increase in the strength of the magnetic field caused the further augmentation of heat transfer. Yamaguchi et al. [193] conducted a similar study to that of Yamaguchi et al. [192] but only introduced heat-generating objects inside the cavity. The results of the thermomagnetic heat transfer showed that increasing the size of the heat-generating objects caused a slight reduction in heat transfer. The smaller the size of the heat-generating objects, the more the heat transferred. Roszko and Fornalik-Wajs [194] studied the thermomagnetic heat and flow behaviours of Ag/water (0.1 vol.%) nanofluid in a cubic cavity under ΔT = 5 – 25 °C and a variable magnetic field (0 – 10 T). They reported augmentation of *Nu* as a function of ΔT and strength of the magnetic field. Also, heat transfer analysis revealed that flow structure and magnetic field were related to *Nu*. The thermal transport in the system was changed due to exposure to the magnetic field.

However, Dixit and Pattamatta [195] published a contradicting report on the exposure of nanofluids to an external magnetic stimulus. They studied the thermo-convection of four non-magnetic DW-based nanofluids (φ = 0.057 – 2 vol.%) of Cu, MWCNT, SiO_2 and G in a square cavity in the absence and presence of a magnetic stimulus (0.13 T – 0.3 T). The results showed that *Nu* of G/DW nanofluid (for all φ) and MWCNT/DW nanofluid (φ = 0.1 vol.%) was enhanced in comparison with DW in the absence of a magnetic stimulus. *Nu* of all

Table 2.5: Correlations for thermo-convection heat transfer in cavities.

Author	Nanofluids	Geometry	Correlation
Ali et al. [179]	Al_2O_3/W	Vertical cylinders	$Nu = (7.899 - 8.571 \times 10^{-9} Ra) \times (1.0 - 15.283\varphi + 387.681\varphi^2) AR^{0.5}$
Ho et al. [161]	Al_2O_3/W	Vertical squares	$Nu_{nf} = CRa_{nf}{}^{n} \left(Pr_{nf,h}/Pr_{nf}\right)^{m} \left(\beta r_{nf,h}/\beta r_{nf}\right)^{p}$
Cadena-de la Peña et al. [154]	AIN and TiO_2/mineral oil	Opened vertical annular	$Nu = 0.496 Ra^{0.17} K^{\left(\frac{1.582}{k}+2.463\right)} AR^{-0.541}$ Maximum deviation = 1.6%
Ali et al. [178]	Al_2O_3/W	Vertical cylinders	$Nu = 1.426(Ra)^{0.119}(1 + 44.097\varphi - 6943.36\varphi^2) AR^{0.137}$
Ghodsinezhad et al. [152]	Al_2O_3/W	Square	$Nu = 0.6091(Ra)^{0.235}(\varphi)^{0.00584}$ (for $\varphi \leq 0.1$) $Nu = 0.482(Ra)^{0.2356}(\varphi)^{-0.026}$ (for $\varphi \geq 0.1$); $R^2 = 0.94$
Ilyas et al. [176]	f-Al_2O_3/THO	Rectangular	$Nu = C(Ra)^{0.04}(1-\varphi)^{-0.015}$; 228≤Pr≤592; 0.97≤1- φ (wt. frac.) ≤1; $C = 4.17\left(\frac{Pr_r}{Pr_r - 0.343}\right)^{2.51}\left(\frac{Pr_r}{K_r{}^{3.76}\beta_r{}^{3.483}}\right)$
Nnanna et al. [169]	Al_2O_3/DIW	Rectangular	$Nu = 16.4e^{-Ra\epsilon\varphi(e^{-m\varphi})}$ ε=4 x 10^{-7}; m=11; $10^5 \leq \varphi Ra e^{-m\varphi} \leq 10^6$
Suganthi and Rajan [175]	ZnO/PG	Cylinder	$Nu = 0.59\ (Ra)^{0.25}$
Choudhary and Subudhi [166]	Al_2O_3/DW	Square	$Nu = 0.1199Pr^{-1/2}(Ra)^{1/4} + 2.17 \times 10^3 Pr^{-1/7}(Ra)^{3/7}$ (φ < 0.01 vol.%) $Nu = 0.132Pr^{-1/2}(Ra)^{1/4} + 1.66 \times 10^3 Pr^{-1/7}(Ra)^{3/7}$ (φ < 0.10 vol.%) $\left(\frac{\delta_{th}}{H}\right)_{NF} = 122.55\ (Ra)^{-0.427}$; ($\varphi$ < 0.01 vol.%) $\left(\frac{\delta_{th}}{H}\right)_{NF} = 44.873\ (Ra)^{-0.3728}$; ($\varphi$ < 0.10 vol.%)

Table 2.6: Thermomagnetic convection of nanofluids in square and rectangular cavities.

Author	Nanofluids (φ)	Cavity dimension	*Ra*	Measured properties	Parameters considered	Remark
			Square			
Dixit and Pattamatta [195]	SiO_2/DW, MWCNT/DW, Graphene/DW, & Cu/DW (0.057, 1, & 2 vol.%)	Cubic (25 x 50 x 50 mm^3) + magnetic field (0.13 T & 0.3 T)	$1 \times 10^6 - 1 \times 10^7$	μ & κ	*Nu*, magnetic field direction and strength and *Ra*	Heat transfer was augmented for all the graphene samples and MWCNT at 0.1 vol.%, in the absence of magnetic field. Generally, the presence of magnetic field deteriorated heat transfer in all the NF samples.
Yamaguchi et al. [193]	Mg-Zn ferrite/kerosene (ND)	Cubic (7.5 mm each side) with a heat-generating object (brass & square) and magnetic field.	Gr=0-160; $Gr_m=1.22 \times 10^3 - 4.4 \times 10^4$	-	*Nu*, *Gr*, Gr_m, *H & d*	The presence of magnetic field enhanced heat transfer irrespective of the size of the heat-generating objects.
Roszko and Fornalik-Wajs [194]	Ag/DW (0.1 vol.%)	Cubical with 0.032 m under magnetic field (10 T)	$2.5 \times 10^6 - 2.2 \times 10^7$	-	Ra_T, Ra_{TM}, *Nu & h*.	*Nu* is a function of the magnetic field and structure of flow. The energy transfer was altered due to the presence of magnetic field.
Yamaguchi et al. [192]	Mg-Zn ferrite/alkyl-naphthalene	Cubic with a magnetic field	Ra ($3.0 \times 10^3 - 8.0 \times 10^3$), Ra_m ($1.0 \times 10^8 - 1.25 \times 10^8$)	-	*Nu*, *Ra* & Ra_m	Presence of magnetic field enhanced heat transfer. Increasing the magnetic strength enhanced heat transfer further.
			Rectangular			
Joubert et al. [88]	Fe_2O_3/DIW (0.05 – 0.3 vol.%)	Rectangle (99 x 96 x 120 mm^3) under magnetic field intensity of 300 G and 700 G.	$1.77 \times 10^8 - 4.26 \times 10^8$	μ	*Nu*, *Ra & h*	Without magnetic field, *Nu* was maximally enhanced by 5.63% for 0.1 vol.% NF, while with magnetic field, an additional maximum augmentation of 2.81% was recorded.

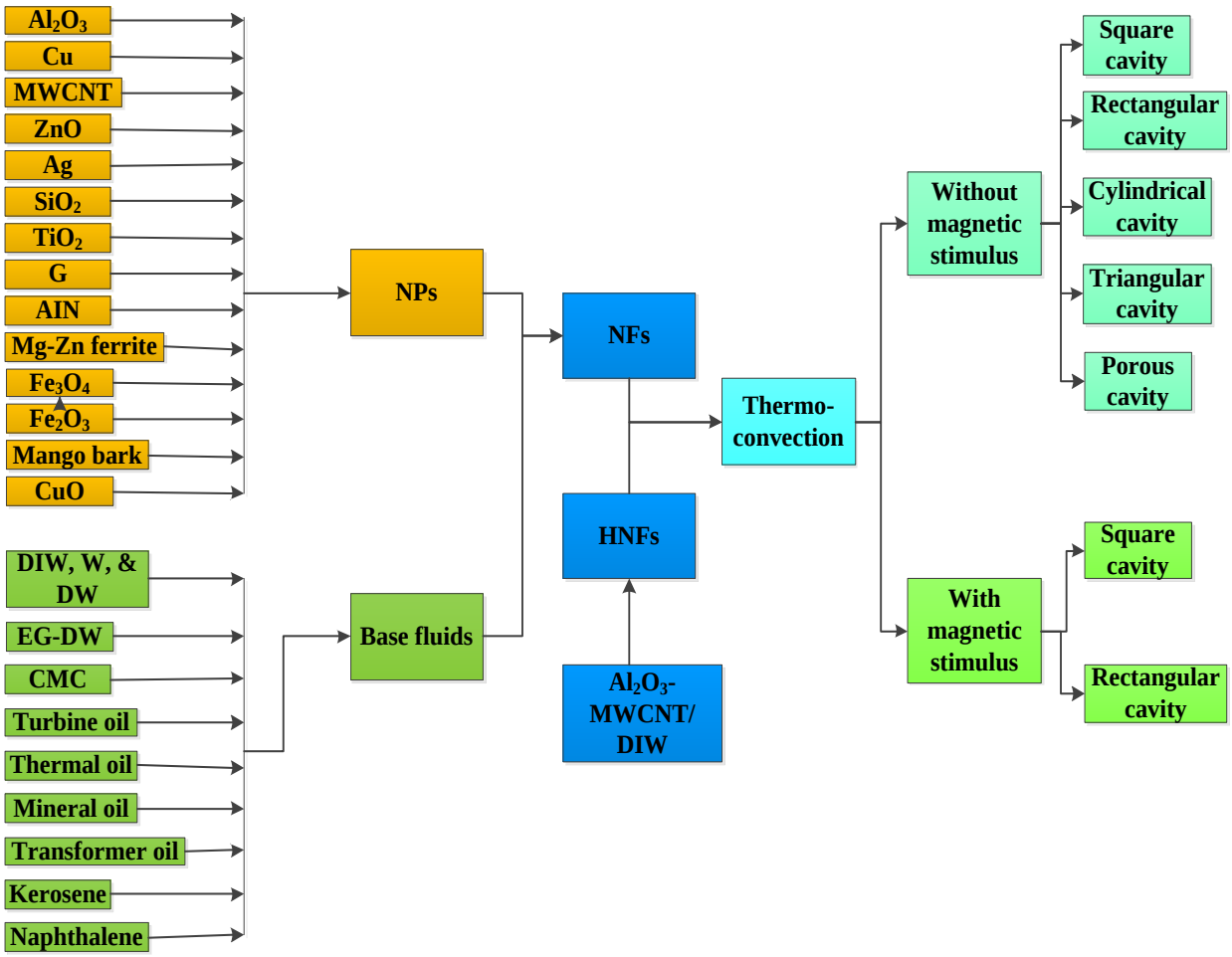

Figure 2.1: Update on experimental thermo-convection of monoparticle and hybrid nanofluids in cavities.

nanofluids was observed to deteriorate in the presence of a magnetic stimulus. This is related to *Ra*, φ, nanofluid type, direction and strength of the magnetic stimulus. It is worth noting that the engaged nanofluids were electrically conducting and non-magnetic in nature.

2.6.2.2 Rectangular Cavities

Joubert et al. [88] investigated thermo-convection heat transfer in a rectangular cavity containing Fe_2O_3/DIW nanofluid (φ = 0.05 – 0.30 vol.%) under constant magnetic stimuli (from permanent magnets) with three different configurations. In the absence of magnetic stimuli, Nu_{av} and h_{av} showed maximum enhancement for φ = 0.1 vol.% in relation to DIW, with 5.63% for Nu_{av}. On imposing the magnetic stimuli, the highest Nu_{av} was observed when the 700 G magnets were positioned above and below the hot wall of the cavity. This caused

Nu_{av} to be augmented by 2.81% (φ = 0.1 vol.%) in comparison with the case without magnetic stimuli. Nu_{av} was found to depend on φ, the strength of the magnetic stimulus and configuration of the magnets.

A picture of the research update on the thermo-convection of nanofluids and hybrid nanofluids in cavities in terms of the types of NPs, HNPs, base fluids, and shapes of the cavity, magnetic stimulus presence and absence, and porosity of cavity is given in Fig. 2.2. The focus of the present study was to fill the gap observed in the literature and this is pictorially represented in Fig. 2.1.

2.7 Current Development

The advent of a special class of nanofluids called "hybrid nanofluids" with improved thermophysical properties resulting from the synergy of utilising two different NPs possessing dissimilar properties has led to investigating the thermo-convection of hybrid nanofluids in diverse cavities. It can be observed from the public domain that there is a dearth of documentation and knowledge concerning thermo-convection and thermomagnetic convection heat transfer performance of hybrid nanofluids in cavities. In the open literature, there are a few studies on the thermo-convection and thermo-magnetic convection of hybrid nanofluids in cavities. However, all of these were carried out using numerical techniques. Takabi and Salehi [196] studied the thermo-convection heat transfer of Al_2O_3/water nanofluid and Al_2O_3-Cu/water (96.2:3.8) nanofluids for φ = 0 – 12 vol.% in a rectangular cavity. They found that the hybrid nanofluids yielded higher heat transfer than the monoparticle nanofluids. Nu_{av} of hybrid and monoparticle nanofluid was noticed to enhance with Ra and φ. At Ra = 1 x 10^6 and 2.0 vol.%, Nu_{av} of monoparticle and hybrid nanofluid was enhanced by 14.40% and 13.78% respectively relative to water.

Tayebi and Chamkha [197] utilised the same hybrid and monoparticle nanofluid (φ = 0 – 12 vol.%) as Takabi and Salehi [196] but with a different ratio of HNPs (Al_2O_3-Cu (67:23)) to

study the thermo-convection heat transfer characteristics of these fluids in a horizontal annulus cavity. Their findings were found to be consistent with those of Takabi and Salehi [196] in that the hybrid nanofluid were better heat transfer and flow media than the monoparticle nanofluid and water; Nu_{av} for monoparticle and hybrid nanofluid was enhanced as *Ra* and φ increased. Mehryan et al. [40] studied numerically the thermo-convection heat transfer performance of the same fluids as used by Takabi and Salehi [196] and Tayebi and Chamkha [197] in a porous square cavity with two types of media in which *Ra* of 10 to 100, φ = 0 to 2% and porosity of 0.3 to 0.9 were considered. Their results showed attenuation of Nu_{av} as φ increased when hybrid and monoparticle nanofluid were used in a porous cavity. A higher heat transfer deterioration was observed for Al_2O_3-Cu/W (96.2%:3.8% wt.%) nanofluids than for Al_2O_3/W nanofluids, which contradicted the outcome of the studies of Takabi and Salehi [196] and Tayebi and Chamkha [197]. Nu_{av} was noticed to reduce with the rise in φ for all the porosity values considered except for 0.9. Izadi et al. [198] numerically investigated the thermo-convection heat transfer of water-based hybrid nanofluids (MWCNT-Fe_3O_4) contained in an inverted T-shaped cavity. They showed that the thermal boundary layer thickness development led to *Nu* deterioration relative to the cavity obstruction ratio. However, *Nu* was noticed to enhance as *Ra* and φ increased. An increase in the heat source AR was noticed to augment heat transfer rate and the best heat transfer performance was achieved when the heat source was located at the cavity centre.

Numerical studies on the thermomagnetic convection of hybrid nanofluids in cavities focused on using hybrid nanofluids and magnetic stimulus as passive and active techniques respectively to benefit heat transfer [190, 199–202]. Mansour et al. [199] numerically examined the thermomagnetic convection of water-based Cu-Al_2O_3 nanofluid saturated into a porous square cavity. They demonstrated that heat transfer was enhanced with a reduction in *Da* and an increase in *B*, and it detracted as *Ha* increased. Also, *Nu* was observed to enhance

with φ, *Ra*, *Ha* and *B*. The use of hybrid nanofluid was noticed to enhance the heat transfer rate. Ashorynejad and Shahriari [201] numerically investigated the thermomagnetic convection heat transfer in a waxy-walled open cavity containing water-based Al_2O_3-Cu nanofluid subjected to a uniform magnetic stimulus. The results showed *Nu* attenuation as *Ha* was increased and its enhancement with an increase in *Ra* and φ. At $Ra = 10^5$, *Nu* was enhanced with an increase in ψ and φ. The highest heat transfer enhancement was reached at *Ha* = 90 and the lowest at *Ha* = 30.

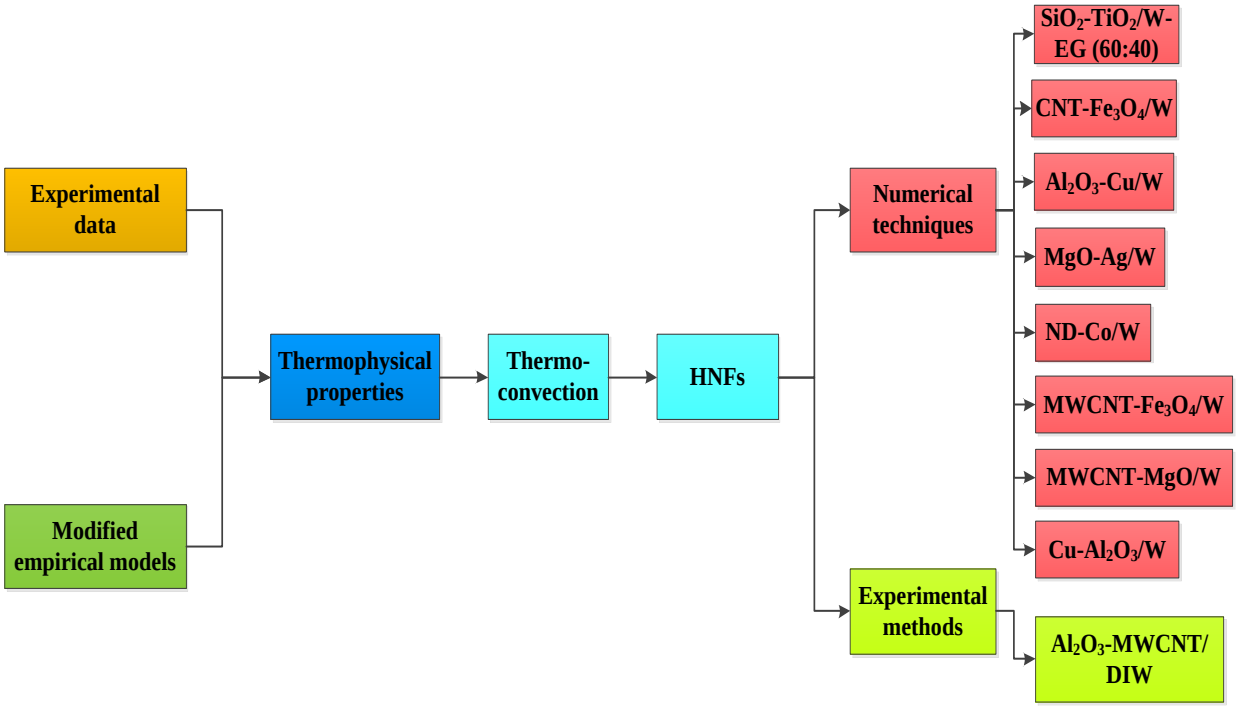

Figure 2.2: Update on utilisation of hybrid nanofluids in thermo-convection studies in cavities.

Rashad and co-workers [202] numerically examined thermomagnetic behaviour in a triangular cavity (heated from the bottom wall) containing Cu-Al_2O_3/water nanofluid. Their results showed enhancement of heat transfer rate with an increase in *Ra* and *D* and a reduction in *B*, but it deteriorated with the rise of *Ha* and Q_p. Increasing φ was observed to be significant when *Ha* was high, *Ra* was low, and *B* and *Da* increased. For hybrid and monoparticle nanofluid, no substantial difference in heat transfer augmentation was observed.

In a recent work, Sajjadi et al. [190] numerically studied the thermomagnetic characteristics in a square cavity saturated with porous media and MWCNT-Fe_3O_4/W nanofluid. The results showed augmentation of heat transfer with an increase in φ but it attenuated as the magnetic stimulus increased. Also, *Nu* was found to be augmented by increasing *Da*, which deteriorated with an increase in *Ha*.

The literature review showed a dearth of experimental studies on the thermomagnetic convection heat transfer performance of hybrid nanofluids in the open domain. In addition, it was noticed that some authors engaged in the modification of empirical and experiment-obtained models and mixture correlations to estimate the thermophysical properties of hybrid nanofluids [39, 40, 197, 198], while others experimentally determined some of these properties [190, 199, 201, 202] utilised in the numerical investigation of thermo-convection and thermomagnetic convection of hybrid nanofluids in cavities. In Fig. 2.2, the current state of hybrid nanofluids utilisation in thermo-convection and thermomagnetic convection is presented.

2.8 CONCLUSION

Nanofluids and hybrid nanofluids have been formulated primarily using a one- or a two-step method and can be characterised for their morphology, size, elemental composition, distribution, functional groups, crystalline structure, surface morphology, dispersion, etc. by various techniques. Because the stability of monoparticle and hybrid nanofluids is highly related to their thermophysical properties and convective heat transfer performance, obtaining stable monoparticle and hybrid nanofluids has become a huge necessity prior to further use. Sonication, pH control and surfactant addition as stability-improving techniques need to be taken seriously and optimising these techniques is paramount to achieving more stable mono-particle and hybrid nanofluids. It is evident from the literature that it is virtually impossible to reproduce works on the formulation of hybrid and monoparticle nanofluids, because all the

required parameters are not provided. Also, monitoring and reportage of monoparticle and hybrid nanofluids stability are of great importance because most studies on thermophysical properties and thermo-convection do not report stability or engage a visual inspection method to check stability, due to this technique not being scientific.

Thermophysical properties (κ_{eff}, μ_{eff}, ρ_{eff}, σ_{eff}, C_p-$_{eff}$, β_{eff}, etc.) of diverse types of nanofluids with various base fluids have been investigated mainly as a function of φ and temperature. The advent of hybrid nanofluids as a new class of monoparticle nanofluids further ignites the need to measure the thermophysical properties of emerging hybrid nanofluids. Most studies on the thermo-convection of monoparticle and hybrid nanofluids in different cavities reported enhancement of heat transfer for $\varphi = \leq 0.20$ vol.%. Increasing φ beyond this limit primarily resulted in deterioration. Stability of monoparticle and hybrid nanofluids outside other factors such as μ_{eff}, ρ_{eff}, Brownian motion and slip mechanism has been linked mainly to the deterioration of heat transfer noticed in thermo-convection studies. To improve the outcomes of thermophysical properties and thermo-convection heat transfer of monoparticle and hybrid nanofluids, their stability is very important. Researchers need to intensify studies on the experimental thermo-convection of new kinds of hybrid monoparticle and nanofluids, especially in terms of the base fluids and the use of magnetic monoparticle and hybrid nanofluids. The lack of publication on the thermomagnetic convection of hybrid and magnetic nanofluids that is experiment-based has created a vacuum that must be filled. Additionally, studies on the thermo-convection and thermomagnetic convection of monoparticle and hybrid nanofluids are strongly recommended to measure the thermophysical properties of the monoparticle and hybrid nanofluids engaged. It is also recommended not to use existing models because these models have been reported to underpredict the thermal properties and considerably affect the convective heat transfer output. The emergence of hybrid nanofluids as new advanced thermal fluids calls for the

development of correlations to estimate the thermophysical properties and *Nu* of thermo-convection of hybrid nanofluids.

Chapter 3

METHODOLOGY

3.1 INTRODUCTION

This chapter gives information about the materials, equipment and procedures engaged in conducting this study. Details of the optimum variables required in the formulation of MHNFs are provided. The experimental procedure of the stability, measurement of thermal properties and thermo-convection performance of MHNFs is highlighted. The development of models for the thermal properties and *Nu* of MHNFs is also discussed.

3.2 MATERIALS AND EQUIPMENT

3.2.1 Materials

NPs of Fe_2O_3 (98% purity; 20-30 nm diameter) and γ-Al_2O_3 (20-30 nm diameter) used in the study were procured from Nanostructured and Amorphous Materials Inc., Houston, Texas, USA, while those of functionalised MWCNT (length: 10-30 μm; inner diameter: 3-5 nm and outer diameter: 10-20 nm) were bought from MKnano Company, Ontario, Canada. Sodium dodecyl sulphate ($\geq$ 98.5% purity) and sodium dodecylbenzene sulfonate (technical grade) were used as surfactants and were sourced from Sigma-Aldrich, Germany. The reason for using surfactants was to improve the homogenisation of the NPs in the base fluids. Deionised water (DIW) was obtained in the laboratory, whereas ethylene glycol (EG) was purchased from Lasec (South Africa.) A rectangular test cell (120.8 mm (L) x 99.7 mm (B) x 113.2 mm (D)) made from acrylic was used as the cavity to contain the test samples. The polyurethane was used as an insulation material when performing the thermo-convection experiment. T-type thermocouples manufactured by Omega Engineering Inc., USA, were used to measure temperatures within and without the test cell. Glassware of volumetric flasks, beakers and conical flasks were also used in the study.

3.2.2 Equipment

A vernier caliper and a metre rule were used to determine the dimensions within and around the cavity. The NPs and surfactants used in this work were measured using a digital weighing balance (Radwag AS 220.R2). Sonication of mixtures of HNPs, surfactants and base fluids was carried out using Qsonica (Q-700; 700 W and 20 kHz). Water baths were used to maintain constant temperatures of the test samples (LAUDA ECO RE1225 and PR20R-30 Polyscience). Electrical conductivity meter (EUTECH Instrument (CON700)), ultraviolet (UV) visible spectrophotometer (Jenway; model 7315), TEMPOS thermal properties analyser (METER Group), vibro-viscometer (SV-10, A&D, Japan), flow meters (Burkert Type 8081), transmission electron microscope (JEOL JEM-2100F) and gaussmeter (5180 model, F.W. BELL, USA) were used to measure electrical conductivity, stability, thermal conductivity, viscosity, volumetric flow rates, morphology and magnetic strength respectively. A data logger (National Instrument; SCXI-1303) with 32 channels and a DC power supply (NIE, model: PS3020 with maximum 20 A and 30 V) were also used in the study. The accuracy of the equipment is provided in Appendix C.

3.3 MAGNETIC HYBRID NANOFLUID FORMULATION

A two-step process of nanofluid formulation was employed in the study. To formulate aqueous MWCNT-ferrofluid (AMF) and Al_2O_3-ferrofluid (AAF), HNPs of MWCNT (20 wt.%) and Fe_2O_3 (80 wt.%), and Al_2O_3 (25 wt.%) and Fe_2O_3 (75 wt.%) were suspended in DIW. The suspension of Al_2O_3 (25 wt.%) and Fe_2O_3 (75 wt.%) into 40 vol.%:60% vol.% mixture of EG-DIW was used to formulate bi-aqueous Al_2O_3-ferrofluid (BAAF). Depending on the type of MHNF to be formulated, the weights of respective NPs and surfactant involved and the volume of the base fluid-type required were measured using the digital weighing balance and volumetric cylinder respectively, based on Eq. 3.1. Sodium dodecyl sulphate (SDS) was found to be suitable for DIW as base fluid, whereas sodium dodecylbenzene sulfonate (SDBS) was observed to be appropriate for EG-DIW. Sonication of the mixture of

HNPs, surfactant and base fluid was conducted using an ultrasonicator (Qsonica). Prior to this step, the mixture contained in a beaker was immersed in a water bath (LAUDA ECO RE1225) and maintained at a constant temperature of 20 °C. This was to avoid build-up of heat, which could damage the NPs during the sonication process.

$$\varphi = \left(\frac{X_{Fe_2O_3}\left(\frac{M}{\rho}\right)_{Fe_2O_3} + X_{Al_2O_3/MWCNT}\left(\frac{M}{\rho}\right)_{Al_2O_3/MWCNT}}{X_{Fe_2O_3}\left(\frac{M}{\rho}\right)_{Fe_2O_3} + X_{Al_2O_3/MWCNT}\left(\frac{M}{\rho}\right)_{Al_2O_3/MWCNT} + \left(\frac{M}{\rho}\right)_{DIW/EG-DIW}} \right) \quad \textbf{3.1}$$

To formulate stable MHNFs, the sonication time (45 min – 300 min), amplitude (60% – 80%) and dispersion fraction (0.4 – 1.2 for AMF; 0.8 – 1.3 for BAAF; 0.5 – 1.2 for AAF) were optimised by measuring the electrical conductivity (EC) of MHNFs using the EC meter. One of the parameters (sonication time, amplitude and dispersion fraction) was varied while the remaining two were kept constant to optimise it through EC measurement. This was done for the three variables to optimise them. The turning point for the obtained EC values was identified as the optimum value, and this indicated the point of critical micelle concentration (CMC) [203]. Dispersion fraction is expressed in Eq. 3.2. Throughout the sonication period, the pulse was made to be active for 5 s and idled for 2 s. The optimal values obtained for the sonication time, dispersion fraction and amplitude were used to formulate the MHNFs for different volume concentrations (φ = 0.05 – 0.40 vol.% for AMF and BAAF and φ = 0.05 – 0.30 vol.% for AAF). For a specific type of MHNF, φ, percent weights of HNPs and volume of base fluid type were employed in Eq. (1) to estimate the weights of the HNPs that would be used to formulate the hybrid nanofluid. Volumes of 70 ml, 100 ml and 1 400 ml of different base fluids (DIW and EG-DIW) were used for the optimisation process, thermal properties measurement and thermo-convection experiment respectively. The weights of surfactants and HNPs used for formulating the MHNFs were estimated and are provided in Appendix A.

$$Dispersion\ fraction = \frac{weight\ of\ surfactant}{weight\ of\ binanoparticles} \quad 3.2$$

3.4 STABILITY AND MORPHOLOGY OF MAGNETIC HYBRID NANOFLUID

The UV visible spectrophotometer was used to measure the absorbance of the formulated MHNFs, which served as an indicator to monitor their stability [156]. Each test sample was measured for 50 h to ensure stability monitoring for a longer period compared with the duration of the experiment. Additionally, a visual examination of MHNF samples was conducted weekly for a month in order to provide a physical check of the stability of the samples. To check the morphology and size of the formulated MHNFs, a transmission electron microscope (TEM) was used.

3.5 EXPERIMENTAL SET-UP AND PROCEDURES

3.5.1 Thermophysical Properties of Magnetic Hybrid Nanofluid

A TEMPOS thermal properties analyser was used to measure κ of samples of AMF, BAAF, AAF, DIW and EG-DIW from 20 to 40 °C at an interval of 5 °C. The instrument was calibrated using standard glycerin supplied by the manufacturer. The κ of the glycerin was determined in triplicate at 20 °C, and the average (0.285 W/m K) was found to agree with κ (0.282 W/m K at 20 °C) of the glycerin provided by the manufacturer. Furthermore, the μ of samples of AMF, BAAF, AAF, DIW and EG-DIW was determined experimentally at the studied temperatures as that of κ using a vibro-viscometer. The viscometer was calibrated prior to its use and thereafter, the μ of DIW was measured from 20 to 40 °C. The obtained viscosities were compared with those provided in the literature [204] for DIW. They were found to agree well and is discussed in Chapter 5.

The β, C_p and ρ of AMF, BAAF and AAF were required for data reduction (described in Subsection 3.6), and these properties were estimated using empirical models that were modified for hybrid nanofluids because they were not measured experimentally. The empirical models for the properties are expressed in Eqs. 3.3 to 3.5 [201].

$$\rho_{MHNF} = \varphi_{Fe_2O_3}\rho_{Fe_2O_3} + \varphi_{Al_2O_3//MWCNT}\rho_{Al_2O_3/MWCNT} + (1 - \varphi_{MHNF})\rho_{DIW/EG-DIW} \quad 3.3$$

$$(\rho\beta)_{MHNF} = \varphi_{Fe_2O_3}(\rho\beta)_{Fe_2O_3} + \varphi_{Al_2O_3/MWCNT}(\rho\beta)_{Al_2O_3/MWCNT} + (1 - \varphi_{MHNF})(\rho\beta)_{DIW/EG-DIW} \quad 3.4$$

$$(\rho C_p)_{MHNF} = \varphi_{Fe_2O_3}(\rho C_p)_{Fe_2O_3} + \varphi_{Al_2O_3/MWCNT}(\rho C_p)_{Al_2O_3/MWCNT} + (1 - \varphi_{MHNF})(\rho C_p)_{DIW/EG-DIW} \quad 3.5$$

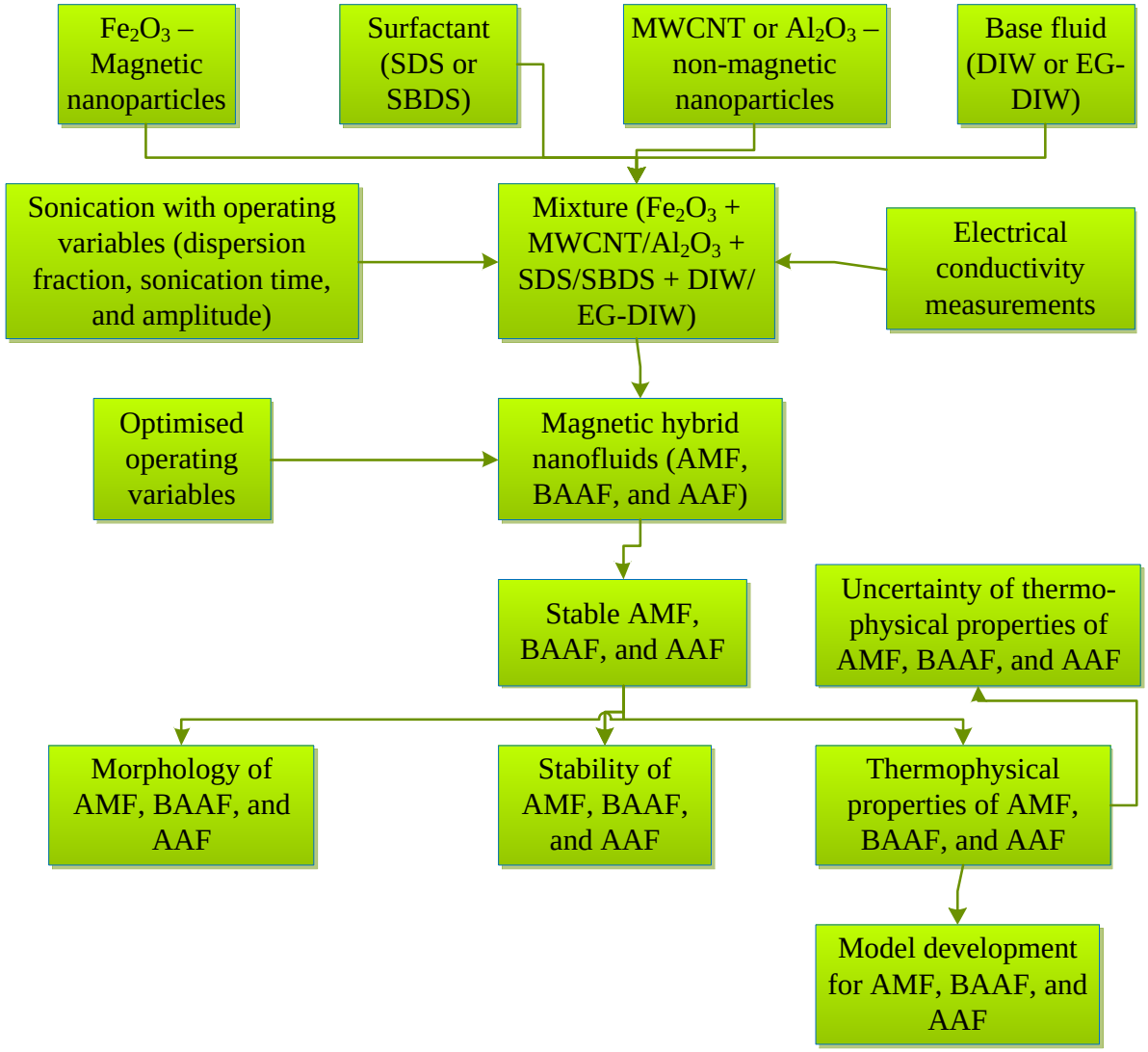

Figure 3.1: Flow chart of formulation, characterisation, measurements and model development of thermophysical properties of MHNFs.

Data from ASHRAE [205] for ρ and C_p of EG-DIW (40:60 vol.%) between 15 to 45 °C were obtained and used in the data reduction process. DIW and EG had β of 2.14 x 10^{-4} and 5.4 x

10^{-4} respectively, and that of EG-DIW was estimated to be 3.56 x 10^{-4}. Also, ρ and C_p data of DIW were sourced from the literature [204].

Enhancement (%) of the thermal properties (viscosity and thermal conductivity) of the MHNFs over the base fluids was estimated using Eqs. 3.6 and 3.7.

$$\mu_e(\%) = \left(\frac{\mu_{MHNF} - \mu_{DIW/EG-DIW}}{\mu_{DIW/EG-DIW}}\right) \times 100 \quad \textbf{3.6}$$

$$\kappa_e(\%) = \left(\frac{\kappa_{MHNF} - \kappa_{DIW/EG-DIW}}{\kappa_{DIW/EG-DIW}}\right) \times 100 \quad \textbf{3.7}$$

A flow chart of the entire process, which involved the formulation, characterisation, measurements and model development of thermophysical properties of MHNFs, is given in Fig. 3.1.

3.5.2 Thermo-convection of Magnetic Hybrid Nanofluid in Cavity

The study of the thermo-convection performance of MHNFs in a rectangular test cell was carried out without and with magnetic stimuli. Samples of AMF, BAAF, AFF, DIW and EG-DIW were charged into the test cell with two of its opposite sidewalls maintained at cold and hot temperatures, while the remaining sides were thermally insulated. The cold and hot sides of the test cell were kept between 15 to 50 °C to attain temperature gradients of 20, 25, 30 and 35 °C. The temperature gradients between the cold and hot sides of the cavity induced buoyancy within the samples contained in the cavity. Water baths (PR20R-30 Polyscience) and heat exchangers (isothermal counterflow shell-and-tube-type) were used to maintain the heated sides of the cavity at the prescribed temperatures. The water baths were connected by way of pipes to the heat exchangers (mounted on the heated sides) to maintain constant temperatures as pre-set for each water bath.

To measure the volumetric flow rates of the water circulated between the baths and heat exchangers, flow meters were mounted on the inlet pipes of the heat exchangers. A flow chart of this experiment is presented in Fig. 3.2. Temperatures within, outside and on the sides of

the cavity were measured using T-type thermocouples. The arrangement of the thermocouples in the cavity is shown in Fig. 3.3. Prior to the start of this experiment, the thermocouples were calibrated between temperatures of 15 to 55 °C at 2.5 °C intervals. Details of the calibration process and the estimation of the uncertainty associated with the thermocouples are presented in Appendices B and C. The thermocouples had an estimated uncertainty of 0.16 °C. It is worth mentioning that the cavity was well insulated inside a wooden box.

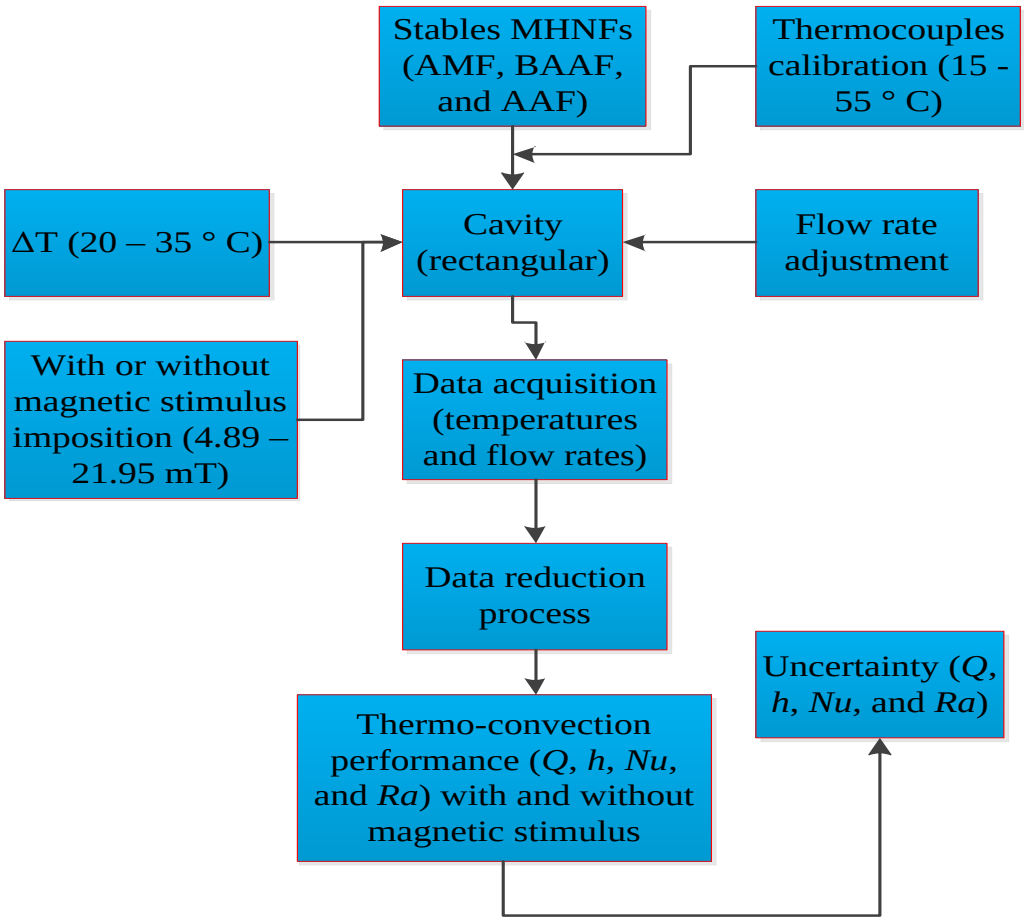

Figure 3.2: Flow chart of thermo-convection of MHNFs in a rectangular cavity.

After 50 min of charging each of the test samples into the cavity, the thermal stability of the samples was achieved. The flow rates of the water baths were regulated until the estimated heat transfer between the hot and cold sides of the cavity was within a maximum difference of 4%. Thereafter, measurements of temperatures and flow rates were acquired directly into a

personal computer already installed with a LABVIEW® software (2014 version) through a data logger (National Instrument; SCXI-1303).

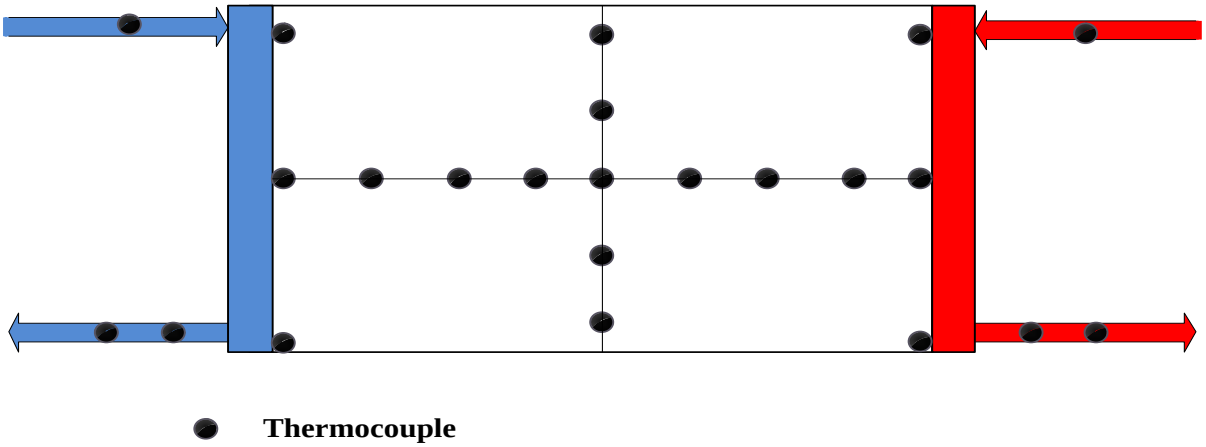

Figure 3.3: Arrangement of thermocouples in the cavity.

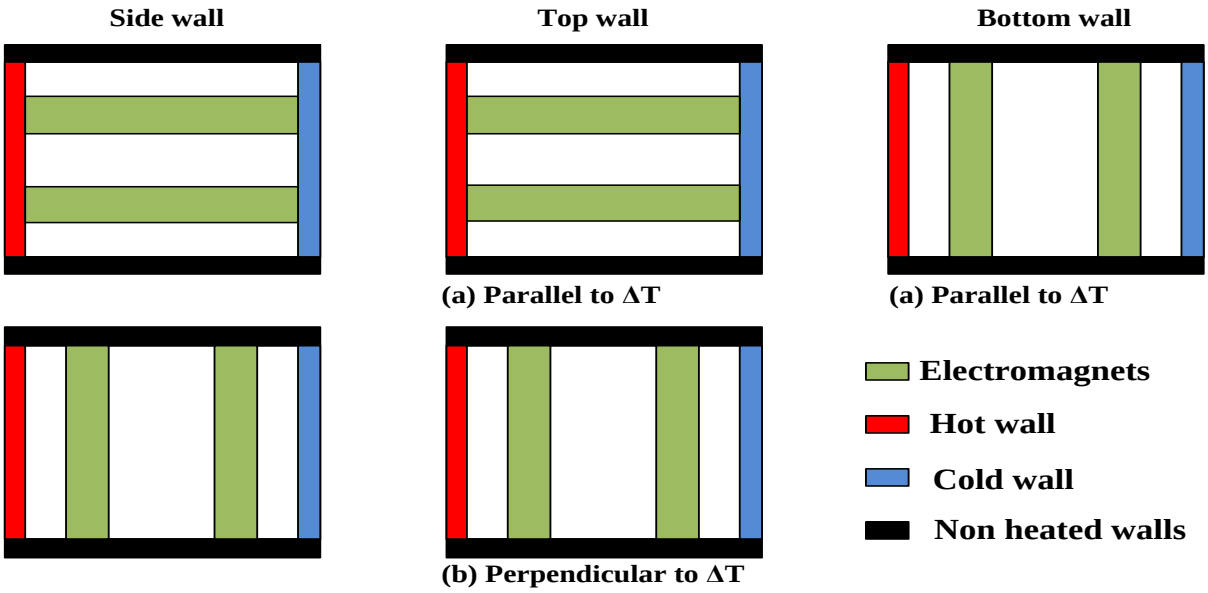

Figure 3.4: Different configurations of electromagnets on the cavity walls.

To investigate the thermo-convection of MHNFs in the rectangular cavity under the influence of magnetic stimuli, samples of AMF, BAAF and AFF with the maximum thermal transport performance were used. Two identical electromagnets (with uniform magnetic stimuli) were placed at the top, bottom and side of the cavity. For the top wall, the electromagnets were placed perpendicular and parallel to the direction of the temperature gradient, while they were

located perpendicular to the temperature gradient direction for the bottom wall. The electromagnets were mounted vertically and horizontally on the sidewall of the cavity. The configurations of the electromagnets on the cavity walls are shown in Fig. 3.4.

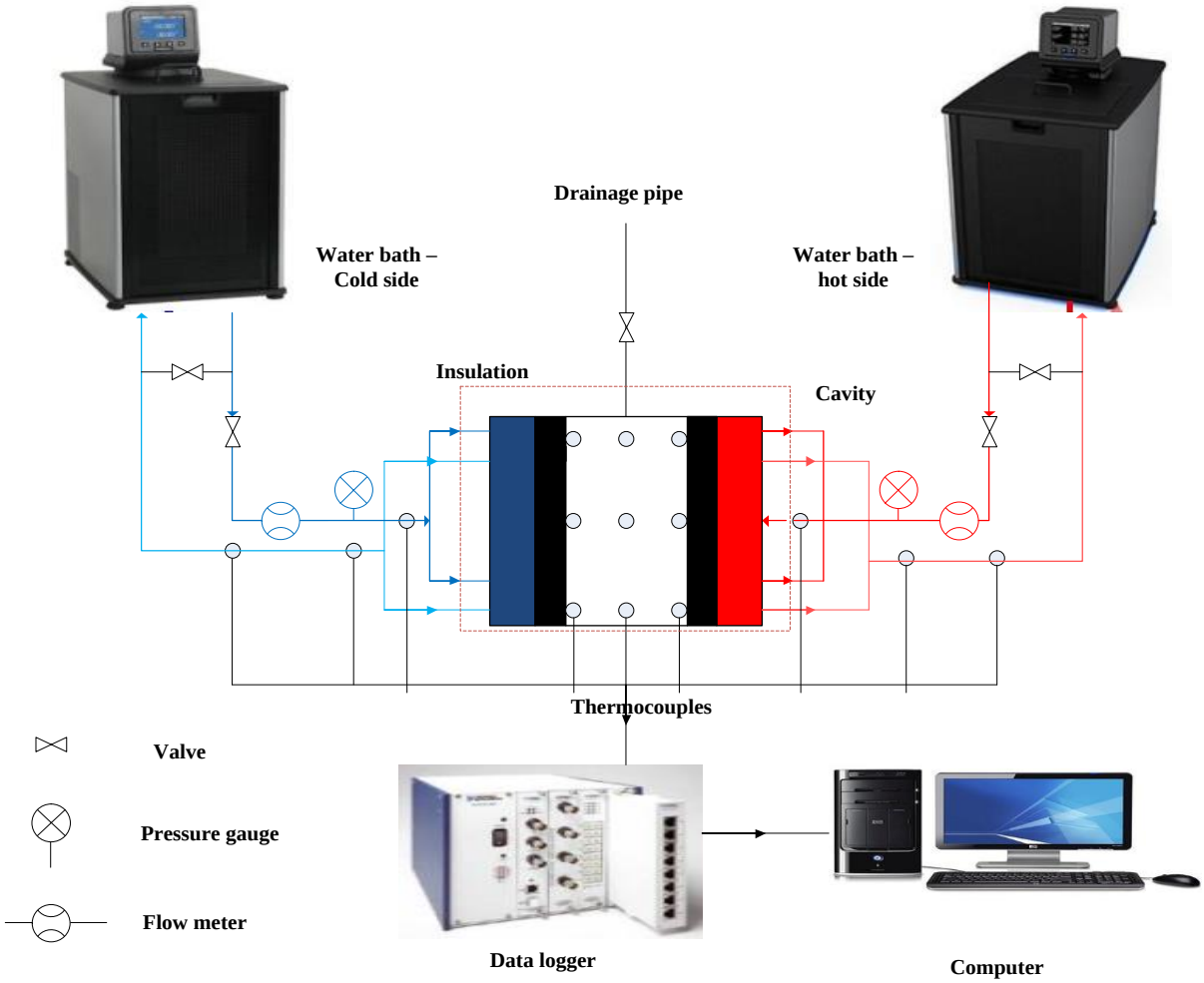

Figure 3.5: Set-up of the thermo-convection experiment.

When the electromagnets were connected to a DC power supply and the voltage knob adjusted, magnetic stimuli were generated as detected using a gaussmeter. As the voltage was increased with a corresponding increase in current, the magnetic stimuli were observed to intensify. An initial magnetic stimulus of 11.84 mT was imposed on the cavity walls, as earlier described. A time span of 10 min was allowed before the commencement of data acquisition. This duration of time was noticed to be most suitable as it allowed effective saturation of the magnetic stimuli and adequate fluid movement within the cavity.

Additionally, the magnetic stimuli imposed on the cavity walls were increased from 4.89 to 21.95 mT to investigate the influence of MHNFs on the thermo-convection performance. The experimental set-up is pictorially presented in Fig. 3.5.

3.6 DATA REDUCTION

The obtained data of the temperatures and flow rates for all test samples of AMF, BAAF, AFF, DIW and EG-DIW in addition to the measured (κ and μ) and estimated (β, C_p and ρ) thermal properties were used in the data reduction process. The data and thermal properties were reduced to *Nu*, *h*, *Q* and *Ra*. The rate of heat transfer between the baths and heat exchangers as the test samples contained in the cavity attained thermal stability was estimated using Eq. 3.8.

$$Q_{av_{(s)}}(W) = \dot{m}_w C_{p(w)} \Delta T \tag{3.8}$$

where

$$\Delta T = \left(T_i - \left(\frac{T_{o,1}+T_{o,2}}{2}\right)\right)_h = \left(\left(\frac{T_{o,1}+T_{o,2}}{2}\right) + T_i\right)_c \tag{3.9}$$

The h_{av}, Ra and Nu_{av} related to the thermo-convection of all test samples in the cavity were evaluated using Eqs. 3.10 – 3.12.

$$h_{av} = \frac{Q_{av}}{A(T_h - T_c)} \tag{3.10}$$

$$Ra = \frac{g\beta_s(T_h - T_c)(\rho_s)^2(C_{p_s})(L)^3}{\mu_s \kappa_s} \tag{3.11}$$

$$Nu_{av} = \frac{h_s L}{\kappa_s} \tag{3.12}$$

3.7 MODEL DEVELOPMENT

3.7.1 Thermophysical Properties

The emergence of hybrid nanofluids and the increasing study of their thermal properties have necessitated the development of models to predict these properties. Also, when AMF, BAAF and AFF were studied for the first time, there were no existing models in the literature that

could predict their κ_{eff} and μ_{eff} thus causing the need to develop new models for the thermal properties of these MHNFs.

3.7.2 Nusselt Number

Owing to the limited number of experimental studies on the thermo-convection performance of nanofluids in cavities and very few models developed from experimental data for the prediction of *Nu*, this study was prompted to develop models in this regard for the test samples (AMF, BAAF and AFF). Experimental data of Nu_{av} for AMF, BAAF and AFF were employed to develop models for predicting Nu_{av}. The margin of deviation (MOD) for the developed models is expressed using Eq. 3.13.

$$MOD\ (\%) = \left(\frac{V_{Exp.} - V_{Pred.}}{V_{Exp.}}\right) \times 100 \qquad \textbf{3.13}$$

3.8 CAVITY VALIDATION

Validation of the cavity was carried out by comparing Nu_{av} data of DIW and EG-DIW obtained in this work with those of *Nu* data estimated using empirical models sourced from the literature. The models proposed by Berkovsky and Polevikov [177], Leong et al. [206] and Cioni et al. [152] for the prediction of *Nu* of water in a cavity are expressed in Eqs. 3.14 to 3.16 respectively. Values of *Ra* and *Pr* for DIW and EG-DIW were substituted into Eqs. 3.14 to 3.16 to obtained *Nu*.

$$Nu = 0.18\left(\frac{Pr}{0.2+Pr}Ra\right)^{0.29} \ (Pr \leq 10^5;\ Ra \leq 10^{10};\ 1 \leq H/L \leq 10) \qquad \textbf{3.14}$$

where: $Pr = \frac{\mu C_p}{k}$

$$Nu = 0.08461Ra^{0.3125} \ (10^4 < Ra < 10^8) \qquad \textbf{3.15}$$

$$Nu = 0.145Ra^{0.292} \ (3.7 \text{ x } 10^8 \leq Ra \leq 7 \text{ x } 10^9) \qquad \textbf{3.16}$$

3.9 UNCERTAINTY ANALYSIS

3.9.1 Thermophysical Properties

The uncertainty associated with the measurements of the μ_{eff} and κ_{eff} of AMF, BAAF and AAF was estimated based on the method used by Adio et al. [64]. For the estimation of μ uncertainty, errors from the formulation (weights of HNPs and volumes of base fluids) of MHNFs, temperature and μ measurement were considered, whereas weights of HNPs, volumes of base fluids and κ measurement were error sources for the κ uncertainty (see Eqs. 3.17 and 3.19). The total uncertainty for κ and μ measurements was estimated using Eqs. 3.19 and 3.20 with the bias components expressed in Eqs. 3.16 and 3.17, and the precision components described in Eq. 3.18. The accuracy of the equipment is provided in Table 3.1. The accuracy of the applicable instruments and the obtained data for the viscosity and thermal conductivity of AMF, BAAF and AAF were substituted into Eqs. 3.17 to 3.21. Details of the uncertainty estimation are provided in Appendix C.

$$U_{b_\mu} = \sqrt{\frac{\Delta m}{m} + \frac{\Delta V}{V} + \frac{\Delta T}{T} + \frac{\Delta \mu}{\mu}} \quad \textbf{3.17}$$

$$U_{b_\kappa} = \sqrt{\frac{\Delta m}{m} + \frac{\Delta V}{V} + \frac{\Delta \kappa}{\kappa}} \quad \textbf{3.18}$$

$$U_{p_{\mu/\kappa}} = \pm(t_{v,p} \times SD_{\mu/\kappa}) \quad \textbf{3.19}$$

$$\delta\mu = U_\mu = \pm\sqrt{\left(U_{b_\mu}\right)^2 + \left(U_{p_\mu}\right)^2} \quad \textbf{3.20}$$

$$\delta\kappa = U_\kappa = \pm\sqrt{\left(U_{b_\kappa}\right)^2 + \left(U_{p_\kappa}\right)^2} \quad \textbf{3.21}$$

3.9.2 Thermo-convection

The uncertainty analysis of the thermo-convection performance of AMF, BAAF and AAF in a cavity was carried out to estimate the error associated with the obtained results. The uncertainty related to *Q*, *Nu* and *h* was estimated using the method reported in the work of Sharifpur et al. [153]. The primary sources of error were temperature and flow rate

measurements and were propagated using Eqs. 3.22 to 3.24. A detailed procedure of the estimated uncertainties is given in Appendix C.

$$\delta\dot{Q} = \left(\left(\frac{\partial\dot{Q}}{\partial\dot{m}}\delta\dot{m}\right)^2 + \left(\frac{\partial\dot{Q}}{\partial C_p}\delta C_p\right)^2 + \left(\frac{\partial\dot{Q}}{\partial T_h}\delta\Delta T\right)^2\right)^{\frac{1}{2}} \quad \textbf{3.22}$$

$$\delta h = \left(\left(\frac{\partial h}{\partial Q}\delta\dot{Q}\right)^2 + \left(\frac{\partial h}{\partial A}\delta A\right)^2 + \left(\frac{\partial h}{\partial T_h}\delta T_h\right)^2 + \left(\frac{\partial h}{\partial T_c}\delta T_c\right)^2\right)^{\frac{1}{2}} \quad \textbf{3.23}$$

$$\delta Nu = \left(\left(\frac{\partial Nu}{\partial h}\delta h\right)^2 + \left(\frac{\partial Nu}{\partial L}\delta L\right)^2 + \left(\frac{\partial\dot{N}u}{\partial\kappa}\delta\kappa\right)^2\right)^{\frac{1}{2}} \quad \textbf{3.24}$$

3.10 CONCLUSION

Details of materials, equipment, characterisation, measurements and experiments involved in this work were given in this chapter. The procedures for the formulation of MHNFs, measurements of thermal properties of MHNFs and the thermo-convection performance of MHNFs in the cavity (with and without magnetic stimuli) were provided. Furthermore, the development of models for the thermophysical properties and *Nu*, and the estimation of uncertainty for thermophysical properties and thermo-convection experiments were described in this chapter.

Chapter 4

FORMULATION, CHARACTERISATION AND STABILITY OF MAGNETIC HYBRID NANOFLUIDS

4.1 INTRODUCTION

This chapter marks the beginning of the presentation of the results obtained in this work. Results of the optimisation of parameters required for the formulation of MHNFs are presented. The morphology and sizes of the formulated AMF, BAAF and AAF were identified using TEM analysis. In addition, the stability of AMF, BAAF and AAF was monitored and reported.

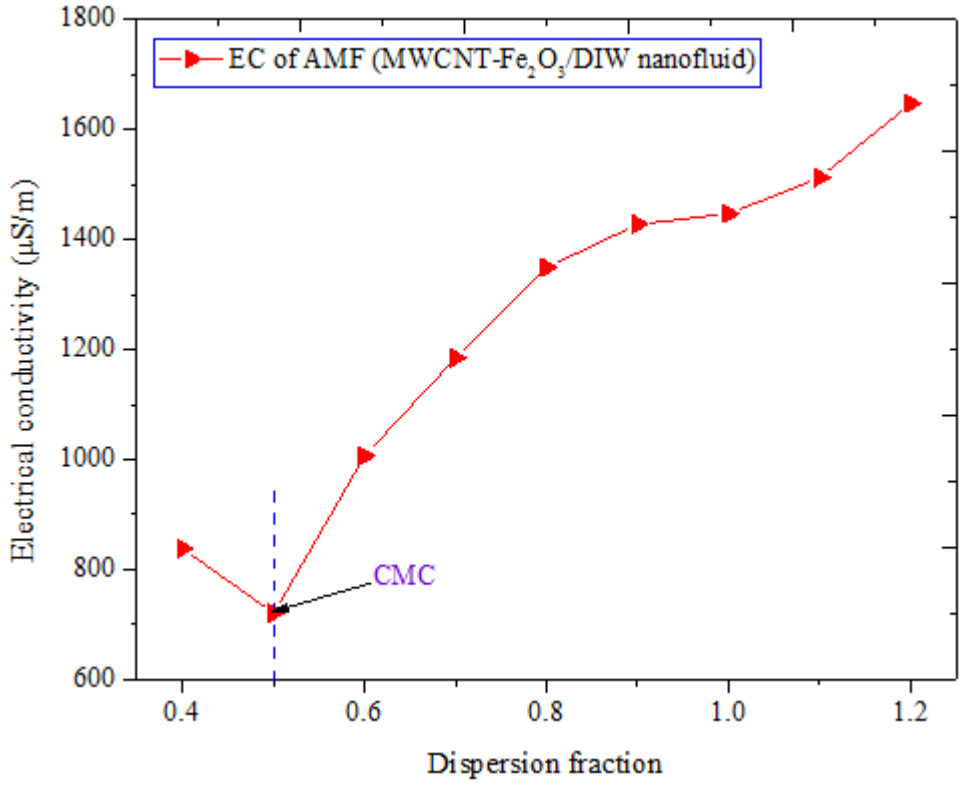

Figure 4.1: Determination of optimum dispersion fraction for AMF formulation.

4.2 FORMULATION OF MHNFs

4.2.1 Formulation of Aqueous MWCNT-Ferrofluid (AMF)

In the formulation of AMF, SDS was used as the surfactant. The weights of SDS, MWCNT NPs and Fe_2O_3 NPs used in the formulation of AMF are given in Appendix A. The three

operating parameters of dispersion fraction of AMF, sonication time and amplitude were optimised through the measurement of EC. Simply put, the CMC was achieved through the measurement of EC. The optimisation of the dispersion fraction of AMF is presented in Fig. 4.1. A reduction in dispersion fraction from 1.2 to 0.5 was noticed to cause a corresponding decrease in EC. A further drop in dispersion fraction (0.4) was observed to increase EC value above that recorded for the dispersion fraction of 0.5. The point (dispersion fraction value of 0.5) where the decreasing EC values increased was the optimal dispersion fraction value or CMC. Fig. 4.2 presents the optimal sonication time required for the formulation of AMF as determined using EC. The EC values were observed to increase with sonication time from 40 min to 120 min, after which EC of AMF decreased with sonication time. The point (sonication time) where the reduction in EC was noticed was the optimum sonication time or CMC.

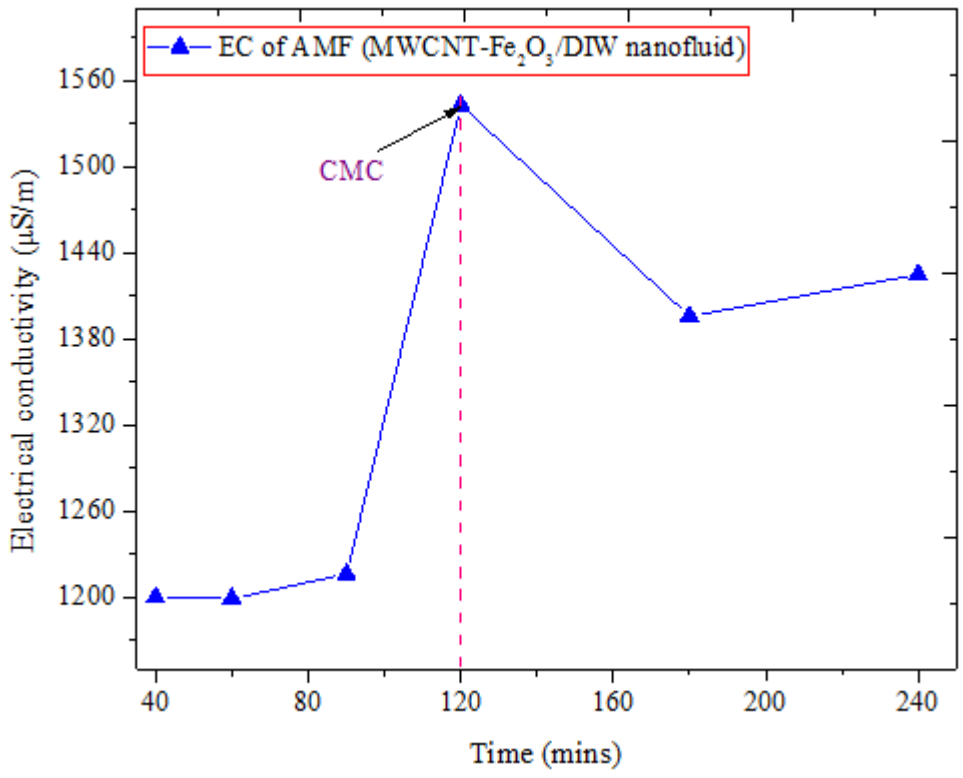

Figure 4.2: Determination of optimum sonication time for AMF formulation.

The amplitude of the sonicator was also optimised in the formulation of AMF. Fig. 4.3 indicates that the optimum amplitude for AMF formulation was 70%. The EC of AMF was noticed to enhance when the amplitude was increased from 60% to 70%, but EC was observed to decrease thereafter with a further increase in amplitude (80%). The obtained optimal values were used in the formulation of 1400 l of AMF for φ = 0.05, 0.1, 0.2, 0.3 and 0.4 vol.% using Eq. 3.1. For the measurement of thermal properties, 100 ml of 1 400 l of AMF was used and the rest engaged in the thermo-convection experiment.

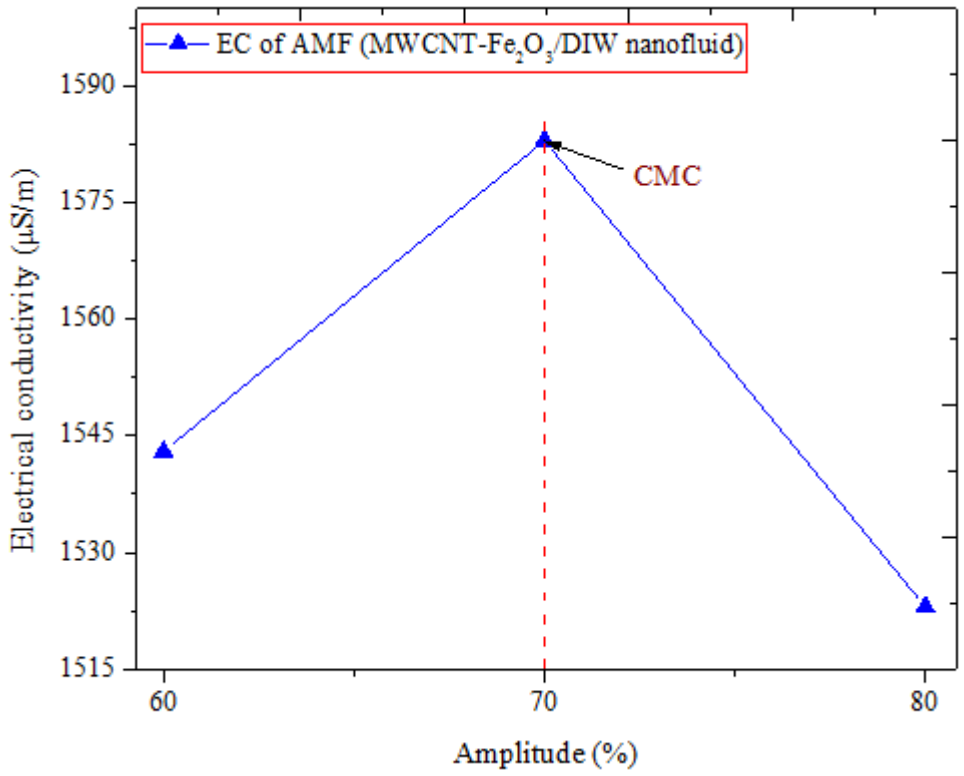

Figure 4.3: Determination of optimum amplitude for AMF formulation.

Garbadeen et al. [22] used gum Arabic (surfactant), sonication time of 40 min, amplitude of 75% and dispersion fraction of 4 to formulate MWCNT/DIW nanofluid, while Joshi and Pattamatta [162] using SDS formulated the same nanofluid using sonication time of 30 min and dispersion fraction of 1. Joubert et al. [88] used SDS, sonication time of 42 min, amplitude of 65% and dispersion fraction of 1 to formulate Fe_2O_3/DIW nanofluid. For hybrid nanofluids, Aghabozorg et al. [207] prepared Fe_2O_3-CNT/W nanofluid (without a surfactant)

using 3 h of sonication. Shahsavar et al. [107] used GA and produced Fe_3O_4-CNT/W nanofluid through stirring followed by 40 min of sonication. In addition, Sundar et al. [96] with a surfactant formulated CNT-Fe_3O_4/DIW nanofluid using 1 h. Comparing the optimal values of 120 min, 0.5 and 70% for sonication time, dispersion fraction and amplitude respectively, for AMF with previous works for mono and hybrid nanofluids, showed that the obtained optimal values were within ranges of published values.

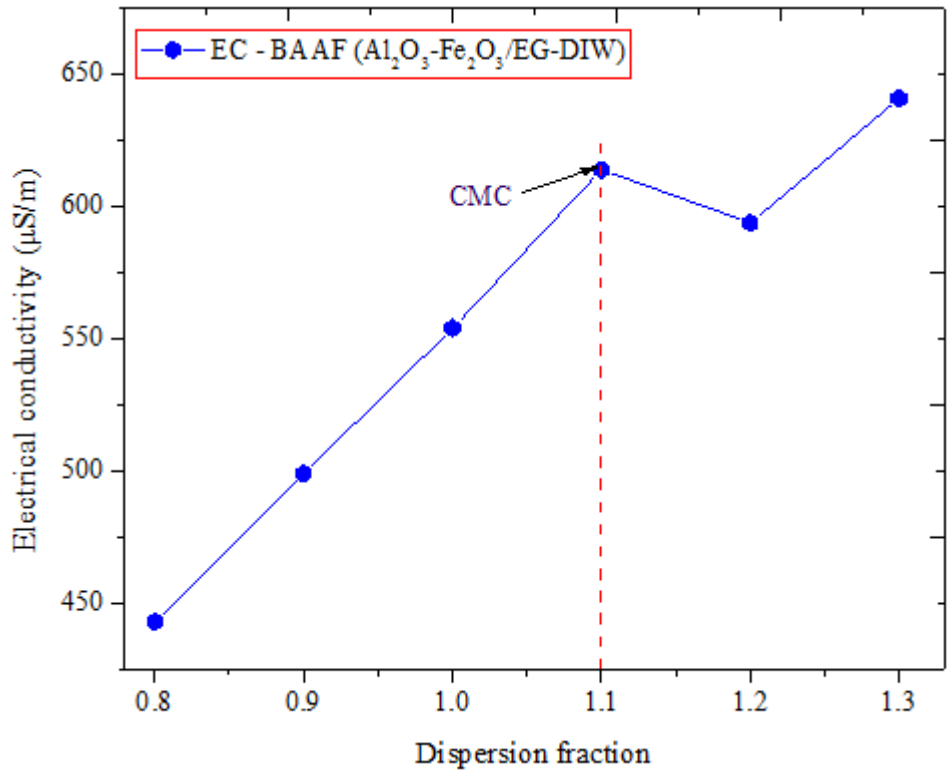

Figure 4.4: Determination of dispersion fraction for BAAF formulation.

4.2.2 Formulation of Bi-aqueous Al_2O_3-Ferrofluid (BAAF)

SDBS was used as the surfactant in the formulation of BAAF; the weights of HNPs and SDBS are provided in Appendix A. The optimisation of dispersion fraction, sonication amplitude and time as key parameters in the formulation of BAAF was carried out by measuring EC to achieve optimum value or CMC. Fig. 4.4 depicts the optimisation of the dispersion fraction of BAAF. The EC was observed to increase with increasing dispersion fraction from 0.8 to 1.1, increasing the dispersion fraction beyond 1.1 yielded reduction in

EC. The dispersion fraction value (1.1) resulting in a decrease in EC was the optimum or CMC. The sonication time was optimised, as displayed in Fig. 4.5. The EC increased from 45 min through to 120 min and thereafter decreased. The optimum sonication time (CMC) was 120 min, which was the point where increasing EC decreased.

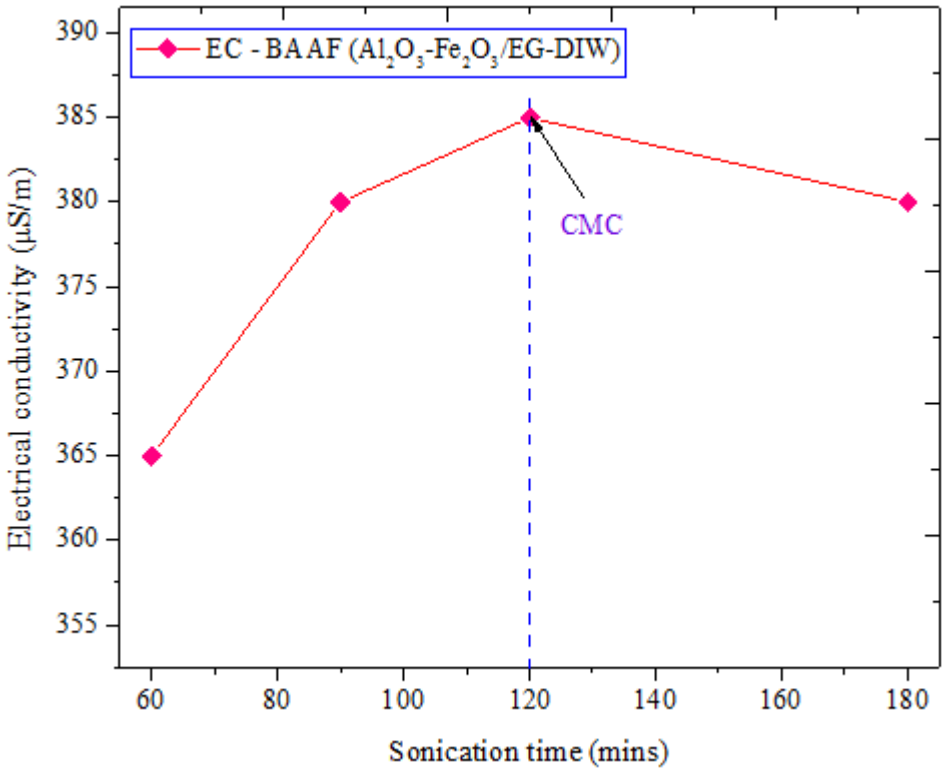

Figure 4.5: Determination of optimum sonication time for BAAF formulation.

Optimisation of the amplitude for the sonicator in the formulation of BAAF was conducted and is presented in Fig. 4.6. The amplitude of 70% was achieved as the optimal value. This is the point with the highest EC value, which was attained on increasing the amplitude from 60% to 70% and thereafter decreased when the amplitude was raised to 80%. The obtained optimum parameters were employed in formulating BAAF at φ = 0.05, 0.1, 0.2, 0.3 and 0.4 vol.%. A volume of 1 400 ml was formulated for each volume concentration with 100 ml used for the measurement of thermal properties and the rest was engaged in the experimental set-up involving thermo-convection.

Solomon et al. [177] sonicated for 40 min to formulate Al_2O_3/EG-DIW nanofluid, while Sarbolookzadeh et al. [109] produced MWCNTs-Fe_3O_4 (50:50)/EG nanofluid by stirring for 2 h and sonicating for 5.5 h. Also, Nadooshan et al. [100] prepared CNT-Fe_3O_4/EG nanofluid after stirring for 2.5 and sonicating for 6.5 h. Comparing the stirring and sonication times with those optimised for BAAF (2 h) showed that the sonication time used to prepare BAAF was within the range reported.

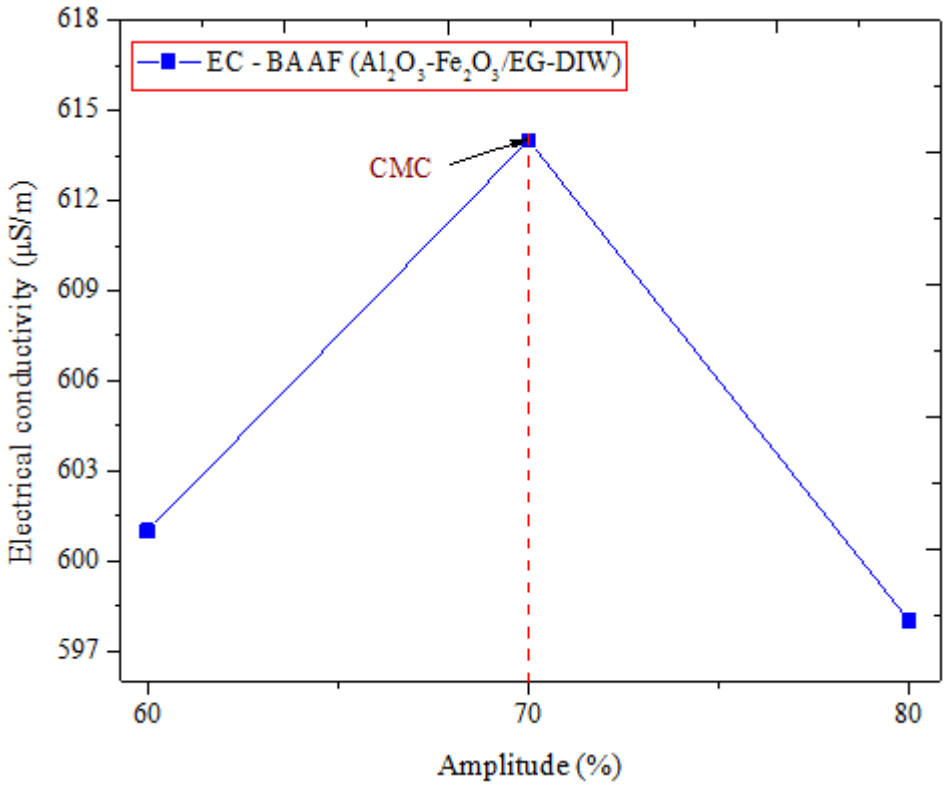

Figure 4.6: Determination of amplitude for BAAF formulation.

4.2.3 Formulation of Aqueous Al_2O_3-Ferrofluid (AAF)

SDS was used as a surfactant in formulating AAF. The weights of HNPs of Fe_2O_3 and Al_2O_3 and SDS used to formulate AAF are given in Appendix A. The dispersion fraction, sonication time and amplitude were optimised through EC measurement to promote the formulation of stable AFF from the use of SDS, HNPs of Al_2O_3 and Fe_2O_3 and DIW. Fig. 4.7 presents the optimisation of the dispersion fraction of AAF. It is obvious that EC values were enhanced with increasing dispersion fraction from 0.5 to 1.0. A drop in the EC of AAF was noticed

with a dispersion fraction of 1.1, thus indicating that the optimum dispersion fraction (or CMC) occurred at 1.0. From Fig. 4.8, it is apparent that the optimum sonication time was 120 min, as this point generally showed a significant reduction in EC or better still, a turning point in EC values when the sonication time was increased from 45 min to 300 min. In addition, Fig. 4.9 indicates that the optimum sonication amplitude was 70%. The EC was observed to increase with the rise in the amplitude from 60% to 70% and EC decreased on increasing the amplitude further to 80%. The optimum values achieved were used to formulate 1 400 ml of AFF at φ = 0.05, 0.1, 0.2, 0.3 and 0.4 vol.%.

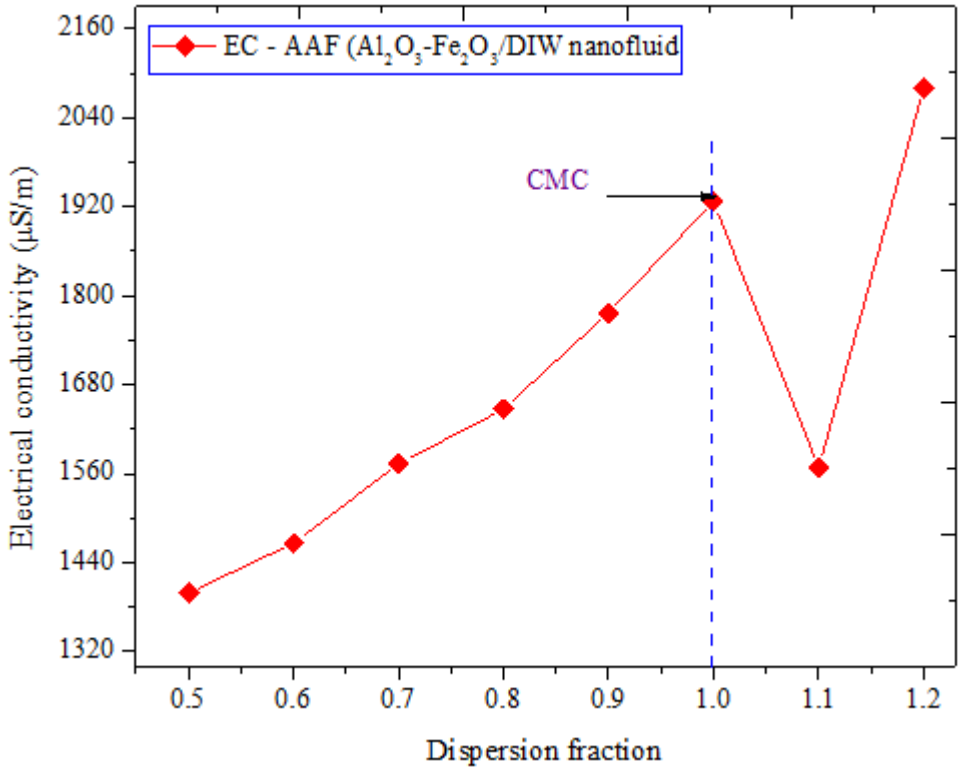

Figure 4.7: Determination of dispersion fraction for AAF formulation.

Sonication time and amplitude of 42 min and 65% respectively and dispersion fraction of 1 were engaged using SDS as a surfactant to formulate Fe_2O_3/DIW nanofluid [88]. However, 15 and 30 min of sonication were required to prepare Al_2O_3/W nanofluid using the same surfactant [151, 162]. In the work of Esfe et al. [128], it took 1 h of stirring and 7 h of sonication to formulate CNTs-Al_2O_3/W nanofluid, whereas it required 6 h of sonication for

Suresh et al. [82] to produce Al_2O_3-Cu (90:10)/W nanofluid using sodium lauryl sulphate as surfactant. Based on the reported sonication time and amplitude, it can be said that the optimised values of 70% (amplitude) and 120 min (sonication time) for BAAF were well within the range of published values.

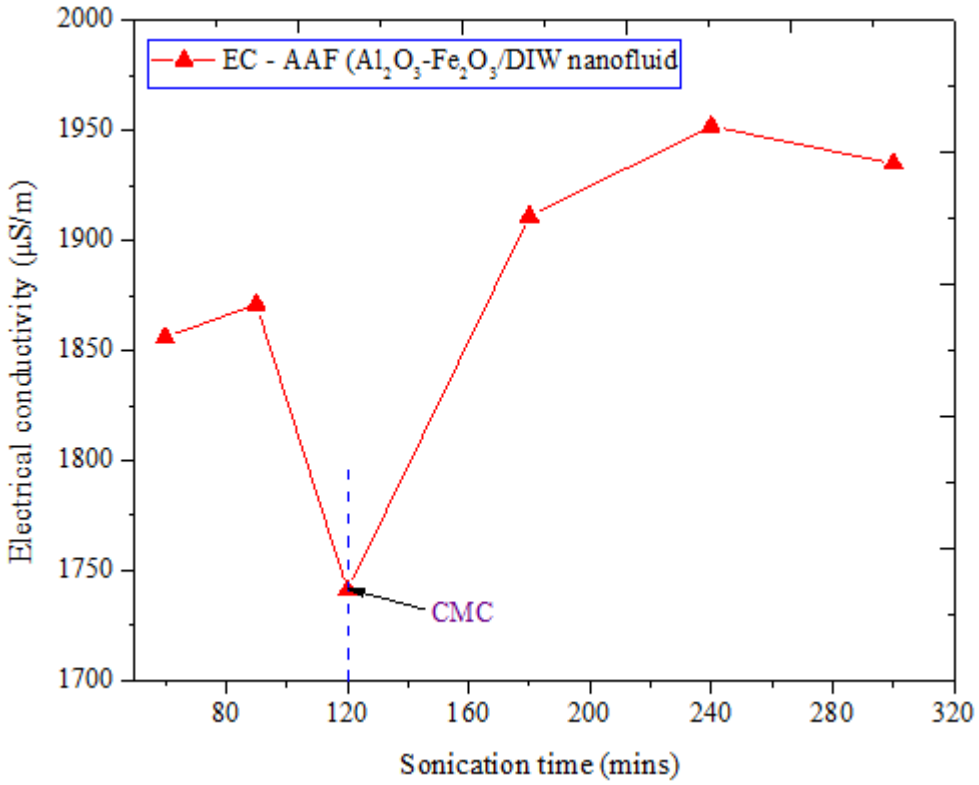

Figure 4.8: Determination of sonication time for AAF formulation.

4.3 CHARACTERISATION AND STABILITY OF MHNFs

4.3.1 Morphology and Stability of AMF

The TEM image of AMF at φ = 0.40 vol.% is presented in Fig. 4.10. The NPs of Fe_2O_3 and MWCNT that made up AMF were identified and were observed to be well suspended in DIW. MWCNT NPs were noticed to be tubular, whereas Fe_2O_3 NPs were spherical. These shapes agreed with those of previous studies [88, 195]. The distribution and amounts of the HNPs, as seen in Fig. 4.10, implied a good degree of stability and percent weights of NPs respectively, which were used in the formulation of AMF. At 100 nm nano-scale, TEM detected that the Fe_2O_3 NPs had sizes ranging from 23.21 nm to 35.31 nm, whereas MWCNT

NPs had outside diameters ranging from 4.35 nm to 18.19 nm. These were found to be about the same as the particle sizes specified by the manufacturers of the HNPs.

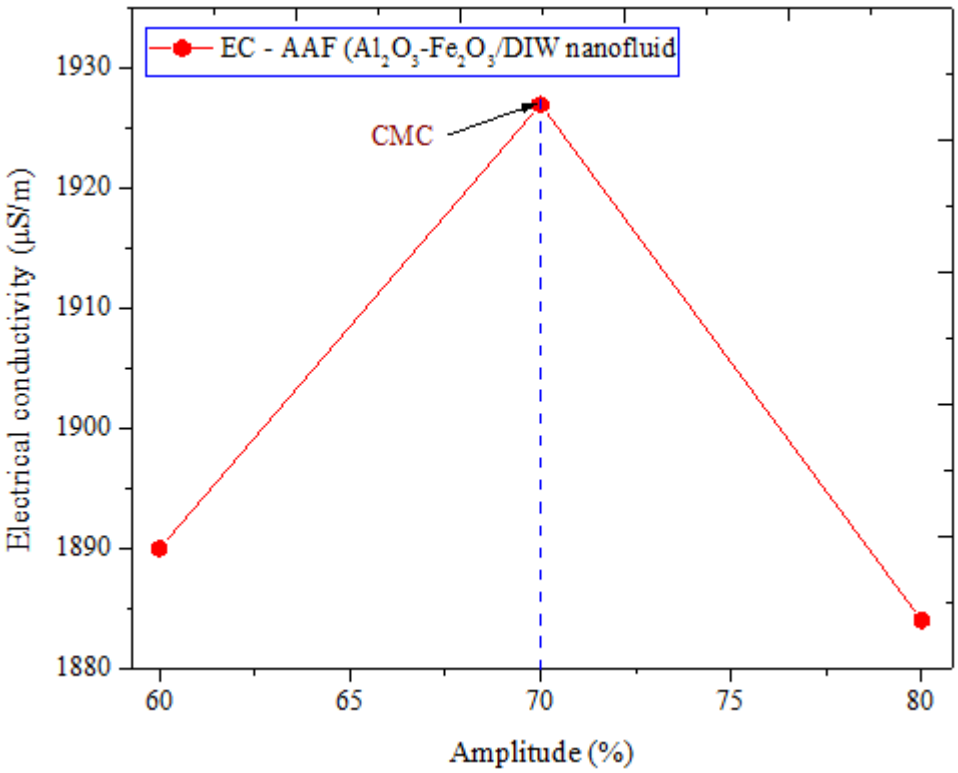

Figure 4.9: Determination of amplitude for AAF formulation.

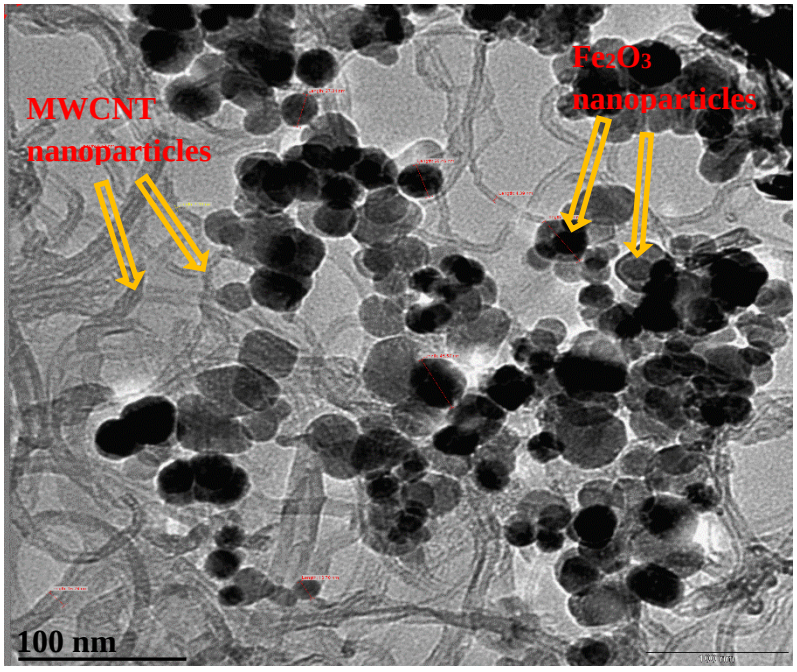

Figure 4.10: TEM image of AMF (φ = 0.40 vol.%).

To monitor the stability of AMF at φ = 0.05 to 0.40 vol.%, the absorbance was measured for 50 h using a UV visible spectrophotometer. The stability of AMF is displayed in Fig. 4.11. The absorbance of each sample was observed to be nearly constant (along with the horizontal) with time. This is an indication of the stability of the HNPs suspended in DIW over a time of 50 h and beyond. From Fig. 4.11, it can also be deduced that absorbance increased with an increase in φ. This observation was found to agree with published works [64, 208]. Absorbances of 1.631, 2.125, 2.341, 2.602 and 3.138 at a wavelength range of 289 nm to 292 nm were recorded for 0.05 vol.%, 0.10 vol.%, 0.30 vol.% and 0.40 vol.% respectively. The wavelengths of Al_2O_3/DIW, CNT/DW, Ag/DW and MWCNT-Ag (0.05:3.0

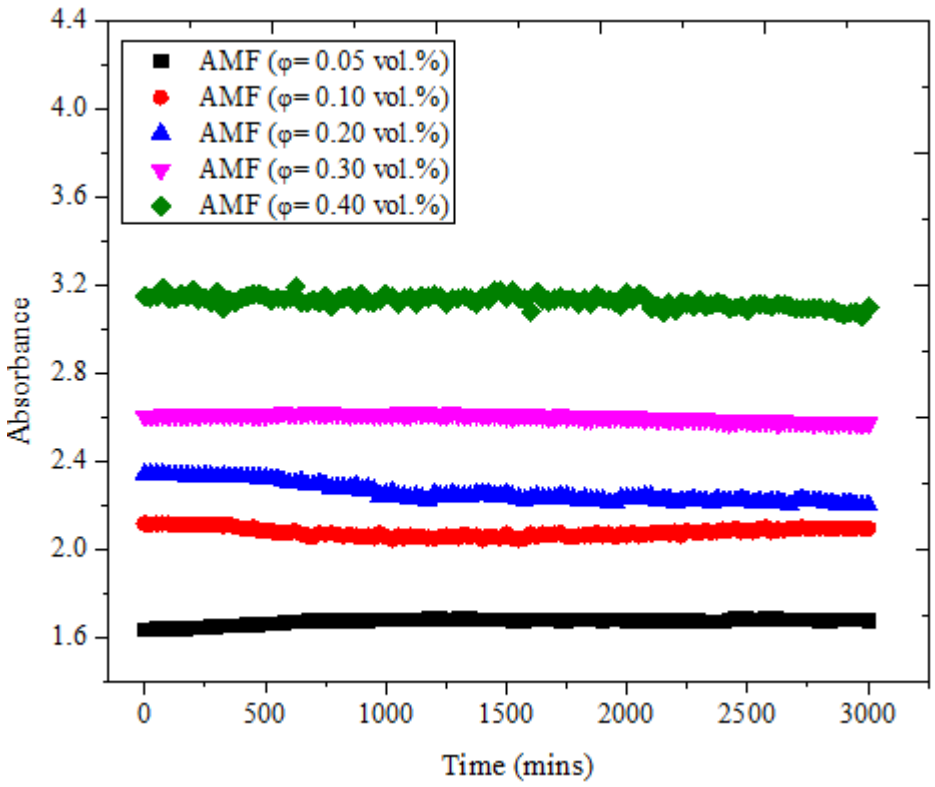

Figure 4.11: Stability of AMF samples over time.

wt.%)/W nanofluids were reported to be 225, 252, 410 and 264 nm respectively [54,72]. The wavelengths determined for AMF were noticed to be slightly higher than those of monoparticle nanofluids of Al_2O_3 and CNT. This can be attributed to the hybridisation of Fe_2O_3 and Al_2O_3 NPs in this work, as could be deduced for the case of MWCNT-Ag

(0.05:3.0 wt.%)/W nanofluid with a wavelength of 264 nm from 252 nm (CNT/DW nanofluid) and 410 nm (Ag/DW nanofluid). The visual inspection of AFM samples for a month showed no sedimentation, which further supported the stability of these samples.

4.3.2 Morphology and Stability of BAAF

The TEM image of BAAF at φ = 0.4 vol.% is provided in Fig. 4.12. Individual NPs of Fe_2O_3 (dark) and Al_2O_3 (light) were observed to be well suspended in the binary base fluid (EG-DIW). Both NPs were found to be spherical and this was consistent with the literature [84, 88]. As seen in Fig. 4.12, the HNPs were stable because they were evenly suspended in the base fluid. Also, their individual quantity in the figure reflected their percent weights. The TEM image of BAAF showed that the Fe_2O_3 and Al_2O_3 NPs had a size range of 16.60 nm to 35.31 nm and 20.50 nm to 34.99 nm respectively. These nano-sizes were noticed to be within the sizes specified by the manufacturers.

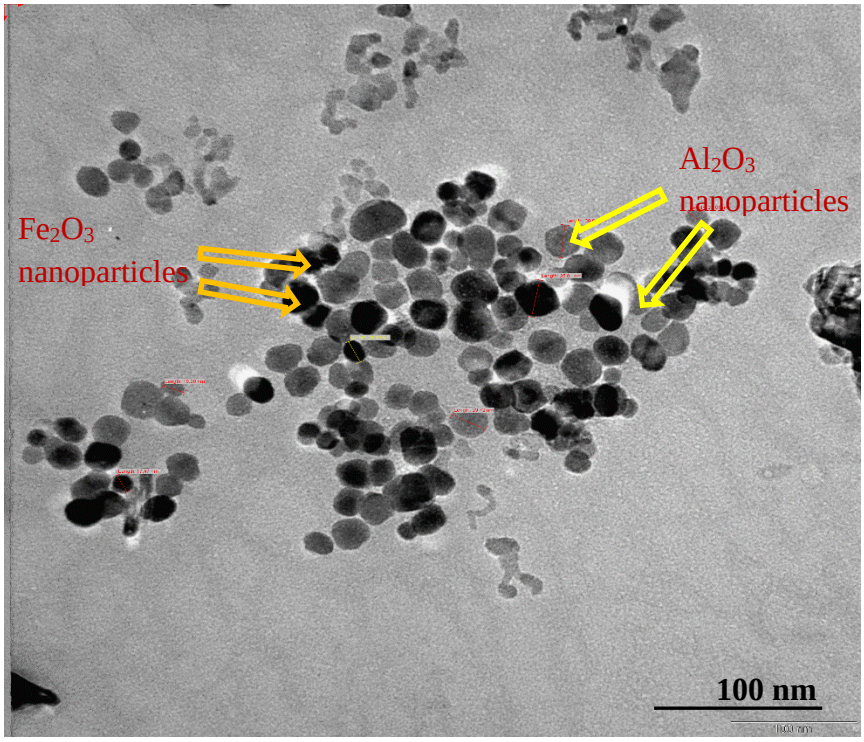

Figure 4.12: TEM image of BAAF (φ = 0.4 vol.%).

A plot of the absorbance of BAAF samples of 0.05, 0.10, 0.20, 0.30 and 0.4 vol.% against time is given in Fig. 4.13. The absorbance was measured as an indicator to monitor the

stability of BAAF over a time span of 50 h. The relatively straight-line trend of the absorbance for each BAAF sample represented good stability over the measured duration. For BAAF samples of 0.05, 0.10, 0.20, 0.30 and 0.40 vol.%, the measured absorbances were 1.628, 2.191, 2.696, 3.068 and 3.604 at a wavelength range of 289 to 299 nm respectively. With a wavelength of 225 nm reported for Al_2O_3 nanofluid [152], the slightly higher wavelengths obtained for BAAF could be linked to the hybridisation of Al_2O_3 NPs with Fe_2O_3 NPs. This finding agreed with the wavelength of 264 nm published for MWCNT-Ag/W nanofluid having an individual wavelength of 252 nm for CNT/DW nanofluid and 420 nm Ag/DW nanofluid [54]. Visual monitoring of BAAF samples for a month revealed that they were stable with no sedimentation.

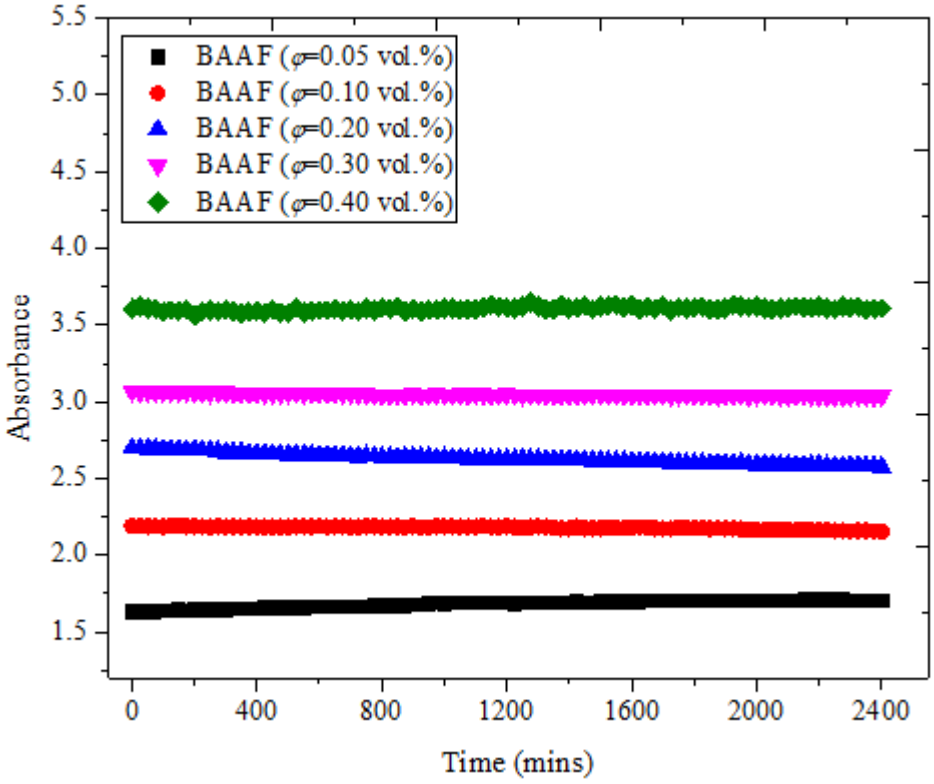

Figure 4.13: Stability of BAAF samples over time.

4.3.3 Morphology and Stability of AAF

An image from the TEM analysis of AAF for sample φ = 0.3 vol.% is shown in Fig. 4.14. Even dispersal of the HNPs into DIW, which connoted good stability, was observed. The

number of each NP displayed in the TEM image also corroborated the percent weight of each NP that was engaged in formulating the sample (0.3 vol.%). As earlier stated for BAAF in Subsection 4.3.2, the Fe_2O_3 and Al_2O_3 NPs were spherical with bright and dark appearances respectively, as can be seen in Fig. 4.14. Nano-size ranges of 20.50 nm to 34.99 nm (Al_2O_3 NPs) and 16.60 nm to 35.31 nm (Fe_2O_3 NPs) were detected with the aid of TEM.

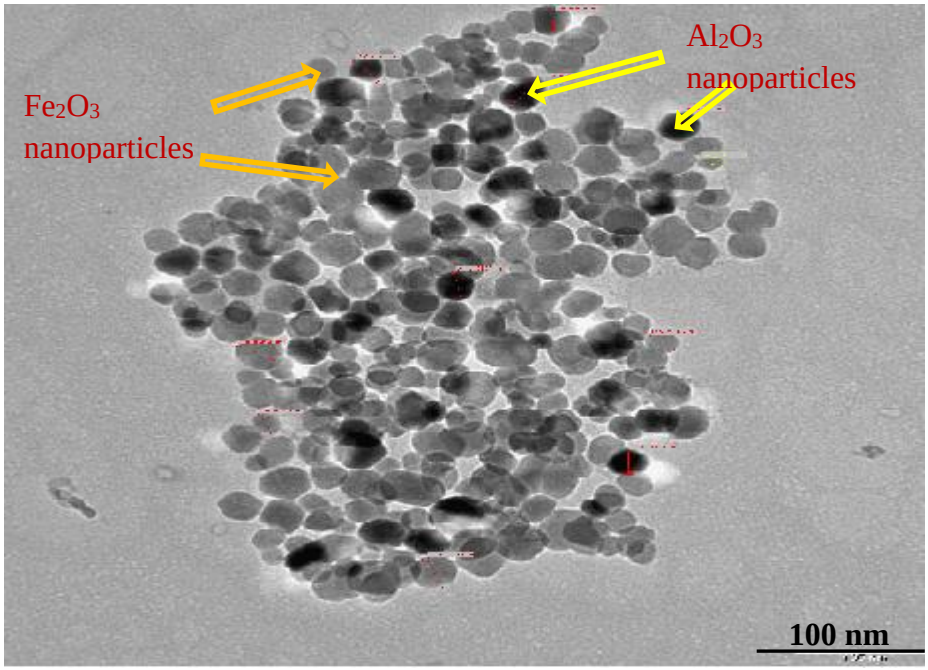

Figure 4.14: TEM image of AAF (φ = 0.3 vol.%).

In Fig. 4.15, the absorbance of AAF was deployed as an indicator to measure the stability. As displayed in Fig.4.15, the absorbance of AAF for φ = 0.05, 0.10, 0.20 and 0.30 vol.% was determined for a period of 50 h. For each AAF sample, the absorbance was noticed to be approximately a straight line, which showed that the sample was stable throughout the studied period and beyond. The absorbances of 2.385, 2.505, 2.804 and 3.186 were measured for φ = 0.05, 0.10, 0.20 and 0.30 vol.% respectively at a wavelength range of 289 to 296 nm. With Al_2O_3/DIW nanofluid reported to have peak absorbance at a wavelength of 225 nm [152], the use of HNPs to formulate AAF was noticed to increase the wavelength at which peak absorbance occurred. The difference observed between wavelengths of monoparticle

and hybrid nanofluids containing identical NPs was also reported by Kumar and Arasu [54], in which work Ag/W, MWCNT/W and MWCNT-Ag/W nanofluids had wavelengths of 410 nm, 252 nm and 264 nm respectively. This observation agreed with what was obtained in this work. Visual inspection of AAF samples also showed they were stable with no sedimentation noticed for a month.

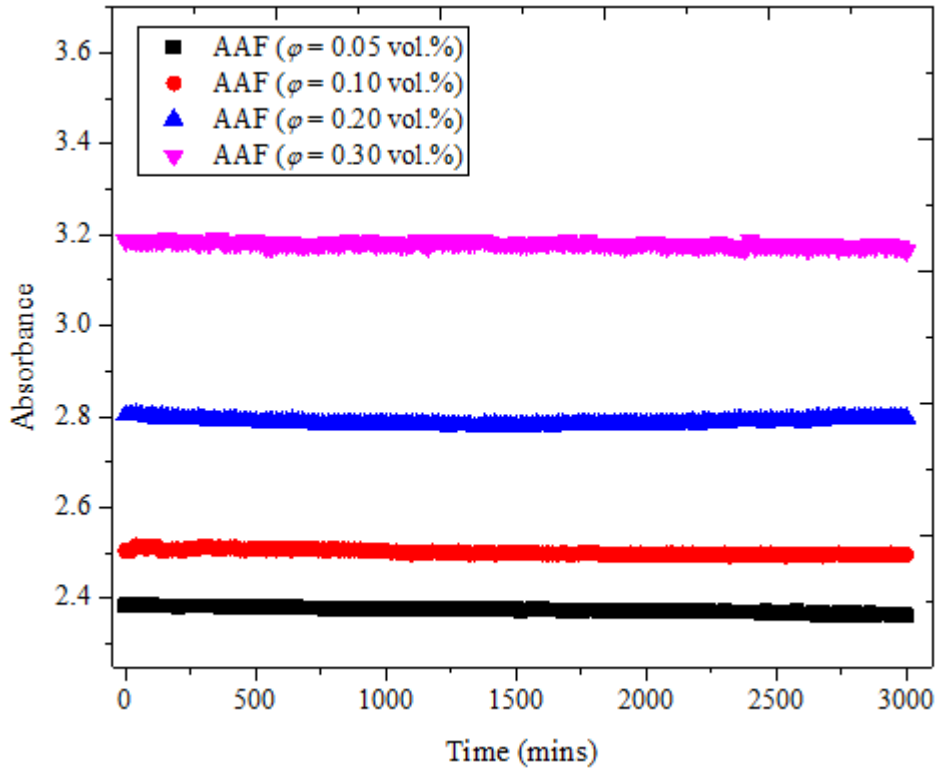

Figure 4.15: Stability of BAAF samples over time.

4.4 CONCLUSION

A review of the literature showed that comprehensive information on the specific values of dispersion fraction (using a surfactant), sonication time, amplitude and pulse used in formulating hybrid and monoparticle nanofluids was generally not provided [51]. Thus, reproducing the experiments to formulate monoparticle and hybrid nanofluids is not possible. In this work, the formulation of AMF, BAAF and AAF at various φ values through operating parameters leading to the attainment of stable MHNFs was optimised by way of EC measurement. The even dispersal of the HNPs into the base fluids identified by TEM images

revealed good stability of MHNFs. The sizes of the HNPs determined using TEM were found to be close to those provided by the manufacturers. Additionally, the stability of AMF, BAAF and AAF as monitored by the absorbance was observed to be stable; hence the experiments involving their thermal properties and thermo-convection (in the presence and absence of magnetic stimuli) were carried out and the findings are presented and discussed in subsequent chapters.

Chapter 5

THERMOPHYSICAL PROPERTIES OF MAGNETIC HYBRID NANOFLUIDS AND MODEL DEVELOPMENT

5.1 INTRODUCTION

The determination of the thermophysical properties of monoparticle and hybrid nanofluids is of utmost importance. These properties serve as indicators for the potential application of the special fluids in various fields of study, especially in thermo-convection studies as carried out in this work. In this chapter, the thermophysical properties (μ_{eff} and κ_{eff}) of stable AMF, BAAF and AAF were measured at the temperatures and φ considered in this study, using the applicable equipment. Furthermore, models were developed for all the MHNFs using the measured data for μ_{eff} and κ_{eff}, because the models for hybrid nanofluids were scarce in the public domain.

5.2 EFFECTIVE THERMAL CONDUCTIVITY OF MHNFs

5.2.1 Effective Thermal Conductivity of AMF

A check on the thermal conductivity meter was carried out by comparing the measured κ of DIW and that obtained from an empirical model published in the literature [204] in order to ascertain the degree of accuracy of the κ values measured using the meter. Fig. 5.1 shows a comparison between the measured κ and the empirically obtained κ at temperatures of 20 to 40 °C. The κ values were observed to increase with a rise in temperature. For both data, an average deviation of 0.20% and an mean absolute error (MAE) of 1.87% were estimated. This revealed a good accuracy for the measured κ.

The κ_{eff} of AMF as a function of temperature and φ is provided in Fig. 5.2. Temperature and φ can be seen to have a positive effect on the κ_{eff} enhancement of AMF. The influence of temperature was observed to be higher than that of φ. It was observed that increasing temperature was higher than that of φ. It was observed that increasing temperature and φ

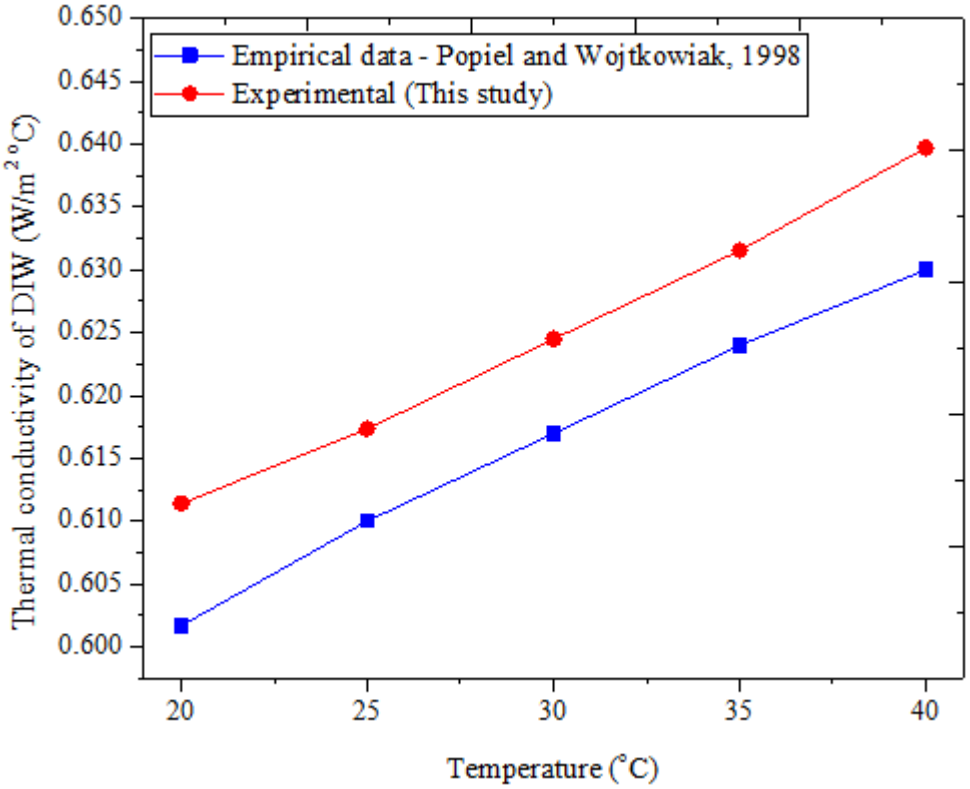

Figure 5.1: Comparison of empirical and measured thermal conductivity values of DIW.

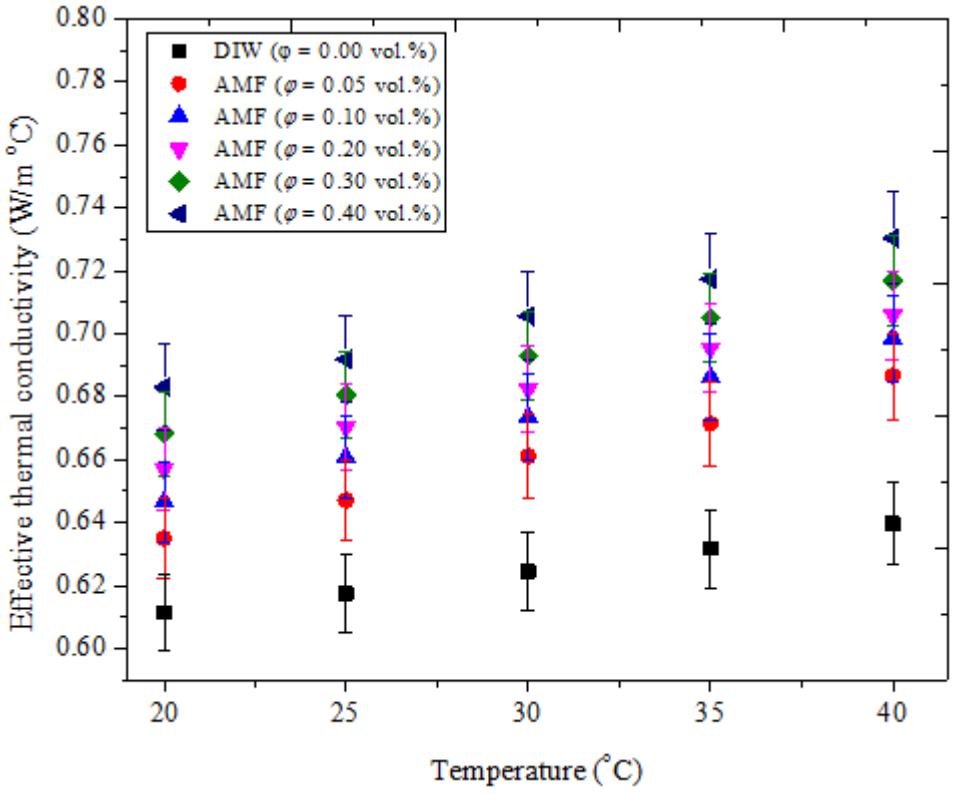

Figure 5.2: Effective thermal conductivity of AMF samples.

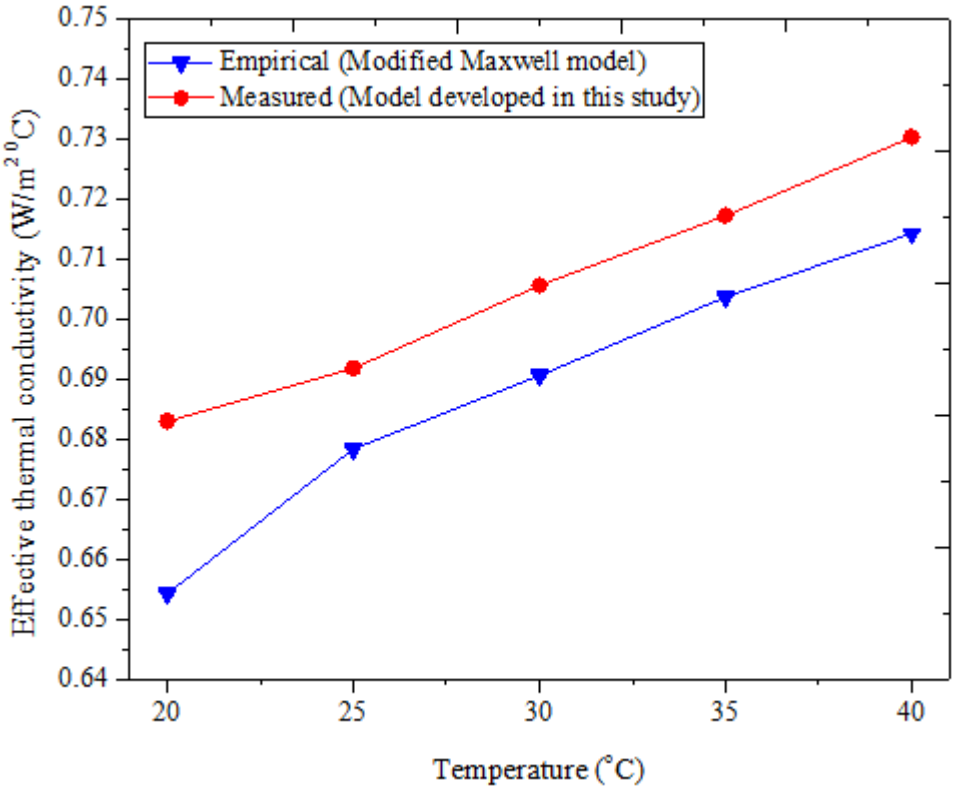

Figure 5.3: Comparison of measured and empirically derived effective thermal conductivity of AMF for φ = 0.40 vol.%.

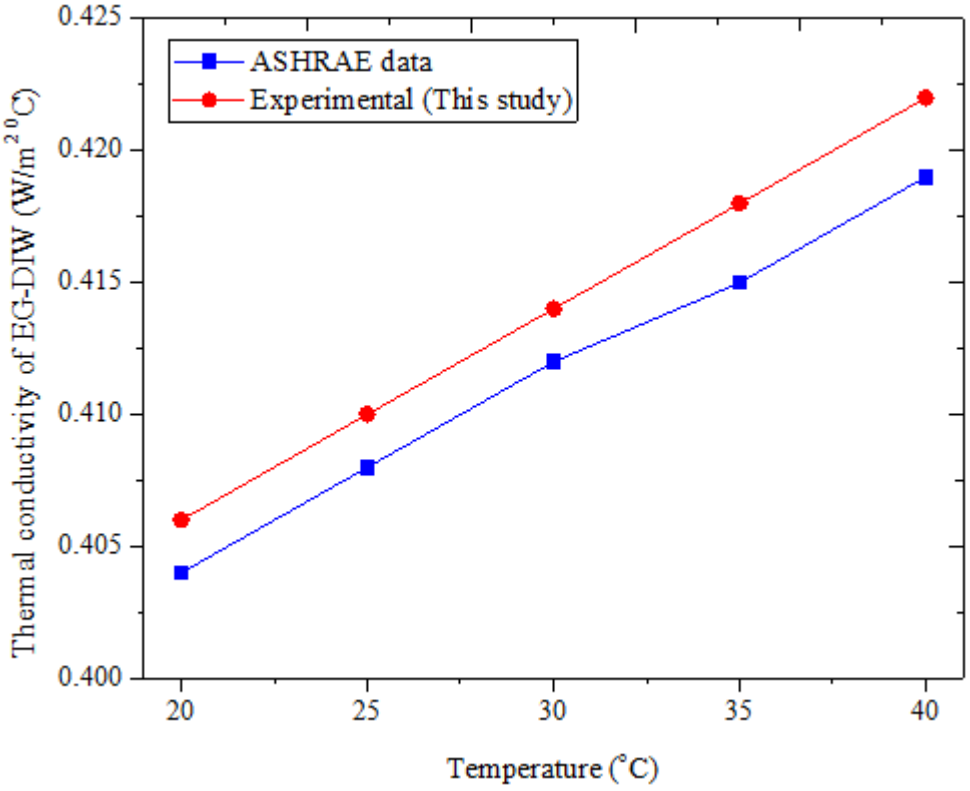

Figure 5.4: Comparison of ASHRAE data and measured thermal conductivity values of EG-DIW.

caused κ_{eff} to enhance and this observation agreed with previously published works [35, 99, 127]. Therefore, suspending Fe_2O_3 and MWCNT NPs into DIW was noticed to improve its κ as both NPs had higher κ values than those of DIW. At the temperature and φ ranges studied, the κ_{eff} of AMF was enhanced by 3.84% to 14.17% relative to κ of DIW. Chen et al. [73] reported that the κ_{eff} of MWCNT (0.05 wt.%)-Fe_2O_3 (0.02 wt.%)/W nanofluid was enhanced by 27.75% for φ = 2.0 vol.%, while Sundar et al. [127] published enhancements of 13.88% to 28.46% for MWCNT (0.26 wt.%)-Fe_3O_4 (0.74 wt.%)/DIW nanofluid at 0.3 vol.% and 20 to 60 °C relative to the base fluids. Enhancements of κ_{eff} by 17.8%, 15.75% and 36.26% were reported for water-based ND (0.72 wt.%)-Fe_3O_4 (0.28 wt.%) nanofluid (0.2 vol.% and 60 °C), ND-CO_3O_4 nanofluid (0.15 wt.% and 60 °C) and Fe_3O_4 (2.428 wt.%)-CNT (1.535 wt.%) nanofluid (1.0 vol.% and 55 °C) respectively compared with their base fluids, for different MHNFs [35, 95, 209]. The κ_{eff} enhancement of AMF was found to be within the range reported in the literature. Furthermore, Kumar and Sonawane [210] reported an enhancement of 6.7% for the κ_{eff} of Fe_2O_3/DIW nanofluid studied at φ = 1.0 – 8.0 vol.% and 30 to 50 °C. A comparison of the κ_{eff} of AMF and that published for monoparticle Fe_2O_3/DIW nanofluid showed that the hybridisation of Fe_2O_3 with MWCNT yielded an increase in κ_{eff}. MWCNT NPs are known to possess significantly higher κ than that of Fe_2O_3 NPs. In addition, the uncertainty associated with the measured κ_{eff} of AMF was evaluated as 2.00% (Appendix C).

The non-availability of a model to predict the κ_{eff} of AMF prompted the development of such a model. The obtained data for the κ_{eff} of AMF at the temperatures and φ considered were employed to develop a model that could be used to predict the κ_{eff} of AMF. The developed model was dependent on temperature and φ, and is expressed in Eq. 5.1. The prediction performance was 98.97% with MAE of 1.40%, MSE of 0.1318, RSME of 0.0107, and MOD of 3.53 and -4.17.

$$\kappa_{AMF} = 2.487 \times 10^{-3} T + 0.1211\varphi + 0.5828 \quad \textbf{5.1}$$

The data for the measured and empirically derived [199] κ_{eff} of AMF were compared and it was observed that the empirical model underestimated the measured data. Fig. 5.3 shows that for φ = 0.40 vol.%, the κ_{eff} of AMF was higher when measured than evaluated using the empirical model. This finding agreed with the report of a previous work that studied the effect of experimental and empirical models on the thermomagnetic convection of nanofluids [211]. It is pertinent to mention that the empirical model, the modified Maxwell model, for the estimation of the κ_{eff} of HNFs was used for comparison purposes. Some of the limited studies on the numerical investigation of the thermo-convection of hybrid nanofluids in cavities used this empirical model for estimating the κ_{eff} of hybrid nanofluids [39, 196,1 97, 212]. The present work revealed that the measurement of the κ_{eff} of hybrid nanofluids was better than evaluating such from the empirical model because the estimated values were lower than the true values.

5.2.2 Effective Thermal Conductivity of BAAF

The κ of EG-DIW obtained experimentally was compared with those published by ASHRAE [205]. Fig. 5.4 presents a comparison of both data at the studied temperatures. The measured data were noticed to be higher than the estimated with MAE of 1.55% and an average deviation of 0.34%. The κ of EG-DIW, as given in Fig. 5.4, was lower than that of DIW, as shown in Fig. 5.1, because DIW had a higher κ than EG and expectedly, the mixture of EG and DIW would have a lower κ value that DIW. The κ_{eff} of BAAF and κ of EG-DIW at the temperatures and φ studied are presented in Fig. 5.5. The κ_{eff} of BAAF was higher than that of EG-DIW and this was due to the addition of HNPs (with higher κ) with increasing φ to the EG-DIW. Again, an increment in temperature and φ was observed to enhance the κ_{eff} of BAAF. This was found to be consistent with the literature regarding the direct effect of temperature and φ on the κ_{eff} of hybrid nanofluids [37, 58, 213].

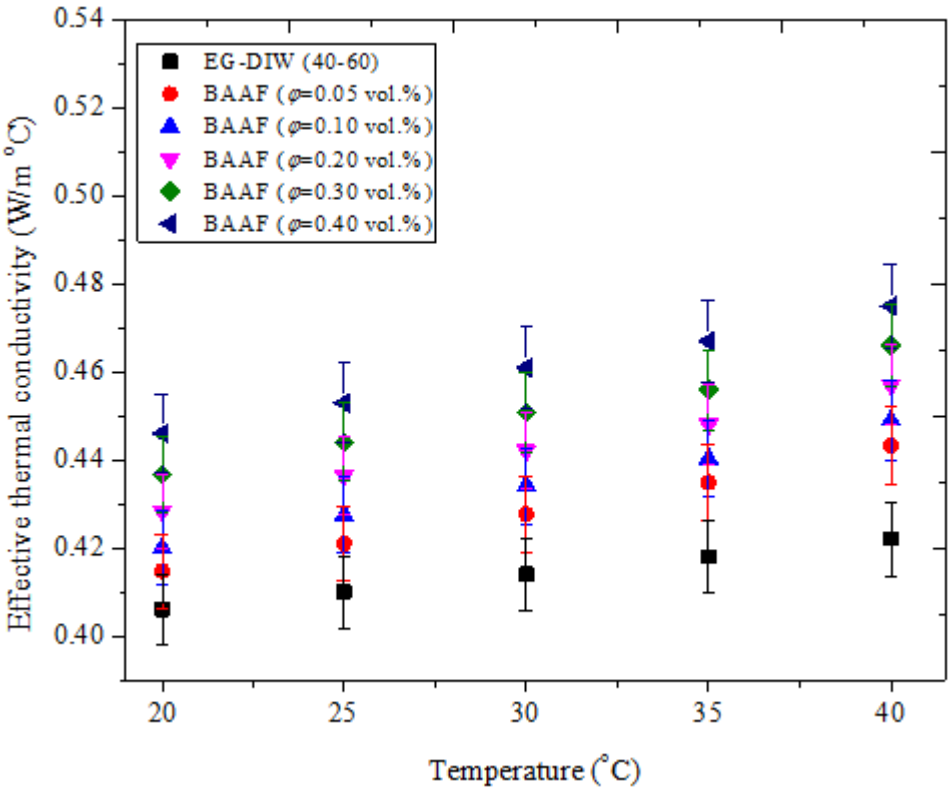

Figure 5.5: Effective thermal conductivity of BAAF samples.

The suspension of HNPs into EG-DIW under increasing temperature and φ was observed to enhance the κ of EG-DIW by 2.14% to 12.56%. Kakavandi et al. [58], Kannaiyan et al. [112], Sundar et al. [35] and Parsian and Akbari [98] published κ_{eff} enhancements of 33% (50 °C and 0.75 vol.%), 45% (60 °C at 2.0 vol.%), 5% to 13.6% (20 – 60 °C at 0.20 vol.%) and 28% (50 °C at 2.0 vol.%) for MWCNT-SiC (50:50)/W-EG (50:50), Al_2O_3-CuO/EG-W (20:80), ND-Fe_3O_4/EG-DW (40:60) and Al_2O_3-Cu (50:50)/EG nanofluids respectively in relation to the base fluids. It can be noticed that the κ_{eff} enhancement obtained for BAAF was within the range reported by previous studies. In addition, Pastoriza-Gallego et al. [69] investigated the κ_{eff} of EG-based Fe_2O_3 and Fe_3O_4 nanofluids at volume fractions of 0.1 to 0.69 and 10 to 60 °C. They found enhancements of 2% to 15% and 1% to 11% for Fe_2O_3/EG and Fe_3O_4/EG nanofluids respectively. Kumar and Sonawane [210] reported 20.33% enhancement for Fe_2O_3/EG nanofluid at 1.0 to 8.0 vol.% and 30 to 50 °C. Hybridising Fe_2O_3 NPs with Al_2O_3

NPs improved the κ_{eff} of BAAF compared with that of Fe_2O_3/EG nanofluid. The uncertainty related to the measurement of κ_{eff} of BAAF was estimated to be 2.00%.

Owing to the lack of studies on the thermophysical properties of BAAF and a model to predict the κ_{eff} of BAAF, the experimental values of κ_{eff} for BAAF were fitted to formulate a model. The developed model is related to both the temperature and φ of the κ_{eff} of BAAF, and it is given as Eq. 5.2. This model can effectively predict the κ_{eff} of BAAF with MAE of 1.22%, MSE of 0.1756, RMSE of 0.0090 and MOD of -2.48% and 2.77%.

$$\kappa_{BAAF} = 1.415 \times 10^{-3}T + 8.939 \times 10^{-2}\varphi + 0.3924 \quad (R^2 > 0.98) \qquad \textbf{5.2}$$

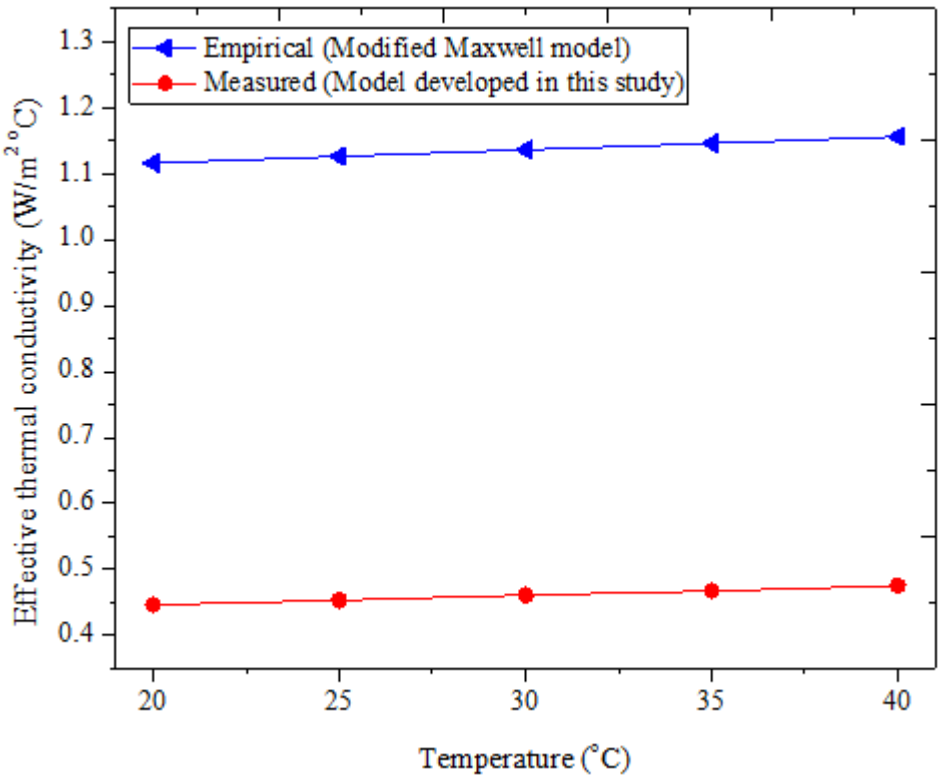

Figure 5.6: Comparison of measured and empirically derived effective thermal conductivity of BAAF for φ = 0.40 vol.%.

A comparison of the developed model with an empirical model (modified Maxwell model) for the prediction of the κ_{eff} of BAAF (φ = 0.40 vol.%), as presented in Fig. 5.6, showed that the obtained values for the latter underestimated those of the former. This was because the

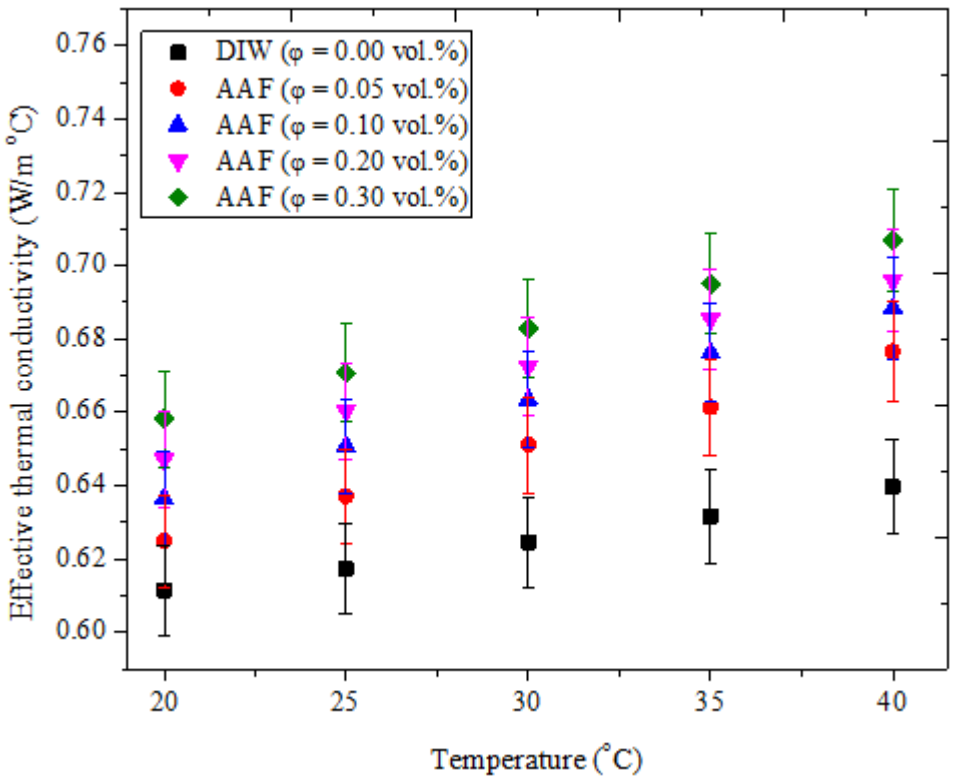

Figure 5.7: Effective thermal conductivity of AAF samples.

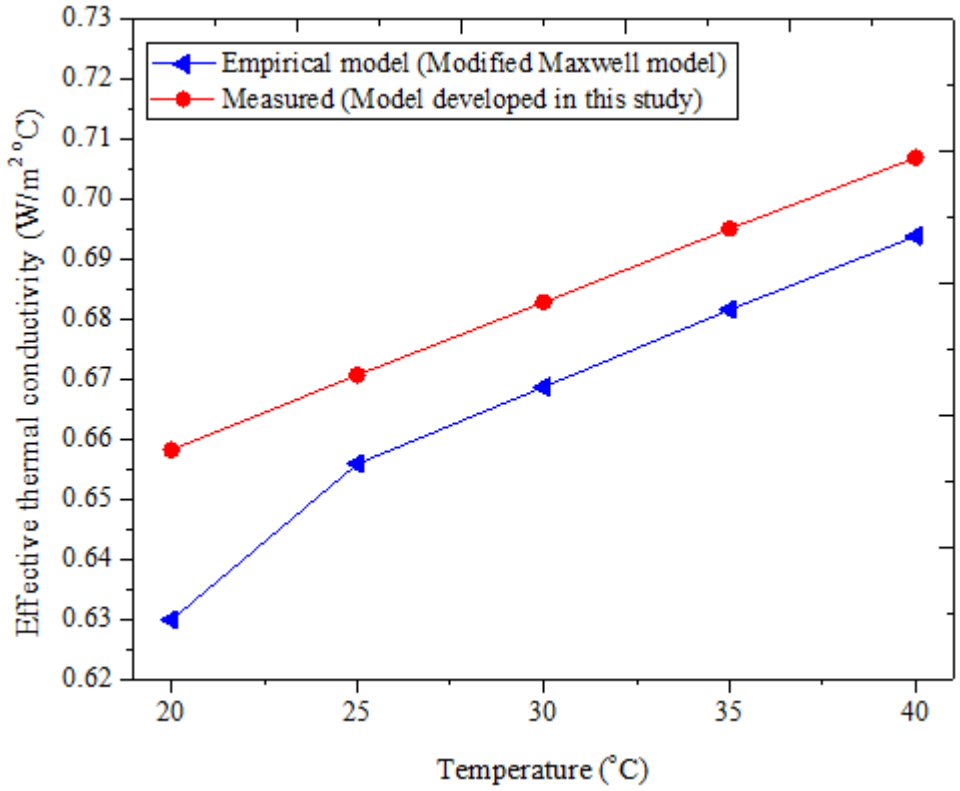

Figure 5.8: Comparison of measured and empirically derived effective thermal conductivity of AAF for φ = 0.30 vol.%.

empirical model was formulated using water as the base fluid and it was not determined experimentally.

Therefore, the use of the empirical model was not applicable to the estimation of the κ_{eff} of BAAF, which was corroborated by Astanina et al. [211], who recommended the use of measured data for the data reduction process involving thermo-convection studies instead of empirically derived data.

5.2.3 Effective Thermal Conductivity of AAF

The κ of DIW and κ_{eff} of stable AAF as a function of temperature and φ are presented in Fig. 5.7. When the temperature of DIW and AAF was increased, κ and κ_{eff} were noticed to enhance with the latter having a higher value than the former. With the suspension of HNPs of Fe_2O_3 and Al_2O_3 into DIW, the κ of DIW was observed to increase. This enhancement was noticed to be a function of φ. It is apparent from Fig. 5.7 that both temperature and φ impacted the enhancement of κ_{eff}. This result was found to be consistent with the literature. The κ_{eff} of AAF recorded an enhancement of 2.21% to 10.51% in relation to κ for the temperature and φ considered in this work. In earlier studies by Esfe et al. [128], Suresh et al. [82] and Abbasi et al. [114], the κ_{eff} of CNT-Al_2O_3/W, Al_2O_3-Cu (90:10)/W, and Al_2O_3-MWCNT/DW nanofluids was enhanced by 18.0% (59 °C at 1.0 vol.%), 12.11% (32 °C at 2.0 vol.%) and 14.75% (1.0 vol.%) respectively relative to the base fluids. It is worth noting that 2.00% was the uncertainty estimated to be associated with the measurement of the κ_{eff} of AAF.

The scarcity of a model for the prediction of the κ_{eff} of AAF led to the fitting of the experimental data of κ_{eff} obtained for AAF. The developed model is expressed in Eq. 5.3 as a function of temperature and φ. The model had MAE of 1.22%, MSE of 0.0864, RMSE of 0.0066, and MOD of -4.25% and 3.88%.

$$\kappa_{AAF} = 2.508 \times 10^{-3} T + 0.1220\varphi + 0.5720 \qquad (R^2 > 98\%) \qquad 5.3$$

The developed model was compared with the empirical model (modified Maxwell model) for the prediction of the κ_{eff} of AAF at a concentration of 0.30 vol.%, as shown in Fig. 5.8. An underestimation of the property was observed, indicating the inability of the empirical model to accurately predict the κ_{eff} of AAF. This result is consistent with that earlier reported for the κ_{eff} of AMF in this work. In addition, the use of experimental data for the prediction of the thermal properties of hybrid and monoparticle nanofluids is preferred above empirical models for the study of natural convection heat transfer of monoparticle and hybrid nanofluids, according to Astanina et al. [211].

5.3 EFFECTIVE VISCOSITY OF MHNFs

5.3.1 Effective Viscosity of AMF

In Fig. 5.9, the measured μ of DIW was compared with that obtained from the literature [204]. Both data agreed with one another with an average deviation of 1.87% and an MAE of 0.74%. The dependence of the μ_{eff} of AMF and μ of DIW on φ and temperature is illustrated in Fig. 5.10. The μ of DIW was observed to increase as the HNPs of Fe_2O_3 and MWCNT were suspended into DIW, due to a higher ρ of HNPs relative to DIW. Thus, increasing φ of AMF from 0.05 to 0.40 vol.% resulted in the enhancement of μ of DIW. A temperature rise was found to lead to depreciation in μ of DIW and μ_{eff} of AMF. The combined effect of φ and temperature for AMF was noticed to enhance μ of DIW by 11.83% to 28.79%. The direct influence of φ and the inverse impact of temperature on the μ_{eff} of AMF was found to agree with the literature [56, 118]. On estimation (using φ and temperature considered in this work), the μ_{eff} of AMF was found to be lower than that reported for monoparticle nanofluids of Fe_2O_3/DW [88] and Fe_3O_4/DW [93]. The introduction of MWCNT NPs to Fe_2O_3 NPs for the formulation of AMF can be attributed to a reduction in μ_{eff}. Previous studies published μ_{eff} enhancements of 1.27-fold to 1.5-fold (0.3 vol.% at 20 – 60 °C), 16.65% to 23.24% (0.1 – 0.3 vol.% at 30 – 60 °C) and 6.45% (0.2 wt.% at 25 °C) for MWCNT (0.26 wt.%)-Fe_3O_4 (0.74 wt.%)/DIW, ND-Ni/DW and TiO_2-CNT/DW nanofluids [79, 127, 214] respectively, which

agreed with the results for AMF. Uncertainty of 2.84% was estimated to accrue to the measurement of μ_{eff} of AMF.

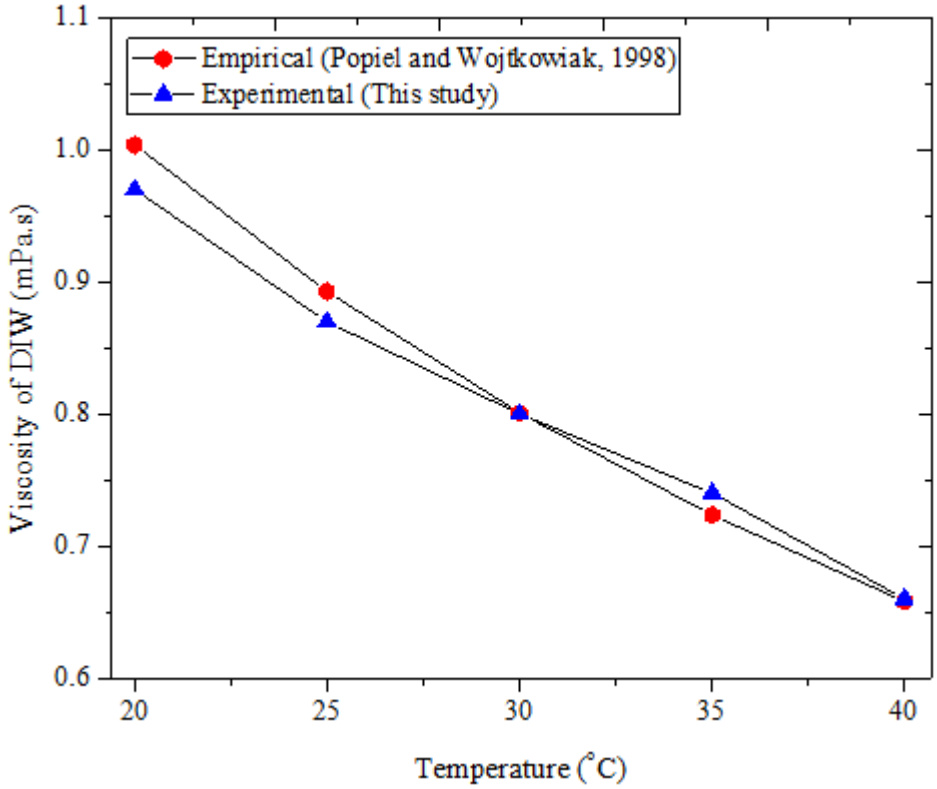

Figure 5.9: Comparison of empirical and measured viscosity values of DIW.

In the absence of a model for predicting the μ_{eff} of AMF, the experimental data as a function of φ and temperature were fitted to obtain a model. Therefore, Eq. 5.4 was developed with an MAE of 1.50%, MSE of 0.0294, RMSE of 0.0176, and MOD of 3.74% and -3.29%.

$$\mu_{AMF} = 0.3049\varphi - 1.5960 \times 10^{-2}T + 1.3588 \qquad (R^2 = 0.981) \qquad 5.4$$

5.3.2 Effective Viscosity of BAAF

In Fig. 5.11, the measured μ of EG-DIW and that obtained from ASHRAE data were compared. An average absolute deviation of 0.33% was estimated for both data. The measured data were noticed to be higher than the ASHRAE data, which agreed with the literature [215]. Expectedly, the μ of EG-DIW was higher than the μ of DIW, as can be seen Figs. 5.9 and 5.11, because the μ of EG was more than the μ of DIW. The μ of EG-DIW and

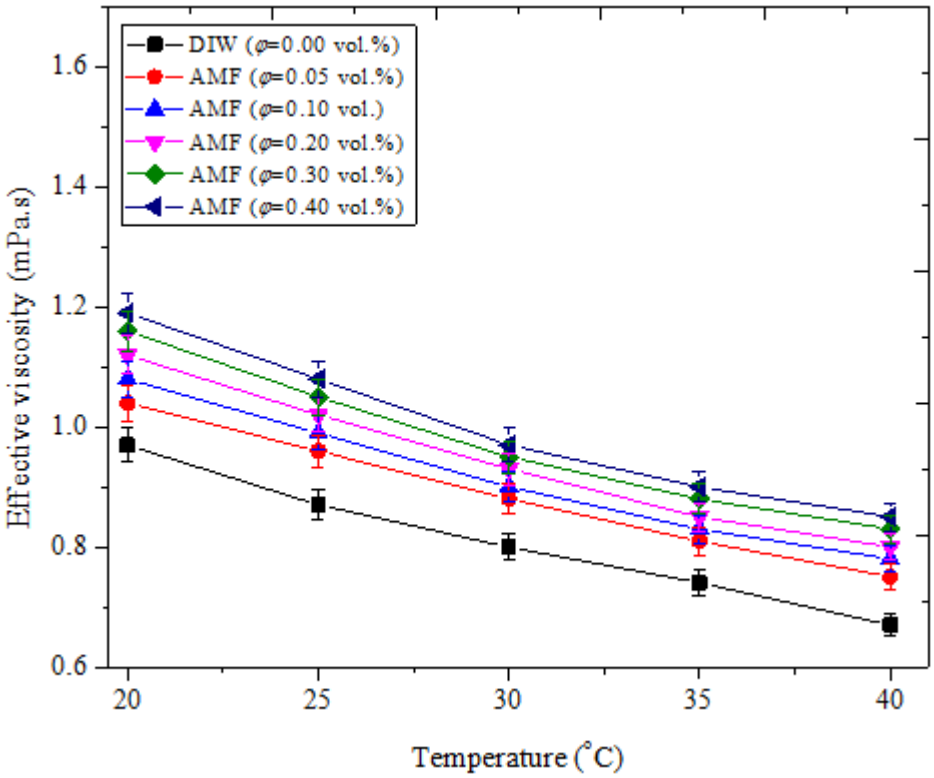

Figure 5.10: Effective viscosity of AMF samples.

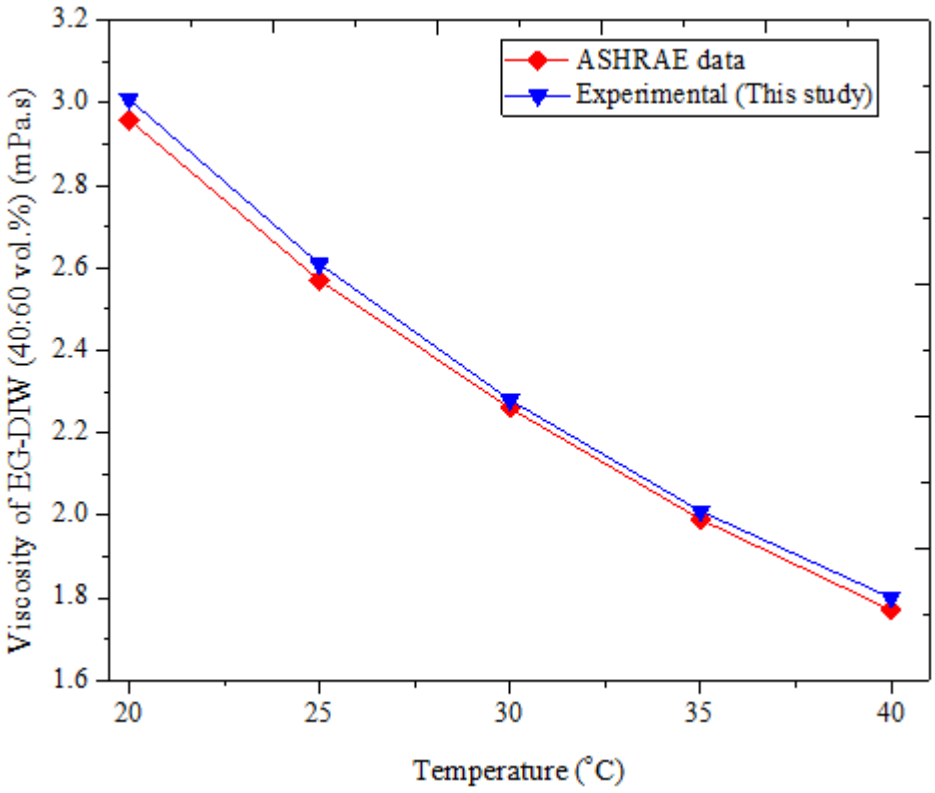

Figure 5.11: Comparison of ASHRAE data and measured viscosity values of EG-DIW.

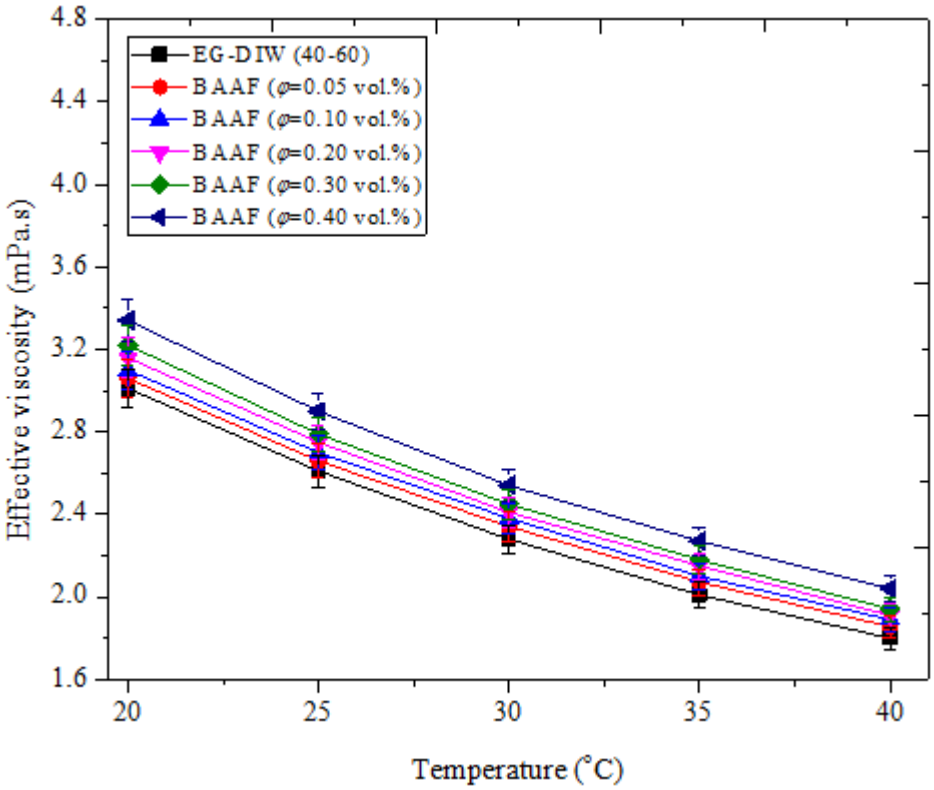

Figure 5.12: Effective viscosity of BAAF samples.

μ_{eff} of BAAF in relation to temperature and φ are presented in Fig. 5.12. Both μ and μ_{eff} were noticed to decrease with temperature rise, while increasing φ was observed to increase μ_{eff}. The addition of HNPs to EG-DIW expectedly enhanced the μ of EG-DIW because HNPs had a higher density than that of EG-DIW. The influence of φ and temperature on the μ_{eff} of BAAF was consistent with previous studies [84, 215]. For the temperature and φ studied, μ_{eff} was augmented by 1.66% to 13.33%. In agreement with this result, Sundar et al. [35], Nabil et al. [52] and Sundar et al. [118] reported enhancements of 1.50-times (0.2 vol.% at 60 °C), 21.3% to 80% (0.5 – 3 vol.% at 30 – 80 °C) and 1.21-times to 1.33-times (0.15 wt.% at 60 °C) for EG-DW (40:60) based ND-Fe_3O_4, TiO_2-SiO_2 and ND-Co_3O_4 (67%:33%) nanofluids respectively. Measurement of the μ_{eff} of BAAF had an estimated uncertainty of 2.99%.

A new model was developed for estimating the μ_{eff} of BAAF from the experimental data within the range of φ and temperature considered in this study. The developed model had

MAE of 2.14%, MSE of 0.0281, RSME of 0.0626, and MOD of 3.60% and -4.49%, as expressed in Eq. 5.5.

$$\mu_{BAAF} = 0.5830\varphi - 6.2070 \times 10^{-2}T + 4.2280 \qquad (R^2 = 0.984) \qquad 5.5$$

5.3.3 Effective Viscosity of AAF

The temperature and φ of the μ_{eff} of AAF are displayed in Fig. 5.13. It can be noticed that the μ_{eff} of AAF was generally higher than the μ of DIW as a result of the suspension of HNPs (denser than DIW) into DIW. When the temperature was increased from 20 to 40 °C, μ_{eff} and μ were seen to reduce gradually. However, increasing φ of AAF was observed to augment μ_{eff}. Under the φ and temperature considered, the μ_{eff} of AAF was enhanced by 4.55% to 20.43%. The μ_{eff} was found to be within the enhancements of 16.65% to 23.24% (0.1 – 0.3 vol.% at 30 – 60 °C) and 6.45% (0.15 wt.% at 60 °C) reported for ND-Ni/DW and TiO_2-CNT/DW nanofluids respectively. Uncertainty of 2.84% was estimated to be associated with the measurement of the μ_{eff} of AAF.

The estimation of the μ_{eff} for AAF and Fe_2O_3-DIW nanofluid obtained in this work and reported by Joubert et al. [88] showed that AAF had a lower μ_{eff} than that of Fe_2O_3-DIW nanofluid. Thus the hybridisation of Fe_2O_3 NPs with 25 wt.% of Al_2O_3 NPs could be traced to the reduction in the μ_{eff} of AAF. A comparison of Figs. 5.10 and 5.13 showed that the values of the μ_{eff} of AMF were slightly higher than those of the μ_{eff} of AAF. This could be linked to AMF having higher ρ and more percent weight of Fe_2O_3 NPs than AAF. Furthermore, comparing Figs. 5.10 and 5.12 showed that the μ_{eff} of AAF was lower than that of BAAF due to the μ of the base fluids. EG had a higher μ than that of DIW and subsequently, the μ of EG-DIW would be more than that of DIW. Additionally, μ_{eff} enhancement of AAF was observed to be more than that of BAAF, which was consistent with previous studies in the literature [35, 95, 118].

A new model that depended on φ and temperature was developed for predicting the μ_{eff} of AAF by fitting the experimental data obtained for AAF in this study. The developed model is expressed in Eq. 5.6. The prediction performance of the model was 96.2% with MAE of 1.73%, MSE of 0.0477, RMSE of 0.0258, and MOD of 2.55% and -2.67%.

$$\mu_{AAF} = 0.3010\varphi - 1.6400 \times 10^{-2}T + 1.3291 \qquad (R^2 = 0.962) \qquad 5.6$$

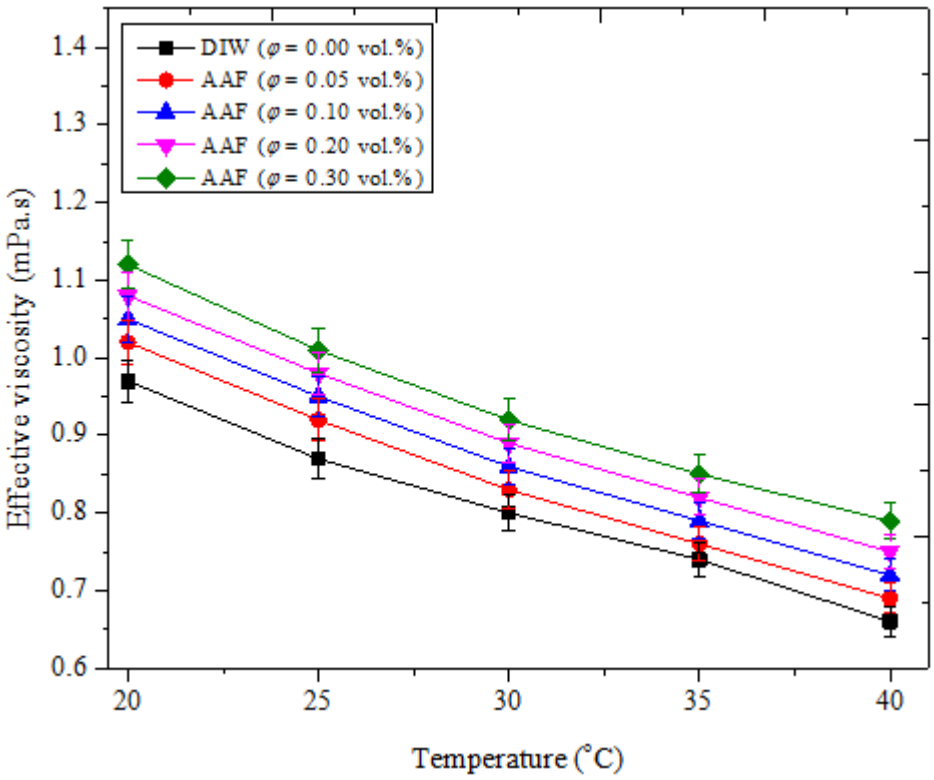

Figure 5.13: Effective viscosity of AAF samples.

5.4 CONCLUSION

The κ_{eff} and μ_{eff} of AMF, BAAF and AAF were measured at the φ and temperature considered in this study. Increasing φ of AMF, BAAF and AAF was noticed to augment κ_{eff} and μ_{eff}, whereas temperature increment only enhanced κ_{eff} and caused a reduction in μ_{eff}. These results were found to agree with previous studies. In comparison with the respective base fluids, enhancements of 3.84% to 14.17%, 2.14% to 12.56%, 2.21% to 10.51% were achieved for the κ_{eff} of AMF, BAAF and AAF respectively. For the μ_{eff} of AMF, BAAF and AAF, augmentations of 11.83% to 28.79%, 1.66% to 13.33% and 4.55% to 20.43%

respectively were attained under φ and temperature considered relative to the corresponding base fluids. In this work, the measured κ_{eff} values followed the order AMF > AAF > BAAF, while for μ_{eff}, the order was BAAF > AMF > AAF. This observation could be attributed to κ and μ of the base fluids, and κ, μ, and ρ of the individual NPs. In addition, models were proposed for the prediction of the μ_{eff} and κ_{eff} of AMF, BAAF and AAF as a function of φ and temperature by way of fitting of the obtained experimental data. Findings from this study revealed that the hybridisation of Fe_2O_3 NPs (base NPs) with MWCNT and Al_2O_3 NPs (doped NPs) resulted in higher κ_{eff} and lower μ_{eff} for AMF, BAAF and AAF than monoparticle nanofluids of Fe_2O_3.

Chapter 6

THERMO-CONVECTION PERFORMANCE OF MAGNETIC HYBRID NANOFLUIDS

6.1 INTRODUCTION

In this chapter, the cavity engaged in the thermo-convection experimental set-up was validated using the base fluids (DIW and EG-DIW) data. The temperature profile of the cavity when filled with samples of DIW, EG-DIW, AMF, BAAF and AAF under varying ΔT is presented in this chapter. This involved the temperatures at the centre and heated walls of the cavity. The thermo-convection performance of the samples in terms of *Ra*, *h*, *Q* and *Nu* was also investigated and the results are reported in this chapter.

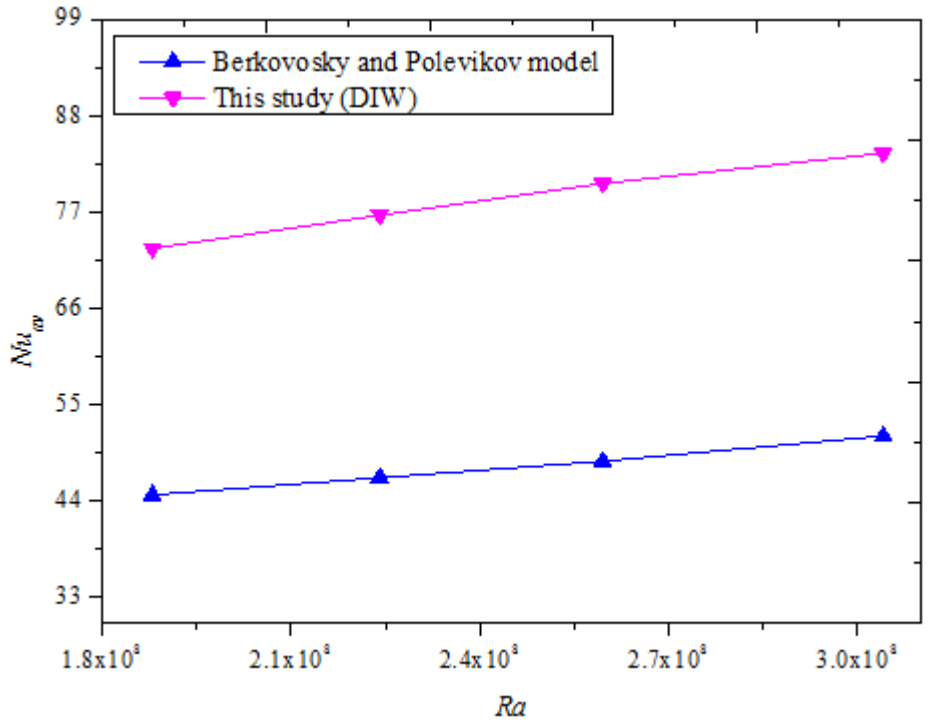

Figure 6.1: Cavity validation for DIW.

6.2 CAVITY VALIDATION

To validate the cavity (rectangular), the Nu_{av} data of DIW and EG-DIW obtained in this study were compared with the *Nu* data estimated from the empirical model proposed by Berkovsky and Polevikov [216]. Figs. 6.1 and 6.2 present the validation of the cavity using DIW and

EG-DIW respectively as base fluids. At *Ra* range of 1.89 x 10^8 to 3.04 x 10^8, the Nu_{av} of DIW was 72.86 to 83.71 (Fig. 6.1), while the Nu_{av} of EG-DIW was 74.42 to 81.79 (Fig. 6.2) at *Ra* of 1.39 x 10^8 to 2.28 x 10^8. From both figures, it can be observed that the experimental data were considerably higher than the data predicted by the model. This indicated that the model underestimated the experimental data. The inability of the model to predict the experimental data of Nu_{av} for both base fluids was found to agree with previous studies [153, 177].

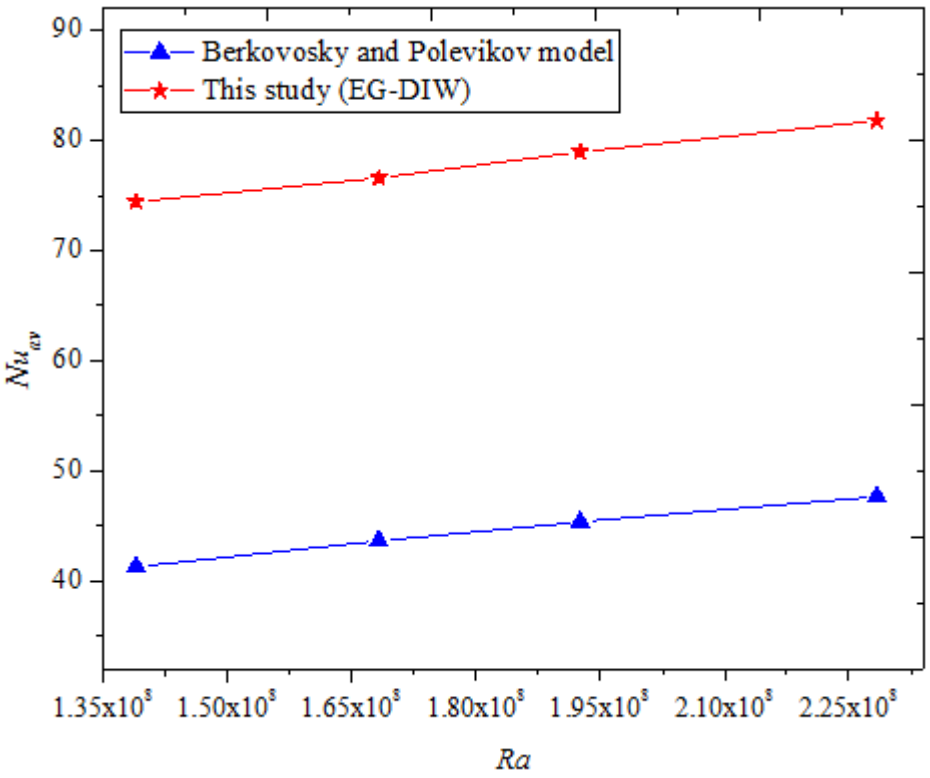

Figure 6.2: Cavity validation for EG-DIW.

6.3 CAVITY TEMPERATURE PROFILES

6.3.1 Temperature Distribution for AMF

Because the thermo-convection experiments were carried out under stable thermal conditions, temperatures were measured using thermocouples at different locations within and outside the cavity, as presented in Fig. 3.3. The temperatures across the mid-section of the cavity (from heated cold wall to hot wall) are presented in Figs. 6.3 to 6.6 for all the tested samples

(DIW and AMF) under different ΔT. Generally, it can be noticed that the measured

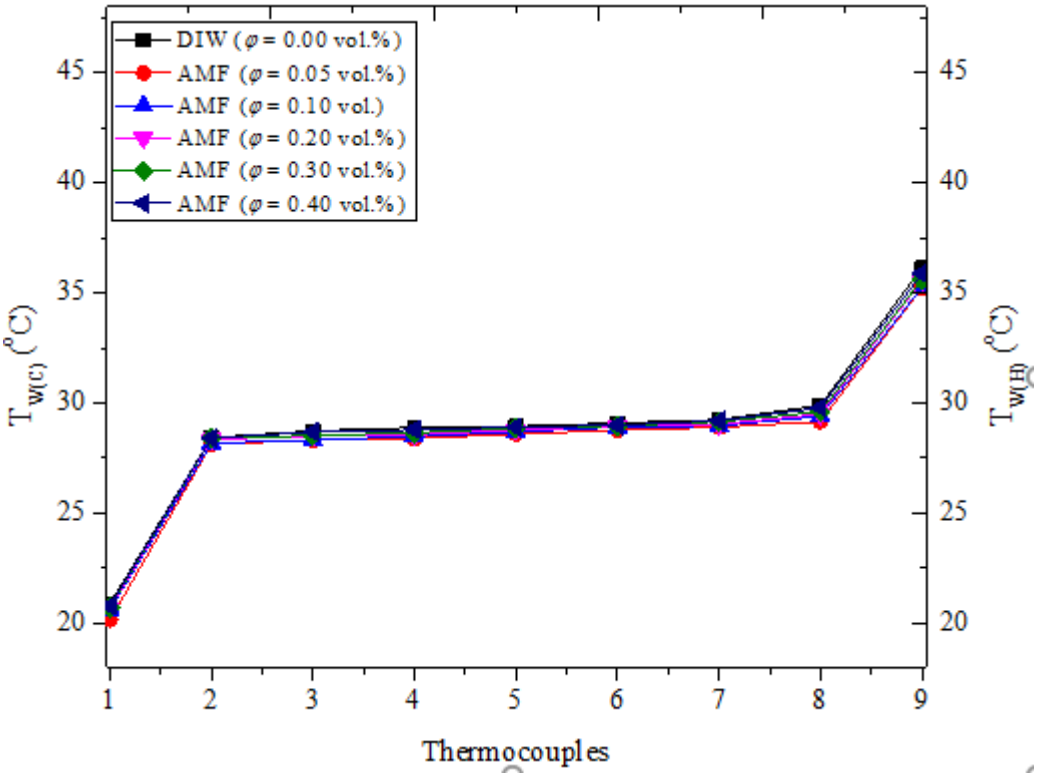

Figure 6.3: Cavity temperature profile for DIW and AMF samples at ΔT = 20 °C.

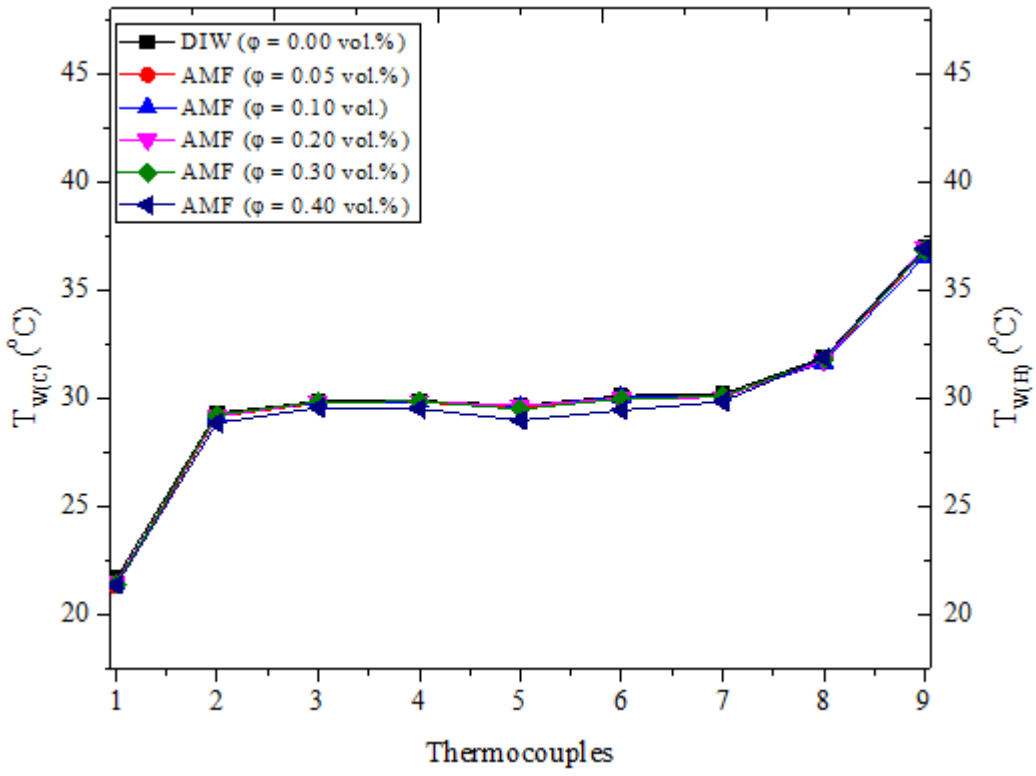

Figure 6.4: Cavity temperature profile for DIW and AMF samples at ΔT = 25 °C.

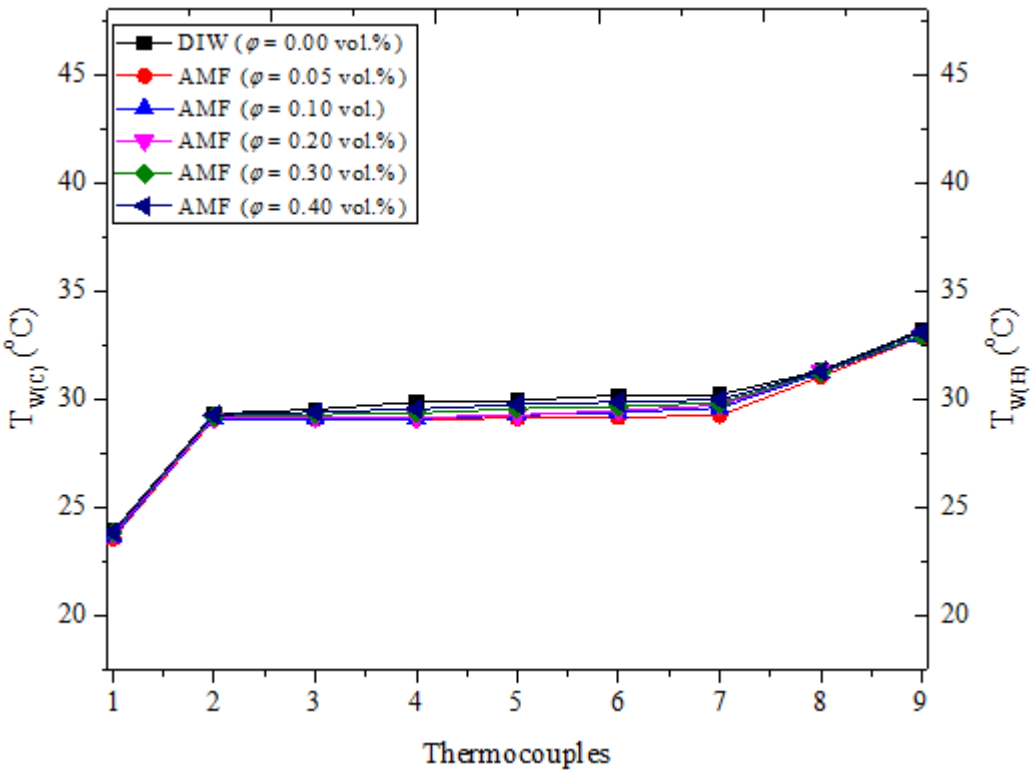

Figure 6.5: Cavity temperature profile for DIW and AMF samples at ΔT = 30 °C.

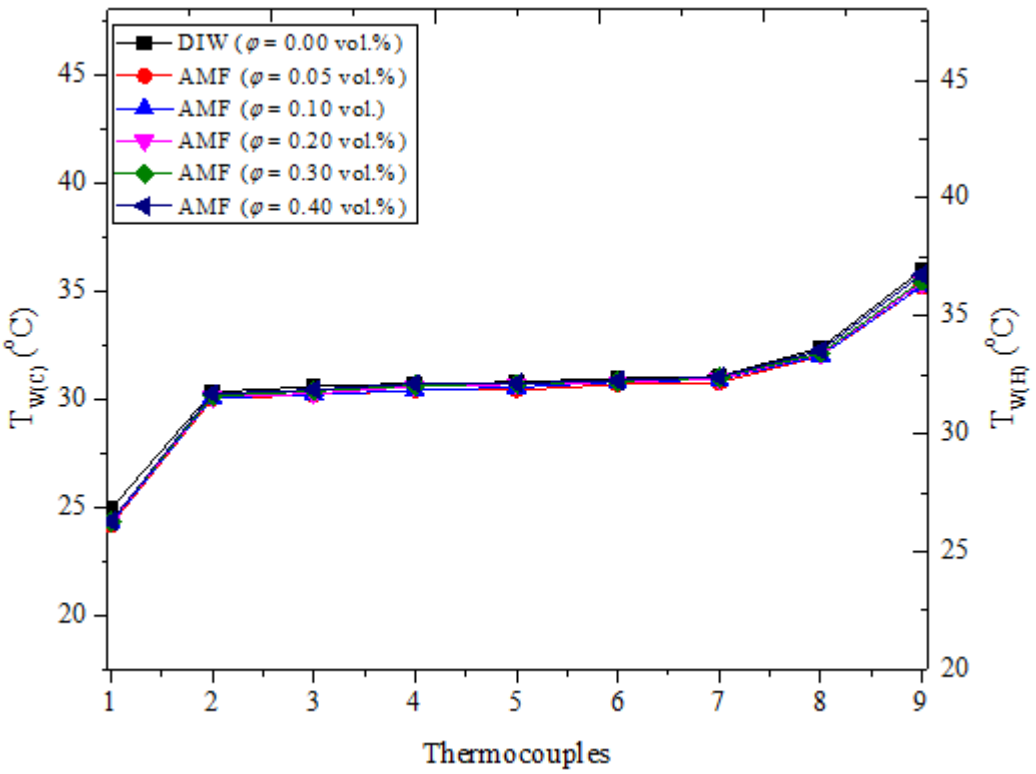

Figure 6.6: Cavity temperature profile for DIW and AMF samples at ΔT = 35 °C.

temperatures for Thermocouples 2 to 7 were relatively similar in value for the tested samples and at all ΔT. DIW was found to have a higher temperature than for the AMF samples. This could be due to the thermal stability reached prior to temperature measurement. Therefore, the suspension of HNPs into DIW caused a very slight reduction in temperature. It is important to note that Thermocouples 8 and 9 were very close compared with Thermocouples 1 and 2, hence the higher temperature reading of Thermocouple 8 in relation to those of 2 to 7. It was obvious that increasing ΔT led to a slight rise in the temperature (around 30 °C) within the cavity and change in wall temperatures; $T_{W(H)}$ decreased while $T_{W(C)}$ increased. Also, the rise in ΔT was noticed to increase ΔT_W for all samples presented in Fig. 6.7. The use of AMF was seen to reduce ΔT_W (cooling effect) in comparison with DIW as ΔT was increased.

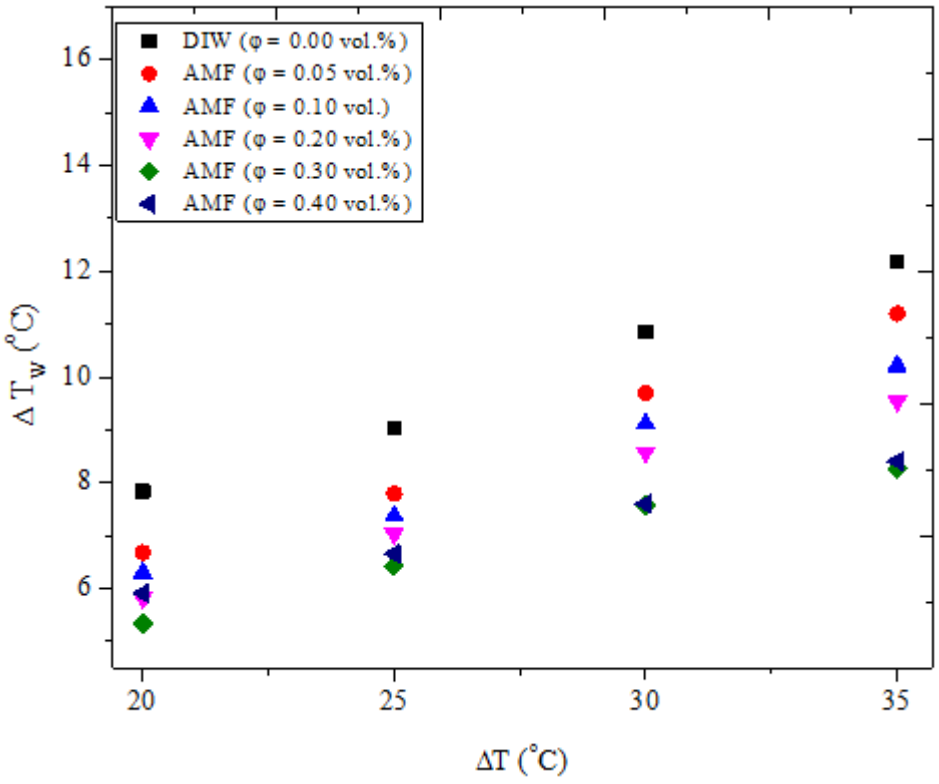

Figure 6.7: Dependence of wall temperature gradient on temperature gradient for DIW and AMF samples.

6.3.2 Temperature Distribution for BAAF

The steady-state temperature profile of the cavity filled with EG-DIW and BAAF samples at various ΔT is illustrated in Figs. 6.8 to 6.11. For the tested samples, the temperatures within the cavity (for Thermocouples 2 – 7) were noticed to be closely similar in value and appeared to be relatively constant. Again, the base fluid (in this case EG-DIW) seemed to have a higher temperature than that of BAAF. In Figs. 6.8 to 6.11, the rise in ΔT was noticed to increase the temperature in the middle of the cavity, except for the extremes (Thermocouples 1 and 9; T_W). Variation in wall temperature (Thermocouples 1 and 9) for all the tested samples was observed as ΔT was increased. A comparison of Figs. 6.3 to 6.6 with Figs. 6.8 to 6.11 showed that the latter had slightly higher temperatures than the former. Thus the use of EG-DIW and BAAF in the cavity led to higher cavity temperature than for DIW and AMF, and this could be due to better heat transfer capacity of DIW and AMF. A direct relationship was noticed between ΔT_W and ΔT, as ΔT increased ΔT_W, as shown in Fig. 6.12.

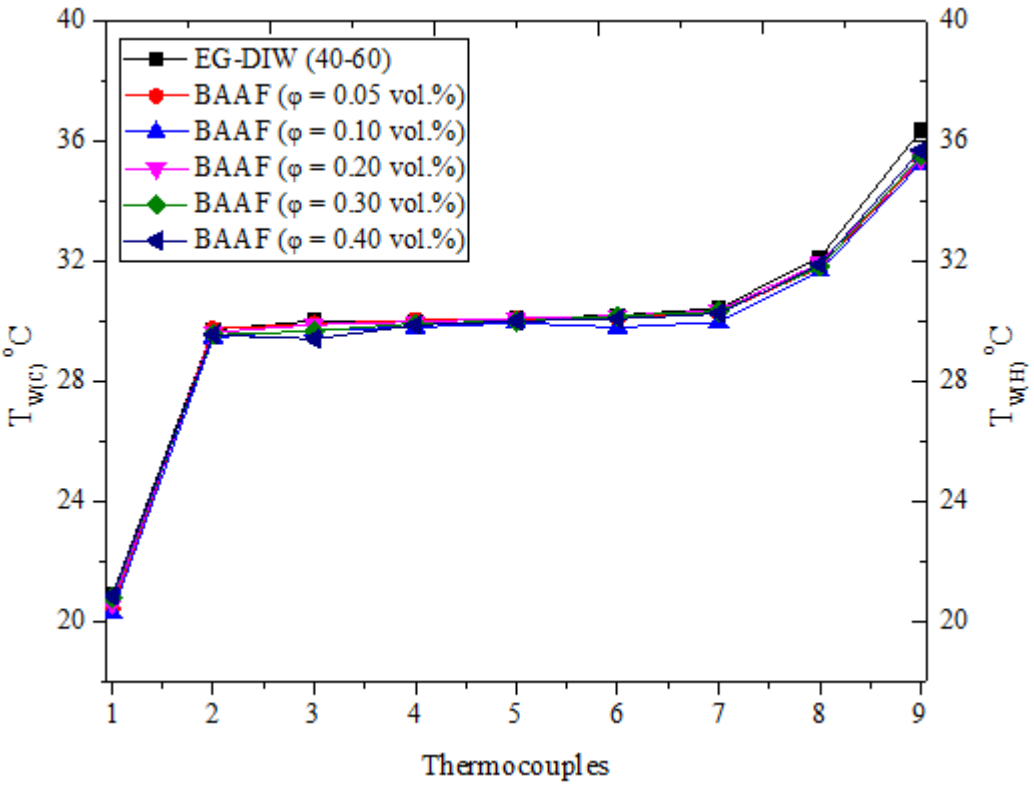

Figure 6.8: Cavity temperature profile for EG-DIW and BAAF samples at ΔT = 20 °C.

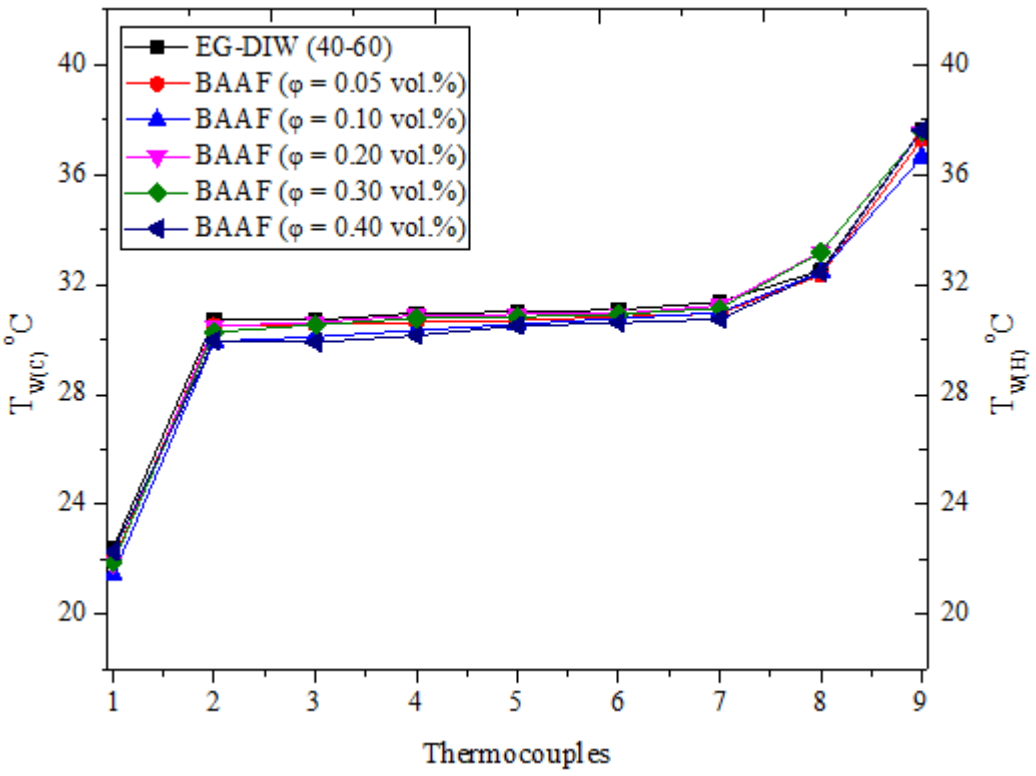

Figure 6.9: Cavity temperature profile for EG-DIW and BAAF samples at ΔT = 25 °C.

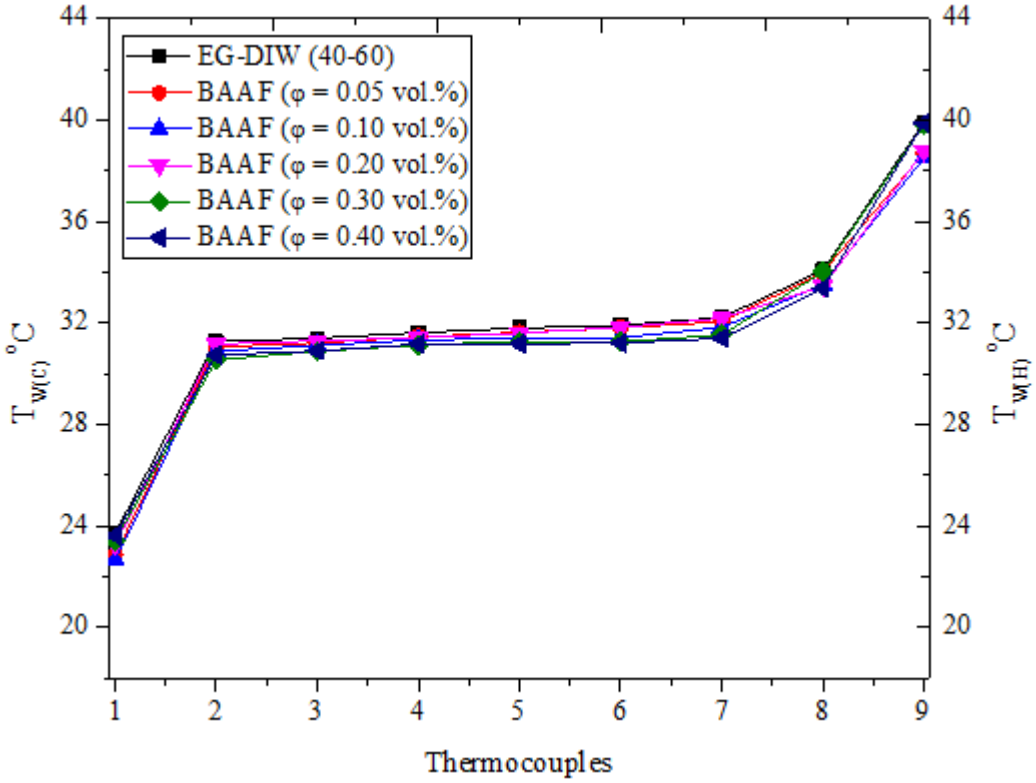

Figure 6.10: Cavity temperature profile for EG-DIW and BAAF samples at ΔT = 30 °C.

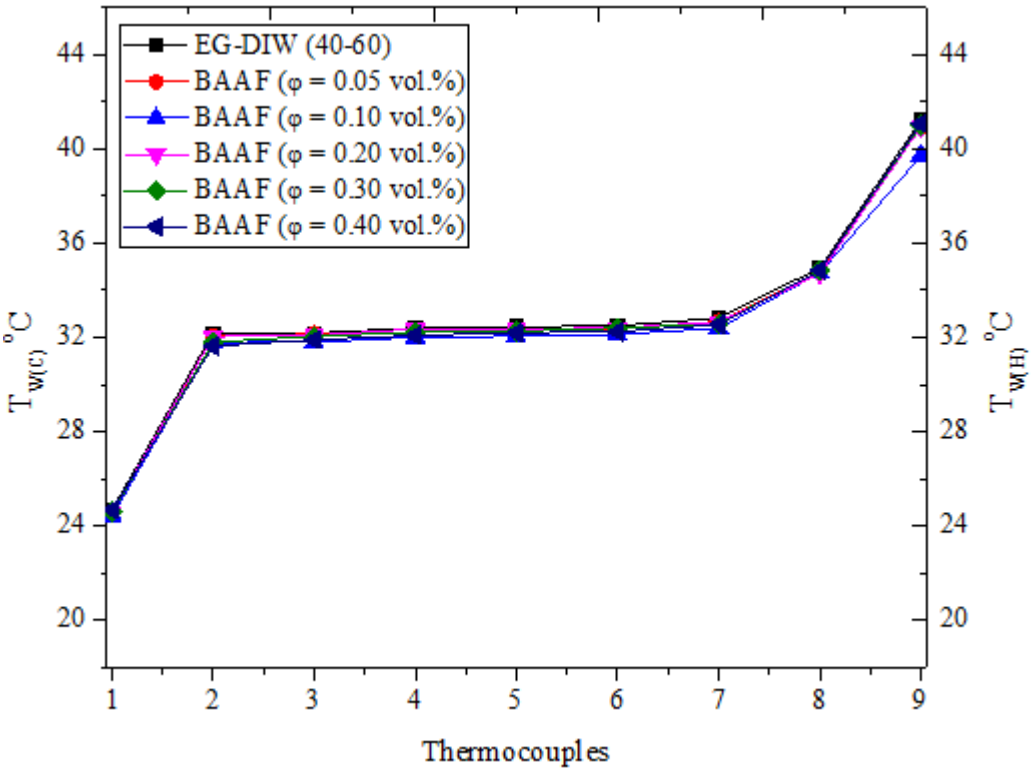

Figure 6.11: Cavity temperature profile for EG-DIW and BAAF samples at ΔT = 35 °C.

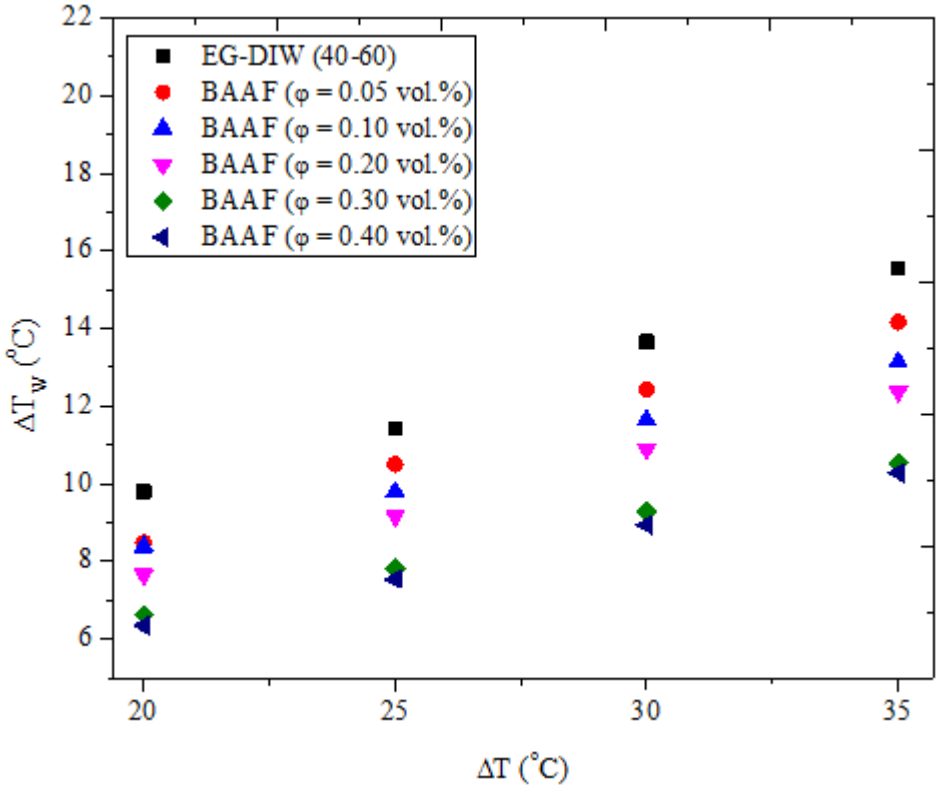

Figure 6.12: Dependence of wall temperature gradient on temperature gradient for EG-DIW and BAAF samples.

6.3.3 Temperature Distribution for AAF

With the thermo-convection experiment conducted at a thermal equilibrium state, Figs. 6.13 to 6.16 show the temperatures at different locations in the cavity for all the tested samples (DIW and AAF). Relatively constant and approximately equal temperatures (Thermocouples 2 – 7) were observed for all the samples and at different ΔT (Figs. 6.13 – 6.16). Higher temperatures were recorded for DIW than for AAF at varying ΔT. Similarly, the temperatures at the walls were higher than those within the cavity since ΔT was imposed on the walls. Increasing ΔT caused a corresponding increase in temperature (27 – 31 °C) within the cavity (Thermocouples 2 – 8) with a variation in T_W (Thermocouples 1 and 9). It was observed that EG-DIW and BAAF samples (Figs. 6.8 – 6.11) had higher cavity temperatures than DIW, AMF and AAF samples (Figs. 6.3 – 6.6 and 6.13 – 6.16). This could be connected to the differences in HNPs and base fluids engaged in the study. Fig. 6.17 indicates that an increase in ΔT was noticed to increase ΔT_W for all the tested DIW and AAF samples.

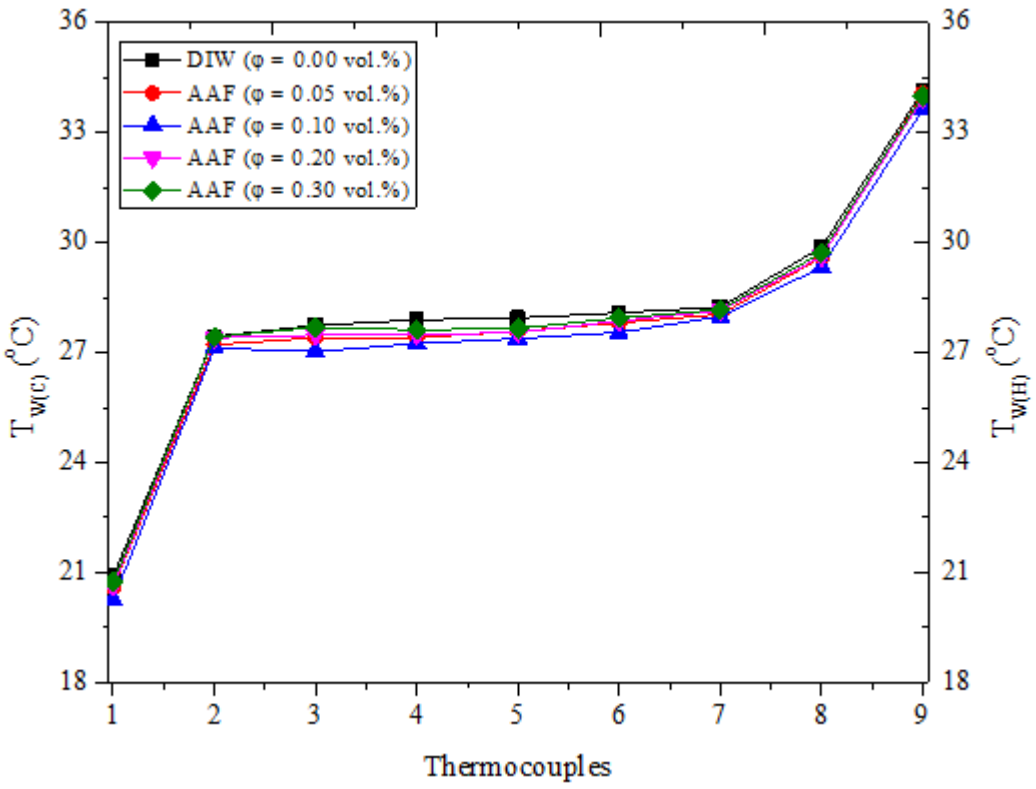

Figure 6.13: Cavity temperature profile for DIW and AAF samples at ΔT = 20 °C.

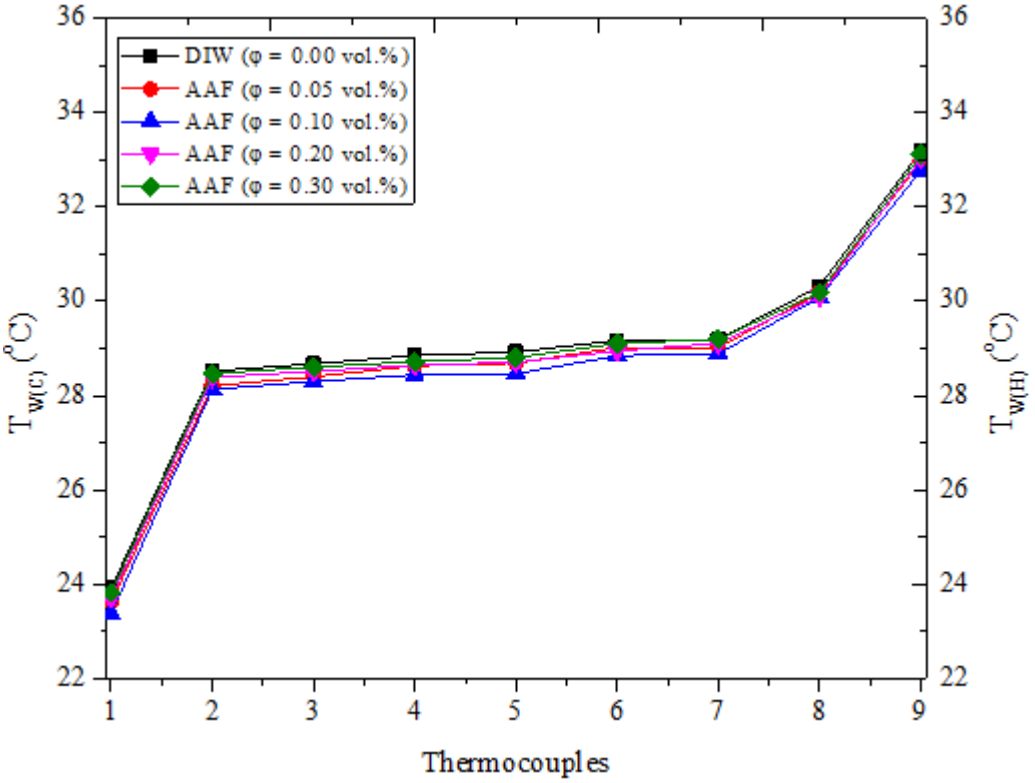

Figure 6.14: Cavity temperature profile for DIW and AAF samples at ΔT = 25 °C.

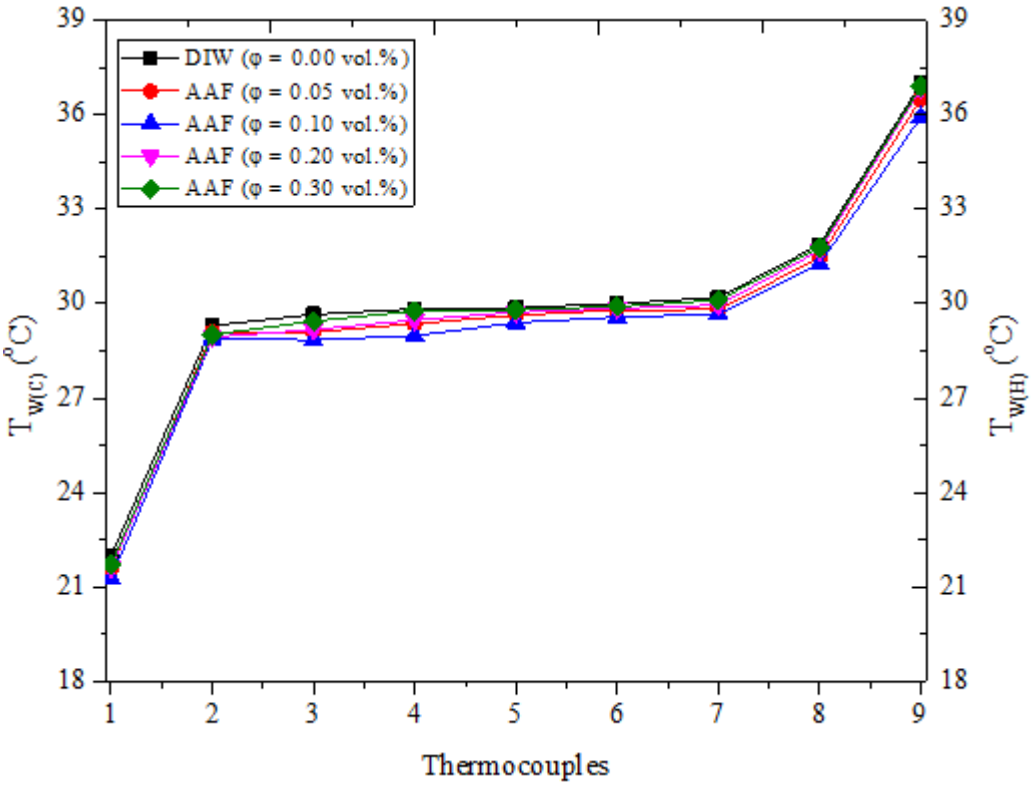

Figure 6.15: Cavity temperature profile for DIW and AAF samples at ΔT = 30 °C.

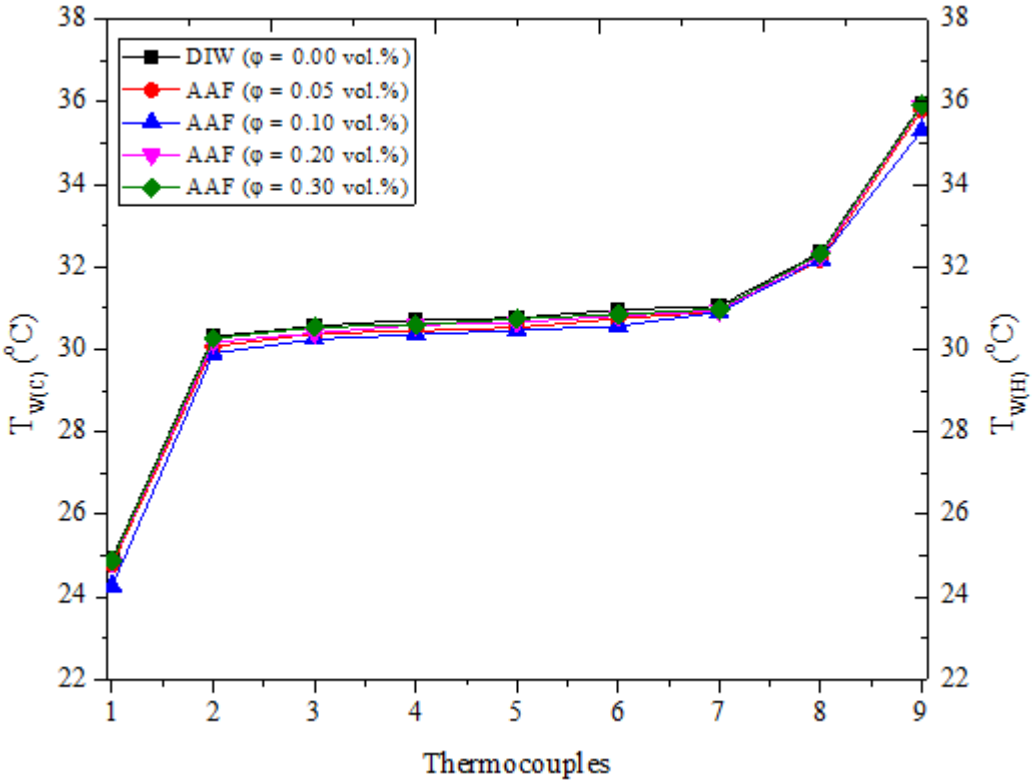

Figure 6.16: Cavity temperature profile for DIW and AAF samples at ΔT = 35 °C.

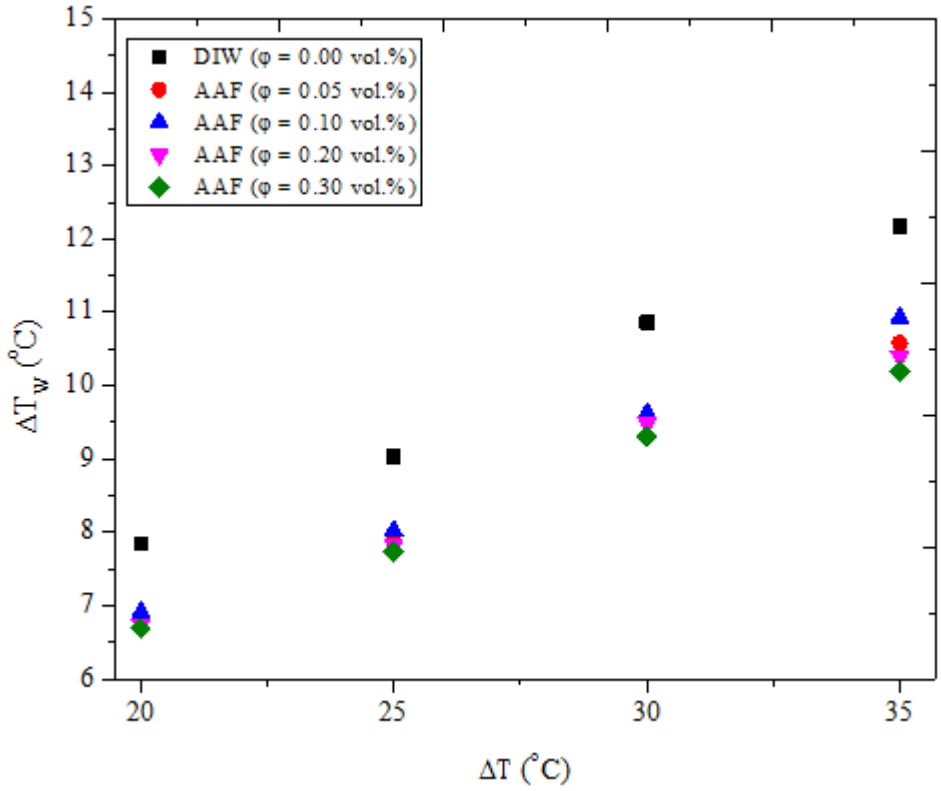

Figure 6.17: Dependence of wall temperature gradient on temperature gradient for EG-DIW and BAAF samples.

6.4 THERMO-CONVECTION PARAMETERS OF MHNFs

6.4.1 Nusselt Number of MHNFs and Model Development

6.4.1.1 Nusselt Number of AMF

An investigation of the thermo-convection heat transfer of DIW and AMF samples in the cavity was conducted and results were presented. The dependence of Nu_{av} on *Ra* at different ΔT for DIW and AMF samples is presented in Fig. 6.18. Increasing *Ra* was observed to enhance Nu_{av} for all the samples with DIW ($1.89 \times 10^8 – 3.04 \times 10^8$) having a higher range of *Ra* than that of AMF ($1.01 \times 10^8 – 2.65 \times 10^8$). The *Ra* values were within the range ($1.00 \times 10^6 – 1.0 \times 10^9$) reported by previous studies [19, 88, 162]. The decrease in *Ra* for AMF samples was due to the suspension of HNPs into DIW, which correspondingly yielded higher Nu_{av} values for some of the AMF samples at different ΔT than for DIW. The influence of an increment in ΔT on *Ra* of DIW and AMF is presented in Fig. 6.19. As ΔT increased, *Ra* was observed to increase with the DIW sample having the highest *Ra*. Figs. 6.18 and 6.19 show that *Ra* and ΔT were directly related to Nu_{av} and this agreed with previous works [151, 152, 195].

Nu of DIW and AMF at the cold and hot walls as a function of ΔT_W is presented in Figs. 6.20 and 6.21. *Nu* at the cold and hot walls of the cavity was found to be enhanced with an increase in ΔT_W. Both figures show that the AMF samples generally had lower values of ΔT_W than those of DIW. It can be observed in Fig. 6.20 that 0.05 vol.% AMF sample had the highest Nu_c (91.80) at the cold wall of the cavity. An identical pattern was noticed for Nu_h at the hot wall with a maximum value of 94.59. This trend for the *Nu* of DIW and AMF samples at both walls of the cavity can be better understood using Nu_{av} presented in Fig. 6.22. The dependence of Nu_{av} on φ and ΔT is shown in Fig. 6.22 with the uncertainty associated. The figure shows that the highest Nu_{av} (93.20) was achieved for 0.05 vol.% AMF at $Ra = 2.65 \times 10^8$ and ΔT = 35 °C, which was an enhancement of 11.30% over that of DIW (Figs. 6.18 and 6.22). AMF samples of 0.10 vol.% and 0.20 vol.% were enhanced by 6.94% and 3.69%,

while samples with φ = 0.30 vol.% and 0.40 vol.% were deteriorated by 0.7% and 2.73% respectively compared with DIW at ΔT = 35 °C. With the use of monoparticle nanofluid of Fe_2O_3/DIW in a rectangular cavity, Joubert et al. [88] reported maximum Nu_{av} of 82.76 and enhancement of 5.63% at Ra = 3.94 x 10^8 and φ = 0.10 vol.% relative to DIW, which was slightly lower that what was obtained in this study. Improvements in Nu by 10%, 35% and 45% were achieved with the use of MWCNT/water nanofluid at φ = 0.10 vol.% in a square cavity, in comparison with Nu of water [22, 151, 195]. Additionally, Giwa et al. [165] reported Nu_{av} enhancements of 11.8 to 17.2% (at ΔT = 55 °C) for 0.10 vol.% Al_2O_3-MWCNT/DIW nanofluid in a rectangular cavity, which were higher than the results obtained in this work.

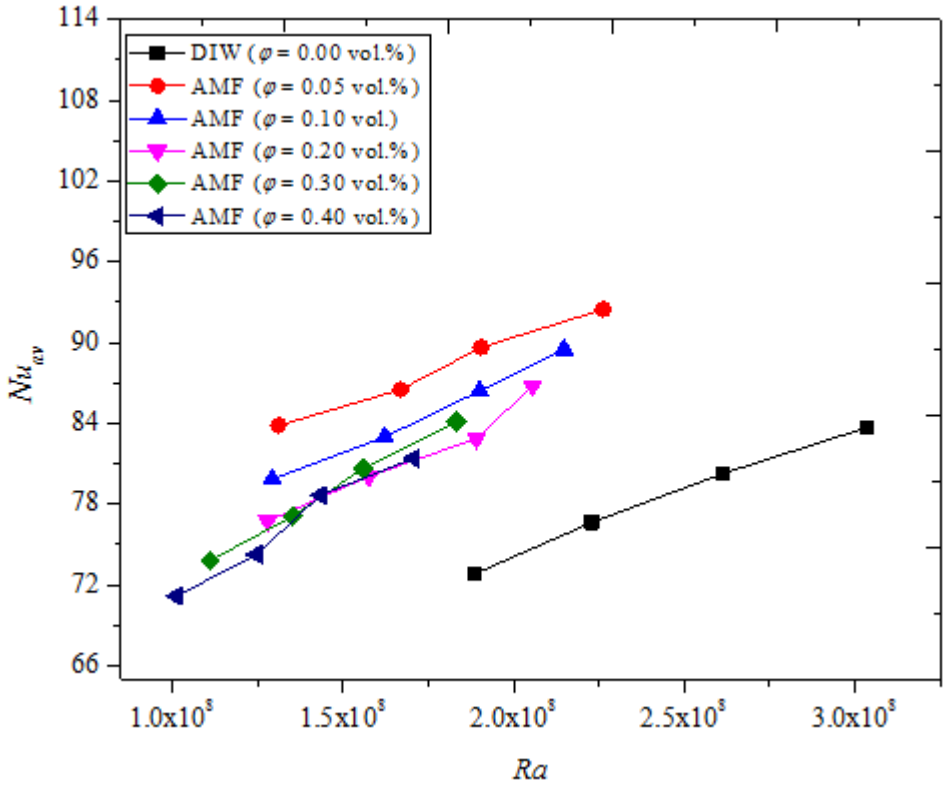

Figure 6.18: Relationship between Nu_{av} and Ra for DIW and AMF samples.

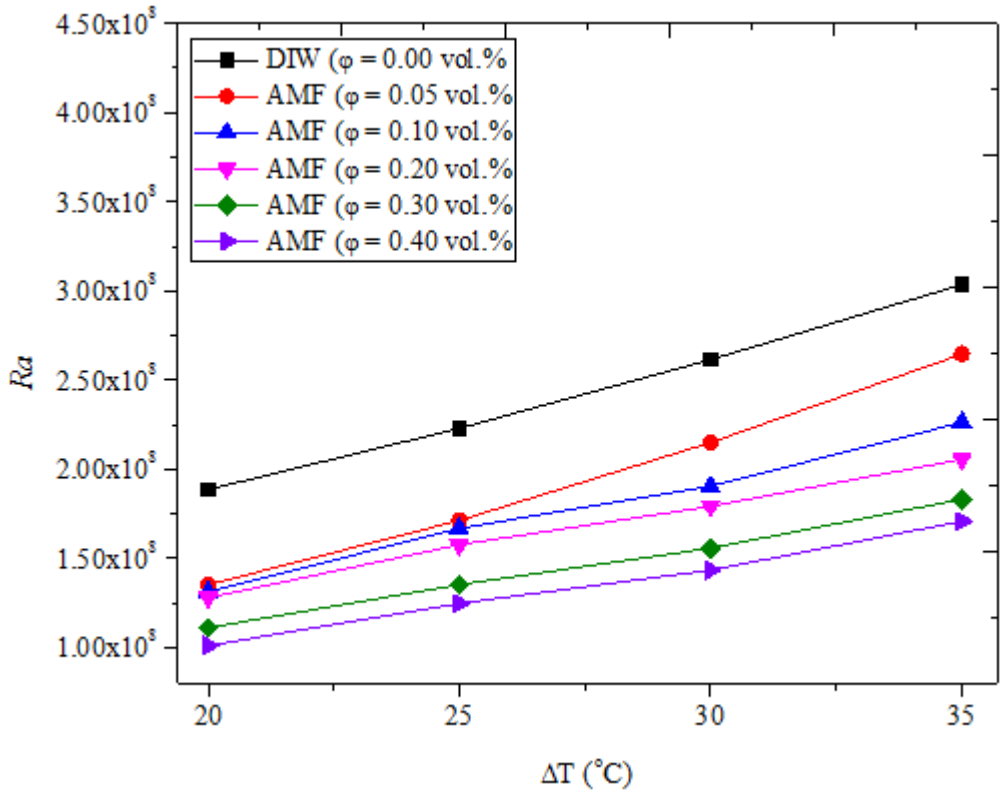

Figure 6.19: Relationship between *Ra* and ΔT for DIW and AMF samples.

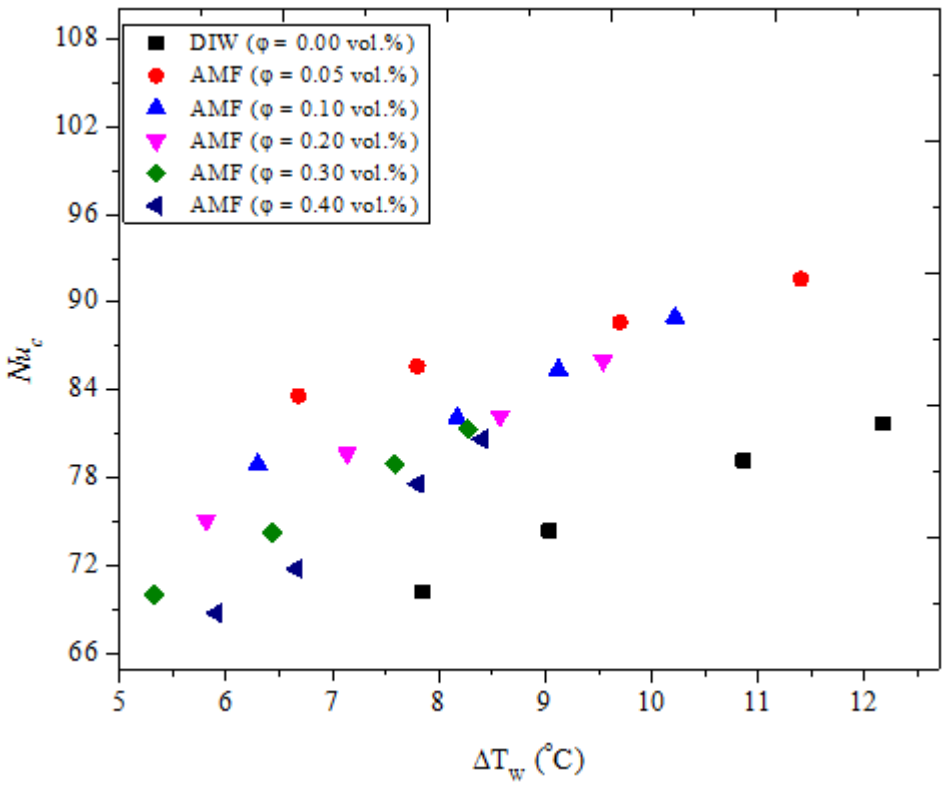

Figure 6.20: Relationship between Nu_c and ΔT_w for DIW and AMF samples.

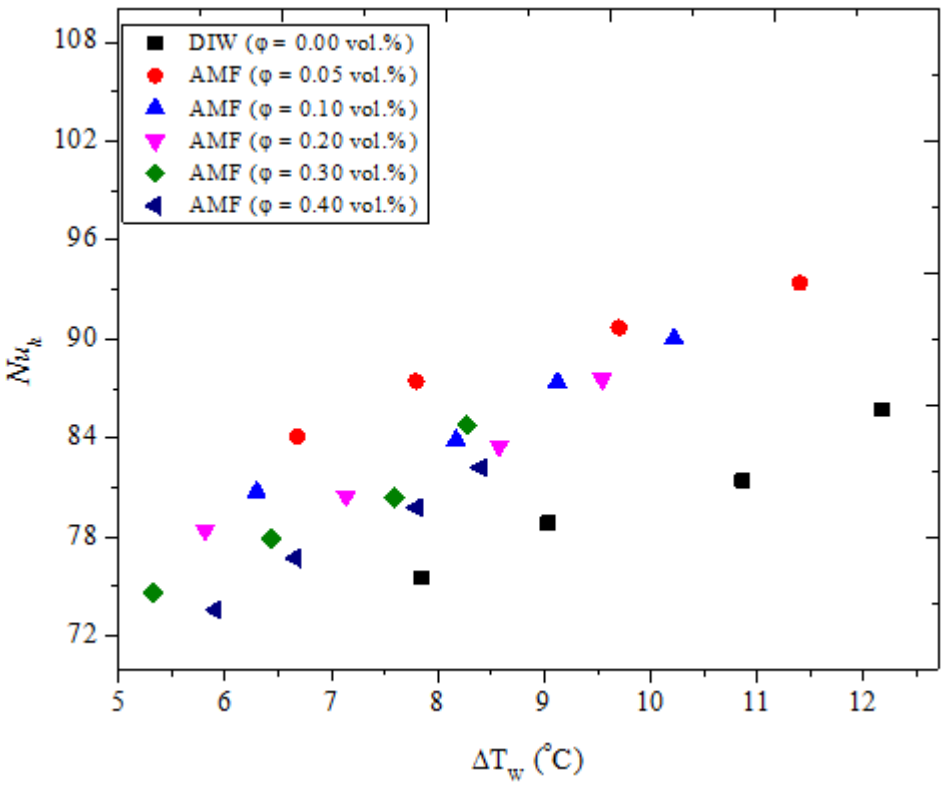

Figure 6.21: Relationship between Nu_h and ΔT_W for DIW and AMF samples.

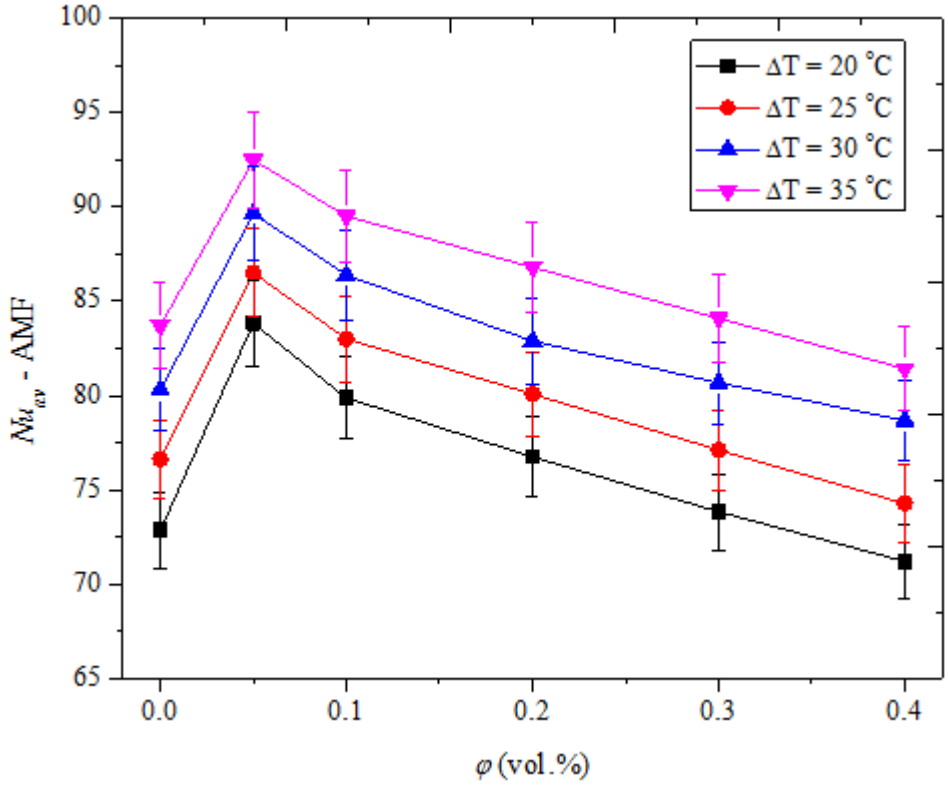

Figure 6.22: Relationship between Nu_{av} and φ for DIW and AMF samples at varying ΔT.

Therefore, the observed enhancement in the present study could be attributed to the hybridisation of Fe_2O_3 NPs with MWCNT NPs to formulate AMF, which was reported earlier in this work to exhibit a lower μ_{eff} than that of Fe_2O_3/DIW nanofluid. Suspending HNPs of Fe_2O_3 and MWCNT in DIW was demonstrated to enhance the μ of DIW by increasing ρ_{eff} of AMF. The increased ρ_{eff} favoured enhancement of buoyancy at lower φ (0.05 vol.% – 0.20 vol.%) after which attenuation (φ = 0.30 vol.% and 0.40 vol.%) was observed. Thus the Nu_{av} of AMF was enhanced for φ = 0.05 vol.% to 0.20 vol.% and deterioration was noticed for higher concentration of AMF, which was consistent with earlier studies [19, 22, 88, 153]. Figs. 6.23 and 6.24 are provided to give a clear pictorial representation of the enhancement and deterioration reported for AMF. Fig. 6.23 shows the dependence of normalised Nu_{av} on ΔT for the AMF samples. The enhancements of Nu_{av} were achieved when φ = 0.05 vol.% to 0.20 vol.% (normalised Nu_{av} of > 1) and attenuation of Nu_{av} occurred at φ > 0.2 vol.% (normalised Nu_{av} of ≤ 1). A similar trend in the appreciation and depreciation of Nu_{av} reported in Fig. 6.23 was observed by the plot of normalised Nu_{av} against *Ra* for AMF, as presented in Fig. 6.24. The scarcity of models in the literature for estimating *Nu* of Fs in cavities informed the fitting of the Nu_{av} data for AMF to develop a model. The proposed model described in Eq. 6.1 was a function of *Ra* and φ. The model could predict the Nu_{av} of AMF by 94.55% with MAE of 1.39%, MSE of 0.0543, RMSE of 0.0176, and MOD of -2.83% and 2.46%. A fit of the model is presented in Fig. 6.25.

$$Nu = 1.79(Ra)^{0.1341}(\varphi)^{-0.0383} \quad \textbf{6.1}$$

6.4.1.2 Nusselt Number of BAAF

The results of engaging EG-DIW and BAAF samples in the cavity to study the thermo-convection heat transfer performance are presented in this section. Nu_{av} as a function of *Ra* for EG-DIW and BAAF is displayed in Fig. 6.26, which shows that as *Ra* increased, Nu_{av} was enhanced with EG-DIW recording the highest values of *Ra* and 0.05 vol.% BAAF affording

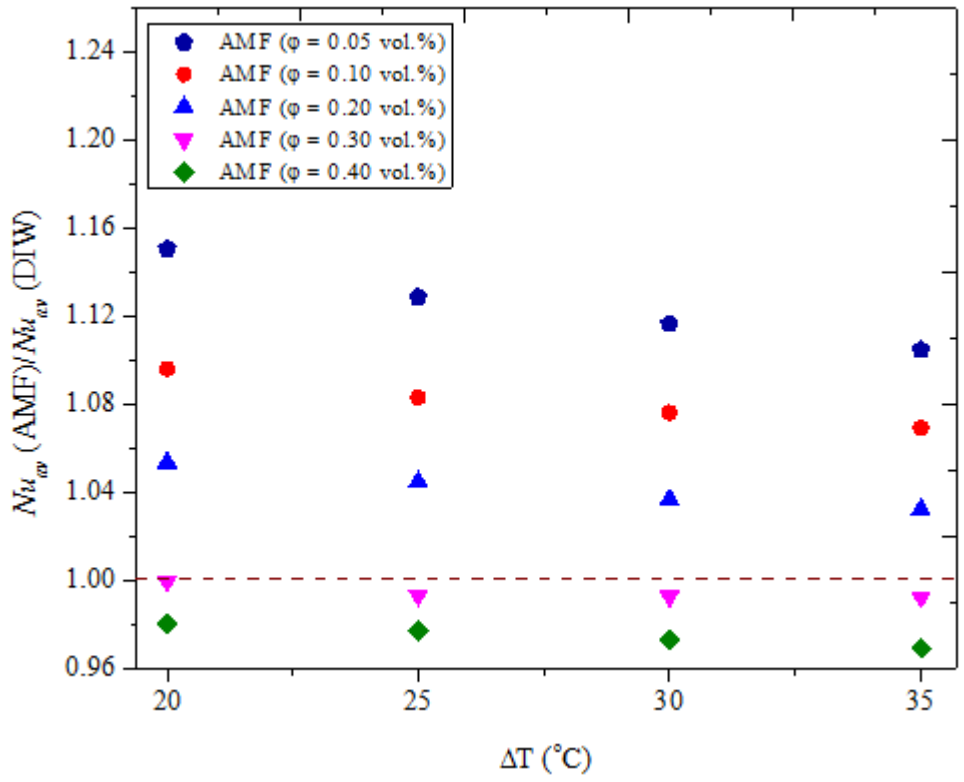

Figure 6.23: Normalised Nu_{av} against ΔT for DIW and AMF samples.

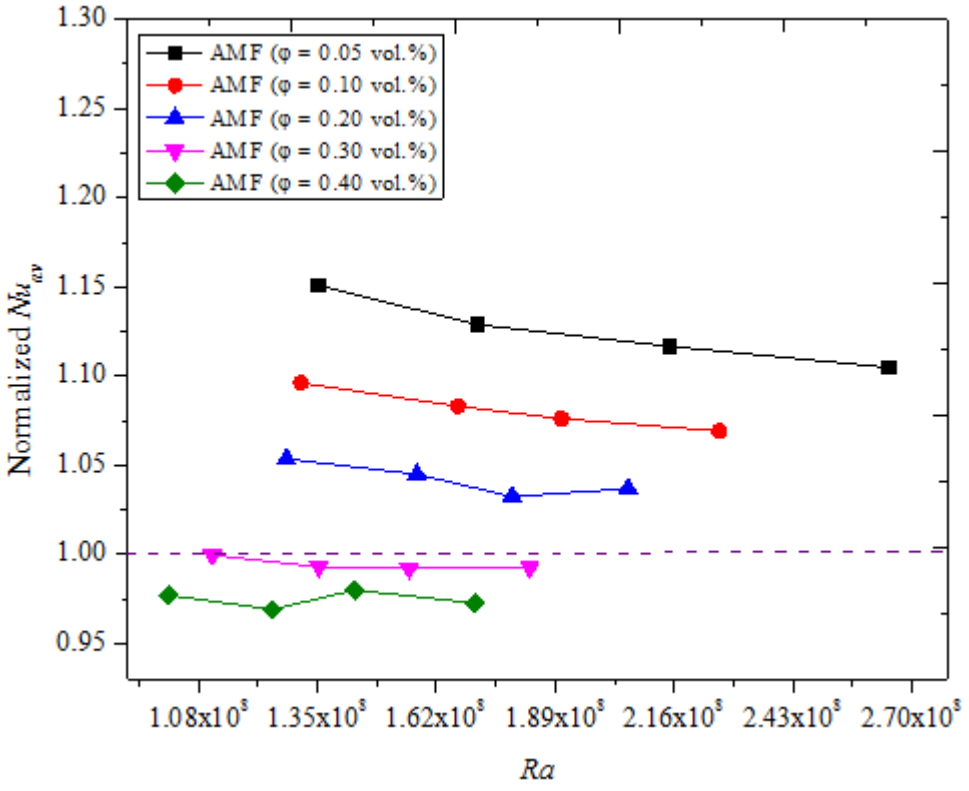

Figure 6.24: Normalised Nu_{av} against *Ra* for DIW and AMF samples.

the maximum value of Nu_{av}. Some BAAF samples were observed to have higher Nu_{av} values than for EG-DIW, which was due to the suspension of HNPs of Fe_2O_3 and Al_2O_3 into EG-DIW to formulate BAAF (Fig. 6.26). *Ra* ranges of 7.06 x 10^7 to 1.63 x 10^8 and 1.39 x 10^8 to 2.28 x 10^8 were involved in this study for EG-DIW and BAAF respectively, which were within *Ra* ranges reported in the literature [151, 153, 177]. In Fig. 6.27, the effect of ΔT on *Ra* is illustrated for EG-DIW and BAAF.

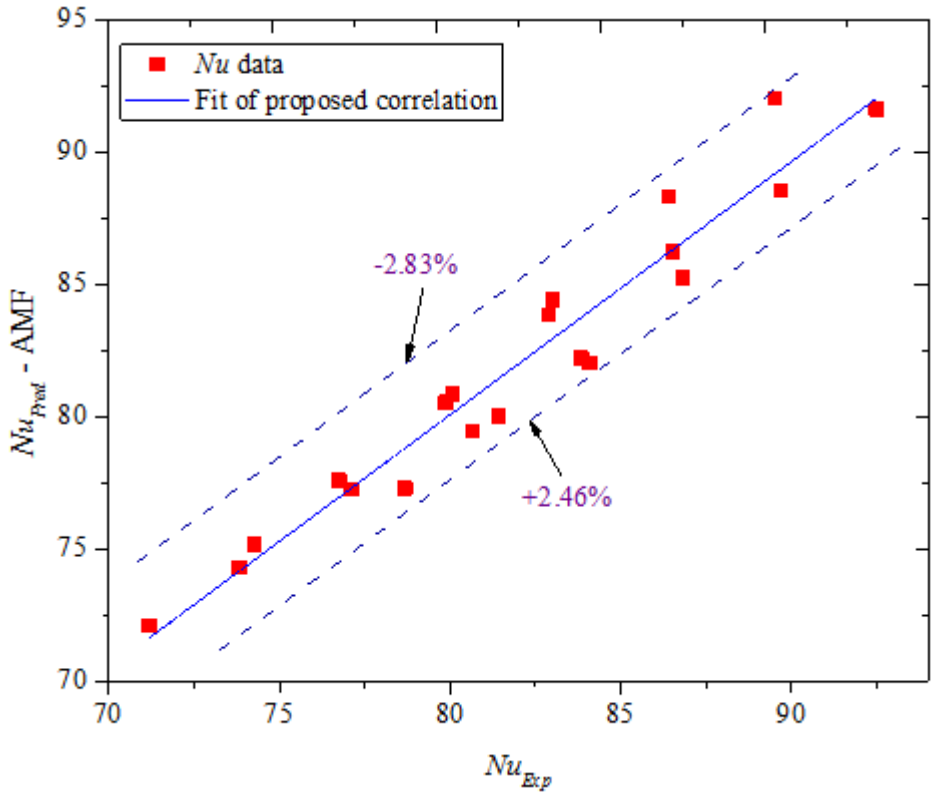

Figure 6.25: Fit of correlation for predicting Nu_{av} of AMF.

A direct relationship was found to exist between ΔT and *Ra* because a rise in ΔT led to an increase in *Ra*. Extending this observation to Fig. 6.26 revealed that as ΔT increased, *Ra* was increased and consequently, Nu_{av} was enhanced [151, 177]. Figs. 6.28 and 6.29 show *Nu* of EG-DIW and BAAF at the cold and hot walls respectively as a function of ΔT_W. Generally, for both figures, *Nu* was enhanced as ΔT_W increased with the 0.05 vol.% and 0.40 vol.% BAAF samples having the highest and lowest *Nu* values respectively, with EG-DIW having the highest ΔT_W values (9.79 – 15.54 °C). At the cold wall of the cavity, the highest Nu_c was

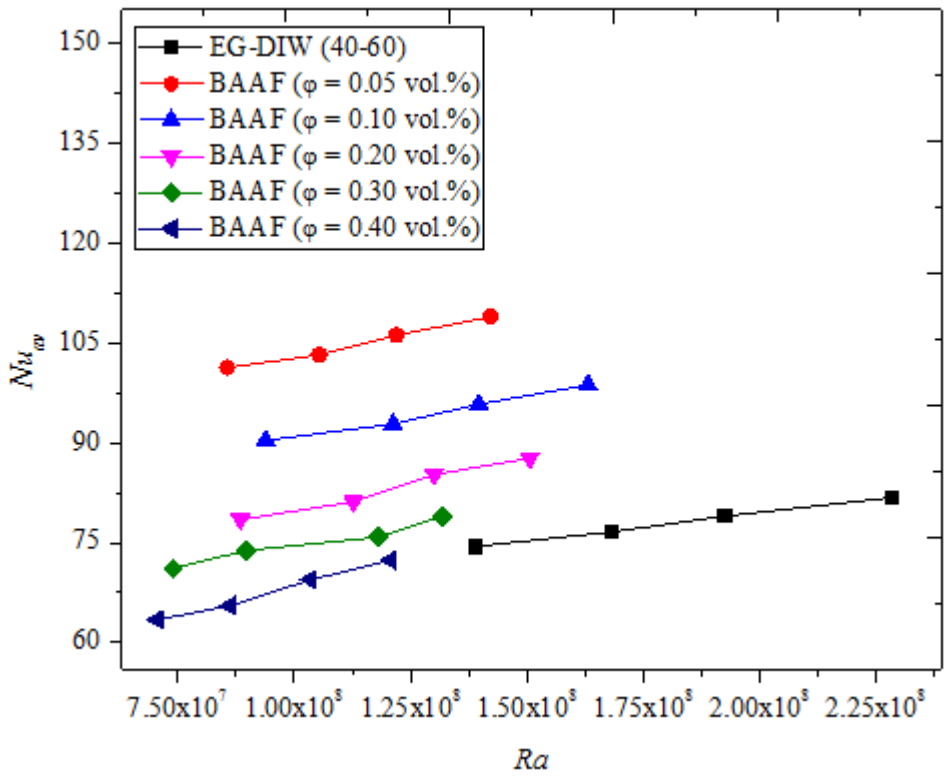

Figure 6.26: Relationship between Nu_{av} and Ra for EG-DIW and BAAF samples.

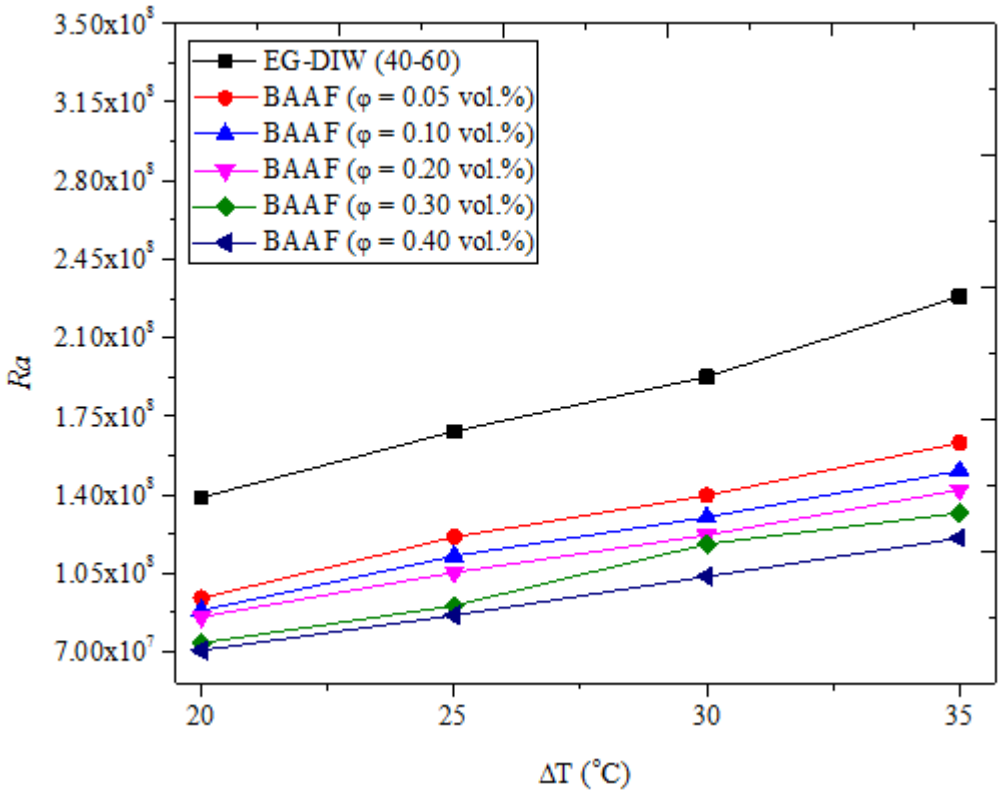

Figure 6.27: Relationship between Ra and ΔT for EG-DIW and BAAF samples.

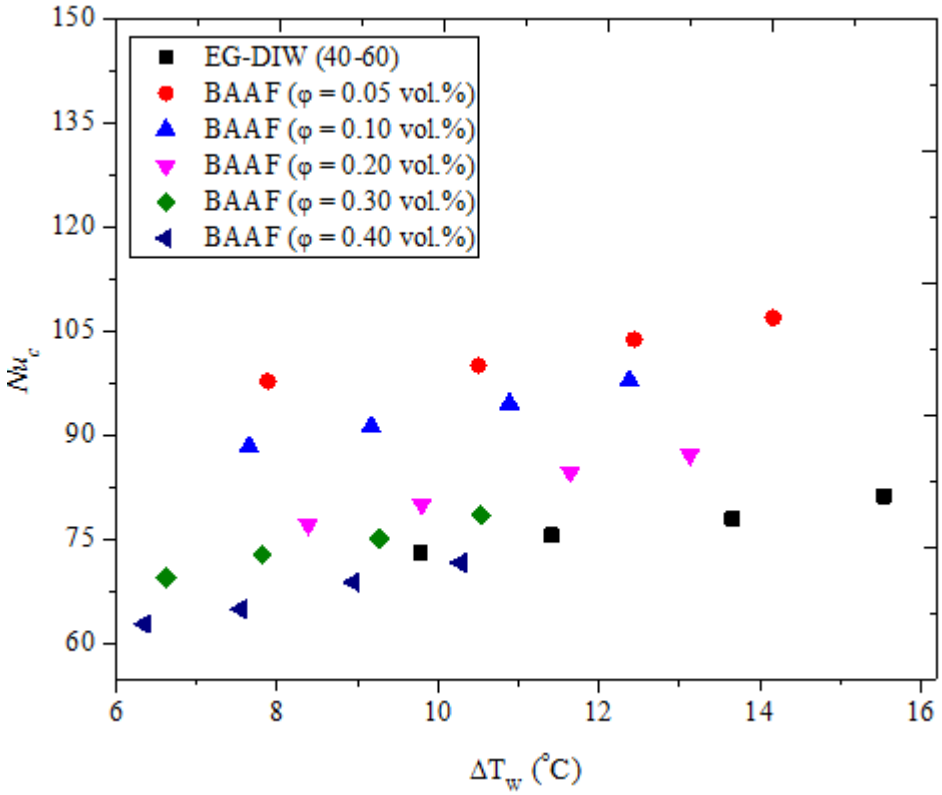

Figure 6.28: Relationship between Nu_c and ΔT_W for EG-DIW and BAAF samples.

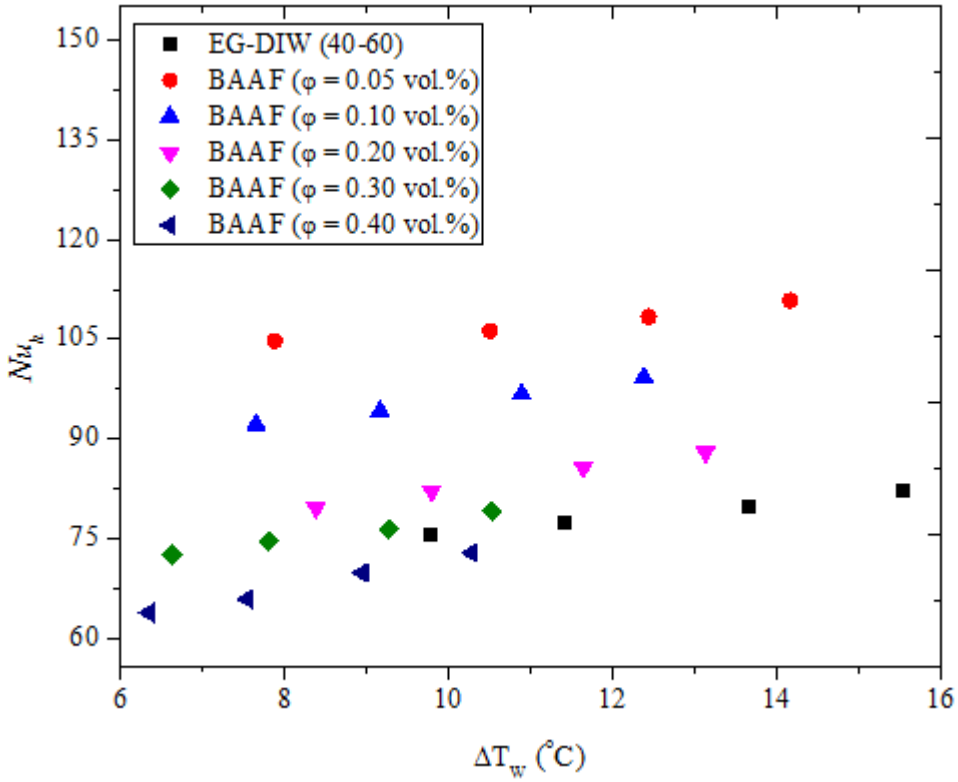

Figure 6.29: Relationship between Nu_h and ΔT_W for EG-DIW and BAAF samples.

attained with BAAF of 0.05 vol.% at ΔT_W = 14.17 °C, whereas 0.40 vol. BAAF achieved the lowest Nu_c (71.71) at ΔT_W = 6.35 °C (Fig. 6.28). Considering the *Nu* at the hot wall of the cavity (Fig. 6.29), the maximum and minimum values of 110.80 and 73.00 were recorded for 0.05 vol.% and 0.40 vol.% BAAF respectively.

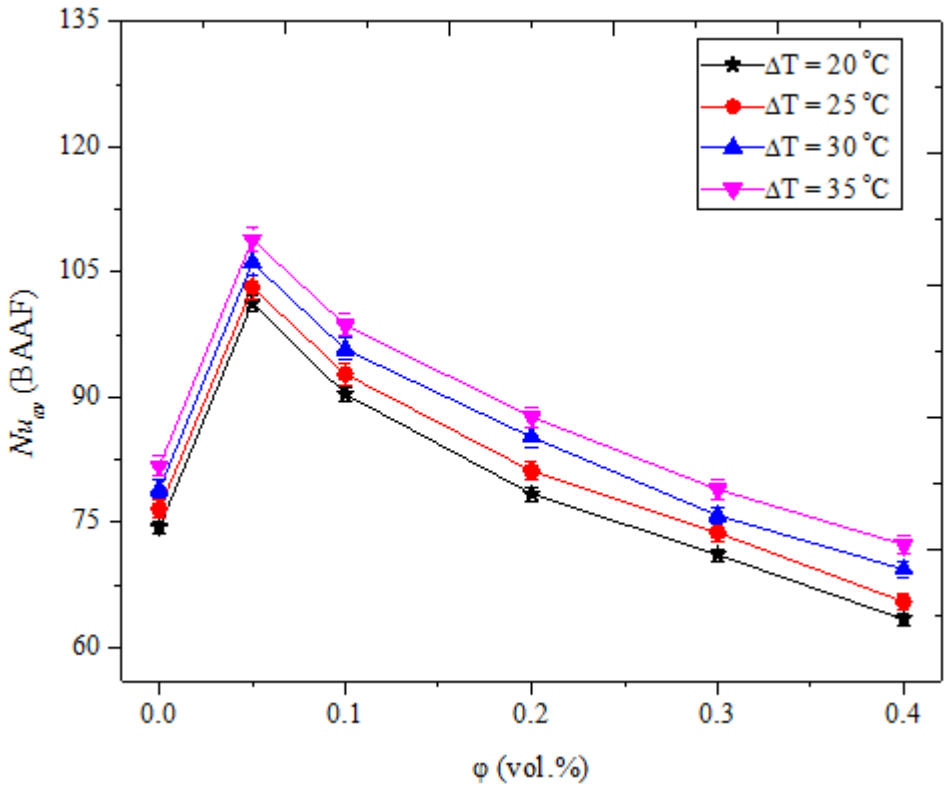

Figure 6.30: Relationship between Nu_{av} and φ for EG-DIW and BAAF samples at varying ΔT.

In Fig. 6.30, the Nu_{av} of BAAF as a function of φ at varying ΔT is presented. The uncertainty of 5.11% associated with Nu_{av} (BAAF) is shown in Fig. 6.30. In this study, the Nu_{av} of EG-DIW was 74.4 to 81.8 at 1.39 x 10^8 to 2.28 x 10^8 and ΔT = 20 to 35 °C, which was lower than the Nu_{av} (45 – 59) of EG-DIW (60:40 vol.%) obtained at ΔT = 20 to 50 °C and 1.4 x 10^8 to 3.5 x 10^8 reported by Solomon et al. [177]. This may be because the Nu_{av} of EG-DIW for this study was achieved at a lower ΔT, EG content, and range of *Ra*. The observed difference in Nu_{av} due to EG:DIW ratio was consistent with the work of Li et al. [158] as heat transfer reduced with an increase in EG content. Fig. 6.30 shows that increasing ΔT was observed to

enhance Nu_{av} but this was not the case for an increase in φ. Nu_{av} was enhanced as HNPs were suspended in EG-DIW for φ = 0.05 vol.%, a further increase in φ (> 0.05 vol.%) showed a reduction in Nu_{av}. Hence the optimum Nu_{av} (108.90) was attained at Ra = 1.63 x 10^8 and ΔT = 35 °C for φ = 0.05 vol.%. The attainment of maximum Nu_{av} at a certain φ value as reported in this work was found to agree with previous studies [151, 153, 177, 195]. At φ = 0.05 – 0.20 vol.%, enhancement of Nu_{av} by 7.15% to 33.14% was observed, whereas a deterioration of 3.46% and 11.54% was noticed for φ = 0.30 to 0.40 vol.% (see Figs 6.31 and 6.32). The optimum enhancement of Nu_{av} (BAAF) was found to be higher than the Nu_{av} of 5.63% and 6.76% published by Joubert et al. [88] and Moradi et al. [180] for Fe_2O_3/DIW (in a rectangular cavity) and Al_2O_3/W nanofluids (in a cylindrical cavity) respectively.

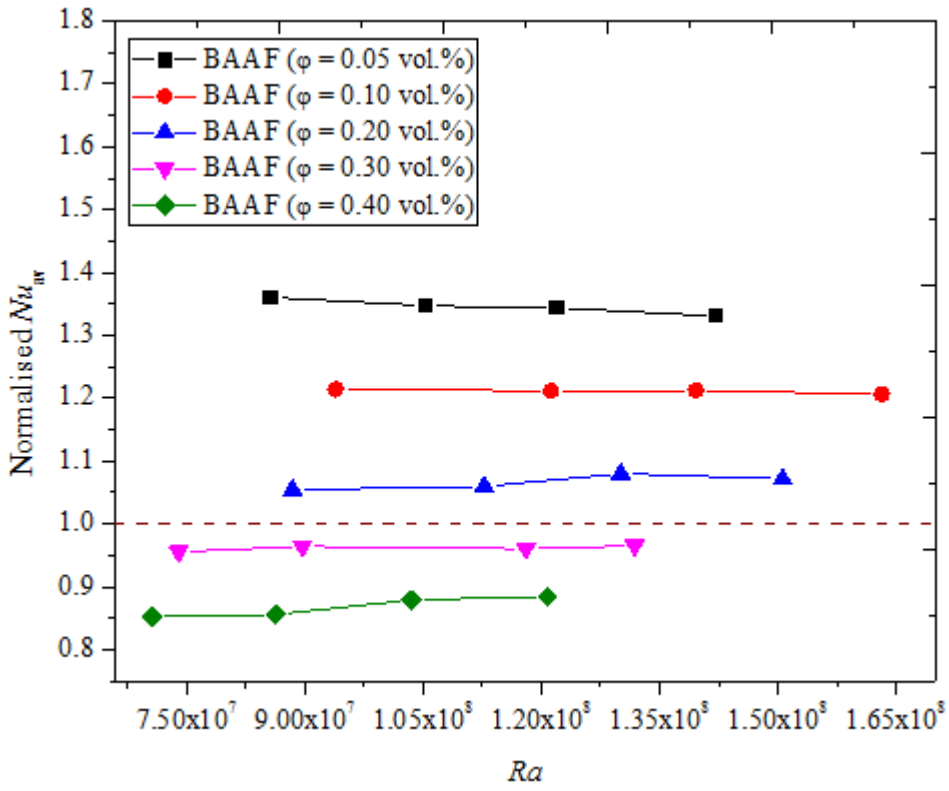

Figure 6.31: Normalised Nu_{av} against Ra for EG-DIW and BAAF samples.

The enhancement and attenuation of Nu_{av} (BAAF) are clearly presented in Figs 6.31 and 6.32. Normalised Nu_{av} (BAAF) as a function of Ra and ΔT both showed augmentation of Nu_{av} when $\varphi \leq 0.20$ vol.% and depreciation for $\varphi \geq 0.20$ vol.%. With a normalised Nu_{av}

(BAAF) value above unity, augmentation occurred and below unity, depreciation was observed. An increase in φ for BAAF resulted in the augmentation of ρ_{eff}, μ_{eff} and κ_{eff}, which caused Nu_{av} enhancement at lower φ ($\leq$ 0.20 vol.%) due to an increase in buoyancy force. However, at higher φ ($\geq$ 0.20 vol.%), ρ_{eff} and μ_{eff} were considerably increased thereby suppressing the effect of increased κ_{eff} and consequently, causing Nu_{av} deterioration because heat transfer was reduced due to buoyancy attenuation. This observation agreed with previous studies [22, 88, 153]. The present study showed that utilising hybrid nanofluid yielded higher Nu_{av} for BAAF. In addition, enhancement reported for Nu_{av} of BAAF was observed to be significantly higher than for AMF. This could be related to lower κ_{eff} of EG-DIW (as expressed in Eq. 3.12), which was augmented through suspension of the HNPs of Al_2O_3 and Fe_2O_3.

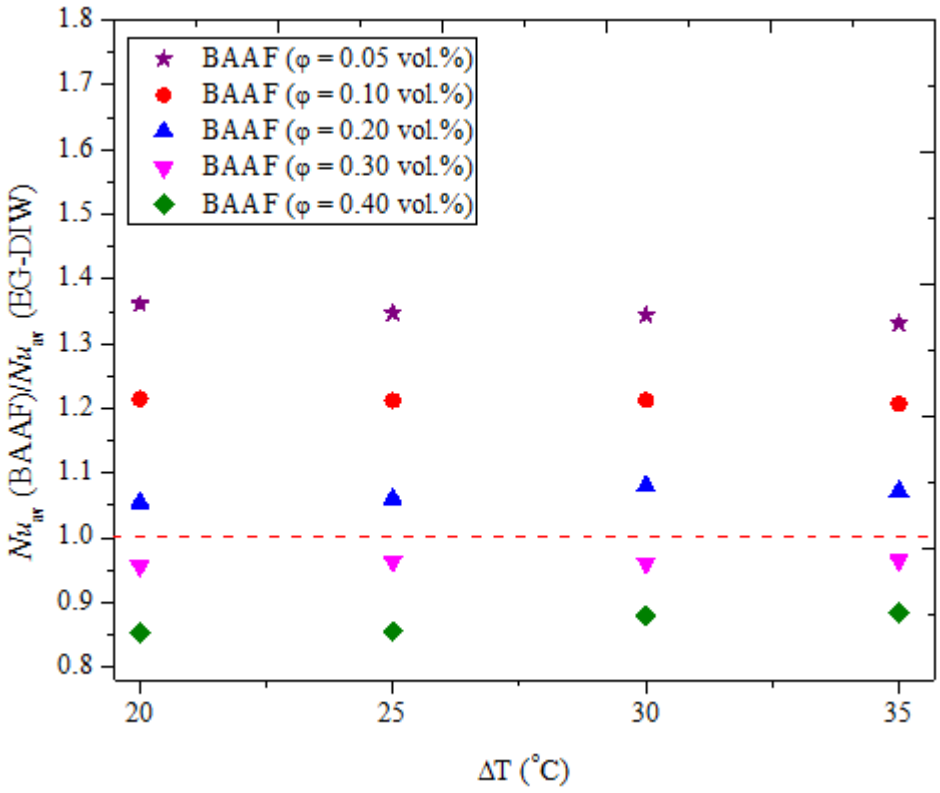

Figure 6.32: Normalised Nu_{av} against ΔT for EG-DIW and BAAF samples.

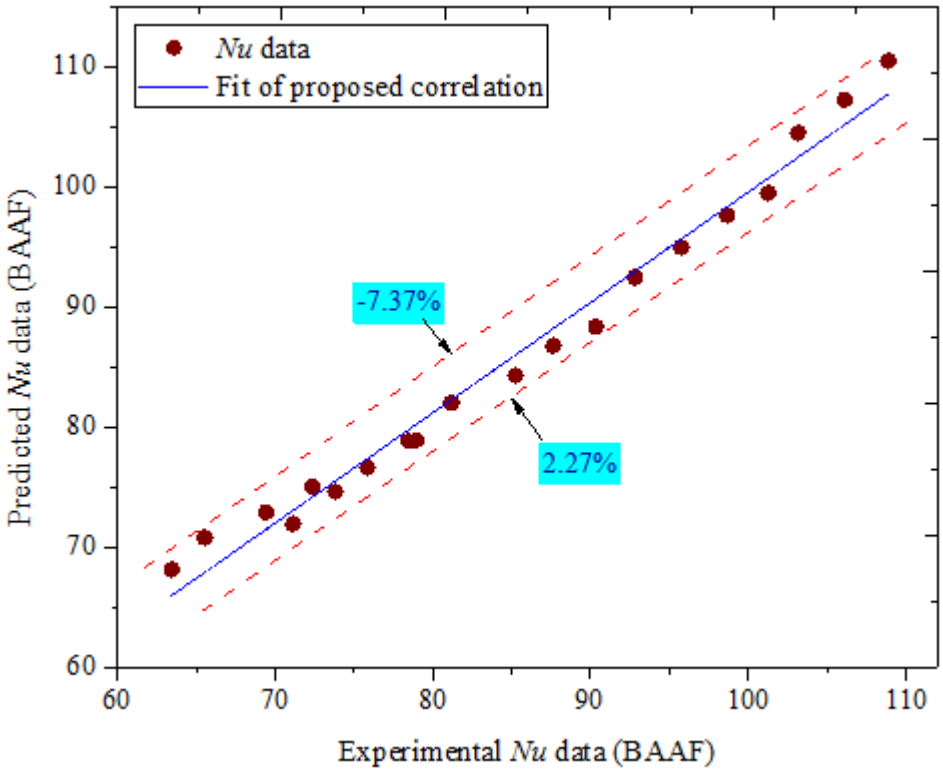

Figure 6.33: Fit of correlation for predicting Nu_{av} of BAAF.

The experimental data of the Nu_{av} of BAAF were fitted into a model for the prediction of Nu_{av}. The developed model is expressed by Eq. 6.2. The model had a coefficient of determination of 0.984, MAE of 1.85%, MSE of 0.0318, RMSE of 1.8062, and MOD of -7.37% and 2.27%. A fit of the correlation of the experimental and predicted data of the Nu_{av} of BAAF is provided in Fig. 6.2.

$$Nu = 0.891(Ra)^{0.235}\varphi^{-0.156} \qquad 6.2$$

6.4.1.3 Nusselt Number of AAF

The thermo-convection heat transfer behaviour of AAF and DIW in the rectangular cavity was studied and the result of the *Nu* parameter is presented in this section. In Fig. 6.34, the dependence of Nu_{av} on *Ra* for samples of AAF and DIW is illustrated. For all the tested samples, Nu_{av} was observed to be directly proportional to *Ra*, which was consistent with the literature [151, 153]. It was observed that DIW had the highest *Ra* values ($1.89 \times 10^8 - 3.04 \times 10^8$) at each ΔT compared with those of AAF ($1.49 \times 10^8 - 2.68 \times 10^8$). Contrary to this

observation, the Nu_{av} values of AAF were noticed to be higher for most AAF samples than

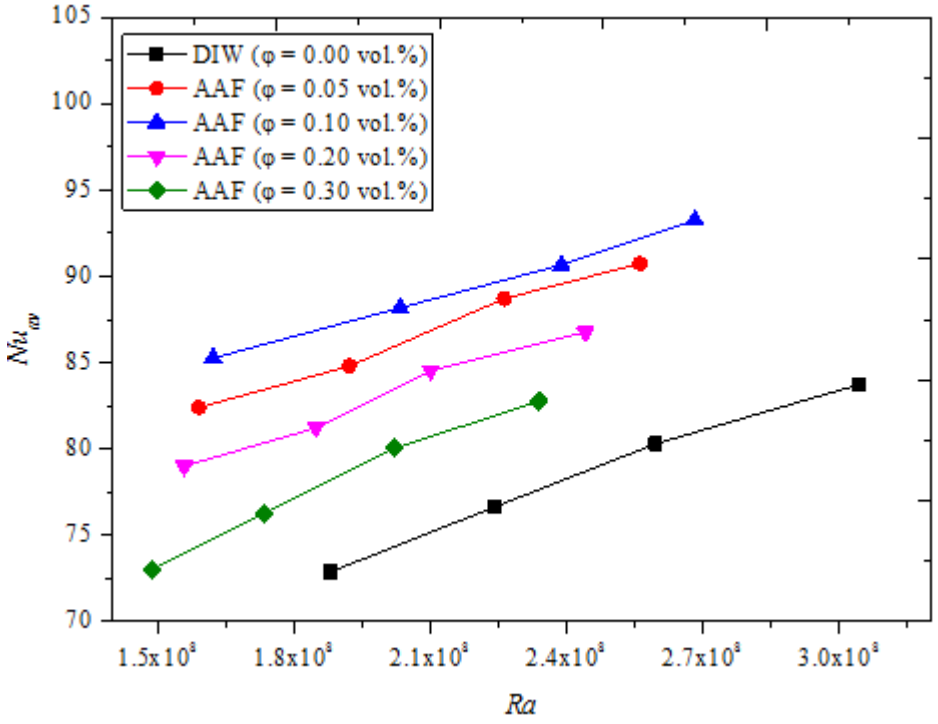

Figure 6.34: Relationship between Nu_{av} and Ra for DIW and AAF samples.

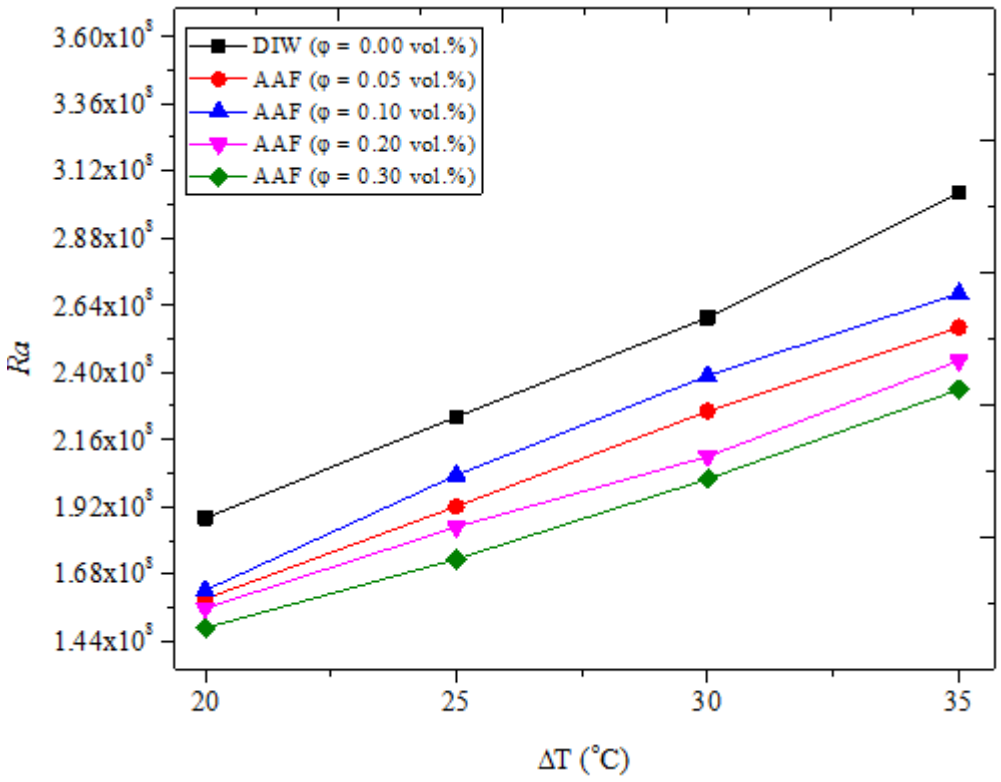

Figure 6.35: Relationship between Ra and ΔT for DIW and AAF samples.

for DIW. The suspension of HNPs (Fe_2O_3 and Al_2O_3) into DIW could be linked to the enhancement of Nu_{av} recorded for BAAF. Fig. 6.35 presents *Ra* as a function of ΔT for AAF and DIW. Increasing ΔT, in turn, increased *Ra* for the tested samples. Thus ΔT rise caused *Ra* increase and consequently, enhanced Nu_{av}.

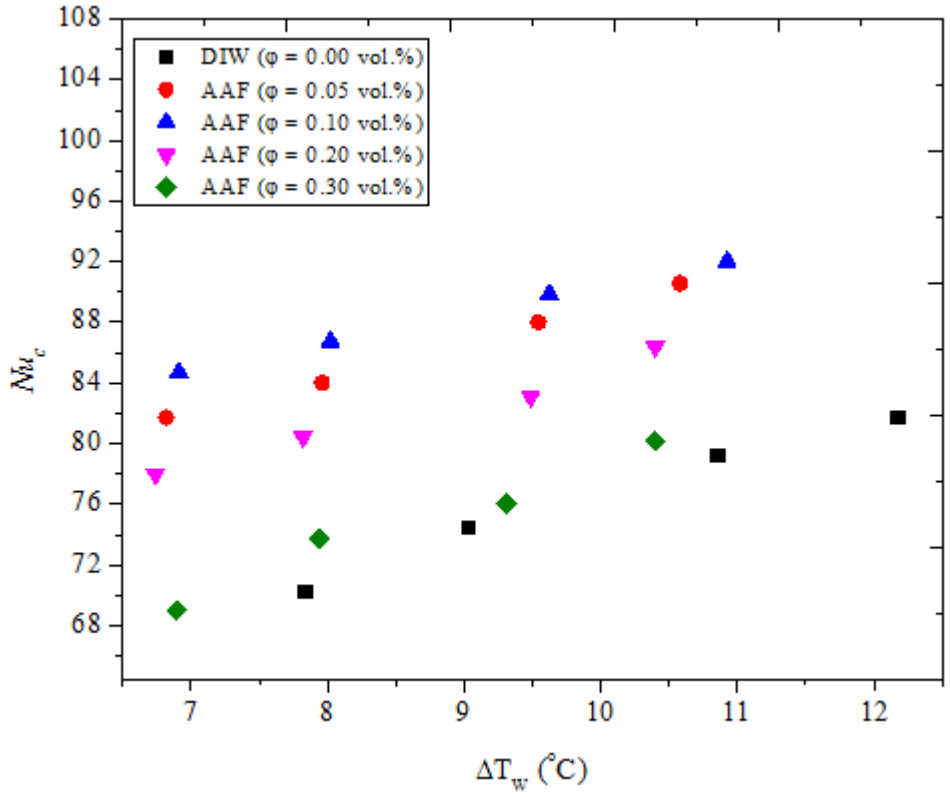

Figure 6.36: Relationship between Nu_c and ΔT_W for DIW and AAF samples.

Figs. 6.36 and 6.37 present the *Nu* parameter for AAF as a function of ΔT_W at the cold and hot walls of the cavity respectively. For the cold wall, Nu_c (AAF) was observed to augment with an increase in ΔT_W (Fig. 6.36). The highest Nu_c (91.06) was recorded for 0.10 vol.% AAF at ΔT_W = 10.93 °C, while DIW had the lowest Nu_c (81.41) at ΔT_W = 7.84 °C. Fig. 6.37 shows that Nu_h was directly related to ΔT_W for AAF and DIW, with 0.10 vol.% AAF yielding the maximum Nu_h of 94.46 (at ΔT_W = 10.93 °C) and DIW having the least value of Nu_h (84.12) at ΔT_W = 7.84 °C. The average of Nu_c and Nu_h for AAF as a function of ΔT is provided in Fig. 6.38. The peak Nu_{av} (92.76) was observed for 0.10 vol.% AAF at *Ra* = 2.68 x 10^8 and ΔT = 35 °C. This maximum Nu_{av} was noticed to be slightly above the Nu_{av} (82.76)

published by Joubert et al. [88] for 0.10 vol.% Fe_2O_3/DIW nanofluid (at 55 °C and *Ra* = 3.94 x 10^8) in a rectangular cavity.

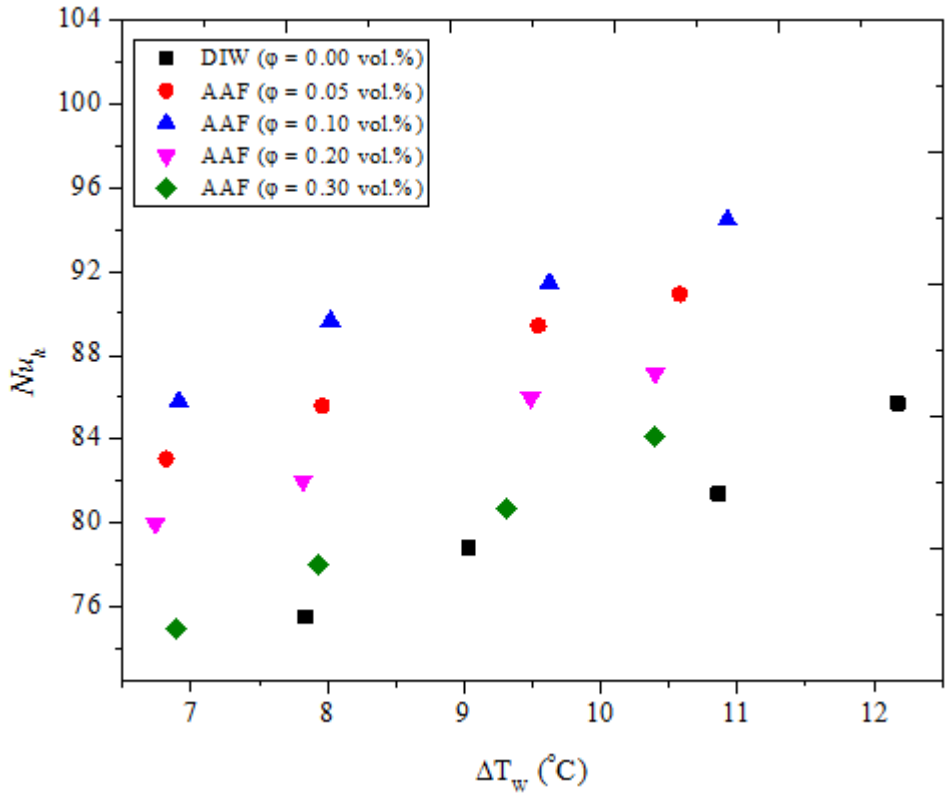

Figure 6.37: Relationship between Nu_h and ΔT_W for DIW and AAF samples.

Nu_{av} (AAF) is displayed as a function of φ and ΔT in Fig. 6.38, which consists of both the augmentation and deterioration scenarios. Relative to DIW, Nu_{av} was noticed to be augmented when $\varphi \geq 0.20$ vol.%, whereas at φ = 0.30 vol.%, attenuation was the case. Accordingly, enhancements of 6.41% (0.5 vol.%.), 10.81% (0.10 vol.%.) and 3.66% (0.2 vol.%.) were recorded for the Nu_{av} of AAF. However, at φ = 0.30 vol.%, Nu_{av} was deteriorated by 1.12%. With a maximum enhancement of 5.63% (Nu_{av}) reported by Joubert et al. [88] for monoparticle nanofluid (Fe_2O_3/DIW), the use of AAF was found to afford a higher Nu_{av} (10.81%), as recorded in this work. This result clearly revealed the effect of hybridising Fe_2O_3 NPs with Al_2O_3 NPs. In addition, enhancements of 6.76% and 11.8% to 17.2% were published for 0.2 vol.% Al_2O_3/W and 0.1 vol.% Al_2O_3-MWCNT/DIW nanofluids, which were lower and higher respectively than the value reported for AAF [52,

66]. As earlier stated in Sub-section 5.3.3, AAF had a lower μ_{eff} than for Fe_2O_3/DIW nanofluid, which probably influenced the improvement in Nu_{av} as lowered μ_{eff} favoured an increase in buoyancy by enhancing heat transfer. At higher φ (0.30 vol.%), the κ_{eff} and μ_{eff} of AAF increased leading to attenuation of Nu_{av} due to reduction in buoyancy force. The scenarios of enhancement and attenuation were clearly presented using normalised Nu_{av} as a function of *Ra* and ΔT as shown in Figs. 6.39 and 6.40 respectively. Figs. 6.39 and 6.40 respectively show that the normalised Nu_{av} value of ≥1 specified appreciation in the Nu_{av} of AAF, while <1 indicated depreciation as a function of *Ra* and ΔT.

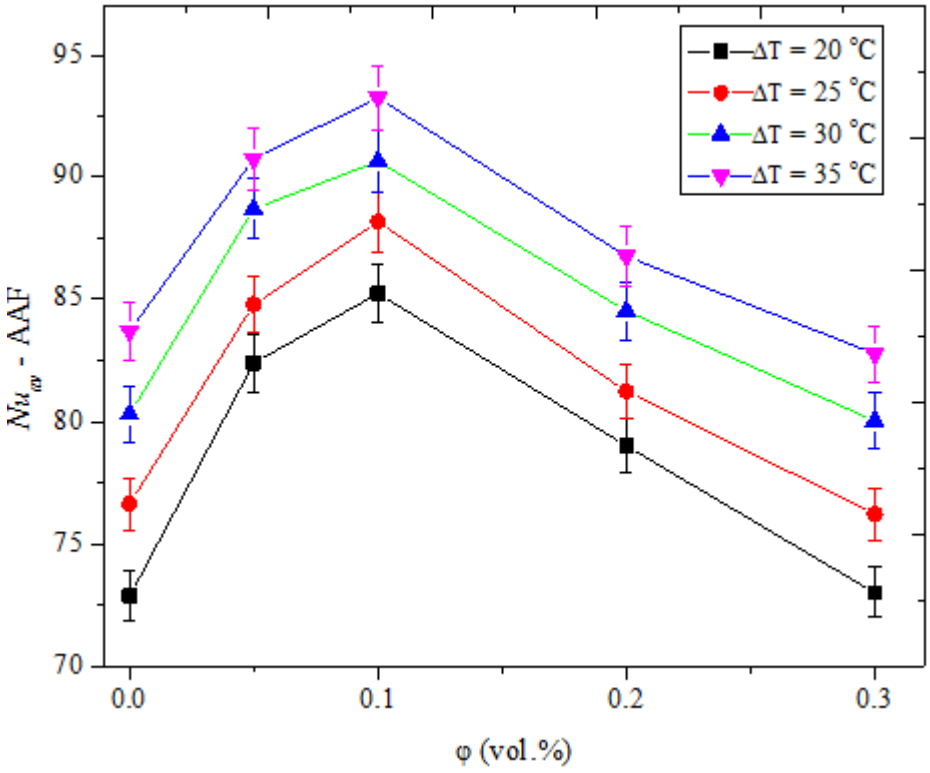

Figure 6.38: Relationship between Nu_{av} and φ for DIW and AAF samples at varying ΔT.

Owing to a limited model for the estimation of the Nu_{av} of nanofluids studied in a cavity, a model was developed by regressing the experimental data of Nu_{av} (AAF). This developed model is given in Eq. 6.3.

$$Nu = 0.721(Ra)^{0.2429}\varphi^{-0.0613} \qquad \textbf{6.3}$$

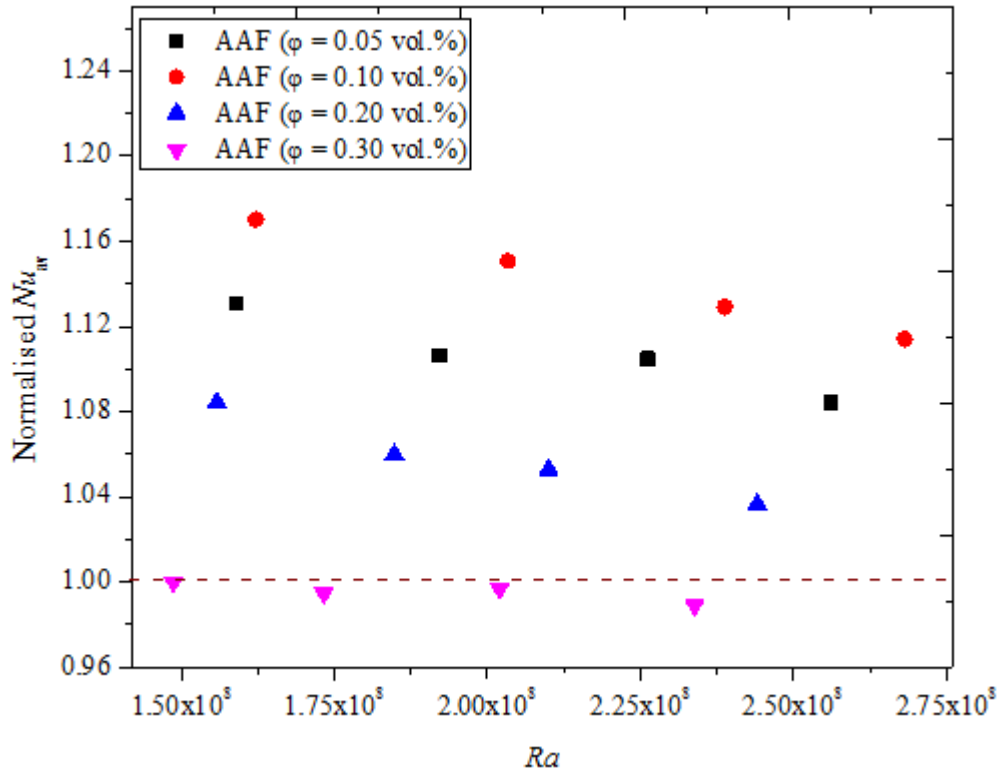

Figure 6.39: Normalised Nu_{av} against Ra for DIW and AAF samples.

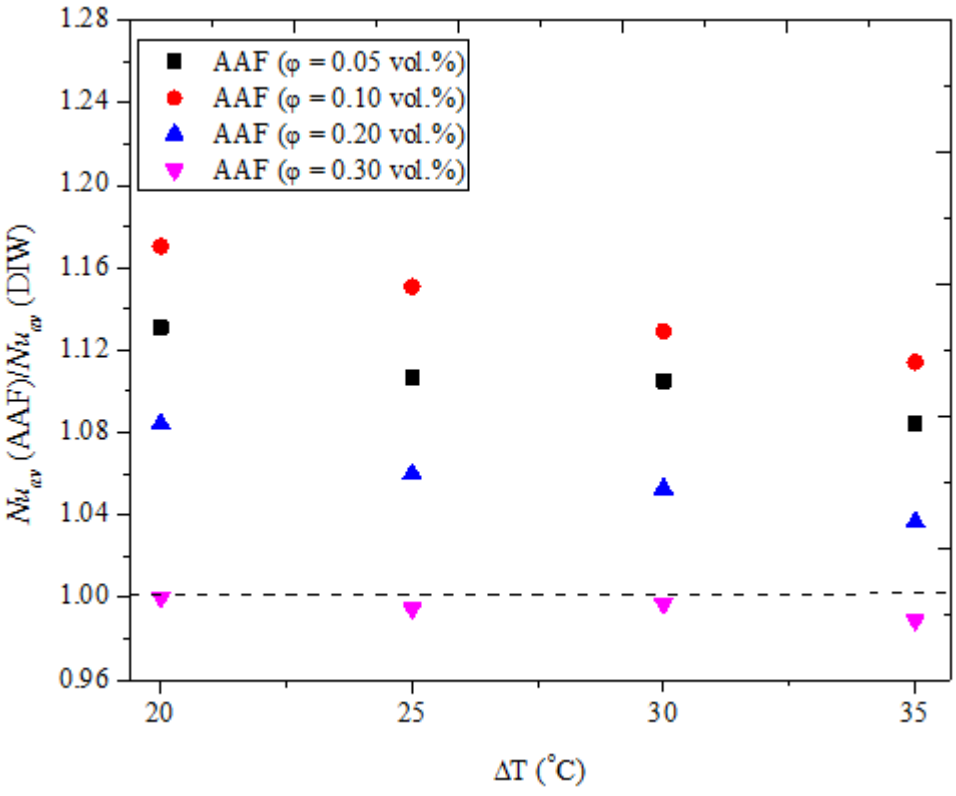

Figure 6.40: Normalised Nu_{av} against ΔT for DIW and AAF samples.

The prediction performance capability of the model was ≈94%. Also, it had a MOD of -2.66% and 2.96%, MAE of 1.498%, MSE of 0.0643, and RMSE of 1.5168. Furthermore, the fit of predicting Nu_{av} (AAF) from experimental data is provided in Fig. 6.41.

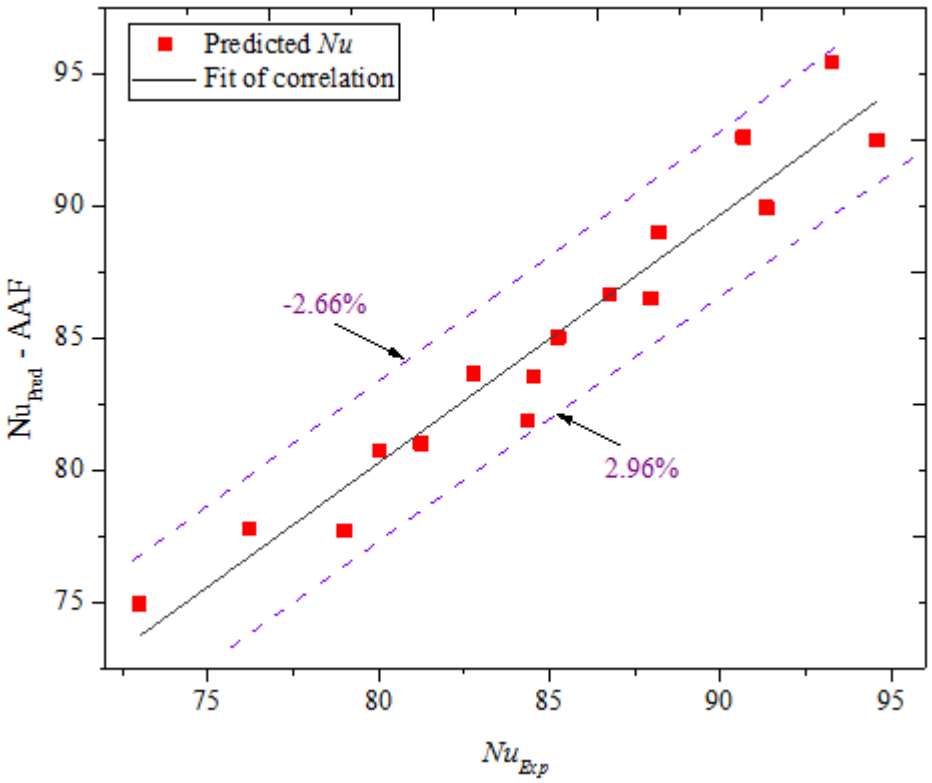

Figure 6.41: Fit of correlation for predicting Nu_{av} of AAF.

6.4.2 Convective Heat Transfer Coefficient of MHNFs

6.4.2.1 Convective Heat Transfer Coefficient of AMF

In the present work, h (h_c, h_h, and h_{av}) was considered as another parameter for the thermo-convection heat transfer investigation of MHNFs (AMF, BAAF and AAF) in the rectangular cavity. The results obtained for h when AMF was used in the cavity were discussed. In Figs. 6.42 and 6.43, the dependence of h_c and h_h on ΔT_W is illustrated. Fig. 6.42 shows that h_c was directly related to ΔT_W because the rise in ΔT increased ΔT_W, which, in turn, enhanced h_c for AMF and DIW. Values of ΔT_W were higher for DIW (7.84 – 12.17 °C) than for AMF (5.33 – 11.40 °C). However, DIW had h_c values lower than for some AMF samples.

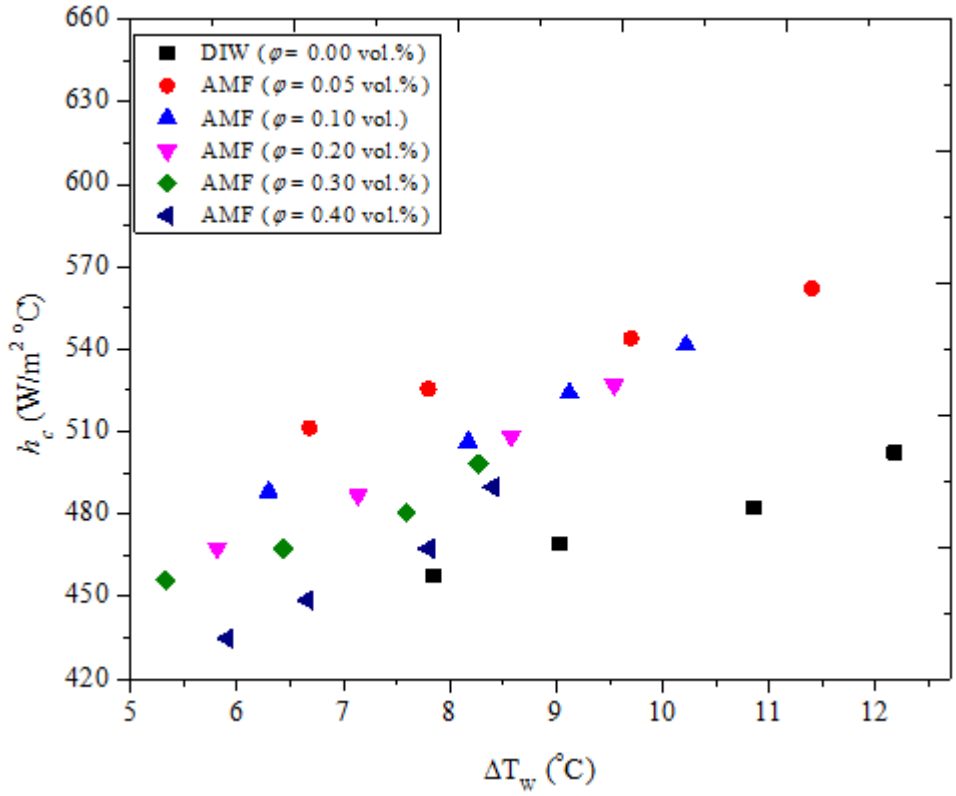

Figure 6.42: Relationship between h_c and ΔT_W for DIW and AMF samples.

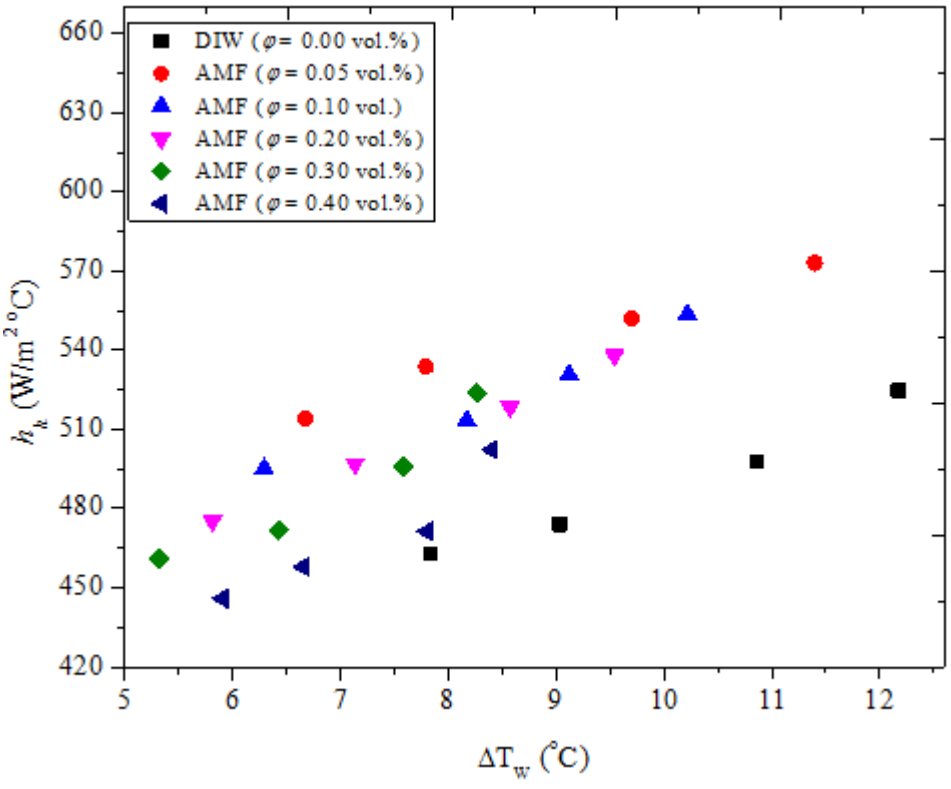

Figure 6.43: Relationship between h_h and ΔT_W for DIW and AMF samples.

The highest h_c (566.94 W/m^2 °C) was attained with 0.05 vol.% AMF at ΔT_W = 11.40 °C. An identical trend was observed between h_c and ΔT_W, and h_h and ΔT_W in Figs. 6.42 and 6.43 respectively. Similarly, the h_h values were noticed to enhance as ΔT_W increased, with h_h = 579.05 W/m^2 °C (for 0.05 vol.% AMF) as the peak value (Fig. 6.43).

Fig. 6.44 illustrates the dependence of h_{av} on φ at different ΔT studied in this work for AMF and DIW. An increase in ΔT was found to augment h_{av} for all the tested samples. Suspending HNPs into DIW enhanced the h_{av} of DIW for some AMF samples. Peak h_{av} (572.99 W/m^2 °C) was observed with 0.05 vol.% AMF sample at ΔT = 35 °C. As φ increased from 0.00 to 0.20 vol.%, an enhancement of h_{av} was noticed, whereas beyond φ = 0.2 vol.% deterioration of h_{av} was the case. The use of AMF in the cavity led to enhancements of h_{av} by 11.59% (0.05 vol.%), 6.62% (0.10 vol.%) and 3.70% (0.20 vol.%), and attenuation of h_{av} by 0.48% (0.30 vol.%) and 3.38% (0.40 vol.%) at ΔT = 35 °C compared with those of DIW.

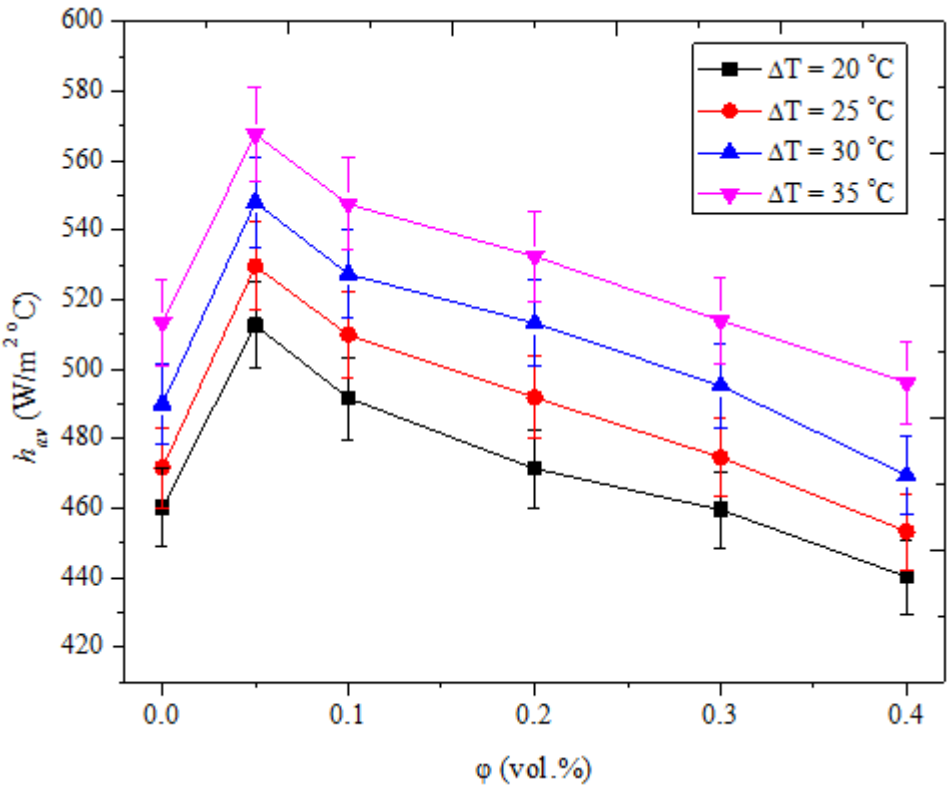

Figure 6.44: Relationship between h_{av} and φ for DIW and AMF samples at varying ΔT.

As earlier discussed, lower μ_{eff} and ρ_{eff} of AMF at φ = 0.05 – 0.20 vol.% were responsible for the enhancement recorded for these concentrations because an increase in buoyancy caused heat transfer enhancement. This was found to be consistent with the literature [151, 153, 162, 195]. Fig. 6.45 shows the normalised h_{av} as related to ΔT for AMF and DIW. Both the enhancement ($\varphi \leq$ 0.20 vol.%) and deterioration ($\varphi \geq$ 0.20 vol.%) of h_{av} (AMF) were indicated by normalised h_{av} of ≥1 and <1 respectively.

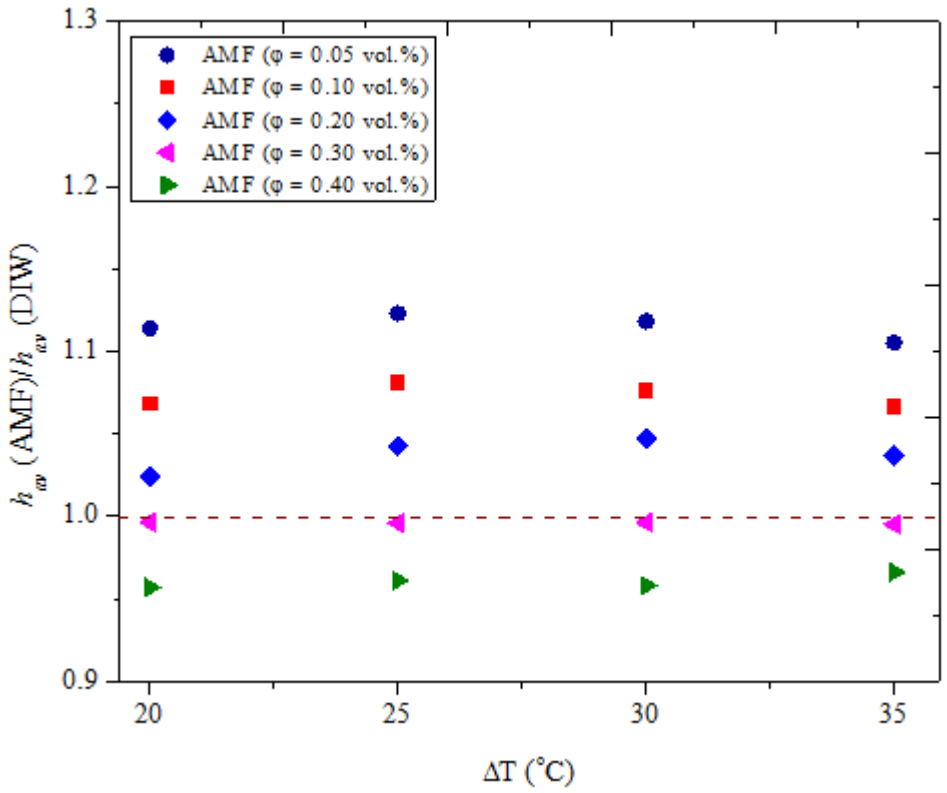

Figure 6.45: Normalised h_{av} against ΔT for DIW and AMF samples.

6.4.2.2 Convective Heat Transfer Coefficient of BAAF

Both Figs. 6.46 and 6.47 present h at the cold and hot walls of the cavity containing BAAF respectively as a dependent ΔT_W. An increase in ΔT_W was observed to enhance h_c and h_h. Of the samples, EG-DIW had the highest ΔT_W (9.79 – 15.54 °C), whereas 0.05 vol.% BAAF yielded maximum h_c (464.94 W/m^2 °C) and h_h (481.48 W/m^2 °C). Figs. 6.46 and 6.47 indicate that only $\varphi \leq$ 0.20 vol.% had h_c and h_h values higher than EG-DIW. In Fig. 6.48, the influence of φ on h_{av} (BAAF) as ΔT increased is presented. A direct relationship was

observed to exist between h_{av} and ΔT because an increase in ΔT resulted in the enhancement of h_{av}. Increasing φ from 0.00 to 0.40 vol.% was noticed to enhance h_{av} to a peak value and further increase in φ caused reduction in h_{av}. At 35 °C and φ = 0.05 vol.%, h_{av} was found to be augmented by 33.17% relative to EG-DIW. Augmentation of the h_{av} of BAAF by 20.75% and 10.21% was observed for φ = 0.10 vol.% and 0.2 vol.%, whereas deterioration of 0.10% and 7.70% was recorded for φ = 0.3 vol.% and 0.4 vol.% respectively compared with EG-DIW. The enhancement of h_{av} (BAAF) obtained in the present study was above 15% (Al_2O_3/DIW nanofluid) [152], 18% (Al_2O_3/W nanofluid) [161] and 12.7% to 19.4% (Al_2O_3-MWCNT/DIW nanofluid) [165] published for thermo-convection of monoparticle and hybrid nanofluids in square and rectangular cavities, although with a different base fluid. Fig. 6.49 presents the normalised h_{av} as a function of ΔT for BAAF and EG-DIW.

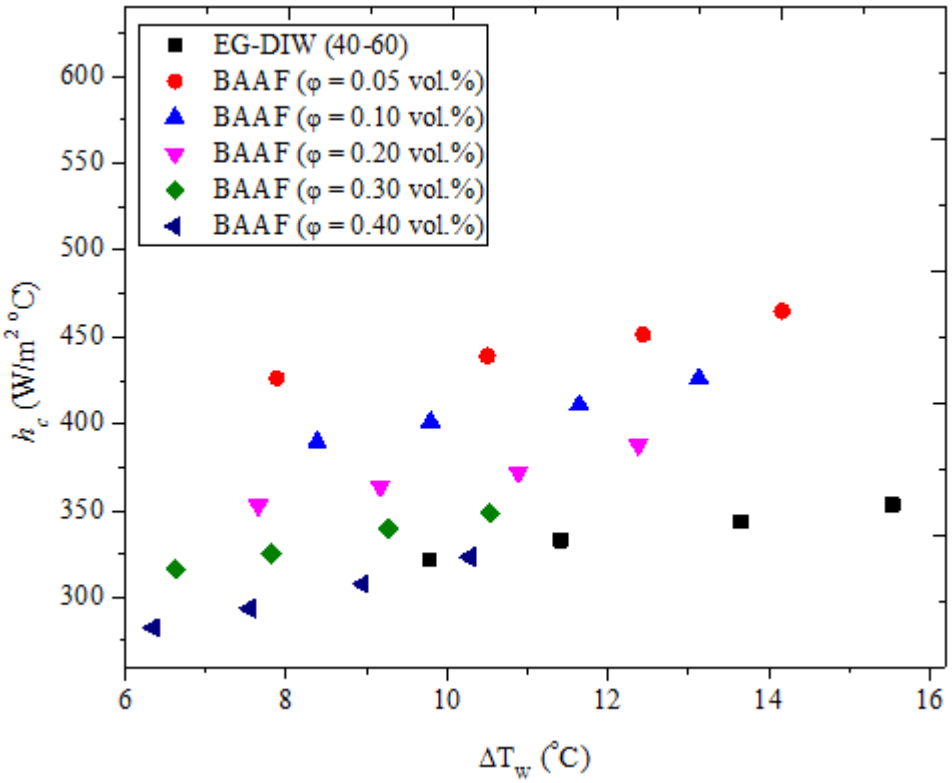

Figure 6.46: Relationship between h_c and ΔT_W for EG-DIW and BAAF samples.

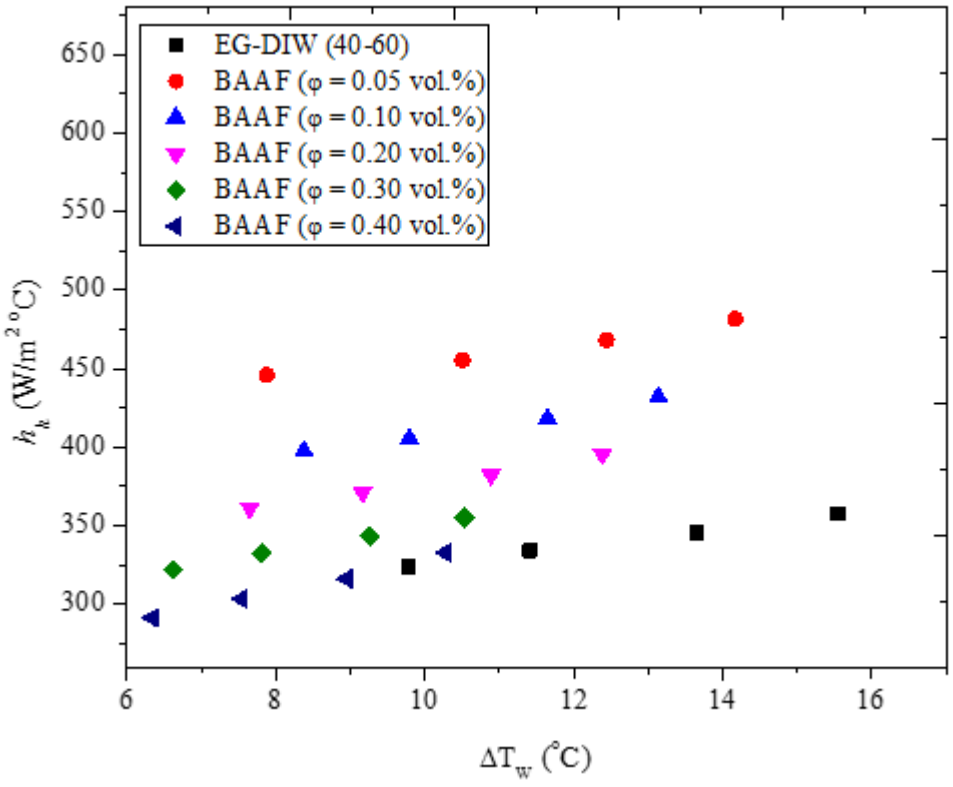

Figure 6.47: Relationship between h_h and ΔT_W for EG-DIW and BAAF samples.

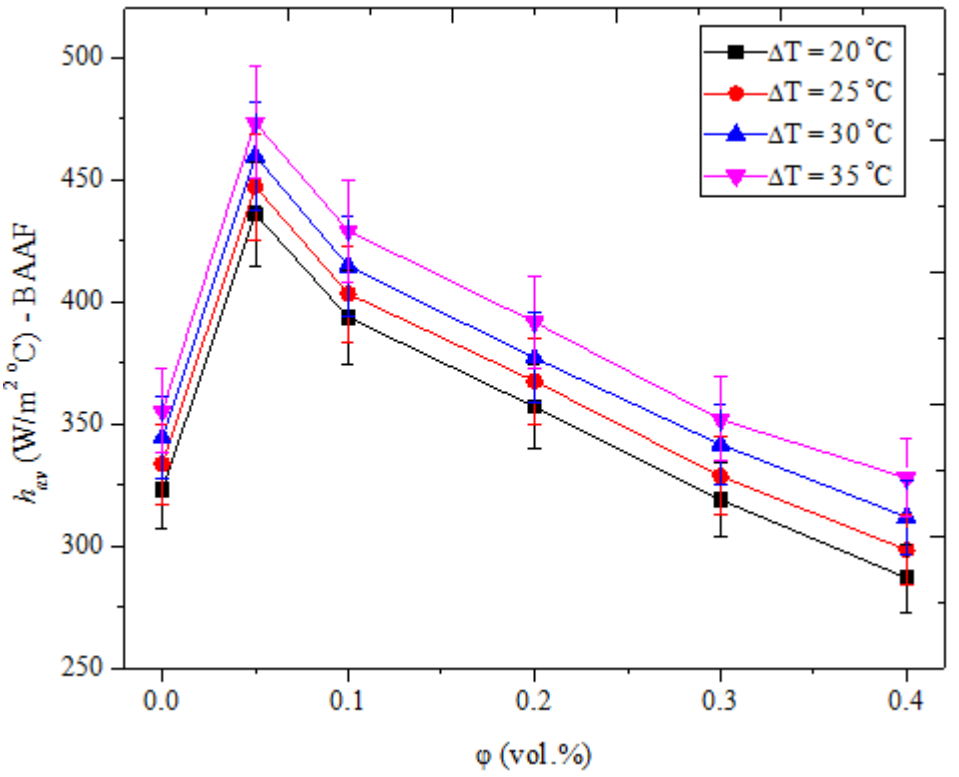

Figure 6.48: Relationship between h_{av} and φ for EG-DIW and BAAF samples at varying ΔT.

With a normalised h_{av} value of ≥1, enhancement of h_{av} was recorded for $\varphi \leq 0.2$ vol.% in comparison with EG-DIW shown in Fig. 6.49. However, a normalised h_{av} of <1 signified deterioration of h_{av} relative to EG-DIW for $\varphi > 0.2$ vol.%.

6.4.2.3 Convective Heat Transfer Coefficient of AAF

In Figs. 6.50 and 6.51, the h_c and h_h of AAF as a function of ΔT_W for AAF and DIW are illustrated. A similar pattern was noticed for both figures relating to h_c and h_h as a dependent of ΔT_W. An increase in ΔT_W led to a corresponding enhancement of h_c and h_h. Also, ΔT_W values were noticed to be the highest for DIW samples, while h_c and h_h were at maximum values for 0.10 vol.% AFF.

The effect of φ on the h_{av} at different ΔT values for DIW and AAF is shown in Fig. 6.52, which indicates that as ΔT increased, h_{av} was augmented. With an increase in φ, the h_{av} of DIW was increased for φ = 0.00 to 0.10 vol.% and thereafter decreased. Fig. 6.52 indicates that the h_{av} (AAF) values for φ = 0.05 to 0.20 vol.% were higher than those of φ = 0.30 vol.%, when compared with the h_{av} of DIW. This indicated augmentation and deterioration of h_{av} in relation to that of DIW. At φ = 0.10 vol.% and ΔT = 35 °C, optimum h_{av} (571.66 W/m^2 °C) was attained, which was an augmentation of 11.92%. The reduction in μ_{eff} for 0.10 vol.% AAF increased buoyancy and heat transfer, which caused h_{av} augmentation, as observed in this study. However, the reverse was the case for φ = 0.30 vol.% with increased μ_{eff}. Augmentations of h_{av} by 15% [152], 18% [161] and 12.7 to 19.4% [165] for monoparticle nanofluids (Al_2O_3/DIW) and hybrid nanofluids (Al_2O_3-MWCNT/DIW) in cavities were found to be higher than those reported for h_{av} (AAF) in the present work. In addition, the h_{av} of AMF and AAF was observed to be lower than that for BAAF.

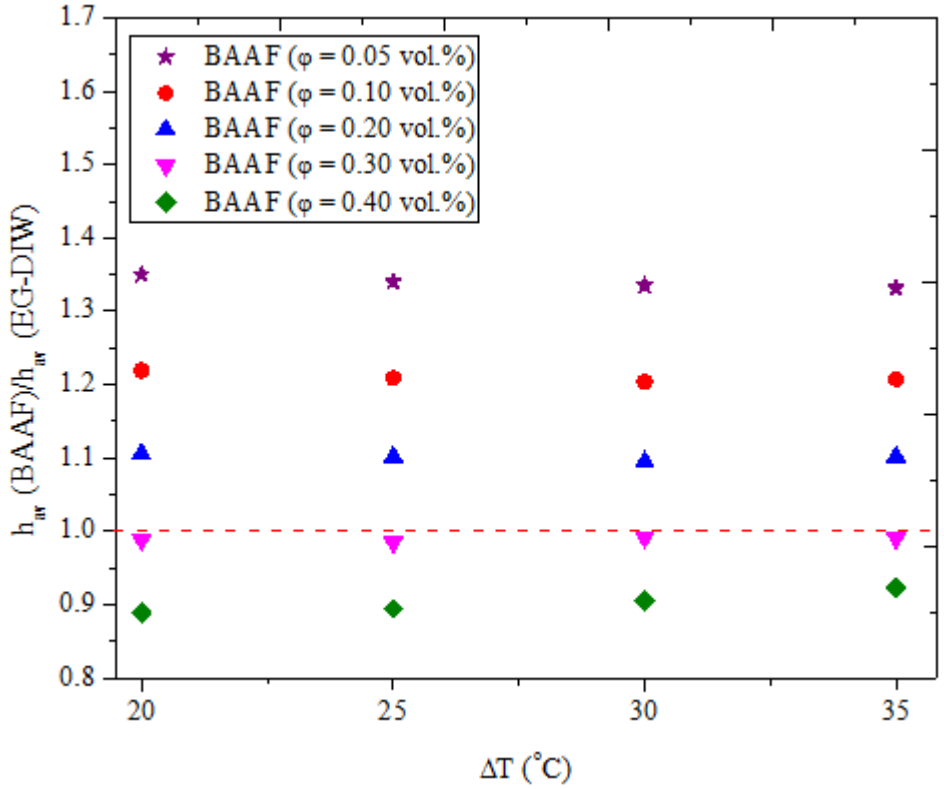

Figure 6.49: Normalised h_{av} against ΔT for EG-DIW and BAAF samples.

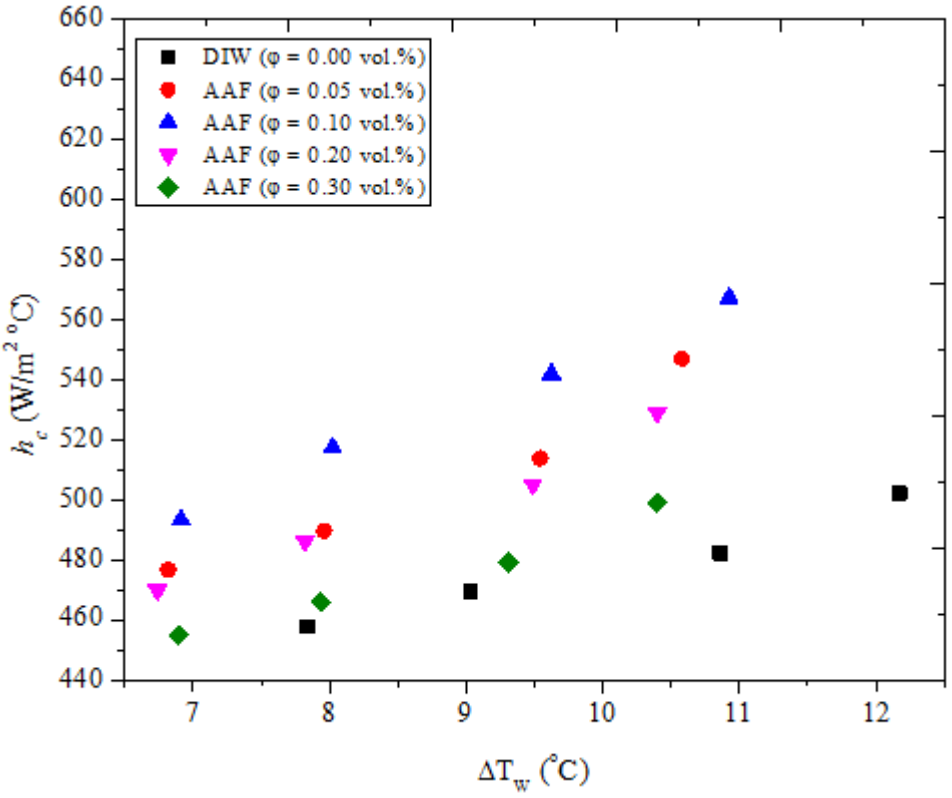

Figure 6.50: Relationship between h_c and ΔT_W for DIW and AAF samples.

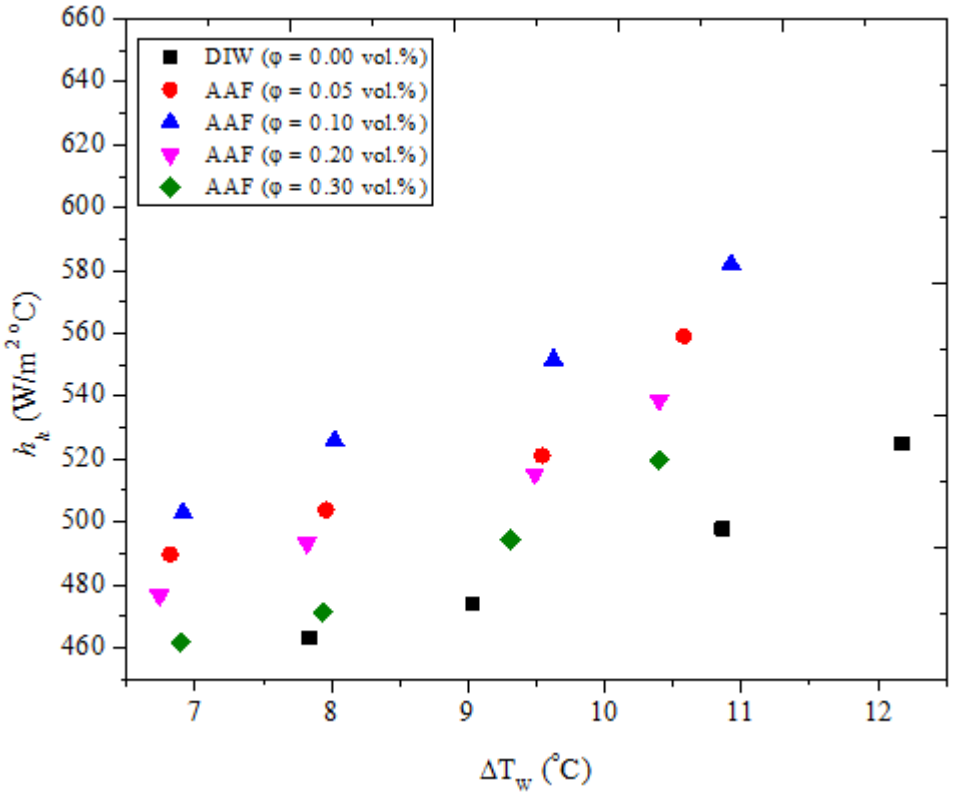

Figure 6.51: Relationship between h_h and ΔT_W for DIW and AAF samples.

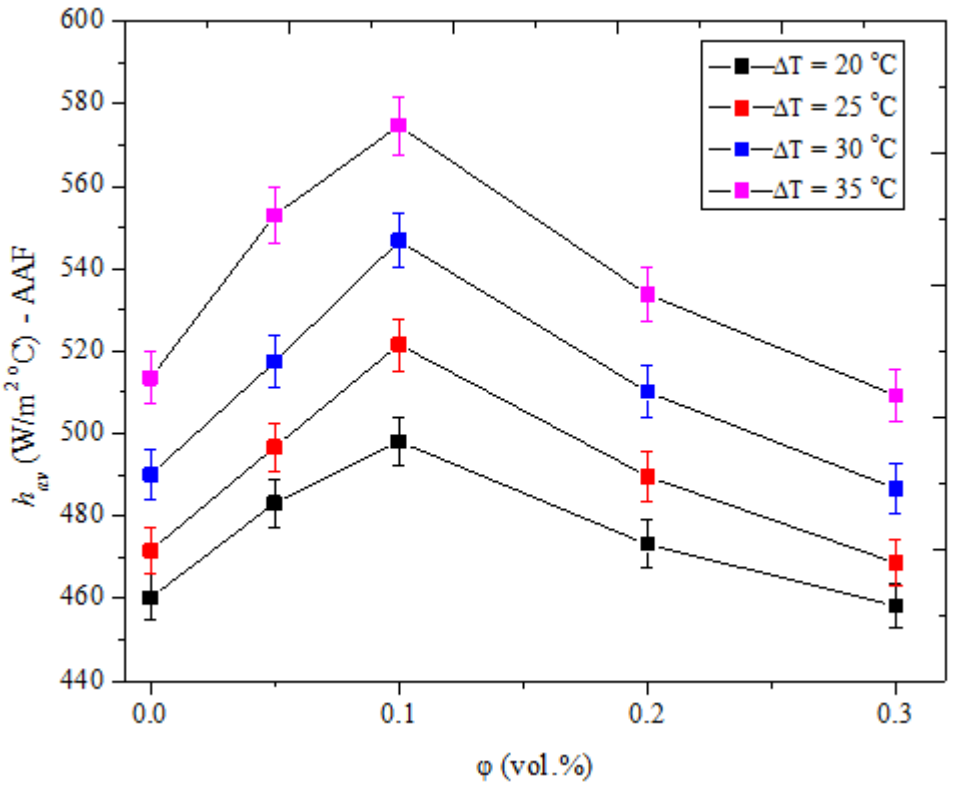

Figure 6.52: Relationship between h_{av} and φ for DIW and AAF samples at varying ΔT.

In Fig. 6.53, the normalised h_{av} of AAF is presented as a function of ΔT in order to properly represent the augmentation and deterioration of h_{av} (AAF) with respect to the h_{av} of DIW. Below normalised h_{av} of 1, deterioration was noticed to occur for φ = 0.30 vol.%, whereas with normalised h_{av} of ≥1, augmentation was recorded for $\varphi \geq 0.20$ vol.%.

6.4.3 Heat Transfer Capacity of MHNFs

6.4.3.1 Heat Transfer Capacity of AMF

The thermo-convection heat transfer of MHNFs in the cavity was studied for the third parameter, Q (Q_c, Q_h and Q_{av}). In Figs. 6.54 and 6.55, the influence of ΔT_W on Q_c and Q_h for DIW and AMF is shown. Increasing ΔT_W enhanced Q_c and Q_h (both figures). DIW had ΔT_W range of 6.68 to 11.40 °C, which was observed to be higher than that of AMF (5.33 – 10.22 °C). Because the patterns in Figs. 6.54 and 6.55 were identical, the Q_c and Q_h of AMF samples with φ = 0.05 to 0.20 vol.% were higher than Q_c and Q_h of DIW. Peak Q_c and Q_h values were 70.52 W and 71.59 W respectively, for 0.05 vol% AMF at ΔT_W = 10.22 °C. The dependence of Q_{av} on φ with an increase in ΔT for DIW and AMF is shown in Fig. 6.56. A rise in ΔT from 20 to 35 °C was noticed to enhance Q_{av}. Increasing φ from 0.00 to 0.40 vol.% resulted in both enhancement and attenuation of Q_{av} (AMF) when $\varphi \leq 0.20$ vol.% and $\varphi >$ 0.20 vol.% respectively. Maximum Q_{av} (AMF) of 572.99 W was achieved with φ = 0.05 vol.% at ΔT = 35 °C. The highest enhancements of 11.21%, 8.36% and 5.52% were recorded for φ = 0.05, 0.10 and 0.20 vol.% respectively compared with DIW. However, Q_{av} was detracted by 0.49% (φ = 0.30 vol.%) and 3.39% (φ = 0.40 vol.%). Fig. 6.57 gives the normalised Q_{av} of AMF (an indicator of the comparison of the Q_{av} of AMF with the Q_{av} of DIW) as a function of ΔT. With normalised Q_{av} of ≥ 1, enhancement was observed for $\varphi \leq$ 0.20 vol.%, but attenuation was the case for $\varphi >$ 0.20 vol.% having normalised Q_{av} of <1.

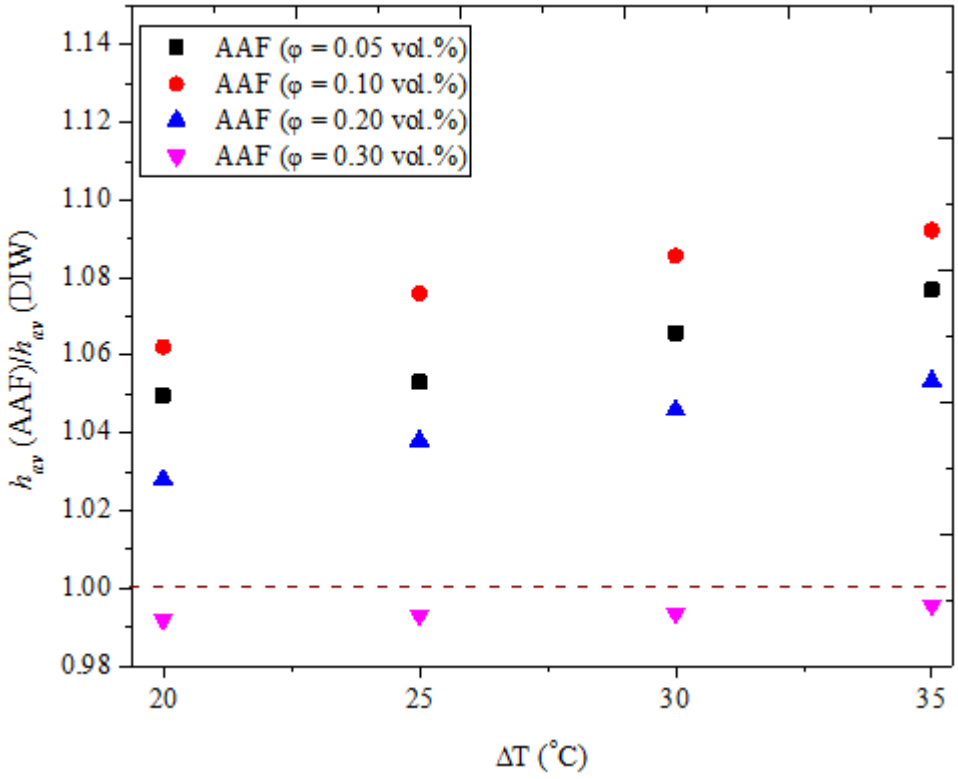

Figure 6.53: Normalised h_{av} against ΔT for DIW and AAF samples.

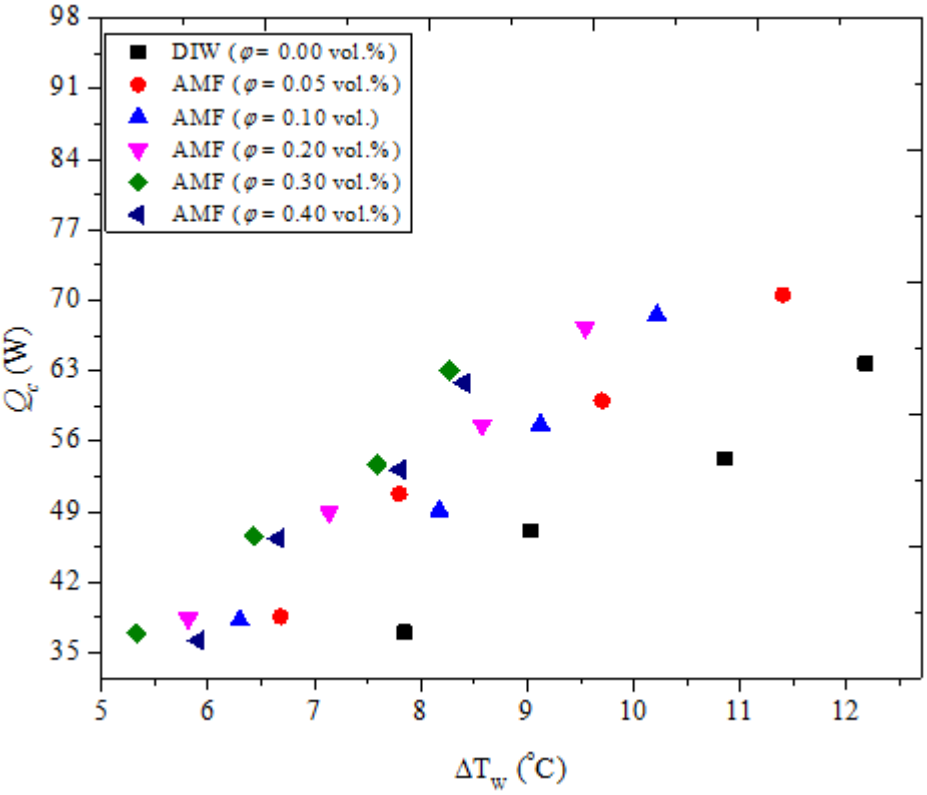

Figure 6.54: Relationship between Q_c and ΔT_W for DIW and AMF samples.

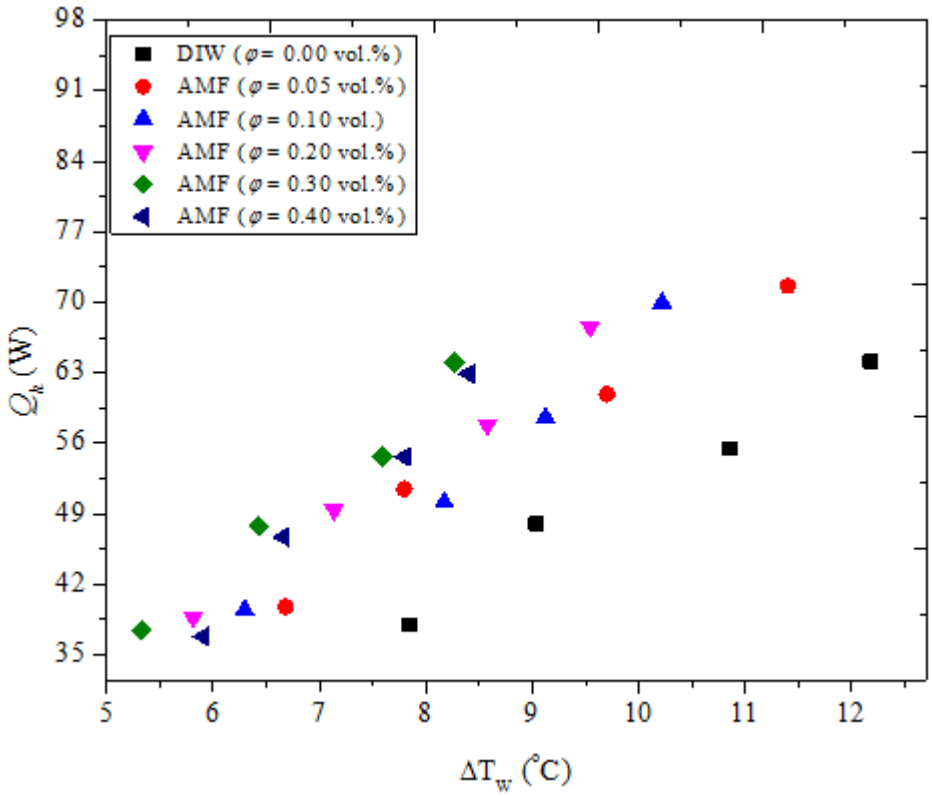

Figure 6.55: Relationship between Q_h and ΔT_W for DIW and AMF samples.

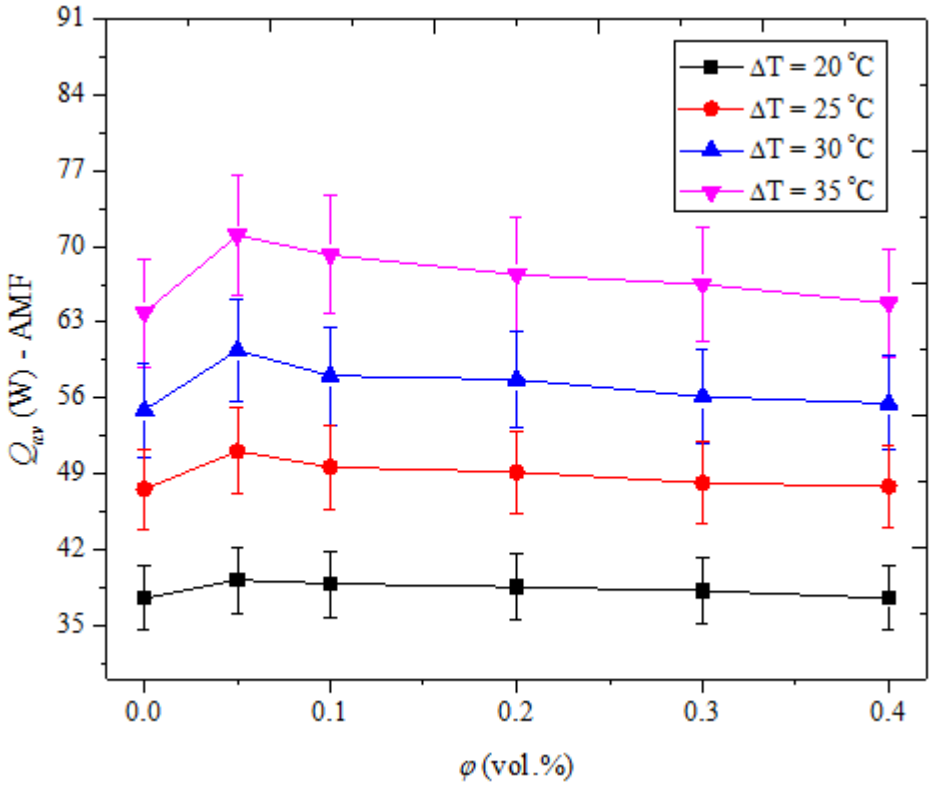

Figure 6.56: Relationship between Q_{av} and φ for DIW and AMF samples at varying ΔT.

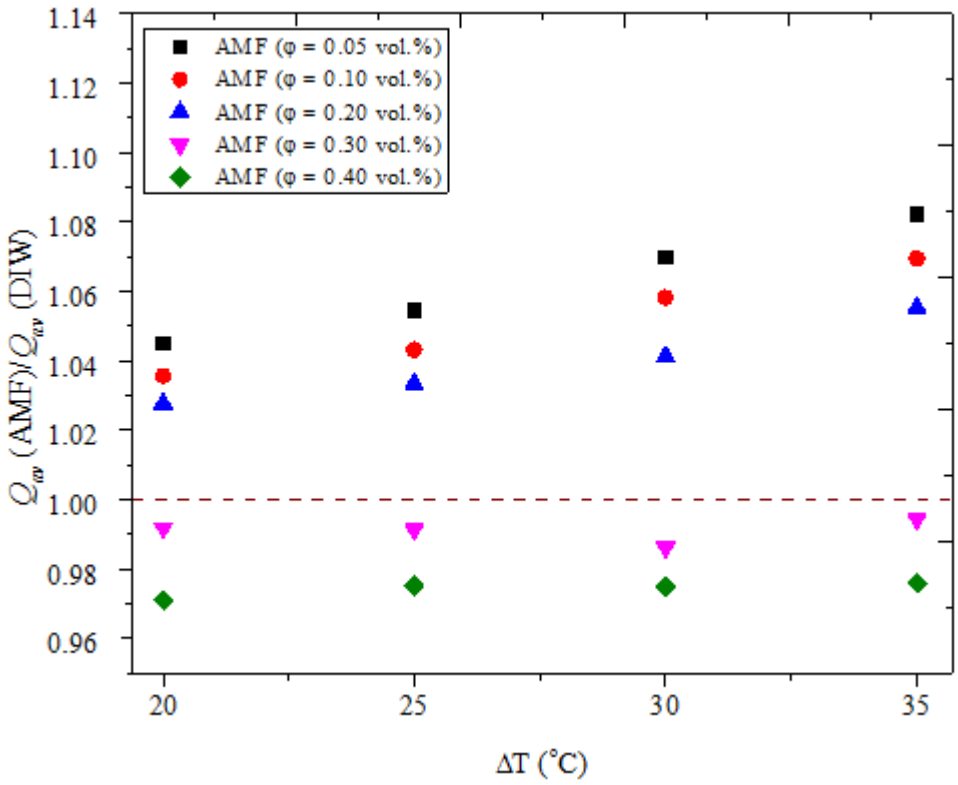

Figure 6.57: Normalised Q_{av} against ΔT for DIW and AMF samples.

The optimum Q_{av} (AMF) recorded in this study was found to be higher than that reported in the literature for TiO_2/DIW (8.2%) and Al_2O_3-MWCNT/DIW (7.2% - 9.8%) nanofluids in rectangular cavities [153, 165].

6.4.3.2 Heat Transfer Capacity of BAAF

The results of the heat transfer capacity of BAAF in the rectangular cavity are presented in this subsection. The Q_c and Q_h of BAAF at the cold and hot walls of the cavity are shown in Figs. 6.58 and 6.59 respectively. With a similar trend observed for Q_c and Q_h as a function of ΔT_W in Figs. 6.58 and 6.59, increasing ΔT_W equally enhanced Q_c and Q_h. Ranges of 6.34 to 15.54 °C, 41.90 W to 69.82 W and 43.37 W to 70.75 W were recorded for ΔT_W, Q_c and Q_h of EG-DIW and BAAF samples respectively. Both figures show that ΔT_W was higher for EG-DIW than for BAAF samples, while Q_c and Q_h values were the highest for 0.05 vol. BAAF. An illustration of the influence of φ on Q_{av} at various ΔT is provided in Fig. 6.60. Again, ΔT increment augmented Q_{av}. As φ increased, Q_{av} enhanced for $\varphi \leq 0.20$ vol.%, after which it

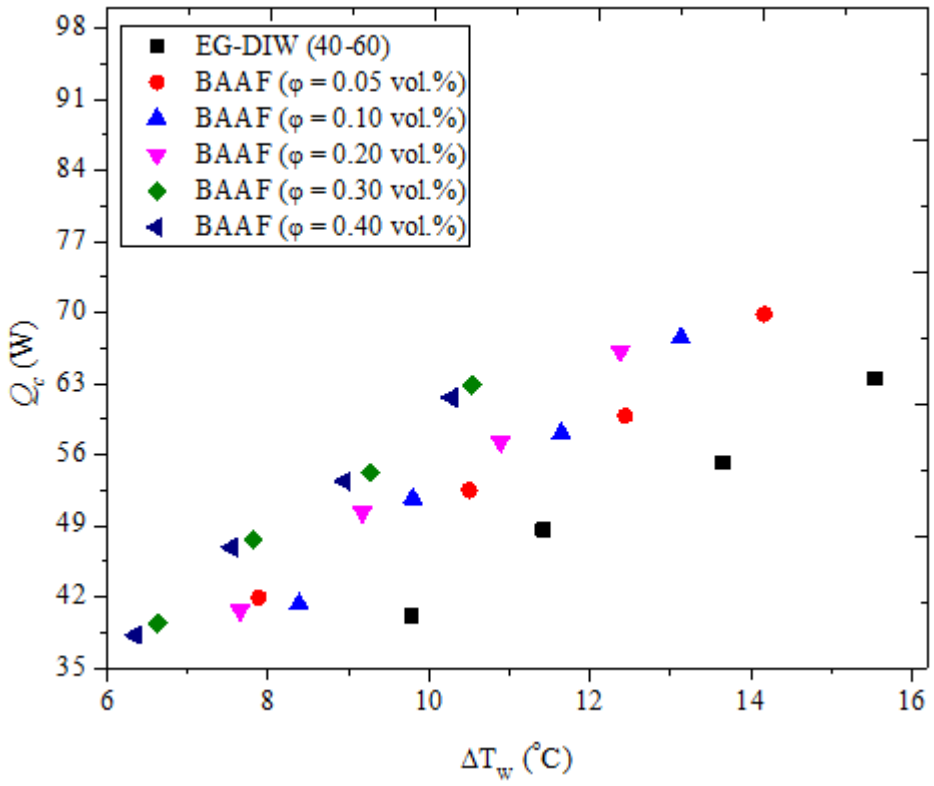

Figure 6.58: Relationship between Q_c and ΔT_W for EG-DIW and BAAF samples.

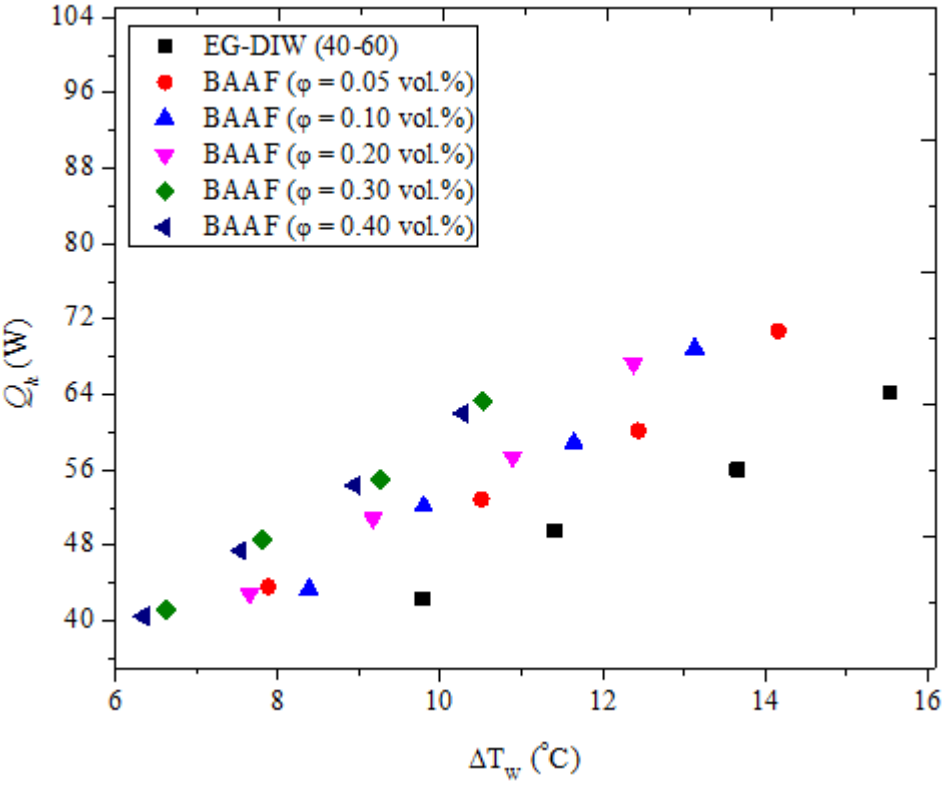

Figure 6.59: Relationship between Q_h and ΔT_W for EG-DIW and BAAF samples.

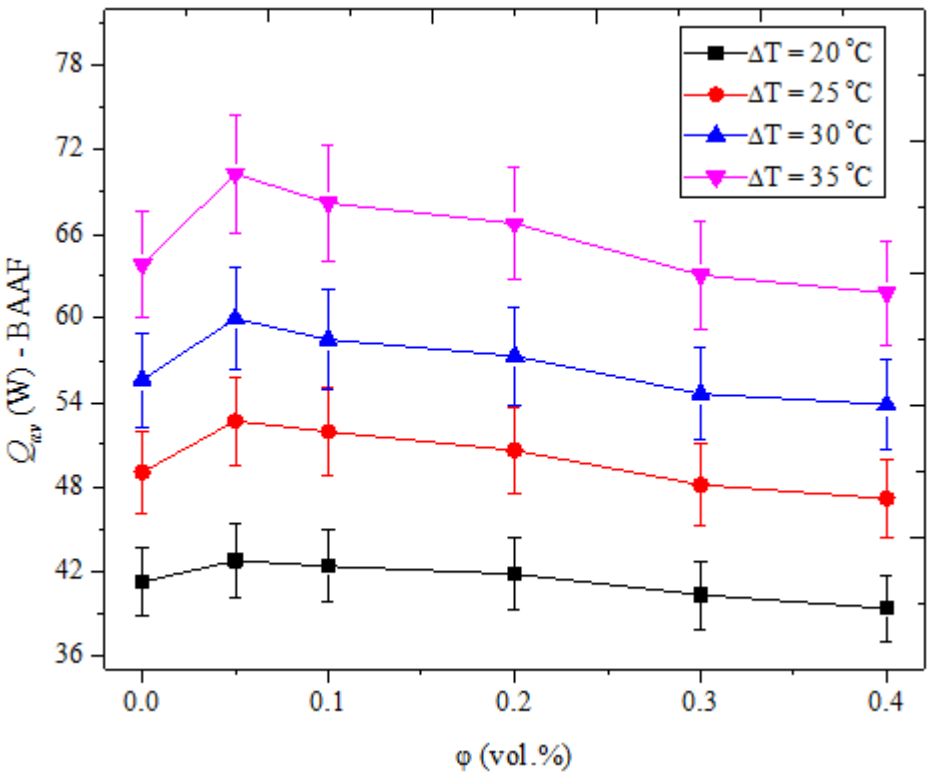

Figure 6.60: Relationship between Q_{av} and φ for EG-DIW and BAAF samples at varying ΔT.

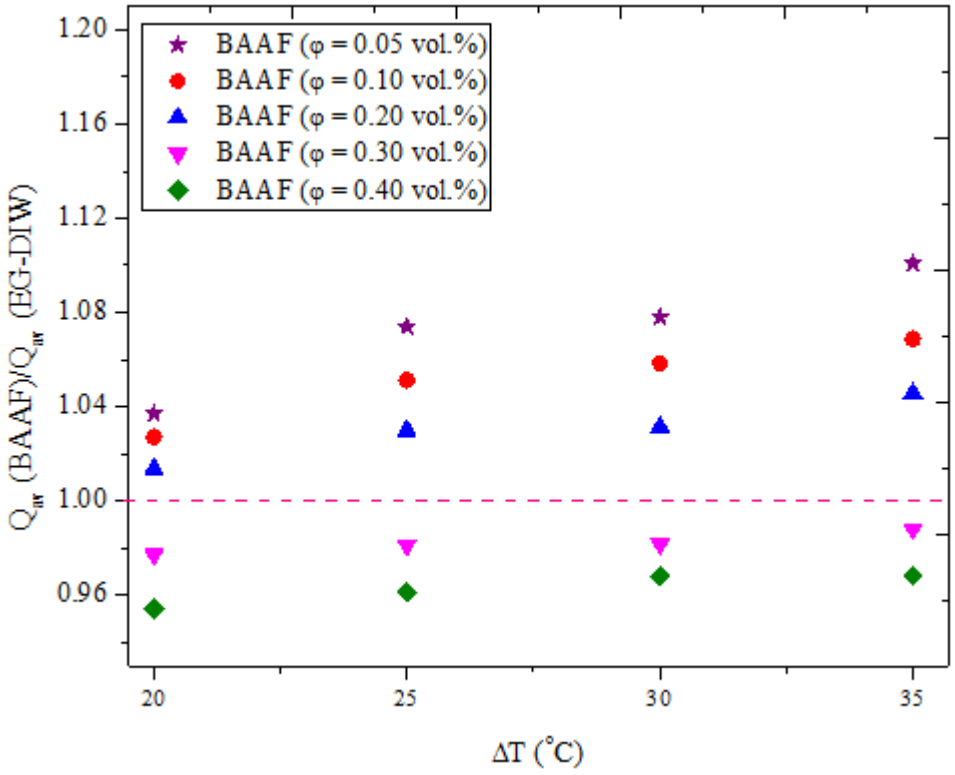

Figure 6.61: Normalised Q_{av} against *Ra* for EG-DIW and BAAF samples.

deteriorated. By this, Q_{av} of $\varphi \leq 0.20$ vol.% was higher than the Q_{av} of EG-DIW and Q_{av} of $\varphi > 0.20$ vol.% was lower than that of EG-DIW. Peak Q_{av} was observed when $\varphi = 0.05$ vol.% with an enhancement of 10.09% relative to EG-DIW at $\Delta T = 35$ °C.

In Fig. 6.61, the dependence of normalised Q_{av} (BAAF) on ΔT is presented. Variation in ΔT was observed to slightly augment normalised Q_{av}. Both the enhancement and deterioration of Q_{av} (BAAF) were indicated by normalised Q_{av} value of above or equal unity and below unity respectively. Thus, at $\varphi \leq 0.20$ vol.% and $\varphi > 0.20$ vol.%, augmentation and attenuation occurred respectively. The peak enhancement of Q_{av} (BAAF) obtained in this study was found to be higher than 8.2% and 7.2% to 9.8% reported for TiO_2/DIW nanofluid [153] and Al_2O_3-MWCNT/DIW nanofluid [165] in rectangular cavities respectively. However, the Q_{av} of BAAF was noticed to be slightly lower than the Q_{av} of AMF, though with different base fluids.

6.4.3.3 Heat Transfer Capacity of AAF

Thermo-convection heat transfer capability of AAF in the cavity was investigated and the results are presented in Figs. 6.62 to 6.65. The influence of ΔT_W on Q_c and Q_h is shown in Figs. 6.62 and 6.63 respectively for AAF and DIW. Both figures show a similar trend of ΔT_W being directly proportional to Q_c and Q_h. ΔT_W was higher for DIW (7.84 – 12.17 °C) than for AAF (6.69 – 10.93 °C). Optimum values of 70.15 W and 71.52 W were obtained for Q_c and Q_h respectively at $\Delta T_W = 10.93$ °C. In Fig. 6.64, the mean of Q_c and Q_h is presented as a function of φ at different ΔT for DIW and AAF. Increasing ΔT was noticed to enhance Q_{av}, whereas an increment in φ augmented Q_{av} for 0.05 to 0.20 vol.% and a further increase caused attenuation of Q_{av} for $\varphi = 0.30$ vol.% and 0.40 vol.%. At $\Delta T = 35$ °C, maximum Q_{av} (AAF) of 70.78 W was achieved with $\varphi = 0.10$ vol.%, which translated to 10.79% in relation to Q_{av} of DIW.

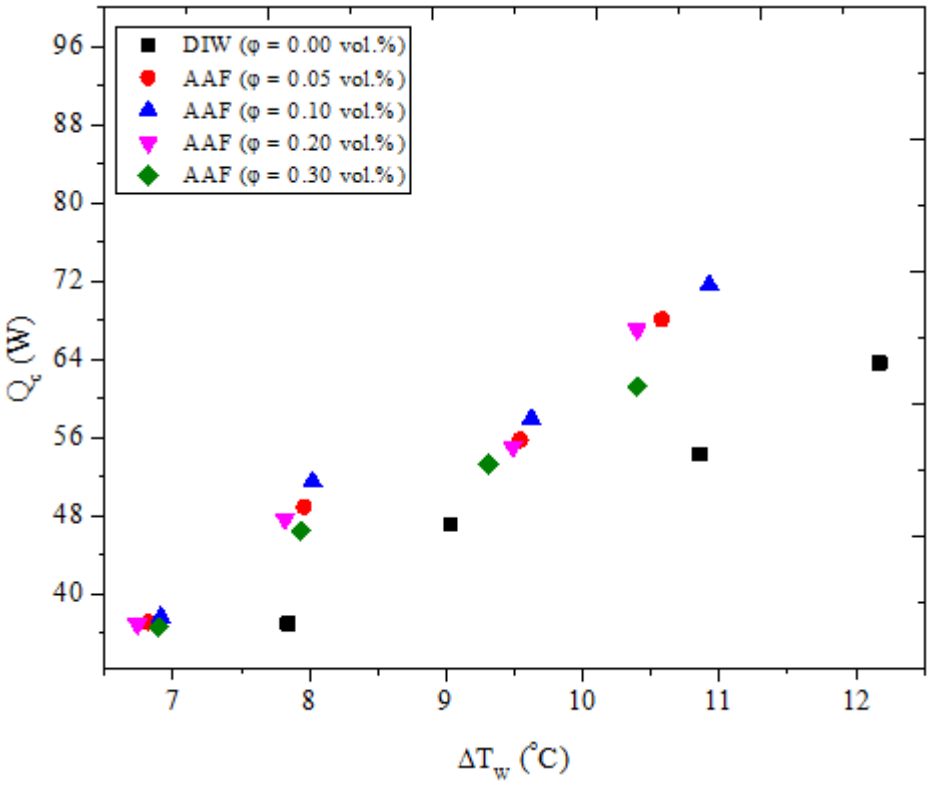

Figure 6.62: Relationship between Q_c and ΔT_W for DIW and AAF samples.

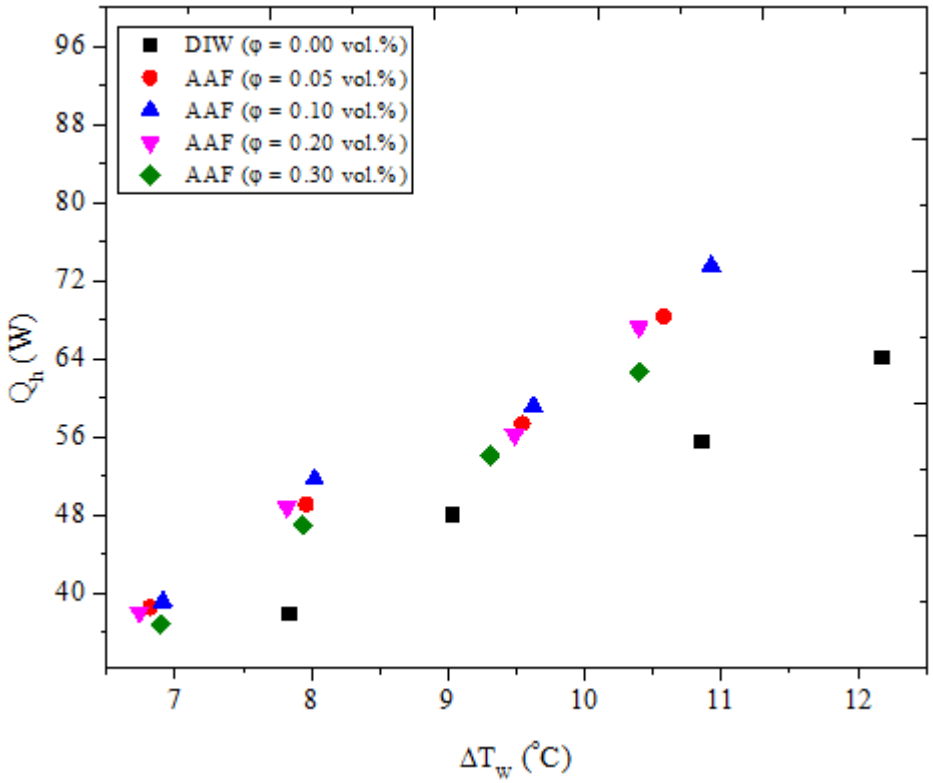

Figure 6.63: Relationship between Qh and ΔTW for DIW and AAF samples.

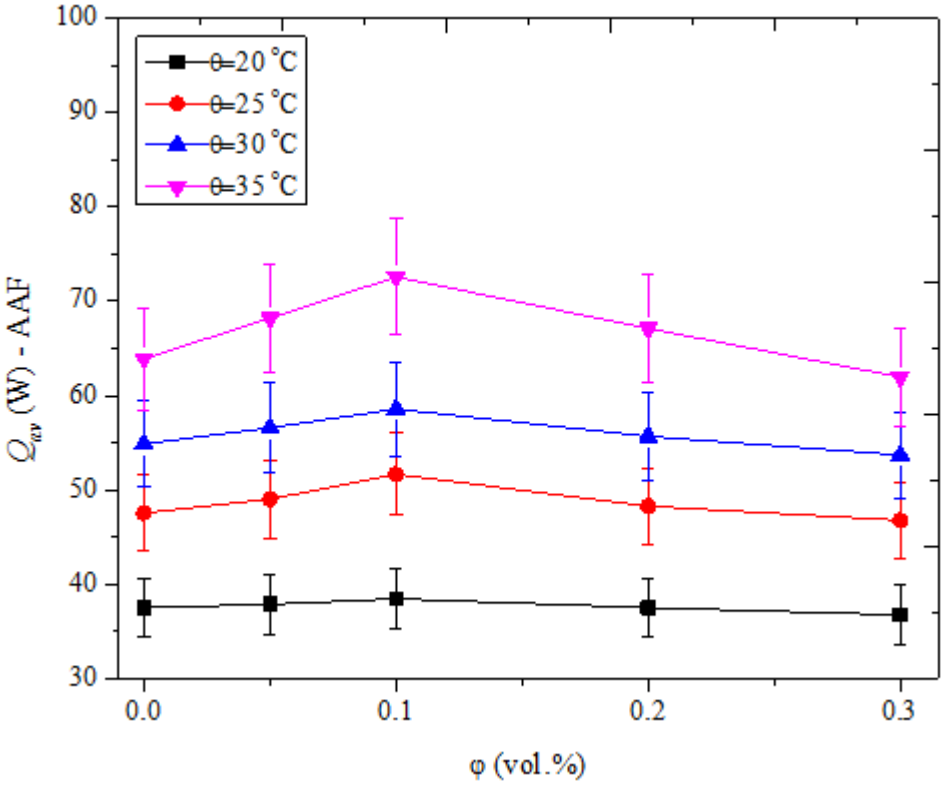

Figure 6.64: Relationship between Q_{av} and φ for DIW and AAF samples at varying ΔT.

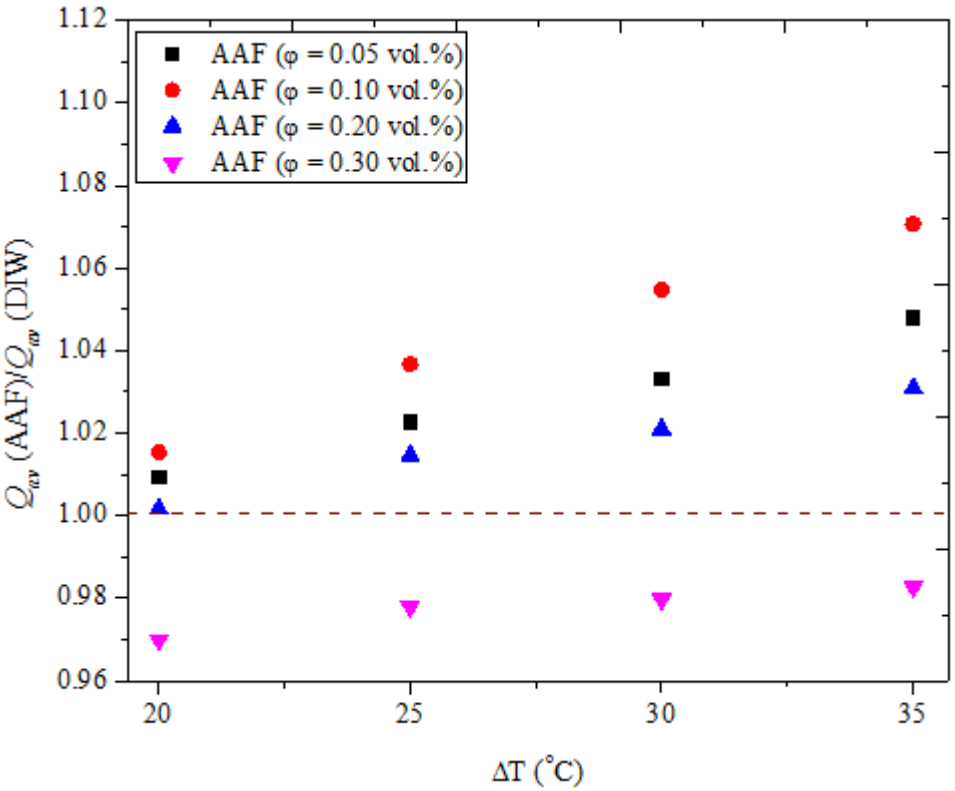

Figure 6.65: Normalised Q_{av} against *Ra* for DIW and AAF samples.

The maximum Q_{av} enhancement obtained in this work was found to be slightly higher than 8.2% and 7.2 to 9.8% published for TiO_2/DIW and Al_2O_3-MWCNT/DIW nanofluids [153, 165] respectively.

Fig. 6.65 displays the normalised Q_{av} as it relates to ΔT for AAF samples. An increment in ΔT was noticed to enhance Q_{av}. Augmentation of Q_{av} (AAF) resulted when normalised Q_{av} was ≥ 1 and deterioration was indicated by normalised Q_{av} value of <1. Thus, at φ = 0.05 to 0.20 vol.%, Q_{av} was enhanced but for φ = 0.30 vol.%, Q_{av} was detracted.

6.5 CONCLUSION

The thermo-convection performance of AMF, BAAF, AAF, DIW and EG-DIW in the rectangular cavity was conducted under varying ΔT and was evaluated using three parameters, namely Nu_{av}, h_{av} and Q_{av}. The temperature profile of the cavity for all the samples engaged in this study was presented in this chapter. Higher and lower temperatures were observed for the hot and cold walls of the cavity respectively in comparison with the approximately equal temperatures of the samples in the middle of the cavity. Samples of AMF, BAAF and AAF were observed to have slightly lower temperatures than those of the base fluids (DIW and EG-DIW). A rise in ΔT led to variation in T_W for the cold and hot walls, while the temperatures of the samples in the cavity increased. For all the samples considered in the study, an increase in ΔT caused a corresponding increase in ΔT_W, which resulted in the enhancement of *Ra*, Nu_{av}, h_{av} and Q_{av}. In addition, the range of ΔT_W for BAAF was noticed to be higher than that of AMF and AAF. Generally, Nu_{av} was observed to be related to ΔT, ΔT_W, φ and *Ra*, while h_{av} and Q_{av} were functions of ΔT, ΔT_W and φ for all the tested samples. *Ra* ranges of 1.01 x 10^8 to 2.65 x 10^8, 7.06 x 10^7 to 1.63 x 10^8 and 1.49 x 10^8 to 2.68 x 10^8 were recorded in this work for AMF, BAAF and AAF respectively, which were found to be within the range of *Ra* reported in the literature for thermo-convection of nanofluids in cavities.

Optimum Nu_{av}, h_{av} and Q_{av} values were achieved when φ = 0.05 vol.% for AMF and BAAF and φ = 0.10 vol.% for AAF, all at ΔT = 35 °C. In this work, the highest values of Nu_{av}, h_{av} and Q_{av} were 93.20, 573.00 W/m^2 °C and 71.06 W; 108.90, 473.21 W/m^2 °C and 70.28 W; and 92.76, 571.66 W/m^2 °C and 70.78 W for AMF, BAAF and AAF respectively in comparison with the respective base fluid values of Nu_{av}, h_{av} and Q_{av}. These values translated to maximum enhancement of 11.33% (Nu_{av}), 11.59% (h_{av}) and 11.21% (Q_{av}) for AMF, 33.14% (Nu_{av}), 33.17% (h_{av}) and 10.09% (Q_{av}) for BAAF, and 10.81% (Nu_{av}), 11.33% (h_{av}) and 10.79% (Q_{av}) for AAF. It can be observed that AMF had the best thermo-convection heat transfer performance, followed by AAF and then BAAF. This finding could be strongly linked to the type of HNPs (which was connected to the thermophysical properties) and base fluids used in formulating MHNFs of AMF, BAAF and AAF. The study revealed that the hybridisation of Fe_2O_3 (base NPs) with MWCNT and Al_2O_3 (dope NPs) to formulate AMF, BAAF and AAF enhanced Nu_{av}, h_{av} and Q_{av}. Relatively higher enhancement of Nu_{av}, h_{av} and Q_{av} for AMF, BAAF and AAF obtained in this study than those previously reported in the literature corroborated the synergetic benefit and effect of hybridising NPs in the formulation of hybrid nanofluids. In addition, the use of AMF and AAF as hybrid nanofluids in a rectangular cavity was found to yield higher enhancement of Nu_{av} than that of monoparticle nanofluid of Fe_2O_3/DIW. Therefore, it is evident that MHNFs of AMF, BAAF and AAF provided improvements in thermo-convection heat transfer.

Chapter 7

THERMOMAGNETIC CONVECTION PERFORMANCE OF MAGNETIC HYBRID NANOFLUIDS

7.1 INTRODUCTION

The influence of uniform magnetic stimuli on the thermo-convection heat transfer performance of MHNFs (AMF, BAAF and AAF) contained in the rectangular cavity was investigated. The samples of AMF (φ = 0.05 vol.%), BAAF (φ = 0.05 vol.%) and AAF (φ = 0.10 vol.%) with the optimum heat transfer capability were studied for the thermomagnetic convection at ΔT = 35 °C. The magnetic stimuli (11.84 mT) were first imposed on the bottom, side (vertical and horizontal) and top (parallel and perpendicular to the ΔT direction) walls of the cavity. Secondly, the wall with the highest enhancement was subjected to increasing magnetic stimuli (4.89 mT – 21.95 mT). In addition, the temperature profile of AMF, BAAF and AAF is presented in this chapter under the influence of magnetic stimuli. Parameters of Nu_{av}, h_{av} and Q_{av} were examined concerning the thermomagnetic convection performance of the mentioned samples in the cavity. The obtained results are presented here.

7.2 CAVITY TEMPERATURE PROFILE UNDER THERMOMAGNETIC CONVECTION

At stable thermal equilibria, the temperatures within the cavity filled with AMF, BAAF and AAF samples (which yielded maximum heat transfer performance) and subjected to the ΔT of 35 °C and magnetic stimuli of 11.84 mT were measured. The temperatures of samples of AMF, BAAF and AAF at different points within the cavity and the heated cavity walls under steady-state thermomagnetic conditions are presented in Figs. 7.1 to 7.3. The figures show that the imposition of magnetic stimuli of 11.84 mT on various walls of the cavity (containing AMF, BAAF and AAF) caused an increase in the temperatures of the tested samples (Thermocouples 2 – 8) and heated walls ($T_{W(C)}$ – Thermocouple 1 and $T_{W(H)}$ - Thermocouple

9) compared with the temperatures recorded for the base case in which no magnetic stimuli were imposed. This was due to the application of external forces (magnetic forces) into the system (cavity containing MHNFs), which resulted in the increase in temperature of the system as agitation and mobility of electrically charged magnetic HNPs increased.

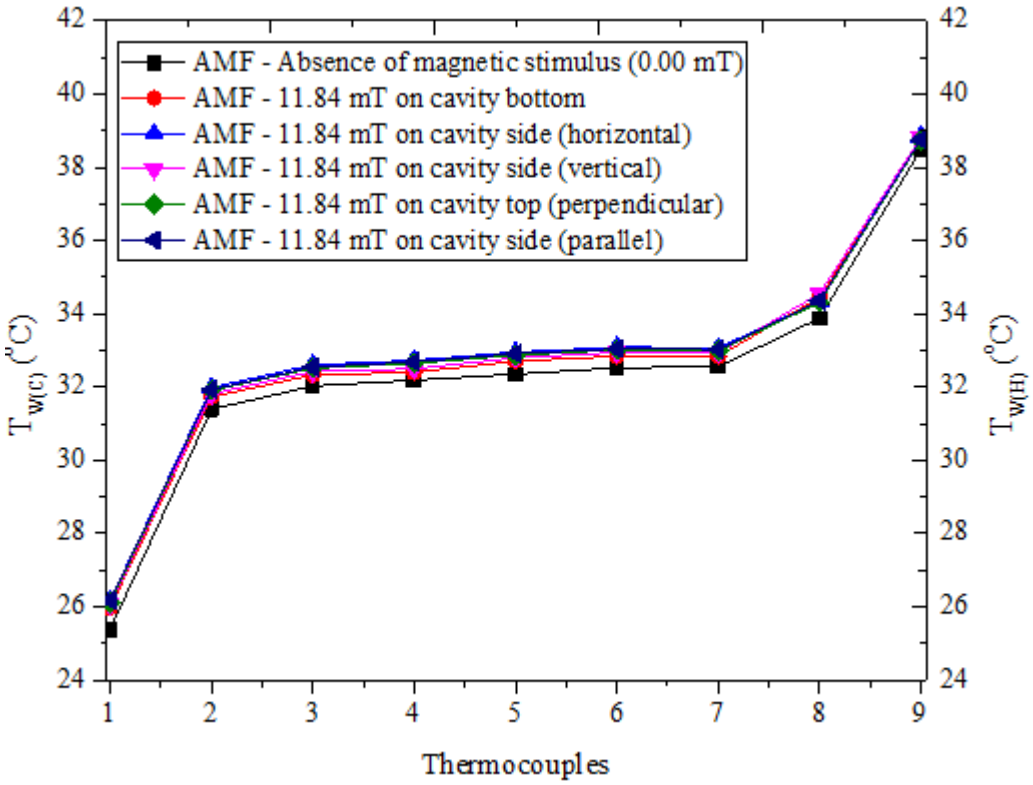

Figure 7.1: Temperature distribution of cavity under magnetic stimuli for 0.05 vol.% AMF.

Slight differences in temperatures were observed for all the samples due to the application of magnetic stimuli on the walls, which were relatively constant within the cavity, except for the point (Thermocouple 8) very close to the hot wall. A close observation of Figs. 7.1 to 7.3 shows that the BAAF sample had the highest temperature (34 – 36 °C) compared with the other samples (32 – 33 °C (AAF) and 33 – 34 °C (AAF)) when magnetic stimuli were imposed on the walls. This was noticed to agree with the temperature profile of the cavity under thermo-convection condition reported in Subsection 6.3.3. The same trend also applied to $T_{W(C)}$ and $T_{W(H)}$ under magnetic stimuli imposition on the walls of the cavity.

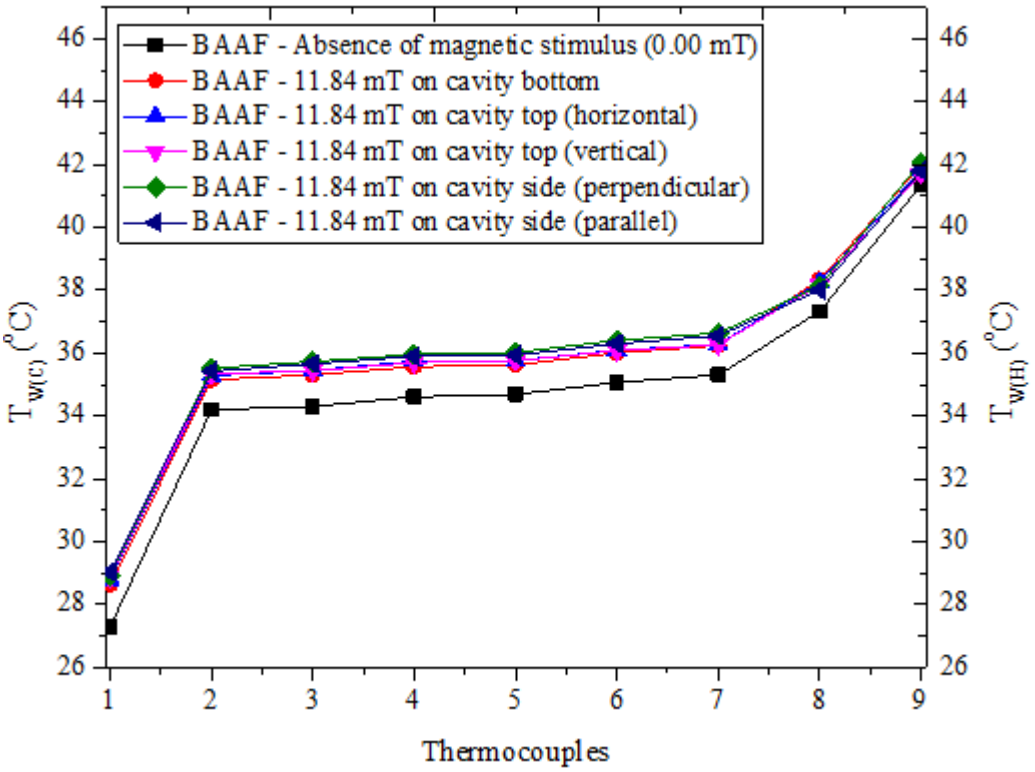

Figure 7.2: Temperature distribution of cavity under magnetic stimuli for 0.05 vol.% BAAF.

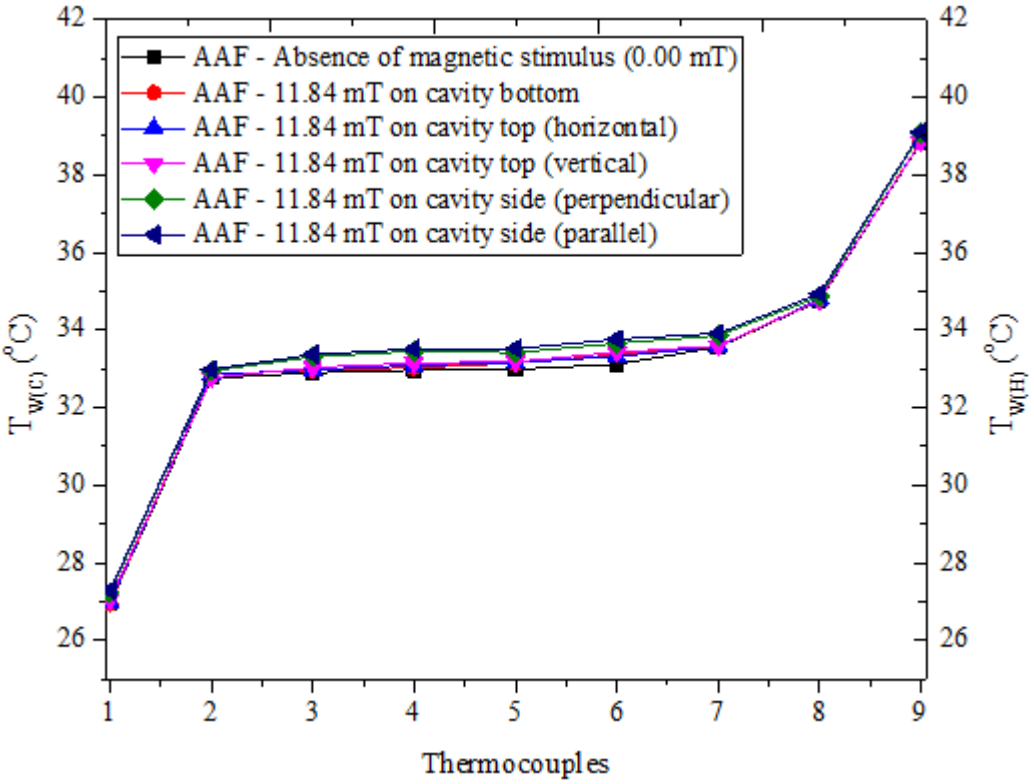

Figure 7.3: Temperature distribution of cavity under magnetic stimuli for 0.10 vol.% AAF.

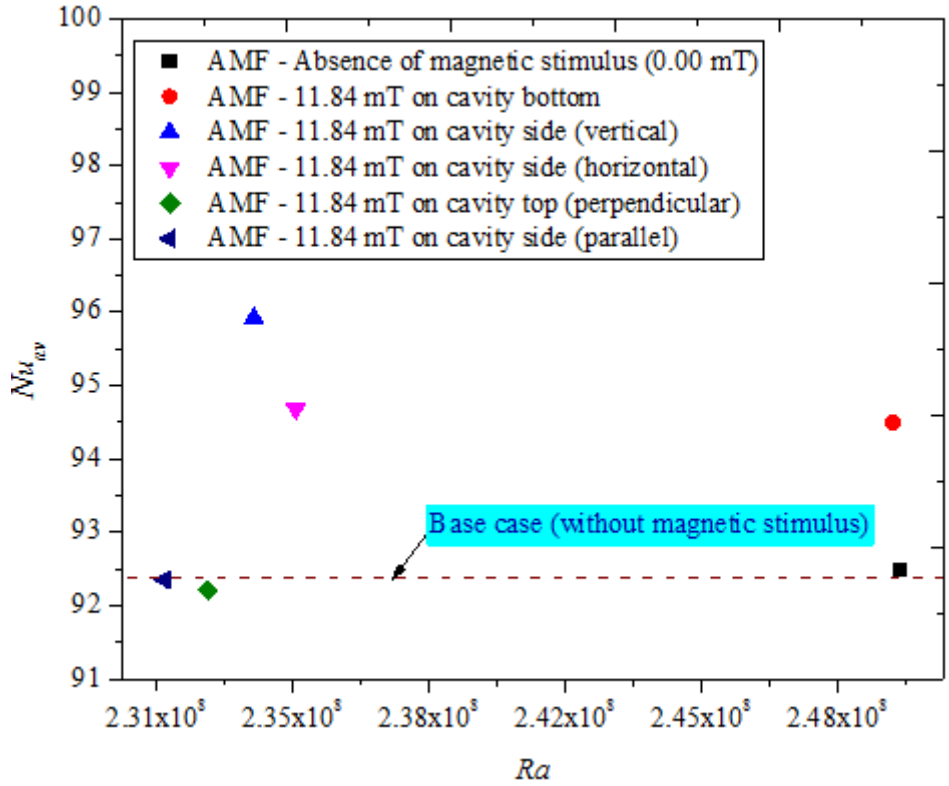

Figure 7.4: Influence of magnetic stimulus imposition on cavity walls for 0.05 vol% AMF sample.

Additionally, the BAAF was noticed to have the highest ΔT_W of the three samples (8.27 – 9.11 °C for AMF; 10.05 – 11.01 °C for BAAF; 6.98 – 7.21 °C for AAF) owing to the subjection of magnetic stimuli on the walls.

7.3 THERMOMAGNETIC HEAT TRANSFER PERFORMANCE OF AMF

With 0.05 vol.% AMF (at ΔT = 35 °C) yielding maximum thermo-convection heat transfer performance, the sample contained in the cavity was exposed to magnetic stimuli by applying the same on the top, bottom and side walls of the cavity. The influence of applying magnetic stimuli of 11.81 mT on the walls of the cavity filled with the AMF sample as related to Nu_{av} is shown in Fig. 7.4. The figure indicates that the imposition of the magnetic stimuli on the bottom and sides led to the enhancement of Nu_{av} in comparison with the base case of no magnetic stimuli. However, deterioration of Nu_{av} was noticed on exposing the top wall to magnetic stimuli. For the bottom, side (vertical and side) horizontal walls, the Nu_{av} was enhanced by 2.17% (Ra = 2.50 x 10^8), 3.71% (Ra = 2.33 x 10^8) and 2.37% (Ra = 2.35 x 10^8)

respectively. It was obvious that the vertical imposition of the magnetic stimuli on the side of the cavity gave the maximum enhancement of Nu_{av}. This result contradicted the work of Dixit and Pattamatta [195], in which deterioration of Nu_{av} of nanofluids was reported on exposing magnetic stimulus to the vertical wall of the square. The enhancement observed by imposing the magnetic stimuli on the bottom and sidewalls of the cavity was due to a rise in the system temperature leading to increased convective flow within the system, which consequently enhanced Nu_{av}. However, the deterioration of Nu_{av} at the top wall on exposure to magnetic stimuli was due to the suppression of the convective flow.

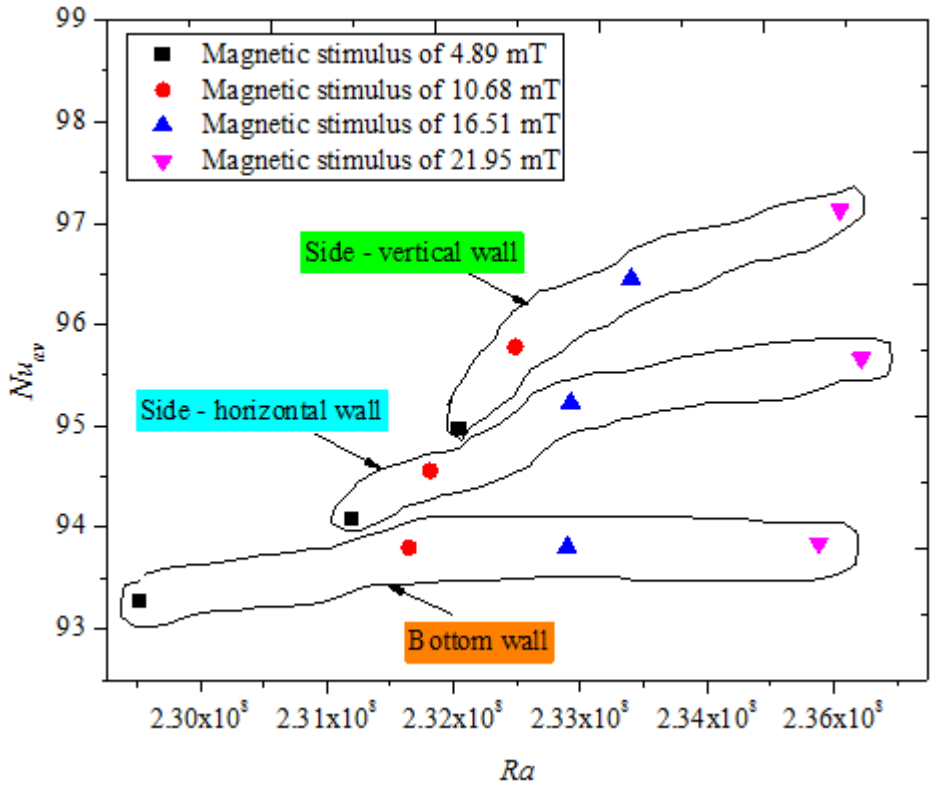

Figure 7.5: Influence of increasing magnetic stimulus on cavity walls for 0.05 vol.% AMF sample.

On achieving Nu_{av} enhancement with the imposition of magnetic stimuli of 11.84 mT on the side and bottom walls of the cavity, these walls were exposed to increasing magnetic stimuli of 4.89 mT to 21.95 mT. Fig. 7.5 shows the influence of increasing magnetic stimuli on the bottom and side walls in terms of the Nu_{av} of AMF. As the magnetic stimuli were increased from 4.89 mT to 21.95 mT, Nu_{av} enhancement of 0.86% to 5.02% relative to the base case of

Nu_{av} (no magnetic stimulus) was recorded. Nu_{av} was enhanced by 0.86% to 1.46%, 1.72% to 3.43% and 2.69% to 5.02% for the bottom, side (horizontal), and side (vertical) walls on exposure to 4.89 mT to 21.95 mT respectively. It could be deduced from this study that an increase in the magnetic stimulus caused a corresponding enhancement of Nu_{av}, which was consistent with previous studies on the enhancement of Nu_{av} of monoparticle nanofluids on exposure to an increment in magnetic stimulus [193, 194].

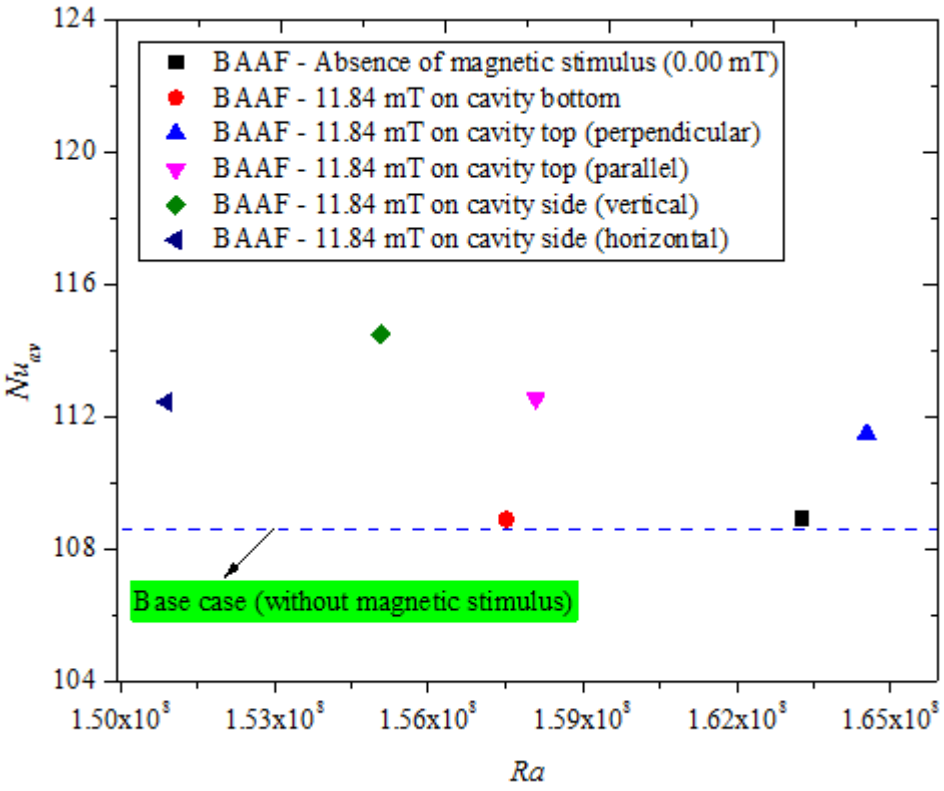

Figure 7.6: Influence of magnetic stimulus imposition on cavity walls for 0.05 vol% BAAF sample.

Joubert et al. [88] reported Nu_{av} enhancement of 2.81% on exposing 0.10 vol% Fe_2O_3/DIW nanofluid (in a rectangular cavity) to 700 G of magnetic stimuli, which was lower than the maximum achieved in this work when magnetic stimuli of 21.95 mT were imposed vertically on the sidewall of the cavity. The Nu_{av} improvement recorded for 0.05 vol.% AMF could be attributed to the hybridisation of Fe_2O_3 NPs with MWCNT NPs, as MWCNT NPs are known to possess κ and lower ρ and μ in comparison with those of Fe_2O_3 NPs [217]. Furthermore,

the Q_{av} of AMF was found to be enhanced by 1.26 to 2.62%, 1.70 to 3.50% and 2.38 to 4.48% on the exposure of the bottom, side (horizontal), and side (vertical) to magnetic stimuli of 4.89 mT to 21.95 mT respectively. Thus the present study revealed that the thermomagnetic convection heat transfer of AMF was strongly dependent on φ, ΔT, utilisation of MHNF and strength of the magnetic stimuli.

7.4 THERMOMAGNETIC HEAT TRANSFER PERFORMANCE OF BAAF

Using BAAF sample (φ = 0.05 vol.%) with the highest thermo-convection heat transfer performance in the rectangular cavity, the thermomagnetic convection of the same sample was investigated. Fig. 7.6 shows the Nu_{av} performance of 0.05 vol.% BAAF at ΔT = 35 °C and under the magnetic stimuli of 11.84 mT imposed on the various walls of the cavity. The exposure of side and top walls of the cavity containing 0.05 vol.% BAAF to the magnetic stimuli of 11.84 mT showed that Nu_{av} was augmented in comparison with the base case, while no sign of augmentation was observed for the bottom wall. When the uniform magnetic stimuli were imposed on the top wall perpendicular and parallel to the direction of ΔT, the Nu_{av} was augmented by 2.37% and 3.34% respectively. For the vertical and horizontal imposition of the magnetic stimuli on the sidewall, augmentation of Nu_{av} (BAAF) was 5.12% and 3.26% respectively. Evidently, the highest augmentation of Nu_{av} (Ra = 1.55 x 10^8) was achieved when the magnetic stimuli were applied vertically on the side of the cavity. With Nu_{av} deterioration of 0.007% on imposing the magnetic stimuli on the bottom wall, it could be said that no noticeable change was observed relative to the base case of no magnetic stimulus. This result agreed with the works of Joubert et al. [88] and Roszko and Fornalik-Wajs [194], namely that the presence of a magnet stimulus augmented Nu_{av} of monoparticle nanofluid of Fe_2O_3/DIW and Ag/DW, and contradicted that of Dixit and Pattamatta [195], which demonstrated that the application of a magnetic field to a square cavity containing nanfluids caused attenuation of Nu_{av}.

The effect of increasing the magnetic stimuli (4.89 mT – 21.95 mT) imposed on the top and sidewalls of the cavity filled with 0.05 vol.% BAAF was examined. The Nu_{av} of BAAF obtained by imposing increasing magnetic stimuli on the top and sidewalls of the cavity is shown in Fig. 7.7. Increasing the magnetic stimuli applied to the top wall from 4.89 mT to10.68 mT resulted in the augmentation of Nu_{av}, but a reduction in Nu_{av} was observed with a further increase in the magnetic strength from 10.68 mT to 21.95 mT. This led to Nu_{av} augmentation by 0.49% to 2.01% and 0.78% to 2.27% on applying the magnetic stimuli (4.89 mT - 10.68 mT) perpendicular and parallel to ΔT direction respectively in comparison with the base case. Similarly, imposing the magnetic stimuli vertically and horizontally on the side of the cavity showed augmentation of Nu_{av} by 3.37% to 3.94% and 1.80% to 2.52% respectively relative to the base case when the magnetic strength was increased from 4.89 mT to 10.68 mT and a decrease in Nu_{av} on increasing from 10.68 mT to 21.95 mT. Additionally, Nu_{av} was appreciated by 0.62% to 3.01% on exposing the bottom wall to increasing magnetic stimuli, in comparison with the case of no magnetic stimuli. The maximum augmentation of Nu_{av} (BAAF) obtained in the present study was higher than the 2.81% reported by Joubert et al. [88], by imposing magnetic stimuli of 700 G (through permanent magnets) on a rectangular cavity containing 0.10 vol.% Fe_2O_3/DIW . The study was found to be consistent with the works of Yamaguchi et al. [192] and Roszko and Fornalik-Wajs [194], which reported Nu_{av} augmentation with increasing magnetic stimulus exposed on the walls of cavities containing nanofluids. However, an exception to this was observed; when the magnetic stimuli were above 13.00 mT, an optimum augmentation of Nu_{av} was noticed at this magnetic stimuli. Similar trends as reported above were observed for Q_{av} (BAAF) under increasing magnetic stimuli. On imposing magnetic stimuli of 4.89 mT, 10.68 mT, 11.84 mT, 16.51 mT and 21.95 mT vertically on the cavity, Q_{av} was augmented by 2.33%, 3.40%, 4.33%, 4.02% and 3.94% respectively.

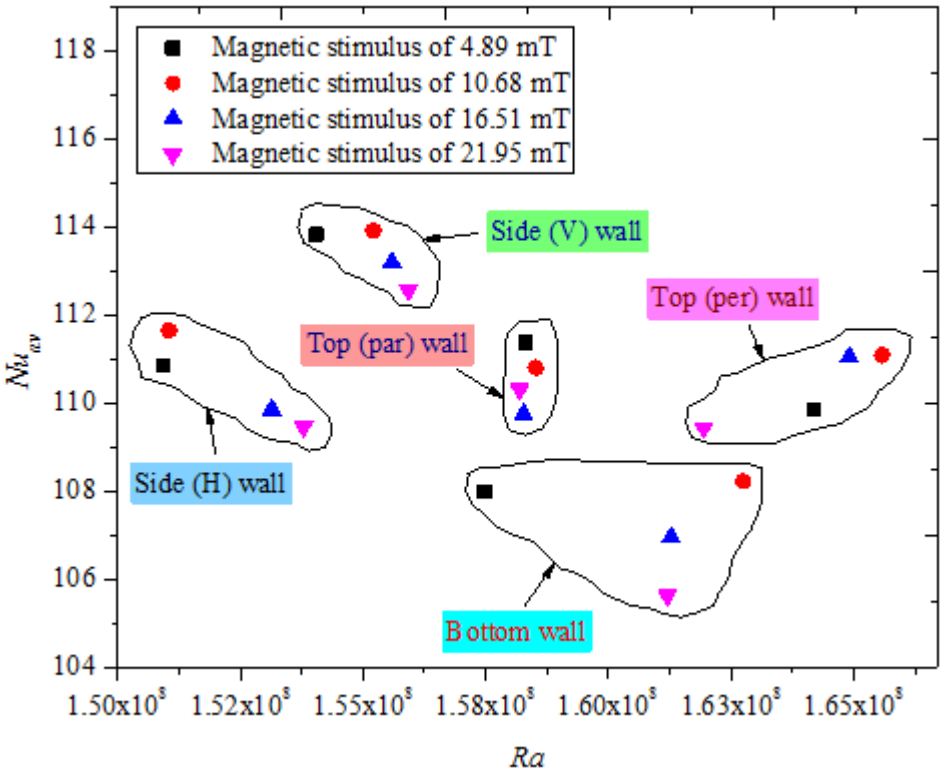

Figure 7.7: Influence of increasing magnetic stimulus on cavity walls for 0.05 vol.% BAAF sample.

7.5 THERMOMAGNETIC HEAT TRANSFER PERFORMANCE OF AAF

With 0.10 vol.% AAF offering the highest thermo-convection heat transfer performance, the influence of exposing the walls of the cavity containing the mentioned fluid to external magnetic stimuli was investigated. The thermo-convection performance (in terms of Nu_{av}) of 0.10 vol.% AAF in a rectangular cavity under the inducement of magnetic stimuli of 11.81 mT is illustrated in Fig. 7.8. Imposing magnetic stimuli of 11.81 mT on the bottom wall, and vertically and horizontally on the sidewall led to an enhancement of $Nu_{av,}$ but those of the top wall (perpendicular and parallel) showed attenuation of Nu_{av}. The vertical and horizontal exposure of the magnetic stimuli on the sidewall of the cavity caused enhancement of Nu_{av} by 2.64% and 1.83% (Ra = 2.01 x 10^8) respectively in comparison with the base case. Imposing the same strength of magnetic stimuli on the bottom wall enhanced Nu_{av} by 1.31% (Ra = 2.01 x 10^8) relative to the base case. The introduction of the magnetic stimuli into the system was noticed to impose magnetic forces on the fluid with the evidence of a rise in the temperature

of the sample, which consequently led to the enhancement of the convective flow within the cavity. The present study conformed to previous studies on the enhancement of Nu_{av} due to the imposition of magnetic stimuli on cavity walls [88, 193, 194]. In contrast, Dixit and Pattamatta [195] reported that Nu_{av} of nanofluids was deteriorated upon exposure to an external magnetic field after Nu_{av} enhancement was reported in the absence of a magnetic field.

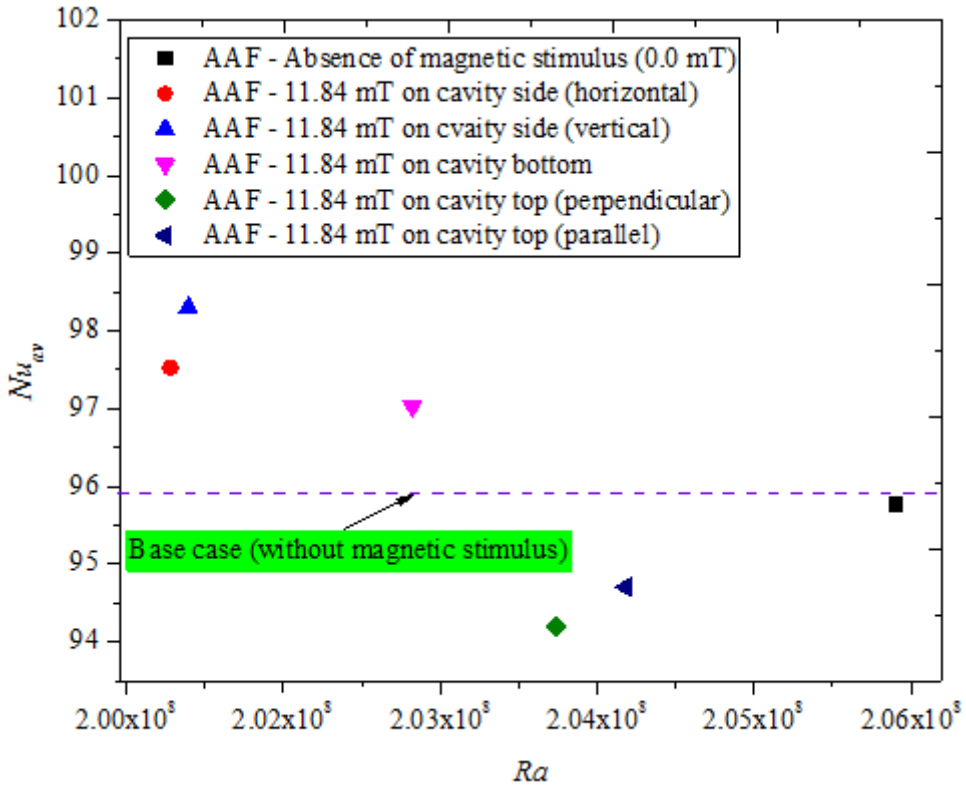

Figure 7.8: Influence of magnetic stimulus imposition on cavity walls for 0.10 vol% AAF sample.

Because the exposure of the magnetic stimuli vertically and horizontally on the sidewall and on the bottom wall caused enhancements of Nu_{av}, the influence of increasing magnetic stimuli from 4.89 mT to 21.95 mT was examined and is shown in Fig. 7.9. The figure shows that increasing the magnetic stimuli imposed on the side- and bottom walls from 4.89 mT to 21.95 mT led to Nu_{av} augmentation. With the vertical and horizontal imposition of the increasing magnetic stimuli (4.89 mT – 21.95 mT) on the side of the cavity, Nu_{av} was augmented by 1.39% to 4.91% and 1.06% to 2.59% respectively relative to the base case.

Additionally, by applying the magnetic stimuli (4.89 mT – 21.95 mT) to the bottom wall, Nu_{av} was augmented by 0.53% to 1.75% in comparison with the base case. Evidently, maximum Nu_{av} enhancement was observed to occur when the magnetic stimuli of 21.95 mT were applied vertically to the sidewall.

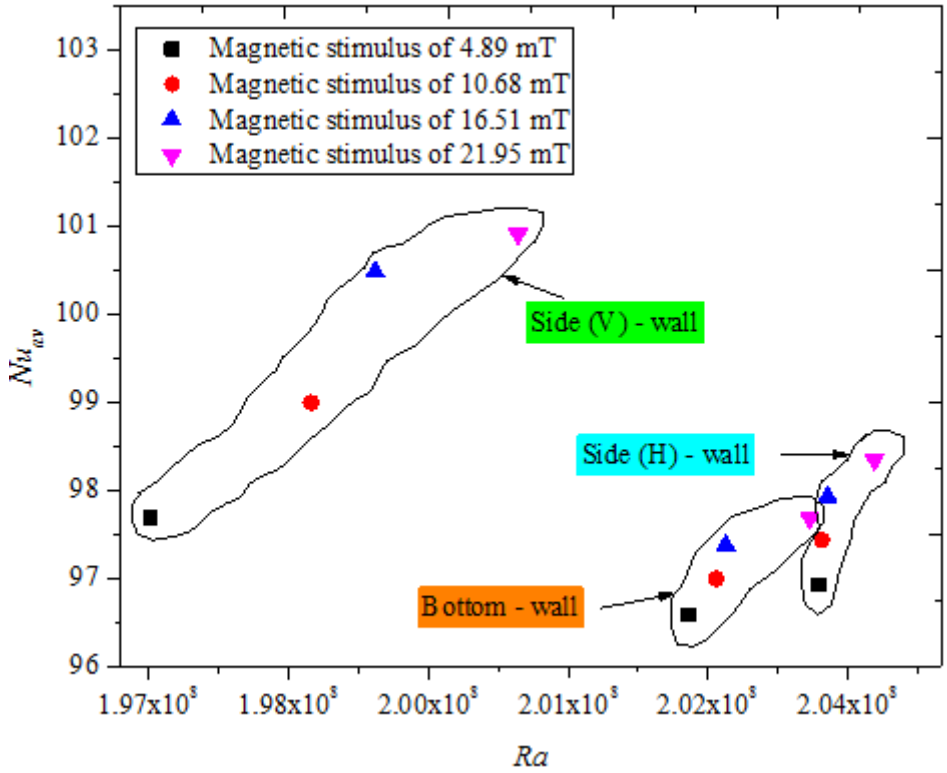

Figure 7.9: Influence of increasing magnetic stimulus on cavity walls for 0.10 vol.% AAF sample.

The result obtained in this study was found to agree with the works of Yamaguchi et al. [192] and Roszko and Fornalik-Wajs [194], which reported enhancement of Nu_{av} on applying increasing magnetic stimuli to the walls of cavities containing nanofluids. By imposing magnetic stimuli of 21.95 mT vertically on the cavity, Q_{av} was enhanced by 4.31%.

7.6 CONCLUSION

The thermomagnetic convection heat transfer of 0.05 vol.% AMF, 0.05 vol.% BAAF and 0.10 vol.% AAF in a rectangular cavity under ΔT of 35 °C was investigated. The temperature profile of the cavity showed that the exposure of the cavity to magnetic stimuli led to an increase in T_W and temperatures of the tested samples compared with the case of no magnetic

stimuli. The temperatures of the samples were approximately constant within the cavity, with slight differences due to the samples used. In addition, the highest T_W and sample temperature were noticed with 0.05 vol.% BAAF sample. Magnetic stimuli of 4.89 mT, 10.68 mT, 11.84 mT, 16.51 mT and 21.95 mT were imposed on the bottom, side- (vertically and horizontally) and top (perpendicular and parallel to ΔT direction) walls of the cavity containing 0.05 vol.% AMF, 0.05 vol.% BAAF and 0.10 vol.% AAF. For all the samples investigated in the cavity under various magnetic stimuli applied to the walls of the cavity, the maximum Nu_{av} and Q_{av} were attained when the magnetic stimuli were vertically imposed on the sidewall. Peak enhancements of 5.02% and 4.48% (0.05 vol.% AMF), 5.12% and 4.02% (0.05 vol.% BAAF) and 4.91% and 4.31% (0.10 vol.% AAF) were obtained for Nu_{av} and Q_{av} respectively relative to base cases of no magnetic stimulus on exposing the magnetic stimuli vertically on the sidewall of the cavity. These enhancements were achieved at magnetic stimuli of 21.95 mT for AMF and AAF samples and 11.84 mT for the BAAF sample. Therefore, increasing magnetic stimuli from 4.89 mT to 21.95 mT enhanced thermomagnetic convection heat transfer for 0.05 vol.% AMF and 0.10 vol.% AAF, whereas enhancement was observed for 0.05 vol.% BAAF when magnetic stimuli increased from 4.89 mT to 13.00 mT.

In this study, higher thermomagnetic convection heat transfer performance was recorded for all the tested samples than for previous studies which mainly engaged monoparticle nanofluids. Therefore, the thermomagnetic convection heat transfer performances achieved in this work could be strongly related to φ, ΔT, strength of magnetic stimuli, use of MHNFs, position and configuration of magnetic stimuli.

Chapter 8

CONCLUSIONS AND RECOMMENDATIONS

8.1 SUMMARY

The limitations imposed by the thresholds of the application of conventional fluids, miniaturisation, surface modification, extension and area/volume ratio reduction as techniques used for the thermal management of energy systems have led to the engineering of a special thermal fluid, nanofluids. The advent of nanotechnology set off the development of NPs used in the formulation of nanofluids. The high heat fluxes generated within state-of-the-art thermal devices and equipment that need to be dissipated at a fast rate have ignited researches the world over on the utilisation of nanofluids as advanced and better thermal media than the traditional fluids of EO, water, EG, TO, etc. Nanofluids have been established to possess improved thermal properties in comparison with conventional fluids, which have improved their convective heat transfer capability.

The vast engineering application of thermo-convection has spurred studies in the use of nanofluids in various types of cavities. In comparison with numerical techniques, few experimental works have been conducted on thermo-convection heat transfer performance of nanofluids in cavities. In addition, different methods have been used to enhance the thermo-convection of nanofluids in cavities, which include AR, cavity inclination, porous cavity, magnetic stimulus, green base fluid, green nanofluid and hybrid nanofluids. There is a dearth of experimental studies on the thermo-convection heat transfer enhancement by way of the use of hybrid nanofluids and magnetic stimulus in the public domain. Therefore, it was the primary focus of this study.

8.2 CONCLUSIONS

In accordance with the objectives of the study, stable MHNFs of AMF, BAAF and AAF at varying φ (0.05 – 0.40 vol.%) were formulated through the optimisation of the parameters

(dispersion fraction, sonication time and amplitude) related to the formulation of stable nanofluids. The stability of AMF, BAAF and AAF was verified using UV visible spectrophotometry and visual inspection techniques with both BAAF and AAF appearing more stable than AMF. TEM characterisation of AMF, BAAF and AAF samples with the highest φ values revealed good suspension of the respective HNPs into the base fluids. The TEM images also showed the spherical shapes of Fe_2O_3 and Al_2O_3 NPs and the rod-like shape of MWCNT NPs in the samples.

The κ_{eff} and μ_{eff} of AMF, BAAF and AAF were experimentally determined at the temperature and φ ranges considered in the study. The κ_{eff} of AMF, BAAF and AAF was found to augment with φ and temperature increase. In comparison with base fluid, AMF showed the highest enhancement for κ_{eff}, followed by BAAF and AAF. The μ_{eff} of AMF, BAAF and AAF was observed to decrease with temperature rise and it augmented with an increase in φ. AMF had the highest μ_{eff} enhancement followed by AAF and then BAAF. The hybridisation of Fe_2O_3 NPs with MWCNT and Al_2O_3 NPs was found to enhance the κ_{eff} of AMF and AAF, and it reduced the μ_{eff} of the same in comparison with monoparticle nanofluids of Fe_2O_3/DIW. The κ_{eff} and μ_{eff} of BAAF were expected to follow the same trend as that of AMF and AAF relative to the base fluid. Models were also developed for AMF, BAAF and AAF from their experimental data of κ_{eff} and μ_{eff} for engineering application. The models were functions of φ and temperature.

Without magnetic stimuli, the thermo-convection heat transfer enhancement of AMF, BAAF and AAF in the rectangular cavity was generally observed when $\varphi \leq 0.2$ vol.%. Beyond φ = 0.2 vol.%, deterioration was usually the case. For AMF and AAF, maximum heat transfer augmentation of 11.21% and 10.79% occurred at φ = 0.05 vol.%, $Ra = 2.65 \times 10^8$ and ΔT = 35 °C and φ = 0.10 vol.%, $Ra = 2.68 \times 10^8$ and ΔT = 35 °C respectively relative to DIW. The obtained Q_{av} improvements for AMF and AAF were observed to be higher than for a

monoparticle nanofluid (Fe_2O_3/DIW) due to the synergy from hybridising Fe_2O_3 NPs with MWCNT and Al_2O_3 NPs. With BAAF, the highest heat transfer of 10.09% was achieved at φ = 0.05 vol.%, Ra = 1.63 x 10^8 and ΔT = 35 °C in relation to EG-DIW. Models for the prediction of the Nu_{av} of AMF, BAAF and AAF were also developed.

By applying magnetic stimuli to the walls (bottom, top and side) of the cavity when samples of AMF, BAAF and AAF with the highest Q_{av} capacity were charged into the cavity, the vertical imposition of the magnetic stimuli on the sidewall was observed to yield the maximum Q_{av}. With AMF and AAF, the highest Q_{av} enhancements of 4.48% and 4.31% were achieved at magnetic stimuli of 21.95 mT respectively compared with the base case of no magnetic stimuli. Furthermore, the use of BAAF showed maximum Q_{av} improvement of 4.02% at magnetic stimuli of 11.84 mT. It was revealed that increasing the magnetic stimuli from 4.89 mT to 21.95 mT caused enhancement of the thermo-magnetic convection Q_{av} for AMF and AAF, while peak enhancement was observed at 13.00 mT for BAAF.

Conclusively, the use of hybrid nanofluids was found to improve both the thermal properties and thermo-convection Q_{av} in comparison with monoparticle nanofluids. Furthermore, the engagement of MHNFs was observed to enhance thermo-magnetic convection Q_{av} in a cavity (rectangular). In addition, DIW-based hybrid nanofluids appeared to be better thermal transport media than EG-DIW-based hybrid nanofluids. Using experimental data of μ_{eff} and κ_{eff} for AMF, BAAF and AAF was observed to be more appropriate for thermo-convection studies than using empirical models for predicting the thermal properties.

8.3 RECOMMENDATIONS

For future studies, the following recommendations are made:

- The percent weight ratios of the hybridised NPs for AMF, BAAF and AAF should be varied to study the ratio which will provide the maximum heat transfer performance under thermo-convection and thermomagnetic convection conditions.

- Because AR, cavity inclination and porosity are techniques for enhancing thermo-convection heat transfer in cavities, there is a need to experimentally investigate the effect of these techniques in cavities using hybrid nanofluids.
- Experimental heat transfer of thermo-convection and thermo-magnetic convection of HNFs and MHNFs in different shapes of cavity such as a cylinder are scarce in the public domain and should be studied .
- With very limited studies on green BFs and GNFs, the use of green BFs and green HNFs for thermo-convection and thermo-magnetic convection is expected to be examined in the nearest future.
- Since magnetic stimuli of over 100 mT have been reported to enhance the viscosity and thermal conductivity of magnetic nanofluids, stronger magnetic stimuli than the one (21.9 mT) used in this study is encouraged to be engaged in investigating the thermo-magnetic convection heat transfer performance of MHNFs in cavities.

REFERENCES

[1] R. Vavrek, J. Chovancová, Assessment of economic and environmental energy performance of EU countries using CV-TOPSIS technique, Ecol. Indic. 106 (2019) 105519.

[2] M. Mahmoodi, Numerical simulation of free convection of a nanofluid in L-shaped cavities, Int. J. Therm. Sci. 50 (2011) 1731–1740.

[3] S.M. Vanaki, P. Ganesan, H.A. Mohammed, Numerical study of convective heat transfer of nanofluids: A review, Renew. Sustain. Energy Rev. 54 (2016) 1212–1239.

[4] R.B. Ganvir, P.V. Walke, V.M. Kriplani, Heat transfer characteristics in nanofluid-A review, Renew. Sustain. Energy Rev. 75 (2016) 451–460.

[5] T. Ambreen, M.H. Kim, Heat transfer and pressure drop correlations of nanofluids: A state of art review, Renew. Sustain. Energy Rev. 91 (2018) 564–583.

[6] M. Gupta, V. Singh, S. Kumar, S. Kumar, N. Dilbaghi, Z. Said, Up to date review on the synthesis and thermophysical properties of hybrid nanofluids, J. Clean. Prod. 190 (2018) 169–192.

[7] H. Masuda, A. Ebata, K. Teramae, N. Hishinuma, Alteration of thermal ccnductivity and viscosity of liquid by dispersing ultra-fine particles (Dispersion of Al_2O_3, SiO_2 and TiO_2 ultra-fine particles), Netsu Bussei. 7 (1993) 227–233.

[8] J.A. Eastman, S.U.S. Choi, S. Li, W. Yu, L.J. Thompson, Anomalously increased effective thermal conductivities of ethylene glycol-based nanofluids containing copper nanoparticles, Appl. Phys. Lett. 78 (2001) 718–720.

[9] S. Lee, S.U.-S. Choi, S. Li, J.A. Eastman, Measuring thermal conductivity of fluids containing oxide nanoparticles, J. Heat Transfer. 121 (1999) 280–289.

[10] S.U.S. Choi, J.A. Eastman, Enhancing thermal conductivity of fluids with nanoparticles, ASME Int. Mech. Eng. Congr. Expo. 66 (1995) 99–105.

[11] J.P. Meyer, S.A. Adio, M. Sharifpur, P.N. Nwosu, The viscosity of nanofluids: A review of the theoretical, empirical, and numerical models, Heat Transf. Eng. 37 (2016) 387–421.

[12] H.Ş. Aybar, M. Sharifpur, M.R. Azizian, M. Mehrabi, J.P. Meyer, A review of thermal conductivity models for nanofluids, Heat Transf. Eng. 36 (2014) 1085–1110.

[13] M. Sharifpur, S. Yousefi, J.P. Meyer, A new model for density of nanofluids including nanolayer, Int. Commun. Heat Mass Transf. 78 (2016) 168–174.

[14] M. Gupta, V. Singh, R. Kumar, Z. Said, A review on thermophysical properties of nanofluids and heat transfer applications, Renew. Sustain. Energy Rev. 74 (2017) 638–670.

[15] S.A. Adio, M. Sharifpur, J.P. Meyer, Investigation into effective viscosity, electrical conductivity, and pH of γ-Al_2O_3-glycerol nanofluids in Einstein concentration regime, Heat Transf. Eng. 36 (2015) 1241–1251.

[16] Y. Xuan, Q. Li, Heat transfer enhancement of nanofluids, Int. J. Heat Fluid Flow. 21 (2000) 58–64.

[17] D. Wen, Y. Ding, Natural convective heat transfer of suspensions of titanium dioxide nanoparticles (nanofluids), IEEE Trans. Nanotechnol. 5 (2006) 220–227.

[18] B.C. Pak, Y.I. Cho, Hydrodynamic and heat transfer study of dispersed fluids with submicron metallic oxide particles, Exp. Heat Transf. 11 (1998) 151–170.

[19] N. Putra, W. Roetzel, S.K. Das, Natural convection of nano-fluids, Heat Mass Transf. Und Stoffuebertragung. 39 (2003).

[20] K.S. Hwang, J.H. Lee, S.P. Jang, Buoyancy-driven heat transfer of water-based Al2O3 nanofluids in a rectangular cavity, Int. J. Heat Mass Transf. 50 (2007) 4003–4010.

[21] S. Yekani Motlagh, S. Taghizadeh, H. Soltanipour, Natural convection heat transfer in

an inclined square enclosure filled with a porous medium saturated by nanofluid using Buongiorno's mathematical model, Adv. Powder Technol. 27 (2016) 2526–2540.
[22] I.D. Garbadeen, M. Sharifpur, J.M. Slabber, J.P. Meyer, Experimental study on natural convection of MWCNT-water nanofluids in a square enclosure, Int. Commun. Heat Mass Transf. 88 (2017) 1–8.
[23] M. Bouhalleb, H. Abbassi, Natural convection in an inclined rectangular enclosure filled by CuO-H_2O nanofluid, with sinusoidal temperature distribution, Int. J. Hydrogen Energy. 40 (2015) 13676–13684.
[24] M. Mahmoodi, S.M. Hashemi, Numerical study of natural convection of a nanofluid in C-shaped enclosures, Int. J. Therm. Sci. 55 (2012) 76–89.
[25] R. Mohebbi, M.M. Rashidi, Numerical simulation of natural convection heat transfer of a nanofluid in an L-shaped enclosure with a heating obstacle, J. Taiwan Inst. Chem. Eng. 72 (2017) 70–84.
[26] K.S. Suganthi, K.S. Rajan, Metal oxide nanofluids: Review of formulation, thermo-physical properties, mechanisms, and heat transfer performance, Renew. Sustain. Energy Rev. 76 (2017) 226–255.
[27] B. Ghasemi, Magnetohydrodynamic natural convection of nanofluids in U-shaped enclosures, Numer. Heat Transf. Part A Appl. 63 (2013) 473–487.
[28] X. Shi, P. Jaryani, A. Amiri, A. Rahimi, E. Hasani, Heat transfer and nano fluid flow of free convection in a quarter cylinder channel considering nanoparticle shape effect, Powder Technol. 346 (2019) 160–170.
[29] Z. Li, M. Sheikholeslami, A.J. Chamkha, Z.A. Raizah, S. Saleem, Control volume finite element method for nanofluid MHD natural convective flow inside a sinusoidal annulus under the impact of thermal radiation, Comput. Methods Appl. Mech. Eng. 338 (2018) 618–633.
[30] M. Sheikholeslami, M. Gorji-Bandpy, K. Vajravelu, Lattice Boltzmann simulation of magnetohydrodynamic natural convection heat transfer of Al_2O_3-water nanofluid in a horizontal cylindrical enclosure with an inner triangular cylinder, Int. J. Heat Mass Transf. 80 (2015) 16–25.
[31] L.T. Benos, E.G. Karvelas, I.E. Sarris, A theoretical model for the magnetohydrodynamic natural convection of a CNT-water nanofluid incorporating a renovated Hamilton-Crosser model, Int. J. Heat Mass Transf. 135 (2019) 548–560.
[32] S.M. Vahedi, A.H. Pordanjani, S. Wongwises, M. Afrand, On the role of enclosure side walls thickness and heater geometry in heat transfer enhancement of water-Al_2O_3 nanofluid in presence of a magnetic field: Sensitivity analysis and optimization, J. Therm. Anal. Calorim. 6 (2019).
[33] S. Jana, A. Salehi-Khojin, W.H. Zhong, Enhancement of fluid thermal conductivity by the addition of single and hybrid nano-additives, Thermochim. Acta. 462 (2007) 45–55.
[34] N. Jha, S. Ramaprabhu, Synthesis and thermal conductivity of copper nanoparticle decorated multiwalled carbon nanotubes based nanofluids, J. Phys. Chem. C. 112 (2008) 9315–9319.
[35] L.S. Sundar, E. Venkata Ramana, M.P.F. Graça, M.K. Singh, A.C.M. Sousa, Nanodiamond-Fe_3O_4 nanofluids: Preparation and measurement of viscosity, electrical and thermal conductivities, Int. Commun. Heat Mass Transf. 73 (2016) 62–74.
[36] L.S. Sundar, K. Shusmitha, M.K. Singh, A.C.M. Sousa, Electrical conductivity enhancement of nanodiamond-nickel (ND-Ni) nanocomposite based magnetic nanofluids, Int. Commun. Heat Mass Transf. 57 (2014) 1–7.
[37] S. Akilu, A.T. Baheta, M.A. Mior, A.A. Minea, K. V. Sharma, Properties of glycerol and ethylene glycol mixture based SiO_2-CuO/C hybrid nanofluid for enhanced solar

energy transport, Sol. Energy Mater. Sol. Cells. 179 (2018) 118–128.
[38] M. Chopkar, S. Kumar, D.R. Bhandari, P.K. Das, I. Manna, Development and characterization of Al_2Cu and Ag_2Al nanoparticle dispersed water and ethylene glycol based nanofluid, Mater. Sci. Eng. B Solid-State Mater. Adv. Technol. 139 (2007) 141–148.
[39] T. Tayebi, A.J. Chamkha, Free convection enhancement in an annulus between horizontal confocal elliptical cylinders using hybrid nanofluids, Numer. Heat Transf. Part A Appl. 70 (2016) 1141–1156.
[40] S.A.M. Mehryan, F.M. Kashkooli, M. Ghalambaz, A.J. Chamkha, Free convection of hybrid Al_2O_3-Cu water nanofluid in a differentially heated porous cavity, Adv. Powder Technol. 28 (2017) 2295–2305.
[41] J.T. Awua, J.S. Ibrahim, A. Kwaghger, M. Sharifpur, J.P. Meyer, Investigation into thermal conductivity of palm kernel fibre nanofluids with mixture of ethylene, 12th Int. Conf. Heat Transf. Fluid Mech. Thermodyn. (2016) 1719–1725.
[42] Q. Li, Y. Xuan, J. Wang, Experimental investigations on transport properties of magnetic fluids, Exp. Therm. Fluid Sci. 30 (2005) 109–116.
[43] K. Oster, C. Hardacre, J. Jacquemin, A.P.C. Ribeiro, A. Elsinawi, Ionic liquid-based nanofluids (ionanofluids) for thermal applications: An experimental thermophysical characterization, in: Pure Appl. Chem., 2019.
[44] Y. Guo, T. Zhang, D. Zhang, Q. Wang, Experimental investigation of thermal and electrical conductivity of silicon oxide nanofluids in ethylene glycol/water mixture, Int. J. Heat Mass Transf. 117 (2018) 280–286.
[45] G. Żyła, J. Fal, Viscosity, thermal and electrical conductivity of silicon dioxide–ethylene glycol transparent nanofluids: Experimental studies, Thermochim. Acta. 650 (2017) 106–113.
[46] S.U. Ilyas, R. Pendyala, M. Narahari, Rheological behavior of mechanically stabilized and surfactant-free MWCNT-thermal oil-based nanofluids, Int. Commun. Heat Mass Transf. 87 (2017) 250–255.
[47] M.K. Abdolbaqi, W.H. Azmi, R. Mamat, K.V. Sharma, G. Najafi, Experimental investigation of thermal conductivity and electrical conductivity of bioglycol-water mixture based Al2O3 Nanofluid, Appl. Therm. Eng. 102 (2016) 932–941.
[48] A.M. Khdher, N.A.C. Sidik, W.A.W. Hamzah, R. Mamat, An experimental determination of thermal conductivity and electrical conductivity of bio glycol based Al_2O_3 nanofluids and development of new correlation, Int. Commun. Heat Mass Transf. 73 (2016) 75–83.
[49] K. Shah, R. V Upadhyay, V.K. Aswal, Influence of large size magnetic particles on the magneto-viscous properties of ferrofluid, Smart Mater. Struct. 21 (2012) 075005.
[50] B. Wei, C. Zou, X. Yuan, X. Li, Thermo-physical property evaluation of diathermic oil based hybrid nanofluids for heat transfer applications, Int. J. Heat Mass Transf. 107 (2017) 281–287.
[51] M.U. Sajid, H.M. Ali, Thermal conductivity of hybrid nanofluids: A critical review, Int. J. Heat Mass Transf. 126 (2018) 211–234.
[52] M.F. Nabil, W.H. Azmi, K. Abdul Hamid, R. Mamat, F.Y. Hagos, An experimental study on the thermal conductivity and dynamic viscosity of TiO_2-SiO_2 nanofluids in water: Ethylene glycol mixture, Int. Commun. Heat Mass Transf. 86 (2017) 181–189.
[53] J.A. Ranga Babu, K.K. Kumar, S. Srinivasa Rao, State-of-art review on hybrid nanofluids, Renew. Sustain. Energy Rev. 77 (2017) 551–565.
[54] D.D. Kumar, A.V. Arasu, A comprehensive review of preparation, characterization, properties and stability of hybrid nanofluids, Renew. Sustain. Energy Rev. 81 (2018) 1669–1689.

[55] S.M. Mousavi, F. Esmaeilzadeh, X.P. Wang, Effects of temperature and particles volume concentration on the thermophysical properties and the rheological behavior of $CuO/MgO/TiO_2$ aqueous ternary hybrid nanofluid experimental investigation, J. Therm. Anal. Calorim. 0 (2019).
[56] S.A. Adio, M. Mehrabi, M. Sharifpur, J.P. Meyer, Experimental investigation and model development for effective viscosity of MgO-ethylene glycol nanofluids by using dimensional analysis, FCM-ANFIS and GA-PNN techniques, Int. Commun. Heat Mass Transf. 72 (2016) 71–83.
[57] M. Sharifpur, S.A. Adio, J.P. Meyer, Experimental investigation and model development for effective viscosity of Al_2O_3-glycerol nanofluids by using dimensional analysis and GMDH-NN methods, Int. Commun. Heat Mass Transf. 68 (2015) 208–219.
[58] A. Kakavandi, M. Akbari, Experimental investigation of thermal conductivity of nanofluids containing of hybrid nanoparticles suspended in binary base fluids and propose a new correlation, Int. J. Heat Mass Transf. 124 (2018) 742–751.
[59] S. Askari, H. Koolivand, M. Pourkhalil, R. Lotfi, A. Rashidi, Investigation of Fe3O4/Graphene nanohybrid heat transfer properties: Experimental approach, Int. Commun. Heat Mass Transf. 87 (2017) 30–39.
[60] S. Nabati Shoghl, J. Jamali, M. Keshavarz Moraveji, Electrical conductivity, viscosity, and density of different nanofluids: An experimental study, Exp. Therm. Fluid Sci. 74 (2016) 339–346.
[61] Z. Said, Thermophysical and optical properties of SWCNTs nanofluids, Int. Commun. Heat Mass Transf. 78 (2016) 207–213.
[62] A. Alirezaie, S. Saedodin, M.H. Esfe, S.H. Rostamian, Investigation of rheological behavior of MWCNT (COOH-functionalized)/MgO - Engine oil hybrid nanofluids and modelling the results with artificial neural networks, J. Mol. Liq. 241 (2017) 173–181.
[63] A. Menbari, A.A. Alemrajabi, Y. Ghayeb, Investigation on the stability, viscosity and extinction coefficient of CuO-Al_2O_3/Water binary mixture nanofluid, Exp. Therm. Fluid Sci. 74 (2016) 122–129.
[64] S.A. Adio, M. Sharifpur, J.P. Meyer, Influence of ultrasonication energy on the dispersion consistency of Al_2O_3-glycerol nanofluid based on viscosity data, and model development for the required ultrasonication energy density, J. Exp. Nanosci. 11 (2016) 630–649.
[65] M. Kole, T.K. Dey, Effect of aggregation on the viscosity of copper oxide-gear oil nanofluids, Int. J. Therm. Sci. 50 (2011) 1741–1747.
[66] X. Ju Wang, D. Sheng Zhu, S. Yang, Investigation of pH and SDBS on enhancement of thermal conductivity in nanofluids, Chem. Phys. Lett. 470 (2009) 107–111.
[67] J.-C. Yang, F.-C. Li, W.-W. Zhou, Y.-R. He, B.-C. Jiang, Experimental investigation on the thermal conductivity and shear viscosity of viscoelastic-fluid-based nanofluids, Int. J. Heat Mass Transf. 55 (2012) 3160–3166.
[68] Z. Aparna, M. Michael, S.K. Pabi, S. Ghosh, Thermal conductivity of aqueous Al_2O_3/Ag hybrid nano fluid at different temperatures and volume concentrations : An experimental investigation and development of new correlation function, Powder Technol. 343 (2019) 714–722.
[69] M.J. Pastoriza-Gallego, L. Lugo, J.L. Legido, M.M. Pineiro, Enhancement of thermal conductivity and volumetric behavior of Fe_xO_y nanofluids, J. Appl. Phys. 110 (2011) 1–9.
[70] A.I. Ramadhan, W.H. Azmi, R. Mamat, K.A. Hamid, S. Norsakinah, Investigation on stability of tri-hybrid nanofluids in water-ethylene glycol mixture, IOP Conf. Ser. Mater. Sci. Eng. 469 (2019).

[71] S. Ebrahimi, S.F. Saghravani, Experimental study of the thermal conductivity features of the water based Fe_3O_4/CuO nanofluid, Heat Mass Transf. 54 (2018) 999–1008.
[72] A. Ghadimi, R. Saidur, H.S.C. Metselaar, A review of nanofluid stability properties and characterization in stationary conditions, Int. J. Heat Mass Transf. 54 (2011) 4051–4068.
[73] L.F. Chen, M. Cheng, D.J. Yang, L. Yang, Enhanced thermal conductivity of nanofluid by synergistic effect of multi-walled carbon nanotubes and Fe_2O_3 nanoparticles, Appl. Mech. Mater. 548–549 (2014) 118–123.
[74] A. Naddaf, S. Zeinali Heris, Experimental study on thermal conductivity and electrical conductivity of diesel oil-based nanofluids of graphene nanoplatelets and carbon nanotubes, Int. Commun. Heat Mass Transf. 95 (2018) 116–122.
[75] M. Hemmat Esfe, A.A. Abbasian Arani, M. Rezaie, W.M. Yan, A. Karimipour, Experimental determination of thermal conductivity and dynamic viscosity of Ag-MgO/water hybrid nanofluid, Int. Commun. Heat Mass Transf. 66 (2015) 189–195.
[76] M.F. Zawrah, R.M. Khattab, L.G. Girgis, H. El Daidamony, R.E. Abdel Aziz, Stability and electrical conductivity of water-base Al_2O_3 nanofluids for different applications, HBRC J. 12 (2016) 227–234.
[77] L. Chen, W. Yu, H. Xie, Enhanced thermal conductivity of nanofluids containing Ag/MWNT composites, Powder Technol. 231 (2012) 18–20.
[78] M. Hajiyan, S. Ebadi, S. Mahmud, M. Biglarbegian, H. Abdullah, Experimental investigation of the effect of an external magnetic field on the thermal conductivity and viscosity of Fe_3O_4-glycerol, J. Therm. Anal. Calorim. 1 (2018) 1–14.
[79] L.S. Sundar, M.K. Singh, A.C.M. Sousa, Turbulent heat transfer and friction factor of nanodiamond-nickel hybrid nanofluids flow in a tube: An experimental study, Int. J. Heat Mass Transf. 117 (2018) 223–234.
[80] E. Esmaeili, R. Ghazanfar Chaydareh, S.A. Rounaghi, The influence of the alternating magnetic field on the convective heat transfer properties of Fe_3O_4-containing nanofluids through the Neel and Brownian mechanisms, Appl. Therm. Eng. 110 (2017) 1212–1219.
[81] S.A. Adio, M. Sharifpur, J.P. Meyer, Factors affecting the pH and electrical conductivity of MgO-ethylene glycol nanofluids, Bull. Mater. Sci. 38 (2015) 1345–1357.
[82] S. Suresh, K.P. Venkitaraj, P. Selvakumar, M. Chandrasekar, Synthesis of Al_2O_3-Cu/water hybrid nanofluids using two step method and its thermo physical properties, Colloids Surfaces A Physicochem. Eng. Asp. 388 (2011) 41–48.
[83] T.T. Baby, S. Ramaprabhu, Experimental investigation of the thermal transport properties of a carbon nanohybrid dispersed nanofluid, Nanoscale. 3 (2011) 2208–2214.
[84] N.N.M. Zawawi, W.H. Azmi, A.A.M. Redhwan, M.Z. Sharif, M. Samykano, Experimental investigation on thermo-physical properties of metal oxide composite nanolubricants, Int. J. Refrig. 89 (2018) 11–21.
[85] S. Ganguly, S. Sikdar, S. Basu, Experimental investigation of the effective electrical conductivity of aluminum oxide nanofluids, Powder Technol. 196 (2009) 326–330.
[86] A. Ijam, R. Saidur, P. Ganesan, A. Moradi Golsheikh, Stability, thermo-physical properties, and electrical conductivity of graphene oxide-deionized water/ethylene glycol based nanofluid, Int. J. Heat Mass Transf. 87 (2015) 92–103.
[87] B. Sun, C. Peng, R. Zuo, D. Yang, H. Li, Investigation on the flow and convective heat transfer characteristics of nanofluids in the plate heat exchanger, Exp. Therm. Fluid Sci. 76 (2016) 75–86.
[88] J.C. Joubert, M. Sharifpur, A.B. Solomon, J.P. Meyer, Enhancement in heat transfer of

a ferrofluid in a differentially heated square cavity through the use of permanent magnets, J. Magn. Magn. Mater. 443 (2017) 149–158.
[89] M. Hadadian, E.K. Goharshadi, A. Youssefi, Electrical conductivity, thermal conductivity, and rheological properties of graphene oxide-based nanofluids, J. Nanoparticle Res. 16 (2014) 1–17.
[90] W. Yu, H. Xie, L. Chen, Y. Li, Enhancement of thermal conductivity of kerosene-based Fe3O4 nanofluids prepared via phase-transfer method, Colloids Surfaces A Physicochem. Eng. Asp. 355 (2010) 109–113.
[91] Y. Xuan, Q. Li, Investigation on convective heat transfer and flow features of nanofluids, J. Heat Transfer. 125 (2003) 151.
[92] N. Tshimanga, M. Sharifpur, J.P. Meyer, Experimental investigation and model development for thermal conductivity of glycerol-MgO nanofluids, Heat Transf. Eng. 37 (2016) 1538–1553.
[93] P. Jamilpanah, H. Pahlavanzadeh, A. Kheradmand, Thermal conductivity, viscosity, and electrical conductivity of iron oxide with a cloud fractal structure, Heat Mass Transf. 53 (2017) 1343–1354.
[94] R. Agarwal, K. Verma, N.K. Agrawal, R. Singh, Sensitivity of thermal conductivity for Al2O3 nanofluids, Exp. Therm. Fluid Sci. 80 (2017) 19–26.
[95] L.S. Sundar, G.O. Irurueta, E. Venkata Ramana, M.K. Singh, A.C.M. Sousa, Thermal conductivity and viscosity of hybrid nanofluids prepared with magnetic nanodiamond-cobalt oxide (ND-Co3O4) nanocomposite, Case Stud. Therm. Eng. 7 (2016) 66–77.
[96] L. Syam Sundar, A.C.M. Sousa, M.K. Singh, Heat transfer enhancement of low volume concentration of carbon nanotube-Fe_3O_4/water hybrid nanofluids in a tube with twisted tape inserts under turbulent flow, J. Therm. Sci. Eng. Appl. 7 (2015) 021015.
[97] S.H. Qing, W. Rashmi, M. Khalid, T.C.S.M. Gupta, M. Nabipoor, M.T. Hajibeigy, Thermal conductivity and electrical properties of hybrid SiO_2-graphene naphthenic mineral oil nanofluid as potential transformer oil, Mater. Res. Express. 4 (2017) 015504.
[98] A. Parsian, M. Akbari, New experimental correlation for the thermal conductivity of ethylene glycol containing Al_2O_3-Cu hybrid nanoparticles, J. Therm. Anal. Calorim. 131 (2018) 1605–1613.
[99] A. Asadi, M. Asadi, A. Rezaniakolaei, L.A. Rosendahl, M. Afrand, S. Wongwises, Heat transfer efficiency of Al_2O_3-MWCNT/thermal oil hybrid nanofluid as a cooling fluid in thermal and energy management applications: An experimental and theoretical investigation, Int. J. Heat Mass Transf. 117 (2018) 474–486.
[100] A. Ahmadi Nadooshan, H. Eshgarf, M. Afrand, Measuring the viscosity of Fe_3O_4-MWCNTs/EG hybrid nanofluid for evaluation of thermal efficiency: Newtonian and non-Newtonian behavior, J. Mol. Liq. 253 (2018) 169–177.
[101] M. Sharifpur, A.B. Solomon, J.P. Meyer, J.S. Ibrahim, B. Immanuel, Thermal conductivity and viscosity of mango bark/water nanofluids, in: 13th Int. Conf. Heat Transf. Fluid Mech. Thermodyn., 2017.
[102] H. Yarmand, S. Gharehkhani, S.F.S. Shirazi, A. Amiri, E. Montazer, H.K. Arzani, R. Sadri, M. Dhari, S.N. Kazi, Nanofluid based on activated hybrid of biomass carbon/graphene oxide: Synthesis, thermophysical and electrical porperties, Int. Commun. Heat Mass Transf. 72 (2016) 10–15.
[103] R. Azizian, E. Doroodchi, B. Moghtaderi, Influence of controlled aggregation on thermal conductivity of nanofluids, J. Heat Transfer. 138 (2015) 1–6.
[104] M. Amani, P. Amani, A. Kasaeian, O. Mahian, I. Pop, S. Wongwises, Modeling and optimization of thermal conductivity and viscosity of $MnFe_2O_4$ nanofluid under magnetic field using an ANN, Sci. Rep. 7 (2017) 17369.

[105] J. Patel, K. Parekh, R. V. Upadhyay, Maneuvering thermal conductivity of magnetic nanofluids by tunable magnetic fields, J. Appl. Phys. 117 (2015) 1–8.
[106] M. Hajiyan, S. Ebadi, S. Mahmud, M. Biglarbegian, Experimental investigation of the effect of an external magnetic field on the thermal conductivity and viscosity of Fe_3O_4 – glycerol, J. Therm. Anal. Calorim. 135 (2019) 1451–1464.
[107] A. Shahsavar, M.R. Salimpour, M. Saghafian, M.B. Shafii, Effect of magnetic field on thermal conductivity and viscosity of a magnetic nanofluid loaded with carbon nanotubes, J. Mech. Sci. Technol. 30 (2016) 809–815.
[108] M.F. Nabil, W.H. Azmi, K.A. Hamid, N.N.M. Zawawi, G. Priyandoko, R. Mamat, Thermo-physical properties of hybrid nanofluids and hybrid nanolubricants: A comprehensive review on performance, Int. Commun. Heat Mass Transf. 83 (2017) 30–39.
[109] S. Sarboolookzadeh Harandi, A. Karimipour, M. Afrand, M. Akbari, A. D'Orazio, An experimental study on thermal conductivity of F-MWCNTs-Fe_3O_4/EG hybrid nanofluid: Effects of temperature and concentration, Int. Commun. Heat Mass Transf. 76 (2016) 171–177.
[110] M.H. Esfe, S. Esfandeh, M. Afrand, M. Rejvani, S.H. Rostamian, Experimental evaluation, new correlation proposing and ANN modeling of thermal properties of EG based hybrid nanofluid containing ZnO-DWCNT nanoparticles for internal combustion engines applications, Appl. Therm. Eng. 133 (2018) 452–463.
[111] T.T. Baby, R. Sundara, Synthesis and transport properties of metal oxide decorated graphene dispersed nanofluids, J. Phys. Chem. C. 115 (2011) 8527–8533.
[112] S. Kannaiyan, C. Boobalan, A. Umasankaran, A. Ravirajan, S. Sathyan, T. Thomas, Comparison of experimental and calculated thermophysical properties of alumina/cupric oxide hybrid nanofluids, J. Mol. Liq. 244 (2017) 469–477.
[113] M. Hemmat Esfe, A.A. Abbasian Arani, M. Rezaie, W.M. Yan, A. Karimipour, Experimental determination of thermal conductivity and dynamic viscosity of Ag-MgO/water hybrid nanofluid, Int. Commun. Heat Mass Transf. 66 (2015) 189–195.
[114] S.M. Abbasi, A. Rashidi, A. Nemati, K. Arzani, The effect of functionalisation method on the stability and the thermal conductivity of nanofluid hybrids of carbon nanotubes/gamma alumina, Ceram. Int. 39 (2013) 3885–3891.
[115] M. Zadkhast, D. Toghraie, A. Karimipour, Developing a new correlation to estimate the thermal conductivity of MWCNT-CuO/water hybrid nanofluid via an experimental investigation, J. Therm. Anal. Calorim. 129 (2017) 859–867.
[116] M. Hemmat Esfe, A.A. Abbasian Arani, M.R. Madadi, A. Alirezaie, A study on rheological characteristics of hybrid nano-lubricants containing MWCNT-TiO_2 nanoparticles, J. Mol. Liq. 260 (2018) 229–236.
[117] K.A. Hamid, W.H. Azmi, M.F. Nabil, R. Mamat, Improved thermal conductivity of TiO_2 –SiO_2 hybrid nanofluid in ethylene glycol and water mixture, IOP Conf. Ser. Mater. Sci. Eng. 257 (2017) 012067.
[118] L. Syam Sundar, M.K. Singh, M.C. Ferro, A.C.M. Sousa, Experimental investigation of the thermal transport properties of graphene oxide/Co_3O_4 hybrid nanofluids, Int. Commun. Heat Mass Transf. 84 (2017) 1–10.
[119] M. Bahrami, M. Akbari, A. Karimipour, M. Afrand, An experimental study on rheological behavior of hybrid nanofluids made of iron and copper oxide in a binary mixture of water and ethylene glycol: Non-Newtonian behavior, Exp. Therm. Fluid Sci. 79 (2016) 231–237.
[120] H. Eshgarf, M. Afrand, An experimental study on rheological behavior of non-Newtonian hybrid nano-coolant for application in cooling and heating systems, Exp. Therm. Fluid Sci. 76 (2016) 221–227.

[121] M. Hemmat Esfe, A. Alirezaie, M. Rejvani, An applicable study on the thermal conductivity of SWCNT-MgO hybrid nanofluid and price-performance analysis for energy management, Appl. Therm. Eng. 111 (2017) 1202–1210.
[122] A.A. Hussien, M.Z. Abdullah, N.M. Yusop, M.A. Al-Nimr, M.A. Atieh, M. Mehrali, Experiment on forced convective heat transfer enhancement using MWCNTs/GNPs hybrid nanofluid and mini-tube, Int. J. Heat Mass Transf. 115 (2017) 1121–1131.
[123] M. Afrand, K. Nazari Najafabadi, M. Akbari, Effects of temperature and solid volume fraction on viscosity of SiO_2-MWCNTs/SAE40 hybrid nanofluid as a coolant and lubricant in heat engines, Appl. Therm. Eng. 102 (2016) 45–54.
[124] N.N. Esfahani, D. Toghraie, M. Afrand, A new correlation for predicting the thermal conductivity of ZnO–Ag (50%–50%)/water hybrid nanofluid: An experimental study, Powder Technol. 323 (2018) 367–373.
[125] S.H. Rostamian, M. Biglari, S. Saedodin, M. Hemmat Esfe, An inspection of thermal conductivity of CuO-SWCNTs hybrid nanofluid versus temperature and concentration using experimental data, ANN modeling and new correlation, J. Mol. Liq. 231 (2017) 364–369.
[126] M. Afrand, D. Toghraie, B. Ruhani, Effects of temperature and nanoparticles concentration on rheological behavior of Fe_3O_4-Ag/EG hybrid nanofluid: An experimental study, Exp. Therm. Fluid Sci. 77 (2016) 38–44.
[127] L.S. Sundar, M.K. Singh, A.C.M. Sousa, Enhanced heat transfer and friction factor of MWCNT-Fe_3O_4/water hybrid nanofluids, Int. Commun. Heat Mass Transf. 52 (2014) 73–83.
[128] M. Hemmat Esfe, S. Saedodin, W.M. Yan, M. Afrand, N. Sina, Erratumto: Study on thermal conductivity of water-based nanofluids with hybrid suspensions of CNTs/Al_2O_3 nanoparticles, J. Therm. Anal. Calorim. 125 (2016) 565.
[129] M.S. Kumar, V. Vasu, A.V. Gopal, Thermal conductivity and rheological studies for Cu-Zn hybrid nanofluids with various basefluids, J. Taiwan Inst. Chem. Eng. 66 (2016) 321–327.
[130] M. Hemmat Esfe, M.R. Sarlak, Experimental investigation of switchable behavior of CuO-MWCNT (85%–15%)/10W-40 hybrid nano-lubricants for applications in internal combustion engines, J. Mol. Liq. 242 (2017) 326–335.
[131] M. Hemmat Esfe, A.A. Abbasian Arani, An experimental determination and accurate prediction of dynamic viscosity of MWCNT(40%)-SiO_2(60%)/5W50 nano-lubricant, J. Mol. Liq. 259 (2018) 227–237.
[132] K.A. Hamid, W.H. Azmi, R. Mamat, K. V Sharma, Heat transfer performance of TiO_2-SiO_2 nanofluids in a tube with wire coil inserts, Appl. Therm. Eng. 152 (2019) 275–286.
[133] R. Prasher, D. Song, J. Wang, P. Phelan, Measurements of nanofluid viscosity and its implications for thermal applications, Appl. Phys. Lett. 89 (2006) 1–4.
[134] P.G. Kumar, V. Kumaresan, R. Velraj, Stability, viscosity, thermal conductivity, and electrical conductivity enhancement of multi-walled carbon nanotube nanofluid using gum arabic, Fullerenes Nanotub. Carbon Nanostructures. 25 (2017) 230–240.
[135] M. Mehrali, E. Sadeghinezhad, S. Tahan Latibari, M. Mehrali, H. Togun, M.N.M. Zubir, S.N. Kazi, H.S.C. Metselaar, Preparation, characterization, viscosity, and thermal conductivity of nitrogen-doped graphene aqueous nanofluids, J. Mater. Sci. 49 (2014) 7156–7171.
[136] G.A. Adewumi, F. Inambao, M. Sharifpur, J.P. Meyer, Investigation of the viscosity and stability of green nanofluids from coconut fibre carbon nanoparticles: Effect of temperature and mass fraction, Int. J. Appl. Eng. Res. 13 (2018) 8336–8342.
[137] U.M. Kallamu, J.S. Ibrahim, M. Sharifpur, J.P. Meyer, Experimental investigation on

viscosity of nanofluids prepared from banana fibre-nanoparticles, 12th Int. Conf. Heat Transf. Fluid Mech. Thermodyn. (2016) 1713–1718.
[138] M. Amani, P. Amani, A. Kasaeian, O. Mahian, F. Kasaeian, S. Wongwises, Experimental study on viscosity of spinel-type manganese ferrite nanofluid in attendance of magnetic field, J. Magn. Magn. Mater. 428 (2017) 457–463.
[139] P.D. Shima, J. Philip, B. Raj, Magnetically controllable nanofluid with tunable thermal conductivity and viscosity, Appl. Phys. Lett. 95 (2009) 1–4.
[140] L. Wang, Y. Wang, X. Yan, X. Wang, B. Feng, Investigation on viscosity of Fe_3O_4 nanofluid under magnetic field, Int. Commun. Heat Mass Transf. 72 (2016) 23–28.
[141] K. Paulovičová, J. Tóthová, M. Rajňák, Z. Wu, B. Sundén, L. Wadsö, T. Tobiáš, P. Kopčansky, M. Timko, V. Lisý, Rheological and thermal transport characteristics of a transformer oil based ferrofluid, Acta Phys. Pol. A. 133 (2018) 564–566.
[142] A. Malekzadeh, A.R. Pouranfard, N. Hatami, A. Kazemnejad Banari, M.R. Rahimi, Experimental investigations on the viscosity of magnetic nanofluids under the influence of temperature, volume fractions of nanoparticles and external magnetic field, J. Appl. Fluid Mech. 9 (2016) 693–697.
[143] A. Amiri, S.N. Kazi, M. Shanbedi, M.N. Mohd Zubir, H. Yarmand, B.T. Chew, Transformer oil based multi-walled carbon nanotube-hexylamine coolant with optimized electrical, thermal and rheological enhancements, RSC Adv. 5 (2015) 107222–107236.
[144] I.M. Shahrul, I.M. Mahbubul, S.S. Khaleduzzaman, R. Saidur, M.F.M. Sabri, A comparative review on the specific heat of nanofluids for energy perspective, Renew. Sustain. Energy Rev. 38 (2014) 88–98.
[145] R.S. Vajjha, D.K. Das, Specific heat measurement of three nanofluids and development of new correlations, J. Heat Transfer. 131 (2009) 071601.
[146] B.X. Wang, L.P. Zhou, X.F. Peng, X.Z. Du, Y.P. Yang, On the specific heat capacity of CuO nanofluid, Adv. Mech. Eng. 2010 (2010).
[147] M.N. Chandran, S. Manikandan, K.S. Suganthi, K.S. Rajan, Novel hybrid nanofluid with tunable specific heat and thermal conductivity: Characterization and performance assessment for energy related applications, Energy. 140 (2017) 27–39.
[148] C.A. Nieto De Castro, S.M.S. Murshed, M.J. V Lourenço, F.J. V Santos, M.L.M. Lopes, J.M.P. França, Enhanced thermal conductivity and specific heat capacity of carbon nanotubes ionanofluids, Int. J. Therm. Sci. 62 (2012) 34–39.
[149] M. Hernaiz, V. Alonso, P. Estellé, Z. Wu, B. Sundén, L. Doretti, S. Mancin, N. Çobanog, The contact angle of nanofluids as thermophysical property, J. Colloid Interface Sci. 547 (2019) 393–406.
[150] H. Karami, S. Papari-Zare, M. Shanbedi, H. Eshghi, A. Dashtbozorg, A. Akbari, E. Mohammadian, M. Heidari, A.Z. Sahin, C.B. Teng, The thermophysical properties and the stability of nanofluids containing carboxyl-functionalized graphene nano-platelets and multi-walled carbon nanotubes, Int. Commun. Heat Mass Transf. 108 (2019) 104302.
[151] P.S. Joshi, A. Pattamatta, Buoyancy induced convective heat transfer in particle, tubular and flake type of nanoparticle suspensions, Int. J. Therm. Sci. 122 (2017) 1–11.
[152] H. Ghodsinezhad, M. Sharifpur, J.P. Meyer, Experimental investigation on cavity flow natural convection of Al_2O_3-water nanofluids, Int. Commun. Heat Mass Transf. 76 (2016) 316–324.
[153] M. Sharifpur, A.B. Solomon, T.L. Ottermann, J.P. Meyer, Optimum concentration of nanofluids for heat transfer enhancement under cavity flow natural convection with TiO_2-water, Int. Commun. Heat Mass Transf. 98 (2018) 297–303.
[154] N.L. Cadena-de la Peña, C.I. Rivera-Solorio, L.A. Payán-Rodríguez, A.J. García-

Cuéllar, J.L. López-Salinas, Experimental analysis of natural convection in vertical annuli filled with AlN and TiO_2/mineral oil-based nanofluids, Int. J. Therm. Sci. 111 (2017) 138–145.
[155] M.A. Sheremet, I. Pop, N. Bachok, Effect of thermal dispersion on transient natural convection in a wavy-walled porous cavity filled with a nanofluid: Tiwari and Das' nanofluid model, Int. J. Heat Mass Transf. 92 (2016) 1053–1060.
[156] A. Brusly Solomon, J. van Rooyen, M. Rencken, M. Sharifpur, J.P. Meyer, Experimental study on the influence of the aspect ratio of square cavity on natural convection heat transfer with Al_2O_3/water nanofluids, Int. Commun. Heat Mass Transf. 88 (2017) 254–261.
[157] A.A. Minea, G. Lorenzini, A numerical study on ZnO based nanofluids behavior on natural convection, Int. J. Heat Mass Transf. 114 (2017) 286–296.
[158] H. Li, Y. He, Y. Hu, B. Jiang, Y. Huang, Thermophysical and natural convection characteristics of ethylene glycol and water mixture based ZnO nanofluids, Int. J. Heat Mass Transf. 91 (2015) 385–389.
[159] K. Kouloulias, A. Sergis, Y. Hardalupas, Sedimentation in nanofluids during a natural convection experiment, Int. J. Heat Mass Transf. 101 (2016) 1193–1203.
[160] Y. Hu, Y. He, S. Wang, Q. Wang, H.I. Schlaberg, Experimental and numerical investigation on natural convection heat transfer of TiO_2-water nanofluids in a square enclosure, J. Heat Transfer. 136 (2014) 022502.
[161] C.J. Ho, W.K. Liu, Y.S. Chang, C.C. Lin, Natural convection heat transfer of alumina-water nanofluid in vertical square enclosures: An experimental study, Int. J. Therm. Sci. 49 (2010) 1345–1353.
[162] P.S. Joshi, A. Pattamatta, Enhancement of natural convection heat transfer in a square cavity using MWCNT/Water nanofluid: an experimental study, Heat Mass Transf. (2017).
[163] Y. Hu, Y. He, C. Qi, B. Jiang, H. Inaki Schlaberg, Experimental and numerical study of natural convection in a square enclosure filled with nanofluid, Int. J. Heat Mass Transf. 78 (2014) 380–392.
[164] O. Mahian, A. Kianifar, S.Z. Heris, S. Wongwises, Natural convection of silica nanofluids in square and triangular enclosures: Theoretical and experimental study, Int. J. Heat Mass Transf. 99 (2016) 792–804.
[165] S.O. Giwa, M. Shafirpur, J.P. Meyer, Heat transfer enhancement of dilute Al_2O_3-MWCNT water based hybrid nanofluids in a square cavity, Proceedings, 16th Int. Heat Transf. Conf. August 10-15, 2018, Beijing, China. (2018) 5365–5372.
[166] R. Choudhary, S. Subudhi, Aspect ratio dependence of turbulent natural convection in Al_2O_3/water nanofluids, Appl. Therm. Eng. 108 (2016) 1095–1104.
[167] S.Z. Heris, M.B. Pour, O. Mahian, S. Wongwises, A comparative experimental study on the natural convection heat transfer of different metal oxide nanopowders suspended in turbine oil inside an inclined cavity, Int. J. Heat Mass Transf. 73 (2014) 231–238.
[168] K. Kouloulias, A. Sergis, Y. Hardalupas, Assessing the flow characteristics of nanofluids during turbulent natural convection, J. Therm. Anal. Calorim. 135 (2019) 3181–3189.
[169] A.G.A. Nnanna, Experimental model of temperature-driven nanofluid, J. Heat Transfer. 129 (2007) 697–704.
[170] C.J. Ho, D.S. Chen, W.M. Yan, O. Mahian, Buoyancy-driven flow of nanofluids in a cavity considering the Ludwig-Soret effect and sedimentation: Numerical study and experimental validation, Int. J. Heat Mass Transf. 77 (2014) 684–694.
[171] A.B. Solomon, M. Sharifpur, J.P. Meyer, J.S. Ibrahim, B. Immanuel, Convection heat

transfer with water based mango bark nanofluids, in: 13th Int. Conf. Heat Transf. Fluid Mech. Thermodyn., Portorož, Slovenia, 2017.
[172] S.U. Ilyas, R. Pendyala, M. Narahari, Experimental investigation of natural convection heat transfer characteristics in MWCNT-thermal oil nanofluid, J. Therm. Anal. Calorim. 135 (2019) 1197–1209.
[173] C. Qi, G. Wang, Y. Ma, L. Guo, Experimental research on stability and natural convection of TiO_2-water nanofluid in enclosures with different rotation angles, Nanoscale Res. Lett. 12 (2017) 1–14.
[174] M.R. Khadangi Mahrood, S.G. Etemad, R. Bagheri, Free convection heat transfer of non Newtonian nanofluids under constant heat flux condition, Int. Commun. Heat Mass Transf. 38 (2011) 1449–1454.
[175] K.S. Suganthi, K.S. Rajan, Improved transient heat transfer performance of ZnO-propylene glycol nanofluids for energy management, Energy Convers. Manag. 96 (2015) 115–123.
[176] S.U. Ilyas, R. Pendyala, M. Narahari, An experimental study on the natural convection heat transfer in rectangular enclosure using functionalized alumina-thermal oil-based nanofluids, Appl. Therm. Eng. 127 (2017) 765–775.
[177] A. Brusly Solomon, M. Sharifpur, T. Ottermann, C. Grobler, M. Joubert, J.P. Meyer, Natural convection enhancement in a porous cavity with Al_2O_3-ethylene glycol/water nanofluids, Int. J. Heat Mass Transf. 108 (2017) 1324–1334.
[178] M. Ali, O. Zeitoun, S. Almotairi, Natural convection heat transfer inside vertical circular enclosure filled with water-based Al_2O_3 nanofluids, Int. J. Therm. Sci. 63 (2013) 115–124.
[179] M. Ali, O. Zeitoun, S. Almotairi, H. Al-Ansary, The effect of alumina–water nanofluid on natural convection heat transfer inside vertical circular enclosures heated from above, Heat Transf. Eng. 34 (2013) 1289–1299.
[180] H. Moradi, B. Bazooyar, A. Moheb, S.G. Etemad, Optimization of natural convection heat transfer of Newtonian nanofluids in a cylindrical enclosure, Chinese J. Chem. Eng. 23 (2015) 1266–1274.
[181] K.G. Pham, S.A. Suslov, The influence of magnetic field on convection in an inclined ferrofluid layer heated from below, J. Phys. Conf. Ser. (2018).
[182] Y. Ma, R. Mohebbi, M.M. Rashidi, Z. Yang, M.A. Sheremet, Numerical study of MHD nanofluid natural convection in a baffled U-shaped enclosure, Int. J. Heat Mass Transf. 130 (2019) 123–134.
[183] B. Ghasemi, S.M. Aminossadati, A. Raisi, Magnetic field effect on natural convection in a nanofluid-filled square enclosure, Int. J. Therm. Sci. 50 (2011) 1748–1756.
[184] M. Sheikholeslami, H.B. Rokni, Magnetohydrodynamic CuO-water nanofluid in a porous complex-shaped enclosure, J. Therm. Sci. Eng. Appl. 9 (2017) 041007.
[185] M. Sheikholeslami, M.B. Gerdroodbary, D.D. Ganji, Numerical investigation of forced convective heat transfer of Fe_3O_4-water nanofluid in the presence of external magnetic source, Comput. Methods Appl. Mech. Eng. 315 (2017) 831–845.
[186] M. Sheikholeslami, A. Shafee, A. Zareei, R. Haq, Z. Li, Heat transfer of magnetic nanoparticles through porous media including exergy analysis, J. Mol. Liq. 279 (2019) 719–732.
[187] N. Makulati, A. Kasaeipoor, M.M. Rashidi, Numerical study of natural convection of a water-alumina nanofluid in inclined C-shaped enclosures under the effect of magnetic field, Adv. Powder Technol. 27 (2016) 661–672.
[188] W.K. Hussam, K. Khanafer, H.J. Salem, G.J. Sheard, Natural convection heat transfer utilizing nanofluid in a cavity with a periodic side-wall temperature in the presence of a magnetic field, Int. Commun. Heat Mass Transf. 104 (2019) 127–135.

[189] H. Nemati, M. Farhadi, K. Sedighi, H.R. Ashorynejad, E. Fattahi, Magnetic field effects on natural convection flow of nanofluid in a rectangular cavity using the Lattice Boltzmann model, Sci. Iran. 19 (2012) 303–310.
[190] H. Sajjadi, A.A. Delouei, M. Izadi, R. Mohebbi, Investigation of MHD natural convection in a porous media by double MRT lattice Boltzmann method utilizing MWCNT-Fe_3O_4/water hybrid nanofluid, Int. J. Heat Mass Transf. 132 (2019) 1087–1104.
[191] H. Moradi, B. Bazooyar, A. Moheb, S.G. Etemad, Optimization of natural convection heat transfer of Newtonian nanofluids in a cylindrical enclosure, Chinese J. Chem. Eng. 23 (2015) 1266–1274.
[192] H. Yamaguchi, X.-D. Niu, X.-R. Zhang, K. Yoshikawa, Experimental and numerical investigation of natural convection of magnetic fluids in a cubic cavity, J. Magn. Magn. Mater. 321 (2009) 3665–3670.
[193] H. Yamaguchi, X.R. Zhang, X.D. Niu, K. Yoshikawa, Thermomagnetic natural convection of thermo-sensitive magnetic fluids in cubic cavity with heat generating object inside, J. Magn. Magn. Mater. 322 (2010) 698–704.
[194] A. Roszko, E. Fornalik-Wajs, Extend of magnetic field interference in the natural convection of diamagnetic nanofluid, Heat Mass Transf. Und Stoffuebertragung. (2017) 1–12.
[195] D.D. Dixit, A. Pattamatta, Natural convection heat transfer in a cavity filled with electrically conducting nano-particle suspension in the presence of magnetic field, Phys. Fluids. 31 (023302 (2019) 1–15.
[196] B. Takabi, S. Salehi, Augmentation of the heat transfer performance of a sinusoidal corrugated enclosure by employing hybrid nanofluid, Adv. Mech. Eng. 2014 (2014).
[197] T. Tayebi, A.J. Chamkha, Natural convection enhancement in an eccentric horizontal cylindrical annulus using hybrid nanofluids, Numer. Heat Transf. Part A Appl. 71 (2017) 1159–1173.
[198] M. Izadi, R. Mohebbi, D. Karimi, M.A. Sheremet, Numerical simulation of natural convection heat transfer inside a $\perp$ shaped cavity filled by a MWCNT-Fe_3O_4/water hybrid nanofluids using LBM, Chem. Eng. Process. - Process Intensif. 125 (2018) 56–66.
[199] M.A. Mansour, S. Siddiqa, R.S.R. Gorla, A.M. Rashad, Effects of heat source and sink on entropy generation and MHD natural convection of Al_2O_3-Cu/water hybrid nanofluid filled with square porous cavity, Therm. Sci. Eng. Prog. 6 (2018) 57–71.
[200] S.A.M. Mehryan, M.A. Sheremet, M. Soltani, M. Izadi, Natural convection of magnetic hybrid nanofluid inside a double-porous medium using two-equation energy model, J. Mol. Liq. 277 (2019) 959–970.
[201] H.R. Ashorynejad, A. Shahriari, MHD natural convection of hybrid nanofluid in an open wavy cavity, Results Phys. 9 (2018) 440–455.
[202] A.M. Rashad, A.J. Chamkha, M.A. Ismael, T. Salah, Magnetohydrodynamics natural convection in a triangular cavity filled with a Cu-Al_2O_3/water hybrid nanofluid with localized heating from below and internal heat generation, J. Heat Transfer. 140 (2018) 072502.
[203] H. Ritacco, J. Kovensky, A. Fernández-Cirelli, M.J.L. Castro, A simplified method for the determination of critical micelle concentration, J. Chem. Educ. 78 (2001) 347.
[204] C.O. Popiel, J. Wojtkowiak, Simple formulas for thermophysical properties of liquid water for heat transfer calculations (from 0 °C to 150 °C), Heat Transf. Eng. 19 (1998) 87–101.
[205] ASHRAE, Handbook - Fundamentals (SI Edition), American Society of Heating, Refrigerating and Air-Conditioning Engineers, Inc., ASHRAE, 2017.

[206] W.H. Leong, K.G.T. Hollands, A.P. Brunger, Experimental Nusselt numbers for a cubical-cavity benchmark problem in natural convection, Int. J. Heat Mass Transf. 42 (1998) 1979–1989.
[207] M.H. Aghabozorg, A. Rashidi, S. Mohammadi, Experimental investigation of heat transfer enhancement of Fe_2O_3-CNT/water magnetic nanofluids under laminar, transient and turbulent flow inside a horizontal shell and tube heat exchanger, Exp. Therm. Fluid Sci. 72 (2016) 182–189.
[208] B. Sun, C. Peng, R. Zuo, D. Yang, H. Li, Investigation on the flow and convective heat transfer characteristics of nanofluids in the plate heat exchanger, Exp. Therm. Fluid Sci. (2016).
[209] A. Shahsavar, M.R. Salimpour, M. Saghafian, M.B. Shafii, An experimental study on the effect of ultrasonication on thermal conductivity of ferrofluid loaded with carbon nanotubes, Thermochim. Acta. 617 (2015) 102–110.
[210] N. Kumar, S.S. Sonawane, Experimental study of Fe_2O_3/water and Fe_2O_3/ethylene glycol nanofluid heat transfer enhancement in a shell and tube heat exchanger, Int. Commun. Heat Mass Transf. 78 (2016) 277–284.
[211] M.S. Astanina, M. Kamel Riahi, E. Abu-Nada, M.A. Sheremet, Magnetohydrodynamic in partially heated square cavity with variable properties: Discrepancy in experimental and theoretical conductivity correlations, Int. J. Heat Mass Transf. 116 (2018) 532–548.
[212] A.M. Rashad, T. Armaghani, A.J. Chamkha, M.A. Mansour, Entropy generation and MHD natural convection of a nanofluid in an inclined square porous cavity: Effects of a heat sink and source size and location, Chinese J. Phys. 56 (2018) 193–211.
[213] P.B. Kharat, J.S. Kounsalye, M. V. Shisode, K.M. Jadhav, Preparation and thermophysical investigations of $CoFe_2O_4$-based nanofluid: A potential heat transfer agent, J. Supercond. Nov. Magn. (2018) 1–11.
[214] L. Megatif, A. Ghozatloo, A. Arimi, M. Shariati-Niasar, Investigation of laminar convective heat transfer of a novel TiO_2-carbon nanotube hybrid water-based nanofluid, Exp. Heat Transf. 29 (2016) 124–138.
[215] K.A. Hamid, W.H. Azmi, M.F. Nabil, R. Mamat, K. V Sharma, Experimental investigation of thermal conductivity and dynamic viscosity on nanoparticle mixture ratios of TiO_2-SiO_2 nanofluids, Int. J. Heat Mass Transf. 116 (2018) 1143–1152.
[216] B. Berkovsky, V. Polevikov, Numerical study of problems on high-intensive free convection, in: Proc. Int. Turbul. Buoyant Convect. Semin., 1977: pp. 443–455.
[217] M.M. Tawfik, Experimental studies of nanofluid thermal conductivity enhancement and applications : A review, Renew. Sustain. Energy Rev. 75 (2017) 1239–1253.
[218] R.J. Moffat, Describing the uncertainties in experimental results, Exp. Therm. Fluid Sci. 1 (1988) 3–17.

APPENDICES

A. Weights of NPs and Surfactants

A.1 Introduction

This section of the appendices presents the estimation of the amounts of NPs and surfactants used in the formulation of AMF, BAAF and AAF samples. The optimum dispersion fractions obtained for the formulation of AMF, BAAF and AAF were used in the estimation of the weights of NPs and surfactants. The amounts of NPs deployed in the formulation of AMF, BAAF and AAF depended on φ, NP percent weight and NP-types hybridised.

A.2 Calculation of Weights of NPs and Surfactants for AMF

NPs of Fe_2O_3 and MWCNT at percent weights of 80% and 20% respectively were suspended in DIW (1 400 ml) to formulate AMF. The dispersion fraction of the surfactant (SDS) was 0.5. Fe_2O_3 NPs had ρ of 5.242 g/cm^3, while MWCNT NPs had ρ of 2.1 g/cm^3. The ρ of individual MHNF was estimated using Eq. A1 as the individual ρ of HNPs and the weight percent were known.

$$\rho_{HNP} = X_{Fe_3O_2}\rho_{Fe_3O_2} + X_{MWCNT/Al_2O_3}\rho_{MWCNT/Al_2O_3} \quad \textbf{A.1}$$

The weight of HNPs was described to be equal to the sum of the individual weight of NPs hybridised, as expressed in Eq. A2.

$$M_{HNP} = M_{Fe_3O_2} + M_{MWCNT/Al_2O_3} \quad \textbf{A.2}$$

The weight of individual NPs was expressed as a multiplication of the percent weight and HNP weight, as given in Eqs. A3 and A4.

$$M_{Fe_3O_2} = X_{Fe_3O_2}M_{HNP} \quad \textbf{A.3}$$

$$M_{MWCNT/Al_2O_3} = X_{MWCNT/Al_2O_3}M_{HNP} \quad \textbf{A.4}$$

Eqs. A1 to A4 were substituted into Eq. 3.1 to estimate the weights of Fe_2O_3 and MWCNT NPs as a function of φ (0.05 – 0.40), as given in Table A1. In addition, the weights of SDS were calculated using Eq. 3.2 and as a dependent of φ.

Table A.2: Weights (g) of NPs and surfactant (SDS) engaged in AMF formulation.

φ	Fe_2O_3	MWCNT	SDS	Total
0.05	2.5849	0.6462	1.6156	4.8467
0.10	5.1724	1.2931	3.2328	9.6983
0.20	10.3552	2.5888	6.4720	19.4160
0.30	15.5483	3.8871	9.7177	29.1531
0.40	20.7519	5.1880	12.9700	38.9099

A.3 Calculation of Weights of NPs and Surfactants for BAAF

In the formulation of BAAF, NPs of Fe_2O_3 and Al_2O_3 at percent weights of 75% and 25% respectively were suspended in EG-DIW (1 400 ml). SDBS was used as the surfactant with a dispersion fraction of 1.1. Fe_2O_3 NPs had ρ of 5.242 g/cm^3, while Al_2O_3 NPs had ρ of 3.97 g/cm^3. The substitution of Eqs. A1 to A4 in Eq. 3.1 was used to calculate the amounts of NPs used in the formulation of BAAF, as provided in Table A2. The weights of SDBS were also estimated using Eq. 3.2 based on φ and dispersion fraction of 1.1.

Table A.3: Weights (g) of NPs and surfactant (SDBS) engaged in BAAF formulation.

φ	Fe_2O_3	Al_2O_3	SDBS	Total
0.05	2.5864	0.8621	4.1382	7.5868
0.10	5.1754	1.7251	8.2806	15.1811
0.20	10.3611	3.4537	16.5778	30.3926
0.30	15.5573	5.1858	24.8916	45.6347
0.40	20.7639	6.9213	33.2222	60.9073

A.4 Calculation of Weights of NPs and Surfactants for AAF

Fe_2O_3 and Al_2O_3 at percent weights of 75% and 25% respectively were suspended in DIW (1 400 ml) to formulate AAF. SDS was used as the surfactant with a dispersion fraction of 1.0. Fe_2O_3 NPs had ρ of 5.242 g/cm^3, while Al_2O_3 NPs had ρ of 3.97 g/cm^3. By substituting Eqs. A1 to A4 in Eq. 3.1, the amounts of NPs used in the formulation of AAF were calculated, as given in Table A3. The weights of SDS were also evaluated using Eq. 3.2 based on φ and dispersion fraction of 1.0.

Table A.4: Weights (g) of NPs and surfactant (SDS) engaged in AAF formulation.

φ	Fe_2O_3	Al_2O_3	SDS	Total
0.05	2.5864	0.8621	3.7934	7.2419
0.10	5.1754	1.7251	7.5906	14.4911
0.20	10.3611	3.4537	15.1963	29.0111
0.30	15.5573	5.1858	22.8173	43.5604

A.5 Conclusion

The weights of NPs and surfactants used in the formulation of AMF, BAAF and AAF in this study were estimated and presented in this section. These weights were observed to be dependent primarily on ρ and percent weight of individual NPs, and φ, as related to the type of MHNFs to be formulated. Additionally, the total amounts of materials (HNPs and surfactants) depended on the types of MHNFs to be formulated, which was related to φ, types of surfactants, dispersion fraction of surfactants, NP percent weight, and the types of NPs combined as HNPs.

B. Calibration of Thermocouples

B.1 Introduction

The calibration of the thermocouples used in the cavity for the thermo-convection and thermomagnetic convection studies of AMF, BAAF and AAF is discussed in this section. The calibration factors of each thermocouple are also presented in this section.

B.2 Calibration of Thermocouples

A thermal bath (PR20R-30 Polyscience; accuracy = ±0.005 °C) was used for the in-situ calibration of the thermocouples at temperatures of 15 to 55 °C with 2.5 °C interval. Temperature measurements of 400 points were acquired at the predetermined temperature using a frequency of 2 Hz and the average was estimated. The calibration process was carried out in triplicate (to reduce error) and the averages of the measured temperature data for the thermocouples were evaluated. For each thermocouple, the average measured temperature was plotted against the reference temperature as determined using PT-100 (thermal bath internal thermocouple) and is presented in Fig. B1. Fitting of the reference and average measured temperature for each thermocouple was conducted to determine the calibration factors using Eq. B1.

$$T_{cal} = mT_{uncali} + c \qquad \textbf{B.1}$$

For the thermocouples, the m and c were utilised as the calibration factors. A linear relationship with $R^2 \approx 1$ was observed between the average measured temperature and the reference temperature for all the thermocouples. This indicated a good correlation between both variables showing excellent behaviour of the thermocouples in measuring the reference temperatures.

Fig. B2 shows the calibrated and uncalibrated temperatures of the thermocouples at some reference temperatures. Scattered temperatures were observed for the thermocouples when

the temperatures were uncalibrated compared with the relatively linear temperatures after calibrating the thermocouples. The reason for using different channels of the data logger was the differences in the calibration factors obtained for the thermocouples.

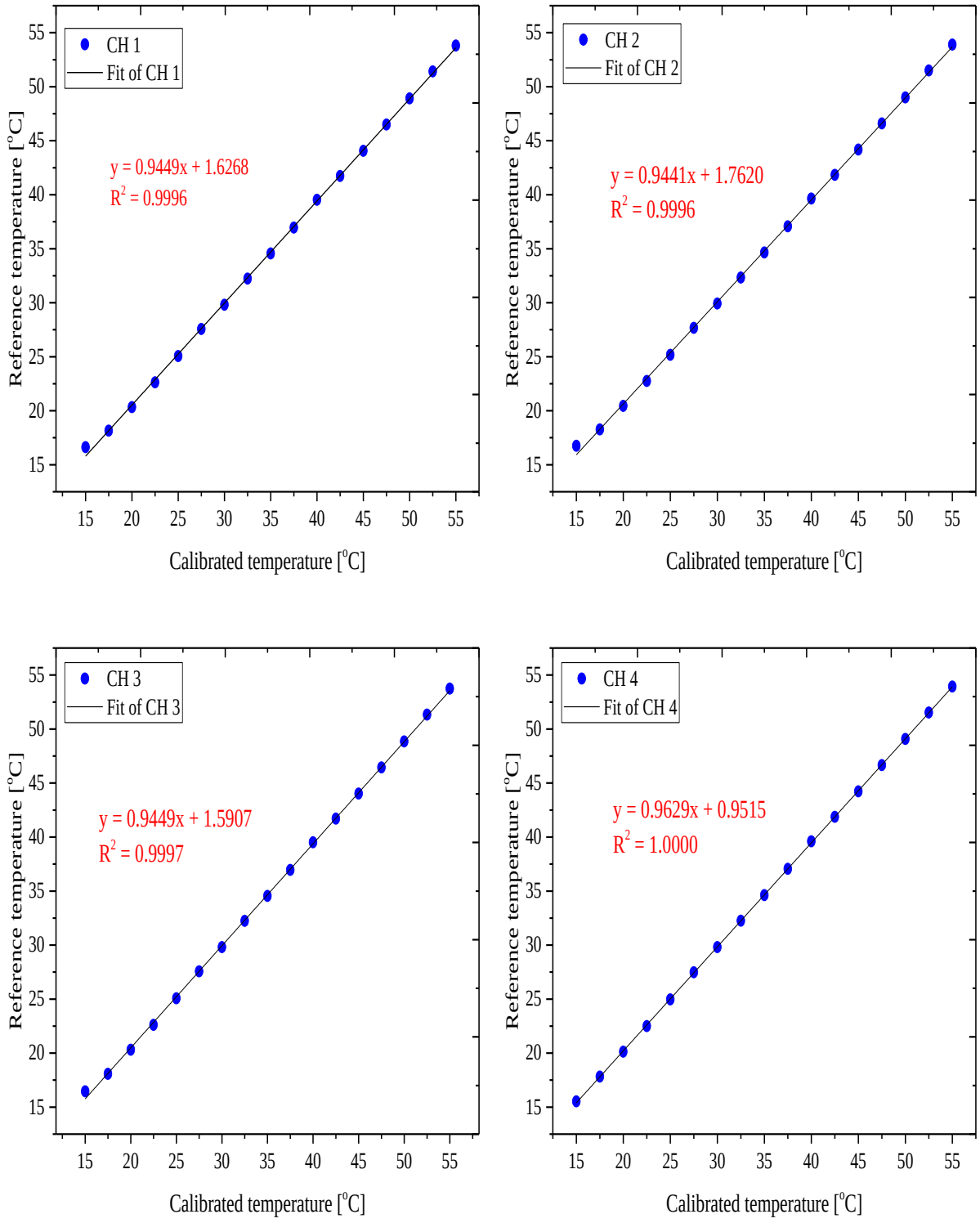

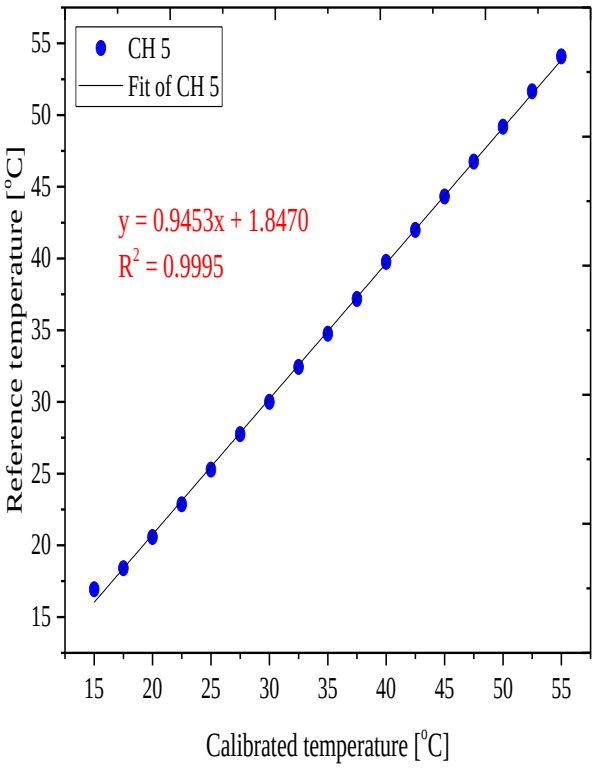
CH 5
Fit of CH 5
y = 0.9453x + 1.8470
R2 = 0.9995
Reference temperature [°C]
Calibrated temperature [°C]

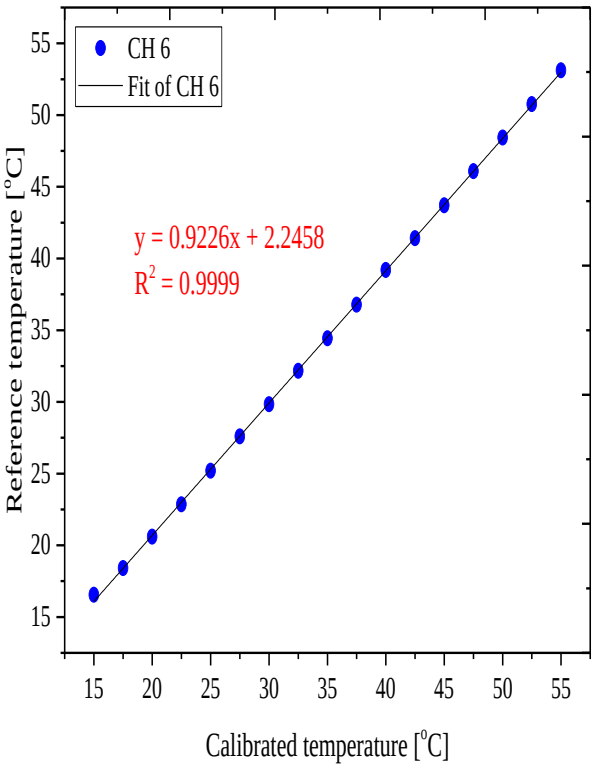
CH 6
Fit of CH 6
y = 0.9226x + 2.2458
R2 = 0.9999
Reference temperature [°C]
Calibrated temperature [°C]

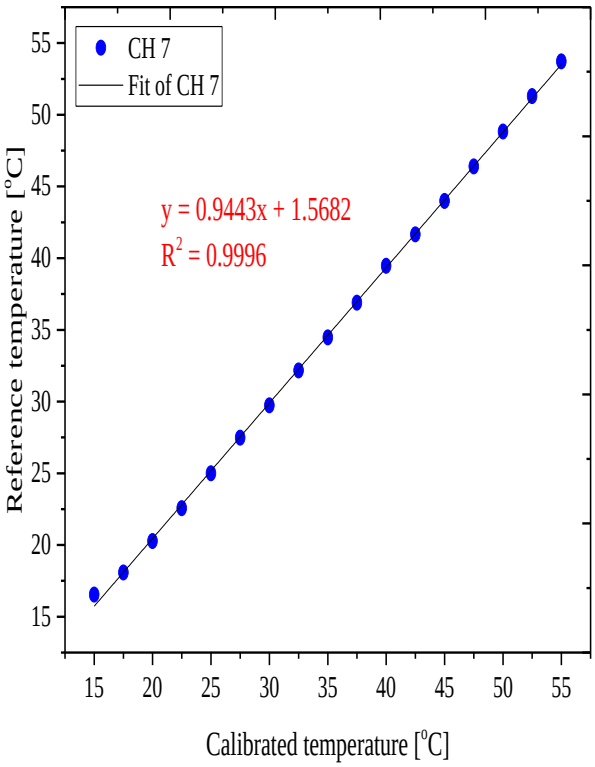
CH 7
Fit of CH 7
y = 0.9443x + 1.5682
R2 = 0.9996
Reference temperature [°C]
Calibrated temperature [°C]

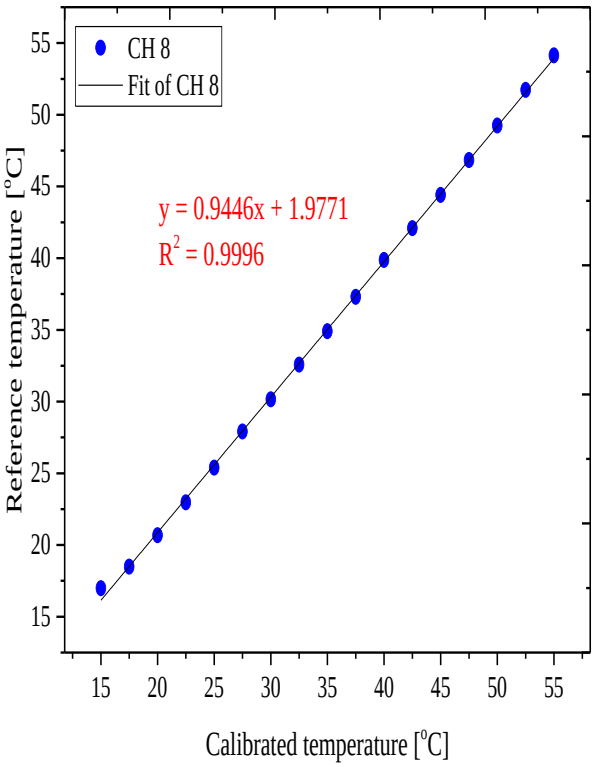
CH 8
Fit of CH 8
y = 0.9446x + 1.9771
R2 = 0.9996
Reference temperature [°C]
Calibrated temperature [°C]

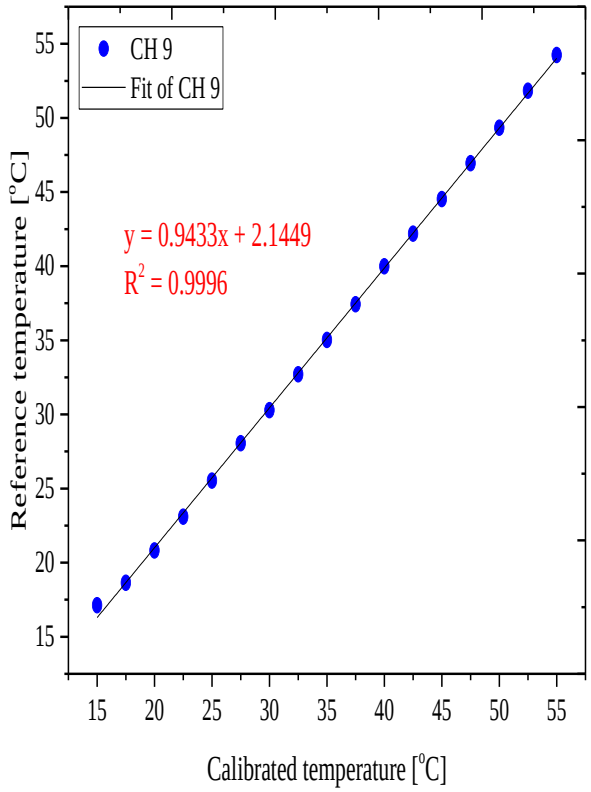
CH 9
Fit of CH 9
y = 0.9433x + 2.1449
R2 = 0.9996
Reference temperature [°C]
Calibrated temperature [°C]

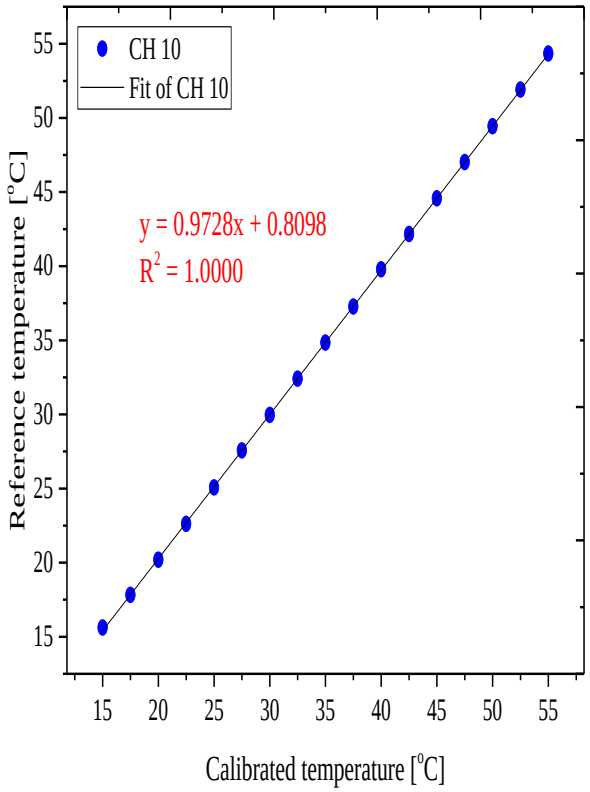
CH 10
Fit of CH 10
y = 0.9728x + 0.8098
R2 = 1.0000
Reference temperature [°C]
Calibrated temperature [°C]

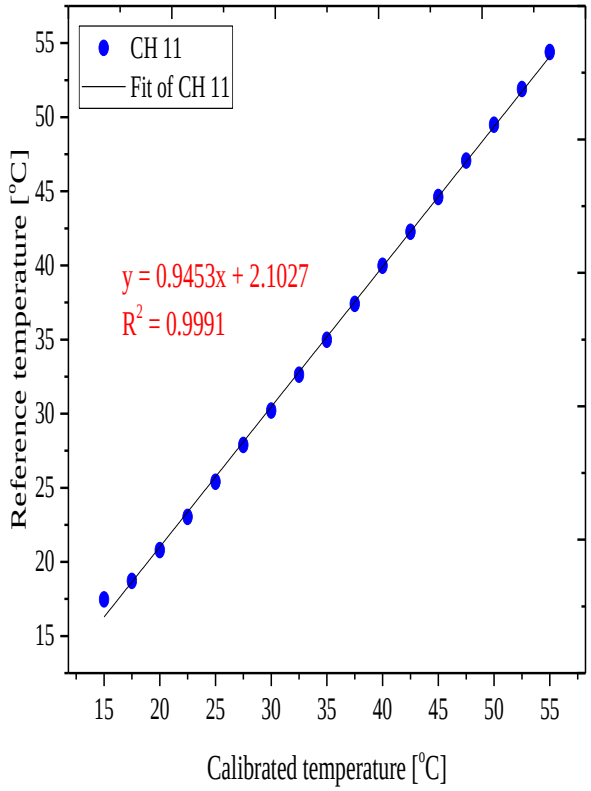
CH 11
Fit of CH 11
y = 0.9453x + 2.1027
R2 = 0.9991
Reference temperature [°C]
Calibrated temperature [°C]

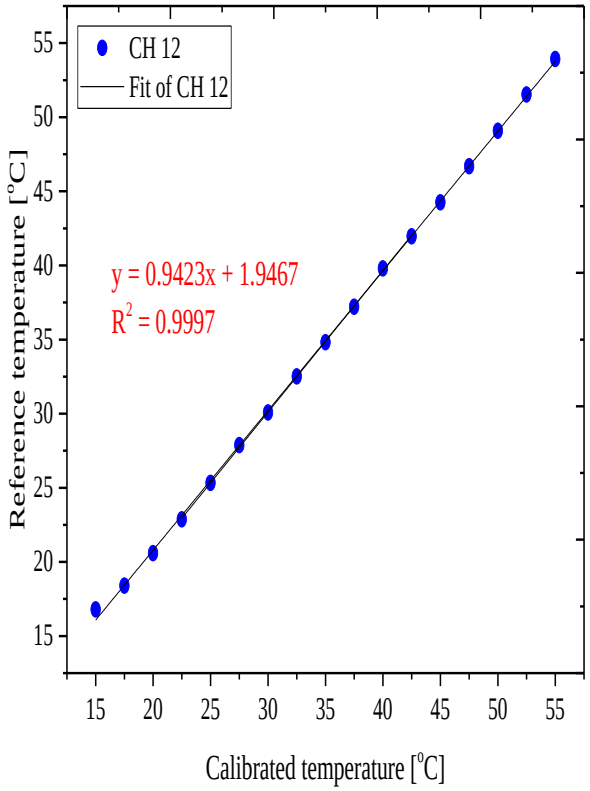
CH 12
Fit of CH 12
y = 0.9423x + 1.9467
R2 = 0.9997
Reference temperature [°C]
Calibrated temperature [°C]

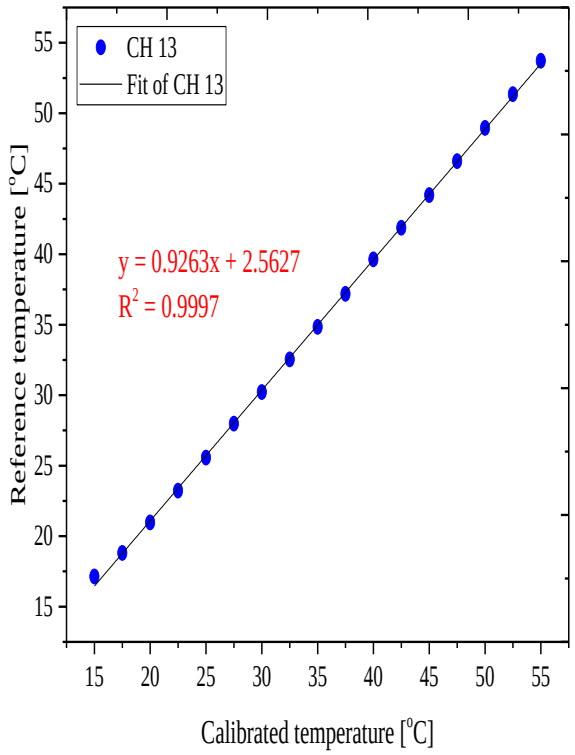
CH 13
Fit of CH 13
y = 0.9263x + 2.5627
R2 = 0.9997
Reference temperature [°C]
Calibrated temperature [°C]

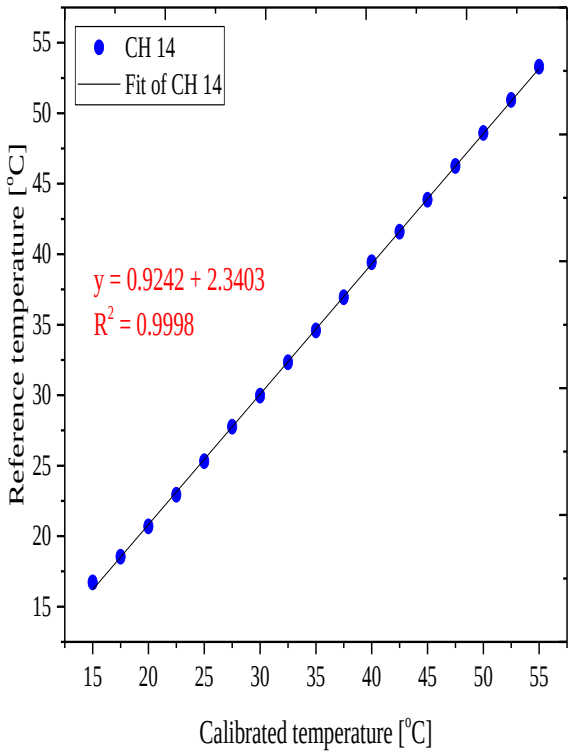
CH 14
Fit of CH 14
y = 0.9242 + 2.3403
R2 = 0.9998
Reference temperature [°C]
Calibrated temperature [°C]

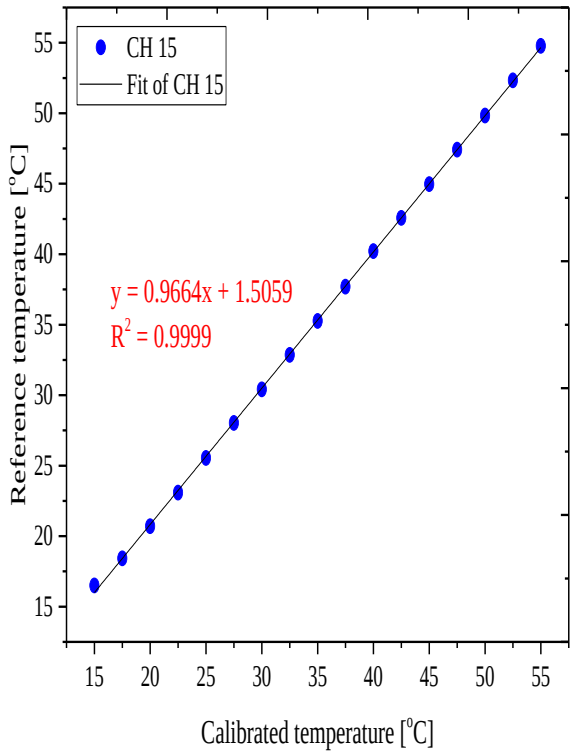
CH 15
Fit of CH 15
y = 0.9664x + 1.5059
R2 = 0.9999
Reference temperature [°C]
Calibrated temperature [°C]

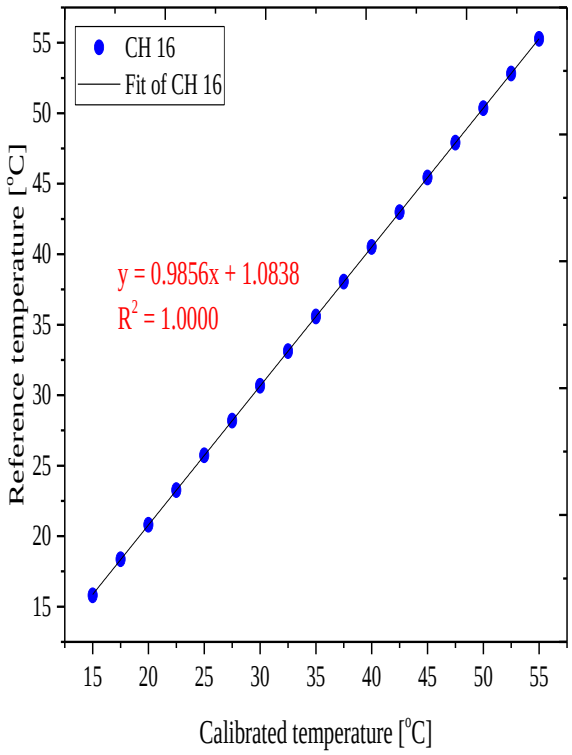
CH 16
Fit of CH 16
y = 0.9856x + 1.0838
R2 = 1.0000
Reference temperature [°C]
Calibrated temperature [°C]

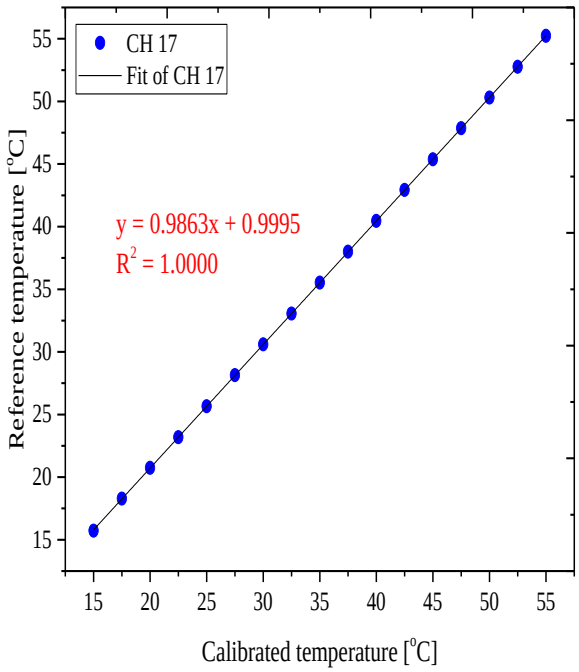
CH 17
Fit of CH 17
y = 0.9863x + 0.9995
R2 = 1.0000
Reference temperature [°C]
Calibrated temperature [°C]

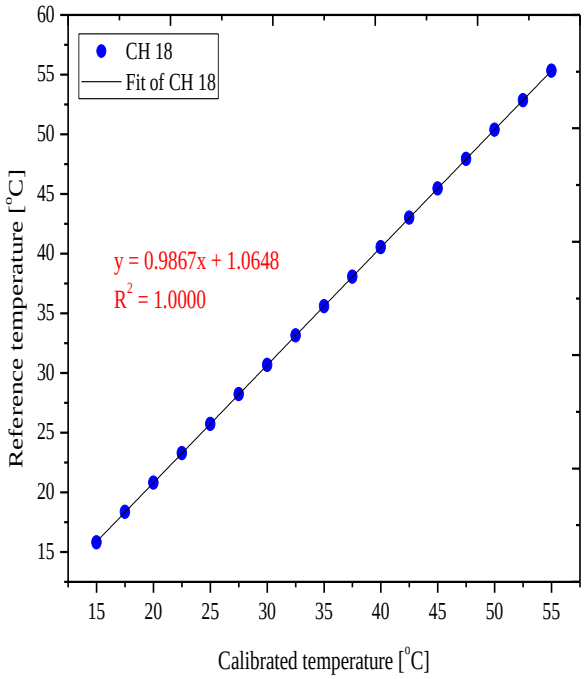
CH 18
Fit of CH 18
y = 0.9867x + 1.0648
R2 = 1.0000
Reference temperature [°C]
Calibrated temperature [°C]

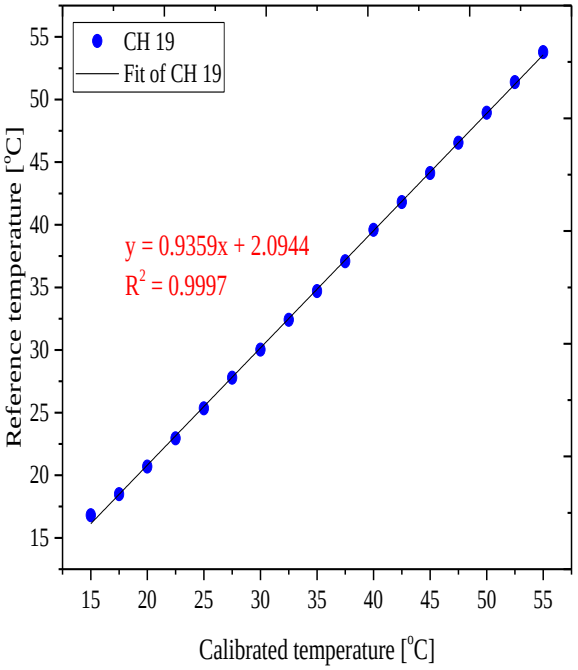
CH 19
Fit of CH 19
y = 0.9359x + 2.0944
R2 = 0.9997
Reference temperature [°C]
Calibrated temperature [°C]

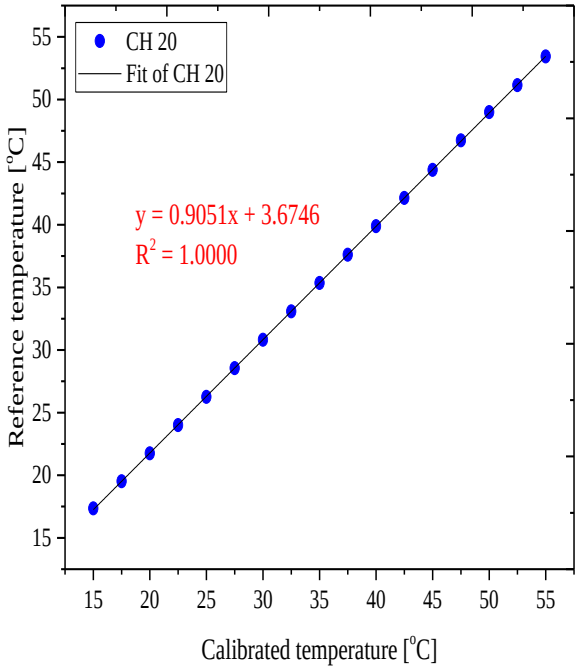
CH 20
Fit of CH 20
y = 0.9051x + 3.6746
R2 = 1.0000
Reference temperature [°C]
Calibrated temperature [°C]

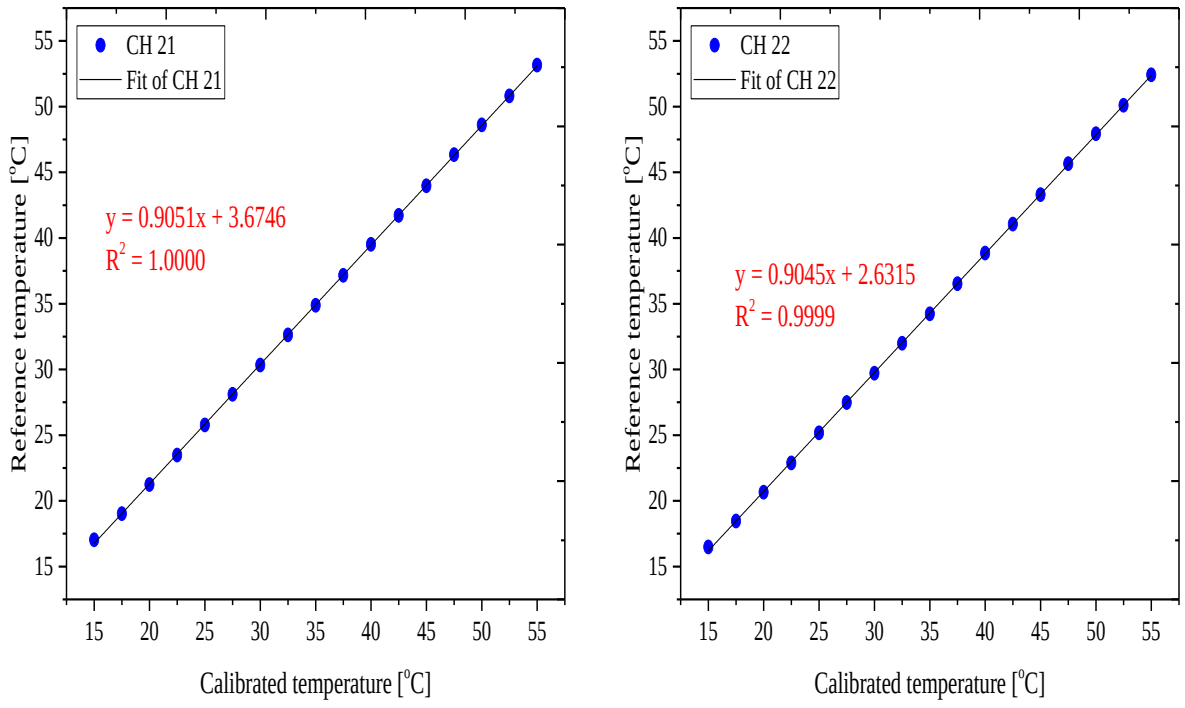

Figure B.8.1: Average measured temperatures of thermocouples against reference temperatures (CH 1 - 22).

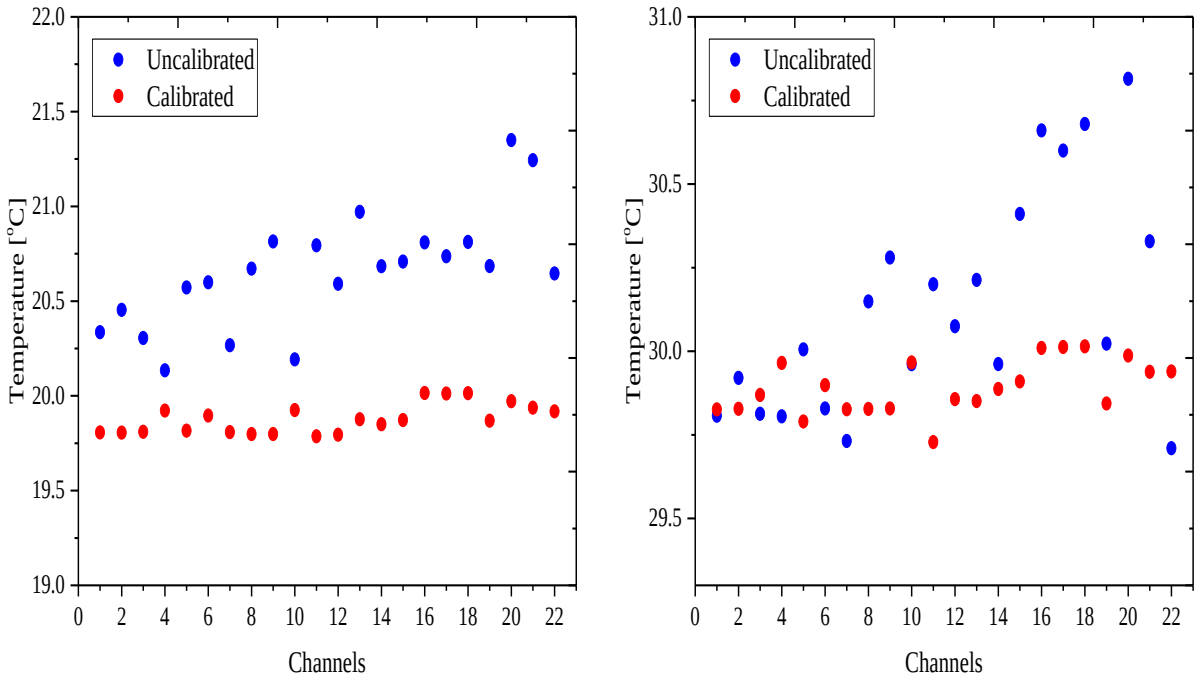

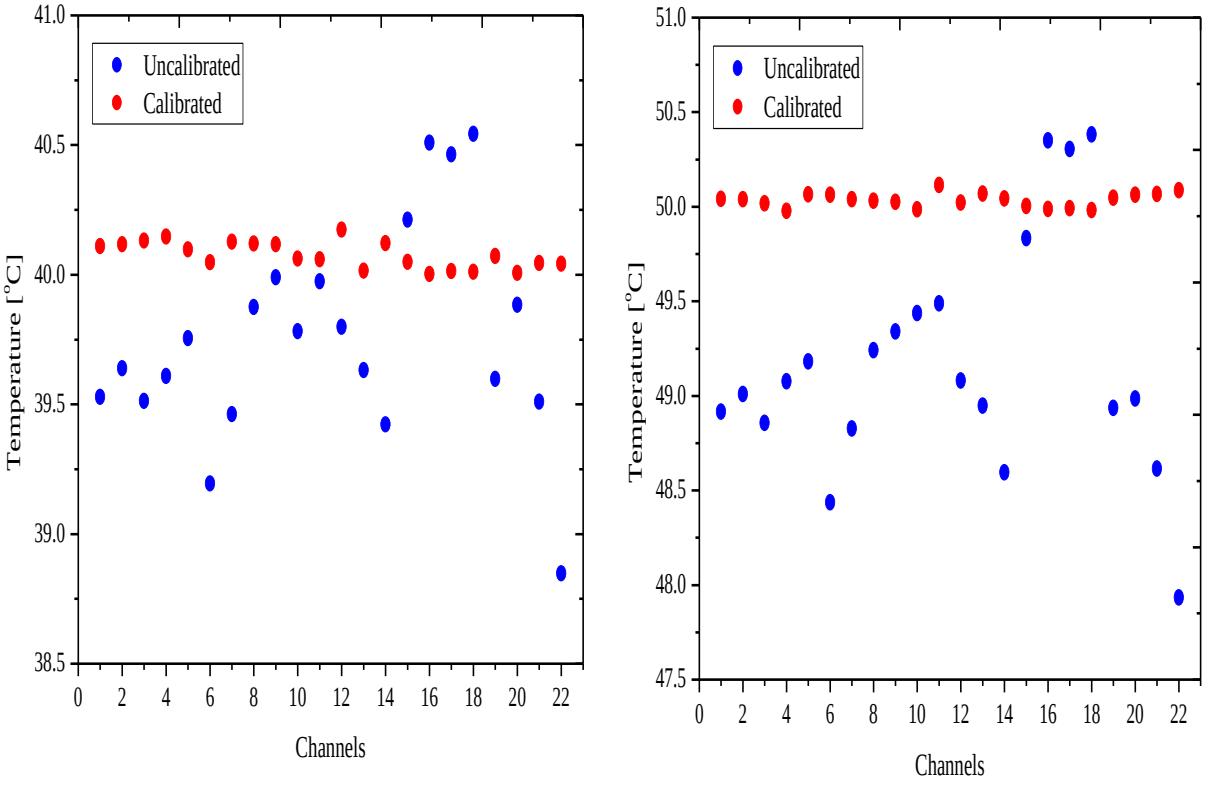

Figure B.8.2: Calibrated and uncalibrated temperatures of thermocouples at 20 to 50 °C

The reason for using different channels of the data logger was the differences in the calibration factors obtained for the thermocouples. Also, the variation in the characteristics of the junction of the thermocouples after soldering them to the different positions could be responsible for the variation in the calibration factors of the thermocouples. After calibration, the average deviation between the average measured temperature of the thermocouples and reference temperatures was 0.169 °C.

B.3 Conclusion

The calibration of the thermocouples was conducted and presented in this section. The thermocouples were calibrated for temperature ranges of 15 to 55 °C using a thermal bath having an accuracy of ±0.005 °C. Linear relationships were noticed to exist between the average measured temperature of the thermocouples and the reference temperature. The average deviation of the thermocouples was 0.169 °C.

C. Uncertainty Analysis

C.1 Introduction

An uncertainty analysis of the parameters pertinent to this work was carried out. This section presents the accuracy of the instruments used in the study (thermophysical properties and thermo-convection) and the estimation of the uncertainties associated with them.

C.2 Theory of Uncertainty Analysis

Basically, bias and precision are two types of errors encountered during measurements. The bias is the error due to measurement accuracy and it is generally given by the instrument manufacturer. This type of error can stem from the imperfection of measuring equipment, calibration, etc. Error due to precision is related to the spread in the data because it is connected to the data precision. The source of this type of error is electrical noise, measurement variation process, etc. The degree of precision and bias errors relates to a probability of 95% in which the estimated error is less than the actual error. For a single measurement, the uncertainty has to do with both precision and bias. Uncertainty is expressed in Eq. C.2.1 [64].

$$\delta x_i = \sqrt{\left(b_i{}^2 + p_i{}^2\right)} \qquad \textbf{C.2.1}$$

where x_i is a single measurement, and δx_i characterises the multiplication of standard deviation by Student's t-variable [218]. The measurement of G was associated with numerous parameters and could be evaluated using a collection of equations.

$$G = G(x_1, x_2, x_3, \ldots\ldots, x_n) \qquad \textbf{C.2.2}$$

With the uncertainties of x_i known, the uncertainty of G could be estimated, as expressed in Eq. C.2.3.

$$\delta G = \frac{\partial G}{\partial X_i}\delta x_i \qquad \textbf{C.2.3}$$

where δG is the sensitivity coefficient used to estimate the effect of x_i on the overall uncertainty. Using the root sum square method, the uncertainty of numerous independent parameters could be estimated.

$$\delta G = \left(\sum_{i=1}^{n}\left(\frac{\partial G}{\partial X_i}\delta x_i\right)^2\right)^{\frac{1}{2}} \quad \text{C.2.4}$$

The precision of the thermocouples was estimated using regression analysis, which is a statistical tool used to establish a mathematical relation between two or more parameters. The *x* value is the known parameter, while the *y* value is determined through measurements. Hence the uncertainty was propagated from the *y* parameter [218]. Eq. C.2.5 was used to estimate the uncertainty of the *y* parameter.

$$\delta y = \pm t S_{yx}\sqrt{\frac{1}{N}+\frac{1}{M}+\frac{(x_i-\bar{x})^2}{S_{xx}}} \quad \text{C.2.5}$$

where S_{xx} is expressed as:

$$S_{xx} = \sum_{i=1}^{N}(x_i-\bar{x})^2 \quad \text{C2.6}$$

S_{yx} was estimated by first evaluating S_{xy}, a and b.

$$S_{xy} = \sum_{i=1}^{N}(x_i-\bar{x})(y_i-\bar{y}) \quad \text{C.2.7}$$

$$b = \frac{S_{xy}}{S_{xx}} \quad \text{C.2.8}$$

$$a = \bar{y} - b\bar{x} \quad \text{C.2.9}$$

$$y_{ci} = a + bx_i \quad \text{C.2.10}$$

$$S_{yx} = \sqrt{\frac{\sum_{i=1}^{N}(y_i-y_{ci})^2}{N-2}} \quad \text{C.2.11}$$

The uncertainty in the *x* parameter was estimated by dividing the uncertainty in *y* by the gradient of the regression line.

$$\delta x = \frac{\delta y}{m} \qquad \text{C.2.12}$$

To obtain the uncertainty in the *x* variable, the uncertainty in *y* was divided by the slope of the regression line.

C.3 Instruments

The accuracy prescribed by the manufacturer was used as the bias for the instruments, while the precision was estimated using the standard deviation of the 1 000 measurement points acquired through the data logger for temperature and flow rate measurements. For the thermal conductivity meter and viscometer, the accuracy (bias) provided by the manufacturers was used. The estimated precision was multiplied by Student's *t*-value with a confidence limit of 95%. The accuracy of the instruments used in the study is given in Table C.3.1.

Table C.3: Accuracy of instruments used in the study.

Instrument	Range	Accuracy
Thermocouple	< 150 °C	±0.1 °C
Weighing balance	10 mg – 220 g	0.001 g
Thermal bath	-200 – 150 °C	± 0.005 °C
Vernier calipers	0.02 mm	0.02 mm
Viscometer	0.3 – 10,000 mPa.s	±3%
Thermal conductivity meter	0.2 – 2.0 W/m K	±10%
Flow meter	0.0666 – 0.3333 l/s	±0.01% of full-scale flow rate + 2% (measured value)
Graduated cylinder	250 ml	± 2.0 ml
Electrical conductivity meter	0 µS - 200 mS	± 1%
Gaussmeter	1 G – 30 kG	±1.1%

C.3.1 Thermocouples

The calibration of the thermocouples was discussed in B.3, where the accuracy of the thermal bath and thermocouples was given as ±0.005 °C and 0.1 °C respectively. The precision was

estimated using Eqs. C.2.5 to C.2.12 with the uncertainty evaluated using Eq. C.2.1. The average uncertainty of the thermocouples was ±0.159%.

C.3.2 Flow Meters

Each of the flow meters had an accuracy of ±0.01% of full-scale flow rate + 2% (measured value) used as the bias. The precision was calculated by multiplying the standard deviation of the flow rate acquired by the data logger by the Student's *t*-value. The uncertainty was then estimated using Eq. C.2.1.

C.3.3 Digital Weighing Balance

The accuracy of the digital weighing balance was 0.001 g and this was used as the bias. The standard deviation of the weights of the HNPs and surfactants (total) for each MHNF as presented in Tables A.3.1 to A.3.3 was obtained and used as the precision. This was multiplied by the Student's *t*-value and Eq. C.2.1 was used to estimate uncertainty.

C.3.4 Thermal Conductivity Meter

Similarly, the accuracy of the thermal conductivity meter was engaged as the bias. The standard deviation of the measurements taken for each MHNF and base fluid was multiplied by the Student's *t*-value and used as the precision. Using Eq. 3.22, which is an extension of Eq. C.1, the uncertainty of κ for MHNFs and base fluids was determined. As mentioned in Appendix A, the volume of the base fluids (DIW and EG-DIW) used in the study was 1 400 ml and the graduated volumetric flash had an accuracy of ±2.0 ml.

C.3.5 Viscometer

With the accuracy of the viscometer used as the bias and the precision calculated from the multiplication of the standard deviation of the measured μ (for MHNFs and base fluids) by Student's *t*-value, the uncertainty of μ (for MHNFs and base fluids) was estimated using Eq. 3.21 (an extension of Eq. C.2.1). It is pertinent to note that the viscometer had an accuracy specified for the temperature sensor associated with μ measurement.

C.4 Parameters

C.4.1 Temperatures

From the known uncertainty of the thermocouples, the uncertainty associated with the measurement of temperatures within and without the cavity was obtained. The uncertainty of the temperature of water flowing from and to the thermal baths was assumed to be equal under adiabatic conduction of close to perfect insulation. This is expressed by Eq. C.4.1.1.

$$\delta T_{in} = \delta T_o \quad \text{C.4.1.1}$$

$$\delta T_{Bulk,H} = \frac{1}{3}\sqrt{\left(\delta T_{o,1}\right)^2 + \left(\delta T_{o,2}\right)^2 + (\delta T_i)^2} \quad \text{C.4.1.2}$$

$$\delta \Delta T = \sqrt{\left(\frac{1}{2}\delta T_{o,1}\right)^2 + \left(\frac{1}{2}\delta T_{o,2}\right)^2 + (\delta T_i)^2} \quad \text{C.4.1.3}$$

$$\delta T_H = \frac{1}{3}\sqrt{\left(\delta T_{H,1}\right)^2 + \left(\delta T_{H,2}\right)^2 + \left(\delta T_{H,3}\right)^2} \quad \text{C.4.1.4}$$

$$\delta T_C = \frac{1}{3}\sqrt{\left(\delta T_{C,1}\right)^2 + \left(\delta T_{C,2}\right)^2 + \left(\delta T_{C,3}\right)^2} \quad \text{C.4.1.5}$$

The uncertainties of the bulk temperature, temperature gradient, temperature hot and cold side of the cavity were estimated using Eqs. C.4.1.2 to C.4.1.5 respectively. It is worth mentioning that T is the absolute temperature used in the correlations for determining the uncertainty of other properties.

C.4.2 Cavity Area

The uncertainty of the cavity area was estimated using Eq. C.4.2.1.

$$\delta A = \sqrt{\left(\frac{\partial A}{\partial W}\delta W\right)^2 + \left(\frac{\partial A}{\partial H}\delta H\right)^2} \quad \text{C.4.2.1}$$

where: $\partial W = \partial H = \partial L$

C.4.3 Thermophysical Properties

To estimate the uncertainty of μ and κ of the base fluids, Eqs. C.4.3.1 to C.4.3.4 representing the correlations developed from the experimental data obtained in this work for μ and κ of the base fluids were used.

$$\kappa_{DIW} = 0.5741 + 1.393 \times 10^{-3}T \quad \text{C.4.3.1}$$

$$\mu_{DIW} = 1.18357 - 0.1271T \quad \text{C.4.3.2}$$

$$\kappa_{EG-DIW} = 0.382833 + 7.17 \times 10^{-4}T \quad \text{C.4.3.3}$$

$$\mu_{EG-DIW} = 3.890357 - 0.05079T \quad \text{C.4.3.4}$$

The empirical formula [204, 205] used for the estimation of the uncertainty of other thermal properties for the base fluids is expressed by Eqs. C.4.3.5 to C.4.3.9.

$$\rho_{DIW} = (999.842594 + 0.067939952T - 0.00909529T^2 + 1.00168 \times 10^{-4}T^3 - 1.120083 \times 10^{-6}T^4 + 6.536332 \times 10^{-9}T^5 \quad \text{C.4.3.5}$$

$$\beta_{DIW} = 8.41 \times 10^{-7}T^3 - 1.55704 \times 10^{-4}T^2 + 0.015892349T - 0.055807193 \quad \text{C.4.3.6}$$

$$C_{p-DIW} = 4.214 - 2.286 \times 10^{-3}T + 4.991 \times 10^{-5}T^2 - 4.519 \times 10^{-7}T^3 + 1.857 \times 10^{-9}T^4 \quad \text{C.4.3.7}$$

$$\rho_{EG-DIW} = 1069.055 - 0.4655T \quad \text{C.4.3.8}$$

$$C_{p(EG-DIW)} = 3.400738 + 0.003362T \quad \text{C.4.3.9}$$

The uncertainties of κ, ρ, β and C_p of the base fluids (DIW and EG-DIW) were estimated using Eqs. C.4.3.10 to C.4.3.13 respectively.

$$\delta\kappa_{bf} = \sqrt{\left(\frac{\partial\kappa_{bf}}{\partial T}\delta T\right)^2} \quad \text{C.4.3.10}$$

$$\delta\rho_{bf} = \sqrt{\left(\frac{\partial\rho_{bf}}{\partial T}\delta T\right)^2} \quad \text{C.4.3.11}$$

$$\delta\beta_{bf} = \sqrt{\left(\frac{\partial\beta_{bf}}{\partial T}\delta T\right)^2} \quad \text{C.4.3.12}$$

$$\delta C_{p-bf} = \sqrt{\left(\frac{\partial C_{p-bf}}{\partial T}\delta T\right)^2} \quad \text{C.4.3.13}$$

With the use of Eq. C.4.3.14 for φ, which is a simple version of Eq. 3.1, the uncertainty of φ was evaluated using Eq. C.4.3.15.

$$\varphi = \frac{v_{hnp}}{v_{hnp}+v_{bf}} = \frac{\frac{m_{hnp}}{\rho_{hnp}}}{\frac{m_{hnp}}{\rho_{hnp}}+v_{bf}} \quad \text{C.4.3.14}$$

$$\delta\varphi = \sqrt{\left(\frac{\partial\varphi}{\partial m_{hnp}}\delta m_{hnp}\right)^2 + \left(\frac{\partial\varphi}{\partial v_{bf}}\delta v_{bf}\right)^2} \quad \text{C.4.3.15}$$

Where:

$$\frac{\partial\varphi}{\partial m_{hnp}} = \frac{\rho_{hnp}v_{bf}}{\left(m_{hnp}+\rho_{hnp}v_{bf}\right)^2} \quad \text{and} \quad \frac{\partial\varphi}{\partial v_{bf}} = \frac{-m_{hnp}\rho_{hnp}}{\left(m_{hnp}+\rho_{hnp}v_{bf}\right)^2}$$

Empirical models for ρ_{hnf}, $C_{p\text{-}hnf}$ and $\beta_{hnf,}$ as expressed using Eqs. C4.3.16 to C.4.3.18, were engaged to estimate their uncertainty as described by Eqs. C.4.3.19 to C.4.3.21 respectively.

$$\rho_{hnf} = (1-\varphi)\rho_{bf} + \varphi\rho_{hnp} \quad \text{C.4.3.16}$$

$$C_{p-hnf} = \frac{(1-\varphi)(\rho C_p)_{bf}+(\rho C_p)_{hnp}}{\rho_{hnf}} \quad \text{C.4.3.17}$$

$$\beta_{hnf} = \frac{(1-\varphi)(\rho\beta)_{bf}+(\rho\beta)_{hnp}}{\rho_{hnf}} \quad \text{C.4.3.18}$$

$$\delta\rho_{hnf} = \sqrt{\left(\frac{\partial\rho_{hnf}}{\partial\varphi}\delta\varphi\right)^2 + \left(\frac{\partial\rho_{hnf}}{\partial\rho_{bf}}\delta\rho_{bf}\right)^2} \quad \text{C.4.3.19}$$

where:

$$\frac{\partial\rho_{hnf}}{\partial\varphi} = \rho_{hnp} - \rho_{bf} \quad \text{and} \quad \frac{\partial\rho_{hnf}}{\partial\rho_{bf}} = 1-\varphi$$

$$\delta C_{p-hnf} =$$

$$\sqrt{\left(\frac{\partial C_{p-hnf}}{\partial \varphi}\delta\varphi\right)^2 + \left(\frac{\partial C_{p-hnf}}{\partial \rho_{bf}}\delta\rho_{bf}\right)^2 + \left(\frac{\partial C_{p-hnf}}{\partial C_{p-bf}}\delta C_{p-bf}\right)^2 + \left(\frac{\partial C_{p-hnf}}{\partial \rho_{hnf}}\delta\rho_{hnf}\right)^2} \quad \textbf{C.4.3.20}$$

where:

$\frac{\partial C_{p-hnf}}{\partial \varphi} = \frac{-(\rho C_p)_{bf}}{\rho_{hnf}}$, $\frac{\partial C_{p-hnf}}{\partial \rho_{bf}} = \frac{C_{p-bf}(1-\varphi)}{\rho_{hnf}}$, $\frac{\partial C_{p-hnf}}{\partial C_{p-bf}} = \frac{\rho_{bf}(1-\varphi)}{\rho_{hnf}}$, and $\frac{\partial C_{p-hnf}}{\partial \rho_{hnf}} =$

$$\frac{-\left((1-\varphi)(\rho C_p)_{bf}+(\rho C_p)_{hnp}\right)}{(\rho_{hnf})^2}$$

$$\delta\beta_{hnf} = \sqrt{\left(\frac{\partial \beta_{hnf}}{\partial \varphi}\delta\varphi\right)^2 + \left(\frac{\partial \beta_{hnf}}{\partial \rho_{bf}}\delta\rho_{bf}\right)^2 + \left(\frac{\partial \beta_{hnf}}{\partial \beta_{bf}}\delta\beta_{bf}\right)^2 + \left(\frac{\partial \beta_{hnf}}{\partial \rho_{hnf}}\delta\rho_{hnf}\right)^2} \quad \textbf{C.4.3.21}$$

where:

$\frac{\partial \beta_{hnf}}{\partial \varphi} = \frac{-(\rho\beta)_{bf}}{\rho_{hnf}}$, $\frac{\partial \beta_{hnf}}{\partial \rho_{bf}} = \frac{\beta_{bf}(1-\varphi)}{\rho_{hnf}}$, $\frac{\partial \beta_{hnf}}{\partial \beta_{bf}} = \frac{\rho_{bf}(1-\varphi)}{\rho_{hnf}}$, and $\frac{\partial \beta_{hnf}}{\partial \rho_{hnf}} =$

$$\frac{-\left((1-\varphi)(\rho\beta)_{bf}+(\rho\beta)_{hnp}\right)}{(\rho_{hnf})^2}$$

To estimate the uncertainty of κ_{hnf}, Eq. C.4.3.22 was employed.

$$\delta\kappa_{hnf} = \sqrt{\left(\frac{\partial \kappa_{hnf}}{\partial \varphi}\delta\varphi\right)^2 + \left(\frac{\partial \kappa_{hnf}}{\partial \kappa_{bf}}\delta\kappa_{bf}\right)^2} \quad \textbf{C.4.3.22}$$

C.4.4 Heat Transfer Rate

The estimation of the uncertainty of the heat transferred (Q) involved the substitution of Eqs. C.4.4.1 to C.4.4.3 into Eq. 3.23.

$$\frac{\partial Q}{\partial \dot{m}} = C_{p-bf}\Delta T \quad \textbf{C.4.4.1}$$

$$\frac{\partial Q}{\partial C_{p-bf}} = \dot{m}\Delta T \quad \textbf{C.4.4.2}$$

$$\frac{\partial Q}{\partial \Delta T} = \dot{m}C_{p-bf} \quad \textbf{C.4.4.3}$$

C.4.5 Convective Heat Transfer Coefficient

Eqs. C.4.5.1 to C.4.5.4 were substituted into Eq. 3.23 to estimate the uncertainty of *h*.

$$\frac{\partial h}{\partial Q} = \frac{1}{(T_h - T_c)A} \quad \text{C.4.5.1}$$

$$\frac{\partial h}{\partial A} = \frac{-Q}{(T_h - T_c)A^2} \quad \text{C.4.5.2}$$

$$\frac{\partial h}{\partial T_h} = \frac{-Q}{(T_h - T_c)^2 A} \quad \text{C.4.5.3}$$

$$\frac{\partial h}{\partial T_c} = \frac{Q}{(T_h - T_c)^2 A} \quad \text{C.4.5.4}$$

C.4.6 Nusselt Number

Similarly, the uncertainty of *Nu* was estimated by substituting Eqs. C.4.6.1 to C.4.6.3 into Eq. 3.24.

$$\frac{\partial Nu}{\partial h} = \frac{L_c}{\kappa} \quad \text{C.4.6.1}$$

$$\frac{\partial Nu}{\partial L_c} = \frac{h}{\kappa} \quad \text{C.4.6.2}$$

$$\frac{\partial Nu}{\partial h} = \frac{-hL_c}{\kappa} \quad \text{C.4.6.3}$$

The uncertainties of parameters and thermophysical properties estimated in this study are presented in Table C.4.5

C.5 Conclusion

The theory and method of uncertainty were highlighted. The accuracy of instruments engaged as the bias and the precision was used to estimate the uncertainty associated with the relevant parameters involved in the study.

Table C.4.5: Estimated uncertainties related to AMF, BAAF and AAF.

Uncertainty	AMF	BAAF	AAF
δT_{CS}	0.0129	0.0129	0.0129
δT_{HS}	0.0407	0.0407	0.0407
δT_{W-H}	0.0953	0.0953	0.0953
δT_{W-C}	0.0591	0.0591	0.0591
$\delta \Delta T_C$	0.0318	0.0318	0.0318
$\delta \Delta T_H$	0.1042	0.1042	0.1042
δT_B	0.0960	0.0960	0.0960
δA	5.02×10^{-5}	5.02×10^{-5}	5.02×10^{-5}
δL	3.33×10^{-4}	3.33×10^{-4}	3.33×10^{-4}
δV	0.0514	0.0514	0.0514
Δm	0.0221	0.0141	0.0191
$\delta \mu_{DIW}$	1.87×10^{-4}	-	1.99×10^{-4}
$\delta \beta_{DIW}$	2.80×10^{-3}	-	2.89×10^{-3}
$\delta \rho_{DIW}$	1.5456	-	1.4492
$\delta C_{p\text{-}DIW}$	0.0348	-	0.0150
$\delta \kappa_{DIW}$	1.42×10^{-4}	-	1.45×10^{-4}
$\delta \mu_{EG\text{-}DIW}$	-	5.48×10^{-3}	-
$\delta \beta_{EG\text{-}DIW}$	-	3.85×10^{-5}	-
$\delta \rho_{EG\text{-}DIW}$	-	0.5026	-
$\delta C_{p\text{-}EG\text{-}DIW}$	-	0.3630	-
$\delta \kappa_{EG\text{-}DIW}$	-	7.74×10^{-5}	-
$\Delta \varphi$	4.86×10^{-4}	1.98×10^{-4}	3.64×10^{-4}
$\delta \rho_{HNF}$	2.1416	0.7689	1.8765
$\delta C_{p\text{-}HNF}$	5.4459	1.4611	5.8334
$\delta \beta_{HNF}$	0.6928	0.0224	0.7396
$\delta \kappa_{HNF}$	2.0029	2.0030	2.0027
$\delta \mu_{HNF}$	2.8422	2.9901	2.8337
$\delta \dot{m}$	1.04×10^{-3}	0.0139	6.82×10^{-4}
δQ	8.4361	6.0196	8.1177
δh	8.0371	4.8797	6.0996
δNu	3.7175	5.1062	3.0556